

**Assigning symmetry terms to molecular orbitals in asymmetric  
Fischer carbenes using FALDI in a theoretical study**

*by*

**Brent Nel<sup>[a]</sup>**

**Supervisor: Jurgens de Lange<sup>[b]</sup>**

**Co-supervisor: Marilé Landman<sup>[c]</sup>**

**Department of Chemistry,**

**University of Pretoria**

Submitted in fulfillment of the requirements of the degree

Master of Science

In the Faculty of Natural and Agricultural Sciences

University of Pretoria

Pretoria

12 December 2021

E-mails: <sup>[a]</sup> [brent1.nel@gmail.com](mailto:brent1.nel@gmail.com)

<sup>[b]</sup> [jurgens.delange@up.ac.za](mailto:jurgens.delange@up.ac.za)

<sup>[c]</sup> [marile.landman@up.ac.za](mailto:marile.landman@up.ac.za)

## Declaration

I, *Brent Nel* declare that the thesis/dissertation, which I hereby submit for the degree *Master of Science* at the University of Pretoria, is my own work and has not previously been submitted by me for a degree at this or any other tertiary institution.



---

*(Signature of Candidate)*

12 December 2021

## Outputs from this work

Brent Nel, Jurgens de Lange. Development of a theoretical FALDI-based framework for the symmetry classifications of molecular orbitals in asymmetric Fischer Carbenes, (Submitted for publication to the Journal of Chemical Theory and Computation).

Brent Nel, Jurgens de Lange. FALDI Molecular Orbital Fragment Analysis to identify bonding modes in various Fischer carbene complexes. (In preparation).

Brent Nel, Marilé Landman and Jurgens de Lange. The Ground State Molecular Orbital Fragment Analysis Between Experimental Fischer Carbenes with X=OEt, NH<sub>2</sub> and NMe<sub>2</sub> and R= 2-(N-Methyl)pyrrolyl. (In preparation).

Brent Nel, Jurgens de Lange and Marilé Landman. FALDI & MO Analysis of intramolecular, non-covalent interactions in Fischer Carbenes, *Proceedings of the 4<sup>th</sup> International Symposium on Halogen Bonding (ISXB4)*, University of Stellenbosch, November 2020. (poster).

## Acknowledgements

I would like to thank my family for the moral, financial and emotional support throughout this journey, to my father who has always been invested in my studies, driving and pushing me to succeed and my mother that continuously provides more love than anyone could ever ask for and my brother with whom I can discuss science. To my fellow students, colleagues and professors I also greatly appreciate the opportunities, encouragement and knowledge shared along the way.

To Prof. Marilé Landman my deepest gratitude goes out to you for the financial support via the National Research Foundation and the early introduction to Inorganic Chemistry, I truly appreciate all the experiences and opportunities you have provided me with.

To my supervisor and mentor Dr. Jurgens de Lange I deeply appreciate your passion for Chemistry, thank you for sharing it with me, for the intellectual stimulation, for the learning opportunities and the ability to grow as a scientist alongside building a friendship. Thank you for believing in my abilities and motivating me to bring out the best in me.

Finally, to my significant other Nicola van den Berg, I would like to thank you for your unconditional love and support that has carried me through this journey, from sharing frustrations to celebrating successes, thank you for the chemistry that we share.

## Abstract

Molecular orbitals (MOs) are one of the most useful tools available for explaining and describing the electronic structure of a chemical system. These MOs are obtainable through different means, which falls under two approaches; the conceptual and computational approach. The conceptual approach is mostly limited to symmetric systems but provides a qualitative and interpretable result, this is obtainable through methods like Symmetry Adapted Linear Combinations (SALCs) of atomic orbitals. While the computational approach applies to any system, irrespective of the symmetry and provides quantitative results but is limited by the interpretability.

In this study, a Fragment, Atomic, Localized, Delocalized, Interatomic (FALDI) electron density decomposition scheme-based approach is investigated that aims to bridge the conceptual and computational approach of MOs. Multiple distinct theoretical chemistry techniques have been used to produce a consistent and accurate model which labels MOs in asymmetric octahedral metal complexes. These techniques include the Quantum Theory of Atoms in Molecules (QTAIM) to obtain the atomic overlap matrix (AOM) which is used in FALDI to obtain electron density (ED). FALDI recovers the localized ED (*loc*-ED) and the delocalized ED (*deloc*-ED) which is needed for the FALDI MO analysis and FALDI fragments. The work illustrates how an asymmetric complex is manipulated into a symmetric function, which is used to obtain the symmetry terms. The symmetric functions are known as Natural Density Functions (NDFs) and is derived using the *loc*-ED of the metal centre. The relationship between the *loc*-ED and the *deloc*-ED can be correlated to recover the delocalized indices (DI) between two atoms interacting whilst assigning symmetry labels. The development of the model was tried and tested on a symmetric model system and a simple octahedral metal centred asymmetric system (Fischer carbene) to ensure consistency and validity.

This study then took the FALDI MO analysis further and considered fragments. Fragments are a summation of diatomic interactions which allow multiple atoms interacting with each other to be considered. Linking the symmetry terms to the metal centre provides the delocalized interactions of the fragments, resulting in a quantitative tool that is also interpretable at a classical level. The result is a method that allows for bonding modes such as  $\sigma$ - and  $\pi$ -character to be recovered while assigning contributions which can be traced back to each molecular orbital origin. The FALDI fragments were applied to multiple asymmetric

Fischer carbene systems to not only further verify the robustness of the method but also to test the limits.

Finally, experimental (with available data) Fischer carbene systems were considered for which novel interpretations and approaches were suggested, which promises a potential future in tuning Fischer carbene systems to achieve the desired chemical traits using the FALDI MO analysis technique.

Keywords: Theoretical Chemistry, Computational Chemistry, FADLI, MOs, QTAIM, SALCs, symmetry, Fischer carbenes

<b>Table of Contents</b>	<b>Page</b>
<b>Cover Page</b>	i
<b>Declaration</b>	ii
<b>Outputs from this work</b>	iii
<b>Acknowledgements</b>	iv
<b>Abstract</b>	v
<b>Table of Contents</b>	vi
<b>List of Figures</b>	xii
<b>List of Tables</b>	xiv
<b>List of Abbreviations</b>	xvi
<b>Chapter 1. Introduction</b>	1
<b>Introduction</b>	2
<b>Background information</b>	3
<b>Problem statement and aims</b>	9
<b>Outline of this dissertation</b>	10
<b>References</b>	13
<b>Chapter 2. Theoretical Background and Developments</b>	16
<b>Introduction</b>	17
<b>Canonical Molecular Orbitals</b>	18
<b>Hartree-Fock Theory</b>	18
<b>Hartree Product wavefunction</b>	19
<b>Electron-electron repulsion</b>	20
<b>The antisymmetry of the wavefunction</b>	21
<b>Slater determinants</b>	21
<b>The Roothaan equations</b>	22
<b>Basis sets</b>	23
<b>Molecular Orbital Theory</b>	25
<b>Atomic orbitals</b>	25
<b>Molecular Orbitals</b>	29

<b>Summary of the Orbital model</b>	31
<b>Density Functional Theory</b>	32
<b>The Existence Theorem of Hohenberg-Kohn</b>	33
<b>The Variational Theorem of Hohenberg-Kohn</b>	34
<b>The Ground State Origin</b>	34
<b>Self-consistent Field of Kohn-Sham</b>	36
<b>Functionals for the Exchange-correlation</b>	38
<b>An overview of DFT</b>	39
<b>Wavefunction Analysis</b>	40
<b>QTAIM</b>	40
<b>Electron density topology</b>	41
<b>Atomic Overlap Matrix</b>	43
<b>Domain averaged Fermi Holes</b>	46
<b>FALDI Density Decomposition scheme</b>	47
<b>Natural Density functions</b>	49
<b>Determination of approximated molecular symmetries through NDF-analysis</b>	50
<b>FALDI Fragments</b>	53
<b>Perspectives</b>	55
<b>References</b>	56
<b>Chapter 3.</b>	60
<b>Chapter 4. FALDI Molecular Orbital Fragment Analysis to identify bonding modes in various Fischer carbene complexes.</b>	71
<b>Abstract</b>	72
<b>Introduction</b>	72
<b>Theoretical Background and Development</b>	76
<b>Computational Details</b>	78
<i>Structures</i>	79
<i>Fragments</i>	79
<b>Results and Discussion</b>	81
<i>Inter-fragment electron delocalization</i>	82
Analysis of the Metal–Carbene ( $[M]\cdots C_{\text{carbene}}$ ) interaction	82
Metal X-group ( $[M]\cdots[X]$ )	88
Metal R-group ( $[M]\cdots[R]$ )	92
Interaction between $C_{\text{carbene}}$ , X- and R-groups	94
Summary: an overview of the Metal–Ligand ( $[M]\cdots[L]$ ) interaction	95



<b>Conclusions</b>	97
<b>References</b>	100
<b>Chapter 5. The Ground State Molecular Orbital Fragment Analysis of Experimental Fischer Carbenes with X=OEt, NH<sub>2</sub> and NMe<sub>2</sub> and R= 2-(N-Methyl)pyrrolyl</b>	103
<b>Abstract</b>	104
<b>Introduction</b>	104
<b>Theoretical Background and Development</b>	107
<b>Computational Details</b>	110
<b>Structures</b>	111
<b>Fragmentations</b>	112
<b>Results and Discussion</b>	113
<i>Investigation of structural parameters</i>	113
<i>The geometric effect imposed by choice of X-group</i>	116
<i>The electronic effect imposed by varying the X-group</i>	121
<b>Binding energies</b>	127
<b>Conclusions</b>	129
<b>References</b>	131
<b>Chapter 6. Summary and conclusions</b>	134
<b>Summary</b>	135
<b>Chapter Breakdown</b>	138
<b>Future Studies</b>	141
<b>References</b>	145
<b>Appendix A</b>	146
<b>Supplementary Information for Chapter 3</b>	146
Section 1: Cartesian Coordinates and Energy of All Molecules Studied.	148
Section 2: Localized Matrix of Cr1 of All Molecules Studied Corresponding the Eigenvalues to Molecular Orbitals.	150
Section 3: Delocalization Matrix Summary for All Molecules Studied Corresponding the Symmetry Terms of Molecular Orbitals Obtained in the Localized Matrix.	155
Section 4: Cr(CO) <sub>6</sub> Natural Density Functions corresponded to the Molecular Orbitals	158
Section 5: Cr(CO) <sub>5</sub> [C(OEt)(Me)] Natural Density Functions	162
Section 6: Cr(CO) <sub>5</sub> [C(OEt)(Me)] Natural Density Functions corresponded to the Molecular Orbitals	163
<b>Appendix B</b>	174
<b>Supplementary Information for Chapter 4</b>	174

<b>Section 1: Cartesian Coordinates and Energies of All Molecules Studied.</b>	175
<b>Section 2: Inter-fragment delocalization of all the molecules in their respective fragments.</b>	187
<b>Section 3: Method of assigning symmetry labels (LMAT) and correlating to the DI contribution (DMAT) on a Molecular orbital level.</b>	188
<b>Section 4: Symmetry decomposition with Inter-fragment delocalization of each R-group for all molecules.</b>	207
<b>Section 5: Symmetry decomposition in terms of energy for each fragment.</b>	209
<b>Section 6: Symmetry decomposition in terms of energy for each R-group.</b>	211
<b>Section 7: MOs contributing majority of the DI in specific interactions for the [M]...[L] interaction.</b>	213
<b>Section 8: MOs contributing majority of the DI in specific interactions for the [M]...C<sub>carbene</sub> bond.</b>	216
<b>Section 9: MOs contributing majority of the DI in specific interactions for the [M]...[X] interaction.</b>	220
<b>Section 10: MOs contributing majority of the DI in specific interactions for the [M]...[R] interaction.</b>	223
<b>Appendix C</b>	228
<b>Supplementary Information for Chapter 5</b>	228
<b>Section 1: Cartesian Coordinates of and Energies of All Molecules Studied.</b>	229
<b>Section 2: Assigning symmetry labels (LMAT) to each of the lowest energy structures.</b>	245
<b>Section 3: The metal cluster interacting with the all ligands [M]...[L] for all frozen dihedrals.</b>	250
<b>Section 4: The fragment analysis of the metal cluster interacting with the carbene carbon [M]...C<sub>carbene</sub> at the frozen dihedrals.</b>	255
<b>Section 5: The fragment analysis of the metal cluster interacting with the X-group [M]...[X] at the frozen dihedrals.</b>	260
<b>Section 6: The fragment analysis of the metal cluster interacting with the R-group [M]...[R] at the frozen dihedrals.</b>	265
<b>Section 7: Inter-fragment delocalization of all the molecules in their respective fragments for the geometric analysis.</b>	270
<b>Section 8: Inter-fragment delocalization of all the molecules in their respective fragments for the electronic analysis.</b>	274
<b>Section 9: Hypothesis testing of the carbonyls interacting with [X] and [R] fragments.</b>	276
<b>Section 10. The fragment analysis of the metal and carbonyls separated interacting with the different fragments at the frozen dihedrals as a geometric analysis.</b>	280



# List of Schemes and Figures

## Chapter 1

<b>Scheme 1. 1.</b> Charge transfer depictions for the $\sigma$ -donor and $\pi$ -acceptor capacity of the carbonyl ligand metal relationship.....	8
--	---

## Chapter 2

<b>Figure 2. 1.</b> Cartesian layout for spherical polar coordinates .....	27
<b>Figure 2. 2.</b> A graphic representation of the spherical coordinates of the atomic orbitals. ....	29
<b>Scheme 2. 1.</b> The process of obtaining localized and delocalized indices.....	45

## Chapter 3

<b>Figure 3.1.</b> Reduced Molecular Orbital Diagram of $\text{Cr}(\text{CO})_6$ . <b>Error! Bookmark not defined.</b>	
<b>Figure 3.2.</b> The Localized Natural Density Functions (NDF's) of $\text{Cr}(\text{CO})_6$ <b>Error! Bookmark not defined.</b>	
<b>Figure 3.3.</b> The Natural Density Functions corresponding to their respective Molecular Orbitals with their contributions. ....	<b>Error! Bookmark not defined.</b>
<b>Figure 3.4.</b> The fifteenth NDF which represents $A_{1g}$ symmetry on the Cr linked to the contributing occupied MO's .....	<b>Error! Bookmark not defined.</b>
<b>Figure 3.5.</b> The Molecular Orbital Diagram of $\text{Cr}(\text{CO})_5\text{C}(\text{OEt})(\text{Me})$ ... <b>Error! Bookmark not defined.</b>	
<b>Figure 3.6.</b> The Natural Density Functions corresponding to their respective Molecular Orbitals with their contributions. ....	<b>Error! Bookmark not defined.</b>
<b>Figure 3.7.</b> The Natural Density Functions corresponding to their respective Molecular Orbitals with their contributions. ....	<b>Error! Bookmark not defined.</b>

## Chapter 4

<b>Scheme 4. 1.</b> Back-bonding in a Fischer carbene.....	74
<b>Figure 4. 1.</b> The skeleton structure of all the Fischer carbenes.....	79
<b>Figure 4. 2.</b> Generalized fragments used for FALDI Fragments MO analysis. The fragments are $[\text{M}] \cdots \text{C}_{\text{carbene}}$ , $[\text{M}] \cdots [\text{X}]$ , $[\text{M}] \cdots [\text{R}]$ , $[\text{X}] \cdots [\text{R}]$ and $[\text{M}] \cdots [\text{L}]$ , where $[\text{M}] \cdots [\text{L}]$ interaction refers to the metal cluster ( $[\text{M}]$ , metal and pentacarbonyl) interacting with the entire carbene ligand ( $[\text{L}]$ which is the $\text{C}_{\text{carbene}}$ , X-group and R-group). ....	80

<b>Figure 4. 3.</b> The geometric effects of changing the X-group whilst the R-group stays the same, using <b>4c</b> and <b>4g</b> to show the planarity disruption between the X- and R-group....	81
<b>Figure 4. 4.</b> The geometric effects of changing the X-group when the R= -CCH forcing planarity between the X- and R-group illustrated by <b>4d</b> and <b>4h</b> .....	82
<b>Figure 4. 5.</b> The molecular orbitals of $\text{Cr}(\text{CO})_5\{\text{C}(\text{NMe}_2)(\text{CCH})\}$ displaying the $[\text{M}]\cdots\text{C}_{\text{carbene}}$ interaction for (i) $\sigma$ and (ii) $\pi$ with an isovalue of 0.02 a.u. ....	85
<b>Figure 4. 6.</b> The most $\pi$ -contributing molecular orbitals for $[\text{M}]\cdots[\text{X}]$ of $\text{Cr}(\text{CO})_5\{\text{C}(\text{X})(\text{CHCHPh})\}$ with (i) $\text{X}=\text{OEt}$ and (ii) $\text{X}=\text{NMe}_2$ with an isovalue of 0.02 a.u.....	90
<b>Figure 4. 7.</b> The $\sigma$ -contributing molecular orbitals for $[\text{M}]\cdots[\text{X}]$ of $\text{Cr}(\text{CO})_5\{\text{C}(\text{X})(\text{CHCHPh})\}$ with (i) $\text{X}=\text{OEt}$ and (ii) $\text{X}=\text{NMe}_2$ with an isovalue of 0.02 a.u.....	91

## Chapter 5

<b>Figure 5. 1.</b> The Fischer Carbene labelling, with the X-group representing the electron-donating group. Where $\text{M}=\text{Cr}$ , <b>5a</b> is $\text{X}=\text{OEt}$ and $\text{R}=\text{2-(N-Methyl)pyrrolyl}$ , <b>5b</b> is $\text{X}=\text{NH}_2$ and $\text{R}=\text{2-(N-Methyl)pyrrolyl}$ and <b>5c</b> is $\text{X}=\text{NMe}_2$ and $\text{R}=\text{2-(N-Methyl)pyrrolyl}$ .....	111
<b>Figure 5. 2.</b> The dihedral angles of the three Fischer carbenes selected for constrained optimizations. The red lines show the dihedral angle ( $\text{Cr}-\text{C}_{\text{carbene}}-\text{C}_{\text{pyrrole}}-\text{N}_{\text{pyrrole}}$ ) that were frozen for the R-group in (i) while the blue lines represent the X-groups dihedral angle ( $\text{Cr}-\text{C}_{\text{carbene}}-\text{O/N-H/C}$ ) that were set to zero at the start of each optimization calculation for the three different X-groups (ii) and (iii). ....	112
<b>Figure 5. 3.</b> Generalized fragments used for FALDI Fragments Molecular Orbital Analysis. Blue: Metal and pentacarbonyl ligands, $[\text{M}]$ . Yellow: $\text{C}_{\text{carbene}}$ ; Orange: R-group, $[\text{R}]$ ; and Green: X-group, $[\text{X}]$ . The carbene ligand as a whole, $[\text{L}] = \text{C}_{\text{carbene}} + [\text{R}] + [\text{X}]$ . ....	113
<b>Figure 5. 4.</b> The interfragment interaction where the $\text{X}=\text{OEt}$ ( <b>5a</b> ) is compared at dihedral angle, $\text{DA}(\text{Cr},\text{C},\text{C},\text{N})$ , of $180^\circ$ (a) and $90^\circ$ (a'). The electrons are shared between fragments (a) $[\text{M}]\cdots\text{C}_{\text{carbene}}$ , (b) $[\text{M}]\cdots[\text{X}]$ (c) $[\text{X}]\cdots[\text{R}]$ . All the isovalues are shown at 0.001 a.u.....	120

## List of Tables

### Chapter 1

Table 1.1 A list of all the complexes investigated in this work.....	11
--	----

### Chapter 2

<b>Table 2. 1.</b> Angular variables without the radial component $r, \theta$ and $\phi$ related to the real angular parts of s, p and d atomic orbitals .....	26
--	----

### Chapter 3

<b>Table 3. 1.</b> The total FALDI-classified symmetry composition of the Cr1–C2 bond in Cr(CO) <sub>6</sub> .....	66
<b>Table 3. 2.</b> The total FALDI-classified symmetry composition of the Cr1–C <sub>CO</sub> bond in Cr(CO) <sub>5</sub> C(OEt)(Me) .....	69
<b>Table 3. 3.</b> The total FALDI-classified symmetry composition of the Cr1–C <sub>carbene</sub> bond in Cr(CO) <sub>5</sub> C(OEt)(Me) .....	69

### Chapter 4

<b>Table 4. 1.</b> The combinations of C <sub>carbene</sub> substituents (X- and R-groups) on Fischer carbenes complexes. ....	79
<b>Table 4. 2.</b> Inter-fragment Delocalization comparison of X=OEt and NMe <sub>2</sub> .....	82
<b>Table 4. 3.</b> Symmetry decomposition for [M]···C <sub>carbene</sub> with X=OEt and NMe <sub>2</sub> .....	83
<b>Table 4. 4.</b> Symmetry decomposition for [M]···[X] interaction with X=OEt and NMe <sub>2</sub> .....	88
<b>Table 4. 5.</b> Symmetry decomposition for the [M]···[R] interaction with X=OEt and X=NMe <sub>2</sub> . ....	93
<b>Table 4. 6.</b> Symmetry decomposition of [M]···[L] interaction with X=OEt and NMe <sub>2</sub> .....	94
<b>Table 4. 7.</b> The total DI of interactions not localized to the metal.....	94

### Chapter 5

<b>Table 5. 1.</b> Comparison of the crystal structures to lowest energy-optimized structures, where the dihedral (N <sub>pyrrole</sub> -C <sub>pyrrole</sub> -C <sub>carbene</sub> -X) and torsion angle (R-C <sub>carbene</sub> -X) represent the angle between the X- and R-groups.....	113
<b>Table 5. 2.</b> The crystal structures bond lengths when the X-group changes <sup>a</sup> .....	115
<b>Table 5. 3.</b> The FALDI MO analysis of X=OEt ( <b>5a</b> ) for various dihedrals DA(Cr,C,C,N) considering the [M]···[L] interaction. ....	117
<b>Table 5. 4.</b> The FALDI fragment population for X=OEt, <b>5a</b> . ....	118
<b>Table 5. 5.</b> The FALDI inter-fragment electron delocalization for X=OEt, <b>5a</b> . ....	119

<b>Table 5. 6.</b> The electrons shared between fragments for the various dihedrals DA(Cr,C,C,N). .....	122
<b>Table 5. 7.</b> FALDI-MO analysis of the [M]··[L] interaction for various X-groups at the lowest energy DA(Cr,C,C,N).....	124
<b>Table 5. 8.</b> The $\sigma$ - and $\pi$ -contribution of the different X groups for Cr··C <sub>carbene</sub> bond .....	126
<b>Table 5. 9.</b> The binding energy of the different X-groups calculated using single point calculations at B3LYP. ....	128

## List of abbreviations

AIM	Atoms in Molecules
AO	Atomic Orbital
AOM	Atomic Overlap Matrix
BCP	Bond Critical Point
B3LYP	Becke's 3-parameter exchange and Lee–Yang–Parr correlation functional
CCP	Cage Critical Point
CP	Critical Point
DAFH	Domain Averaged Fermi Hole
Deloc	Delocalized
DFT	Density Functional Theory
DI	Delocalized Indices
DMAT	Delocalized Matrix
ECP	Effective Core Potentials
ED	Electron Density
EVec	Eigenvector
FALDI	Fragment Atomic Localized Delocalized Interatomic
Frag	Fragment
GGA	Generalized Gradient Approximation
HF	Hartree-Fock
LCAO	Linear Combination of Atomic orbitals
LEVals	Localized eigenvalues
LI	Localized Indices
LMAT	Localized Matrix
Loc	Localized
MLCT	Metal to Ligand Charge Transfer
MO	Molecular Orbital
MOT	Molecular Orbital Theory
MP2	second-order Moller-Plesset Perturbation theory
NCP	Nuclear Critical Point
NDF	Natural Density Function
NL	Non-Localized
PBEPBE	Perdew, Burke and Ernzerhof's exchange and correlation functional
PES	Potential Energy Surface
Ph	Phenyl
PM3	Parametric Method 3
QCT	Quantum Chemical Topology
QTAIM	Quantum Theory of Atoms in Molecules
RCP	Ring Critical Point
SALCs	Symmetry Adapted Linear Combinations of atomic orbitals
SCF	Self Consistent Field
VWN	Vosko, Wilks and Nusair local density functional
XC	Exchange Correlation



# **Chapter 1.**

## **Introduction**

## Introduction

Observable physical and chemical properties – or descriptive chemistry – can often be adequately explained through various chemical theories – or fundamental chemistry. In particular, *electronic* structure underpins a complete description of quantum chemistry<sup>1, 2</sup> which is relatable to general conceptual chemistry through the molecular structure hypothesis. At the heart of this hypothesis is the concept of a chemical bond – the collection of forces acting on atoms to form molecules. Chemical bonds are ubiquitous with chemistry and therefore critically important to understand many chemical applications, from engineering to biology. Chemical bonds are, however, *noumena*, and no chemical bond operator exists in quantum mechanics. Accurately describing chemical bonds and atomic interactions therefore remains a challenge that has conceived an entire chemical language to describe and classify. One of these linguistic tools is that of molecular orbitals (MOs). While MOs were originally a mathematical construct to allow systematic variation of a molecular wavefunction, MO theory (MOT) has since become one of the conceptual languages chemists use to describe electronic structure. MOs provide a molecular-wide, holistic description of a molecule's chemical structure. Chemists, on the other hand, utilize an atomistic, reductionist description of a molecule. Herein lies one of the paradoxical dichotomies of MOT – an attempt to accurately and precisely describe molecular electronic structure in a manner that recovers the molecular-wide wavefunction but can be interpreted in terms of atoms, functional groups and chemical bonds. That said, MOT has evolved to be one of the most useful theories to *conceptually* describe the electronic structure of molecules.

The emergence of computational chemistry as a subdiscipline of theoretical chemistry in the last few decades has significantly altered the manner through which we describe electronic structures. The quantum mechanics behind the scenes is often elegant and rather beautiful for the appreciative audience, but to some experimental chemists meaningless without interpretation and thus easily ignored. This is where computational and theoretical chemistry have been bridging the gap over the years – by systematically allowing previously conceptual approaches to be exactly calculated and quantified. Furthermore, advances in theory together with technological advances have made delving into computational modelling increasingly simpler. Density Functional Theory (DFT) is an excellent example of this being developed in the 1960s<sup>1, 2</sup> but only becoming relevant and widely used and accepted in the 1990s.

At the forefront of this work is the electronic structure, and how we as chemists can describe it. In particular, we investigate the electronic structure of Fischer carbene complexes, primarily due to the excellent canvas that these complexes' electronic structures represent. In the remainder of this chapter I first present background information on a number of relevant topics, followed by a statement of the research problem we aim to solve. Finally, a short overview of our approach is provided, in terms of a description of each chapter of this work.

## **Background information**

### *Applications of electronic structures*

Models of electronic structure are important to the study of chemistry in general, and is a cross-cutting component of almost all fields of chemistry. However, there are a number of applications within chemistry for which an exact understanding of electronic structure is critical. Below, we discuss examples of these applications.

Humanity have many made significant scientific and technological leaps in the last 100 years, but with solving one problem, we often create a new one. The energy crisis is a prime example of this unfortunate tendency – access to electricity vastly improves livelihoods but comes at the cost of our planet's natural resources. In order to meet rising electricity demands whilst preserving natural resources, alternative and renewable methods of electricity generation – such as solar cells – are critically important. Solar cells have been around for 181 years, since Alexandre Edmond Becquerel observed the first photovoltaic effect in a conductive solution exposed to light in 1839.<sup>3, 4</sup> One of the central research questions in the field of solar cells revolves around the molecular mechanism of converting solar energy into electrical energy. Inorganic semiconductor materials have been the best for this conversion and have provided good efficiency but are relatively expensive and difficult to manufacture. An emerging alternative is organic-based photovoltaic systems, which are attractive since organic materials are cheap, abundant and renewable. The primary problems with these systems, however, are their light-harvesting efficiencies and stabilities in the presence of oxygen and water. The bandgap is the primary reason for the efficiency difference between organic and inorganic semiconductors, where the former have a much smaller bandgap compared to the sizeable gap in the latter.<sup>5</sup> The bandgap is predominantly determined by the holistic electronic structure of a semiconductor. Therefore, exact understanding of electronic structures will allow for the efficient rational design of novel light-harvesting materials through bandgap engineering.

Another prime example that vitally requires an understanding of the electronic structure is catalysis. Many industrial processes use specific catalysts to increase yield, lower temperatures of reactions and even drive the selective formation of specific processes.<sup>6-10</sup> We also often associate electroneutral reactions with heterogeneous catalysis, where complete or partial charge transfers occur between the solid catalyst and the reactant. Work already done in 1969 by Gerischer illustrates the connection between charge transfer and catalysis and some of the molecular mechanisms of charge transfer.<sup>11</sup> The mechanisms of many catalysts are therefore highly dependent on their electronic structure. Again, holistic understanding of the electronic structure can lead to the better rational design of catalysts and optimization of chemical properties with specific chemical characteristics.

### *Electronic structure models of transition metal complexes*

While electronic structures are important in the understanding of all chemistries, they are at centre stage in the study of transition metal complexes. One of the popular electronic structure models is the electrostatic model of bonding, also known as crystal-field theory, and its quantum chemical cousin, ligand-field theory.<sup>12</sup> One of the central findings of both crystal- and ligand-field theories is the splitting of  $d$  atomic orbitals that occur when a metal is complexed. These split orbitals have different energy levels, which are then used to explain magnetic properties, thermodynamics and optical spectra.<sup>12</sup> An important consideration of both theories is, however, molecular symmetry.  $d$ -level splitting, as well as the landscape of bonding within ligand field theory, can only be described adequately and accurately in a molecule with a high order of symmetry. This includes symmetrical octahedral, tetrahedral and square-planar geometries. In this work, we will primarily focus on octahedral complexes.

Symmetrical octahedral complexes have two sets of energy levels describing the  $d$  orbitals: the lower energy and triply degenerate set of  $t_{2g}$  orbitals and the doubly degenerate set of higher energy  $e_g$  orbitals, separated by an energy gap or bandgap.<sup>12</sup> The bandgap also goes by a few other names such as the octahedral splitting parameter or ligand field splitting parameter,  $\Delta_o$ .  $\Delta_o$  carries tremendous utility, and can be used to predict a large-range of chemical phenomena.<sup>12</sup> In addition, correspondence of predicted  $\Delta_o$  with experimental results provides evidence for some of ligand-field theory's other predictions – such as the manner through which MOs are formed from symmetry-adapted atomic and ligand orbitals. Unfortunately, these tremendous insights only applies to highly symmetrical molecules, as the fundamentals of ligand-field theory depend on the symmetry operations allowed by point-

group symmetries. MO-based perturbation theory<sup>13</sup> allows for extension into complexes with a lower degree of symmetry, but the complexity of perturbation theory quickly outstrips its usefulness.

Ligand-field theory's utility and predictive power primarily relies on MOs. The construction of MOs are been defined in most cases by group theory<sup>14</sup> which not only allows derivation of MOs for symmetrical molecules but also affords a chemically-intuitive interpretation. Therefore, MOs in symmetrical molecules can be used to understand a wide range of chemical and physical phenomena, including reactivity, photophysical properties and stability.<sup>13</sup> Developments in computational methods have allowed for the variational quantum mechanical determination of MOs, thereby removing the requirement of symmetry. Unfortunately, with the exception of frontier MOs (highest occupied and lowest unoccupied MOs), exact and accurate interpretation of MOs still require some degree of symmetry to be present.

MOT forms a large part of many undergraduate curricula, and in particular, the MOs of diatomic molecules. Simple molecules like carbon monoxide (CO), molecular oxygen (O<sub>2</sub>) and dinitrogen (N<sub>2</sub>) are often used to teach Mos and provide an essential foundation to understanding MOs. Due to the complexity of MOs as a result of asymmetry, MOT is often not taught past the diatomic level. If the course is advanced, it includes triatomic molecules and maybe even inorganic molecules that are admittedly complex, but the example often stops at the symmetric Cr(CO)<sub>6</sub> as the example.<sup>15, 16</sup> In polyatomic molecules, conceptual (i.e. non-variational) MOs are determined through a methodology called symmetry-adapted-linear combinations (SALCs) of atomic orbitals (AO). The SALC-AO approach is fully based on group theory, but describes each MO in terms of chemically-relevant constituents. For instance, in Cr(CO)<sub>6</sub>, a specific MO with *t*<sub>2g</sub> symmetry must form of Cr atoms' AOs with *t*<sub>2g</sub> symmetry (e.g. 3*d*<sub>xy</sub>) and CO SALCs with *t*<sub>2g</sub> symmetry (e.g. π\*<sub>C-O</sub>). Therefore, a *t*<sub>2g</sub> MO can be described as π-backbonding between a metal *d*<sub>xy</sub> orbital and π-antibonding orbitals on the ligands.

Unfortunately, the extreme interpretive power that the SALC-AO approach affords chemists are lost the moment a single degree of symmetry is broken. For instance, when a single CO ligand in Cr(CO)<sub>6</sub> is replaced by a similar CN<sup>-</sup> ligand, all MOs consist of only the lowest symmetry term *a*.<sup>14</sup> No inferences can be made with regards to ligand SALCs or metal AOs in terms of MO formation. While extrapolations can be made from systems with higher symmetry,<sup>17</sup> these often require complex perturbative approaches<sup>13</sup> to be accurate and are still

limited to the extent to which symmetries can change. However, when an asymmetric system lies before the most chemists with an abstracted appearing mixed computer-generated orbital picture, not much interpretation and chemically-useful information can be extracted. Therefore, the electronic structures of asymmetrical transition metal complexes are extremely difficult to discern, especially in terms of MOs.

#### *Density-based methods*

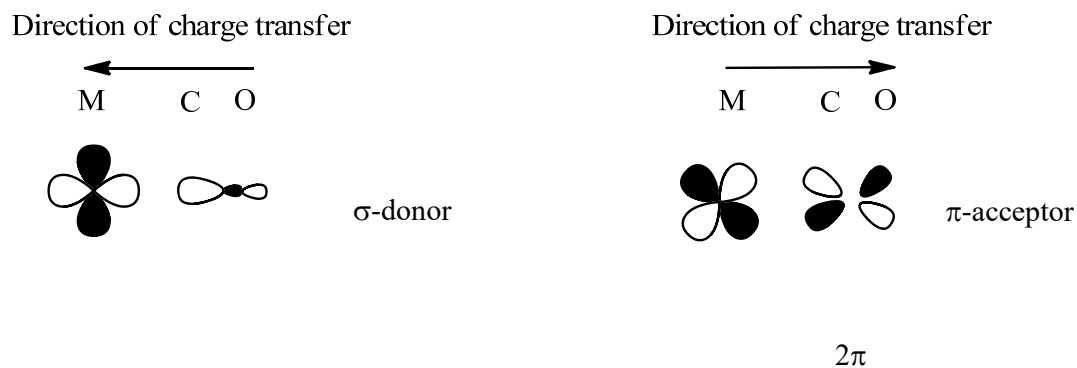
As discussed above, MOs provide a predictive and chemically intuitive interpretation of electronic structure, but their easy interpretation is limited to highly symmetrical systems. Computational (variational) MOs provide the means to calculate MOs for asymmetric systems, but are nearly impossible to interpret due to their holistic, delocalized natures. Electron density-based approaches, on the other hand, such as the Quantum Theory of Atoms in Molecules (QTAIM)<sup>18</sup> and Quantum Chemical Topology (QCT)<sup>19</sup> methods in general, provide an entirely different approach. Specifically, QCT methods allow for a highly *atomistic* description of molecules, and are therefore relatively easy to interpret by chemists. Unfortunately, while QCT methods include holistic elements, to fully recover molecular-wide properties usually require consideration of multiple variables over multiple atoms, making interpretation possible but overly complex.

QTAIMs' delocalization and localization indices (DIs and LIs respectively) provide an approach that can bridge the holistic MOT with atomistic QCT.<sup>20, 21</sup> As a result, LIs and DIs have become popular in molecular structures and models of bonding.<sup>22</sup> Unfortunately, QTAIM's LIs and DIs are still somewhat difficult to interpret, especially for larger molecules. In addition, while the link between MOT and LIs and DIs were shown, the two approaches are still worlds apart – to the point that some theoreticians fully restrict their analyses to either orbital- or density-based approaches. This led to the eventual yet recent development of the Fragment, Atom, Localized, Delocalized, and Interatomic (FALDI) Charge Density Decomposition Scheme,<sup>23</sup> based on concepts of Domain Averaged Fermi Holes (DAFH).<sup>24-26</sup> FALDI fully recovers the holistic nature of the wavefunction whilst providing chemically-intuitive, atomistic interpretations. With a new powerful technique in hand, tackling an old problem such as interpreting molecular orbitals seemed inviting.

#### *Model organometallic compounds*

We can approach the development of any new process or method from many angles and perspectives. Introducing a ‘gold-standard’ is however one of the best ways to develop something that improves on the previously existing methods/models and ideas whilst keeping the authenticity of an effective method that will be more easily accepted. To tackle the ‘golden-standard’ approach in this work, well-studied systems that are accepted in the chemical community are needed and at the core of this work, symmetry is a vital component. As a symmetrical model compound, we have selected the familiar  $\text{Cr}(\text{CO})_6$  complex. A comparable, yet asymmetric model of  $\text{Cr}(\text{CO})_5\{\text{C}(\text{OEt})(\text{Me})\}$  is selected as an asymmetric model compound. These two systems provide the baseline for any theoretical developments made in this study. These complexes are well-known and easily synthesised, with  $\text{Cr}(\text{CO})_6$  even available in a bottle for purchase, making them real and suitable for experimental comparison if desired. A short description and background of each is given below.

Chromium hexacarbonyl,  $\text{Cr}(\text{CO})_6$ , is a common chemical used for many chemical applications; ranging from organometallic synthesis and catalysis to thin film deposition of metals, surface chemistry, photophysics and photochemical dissociation of metal-ligand bonds<sup>27-30</sup> to name a few. Theoretically, it has also become a well-studied molecule premiering in energetic studies,<sup>31</sup> DFT studies regarding vibrational spectra<sup>32</sup> and semiempirical MO models.<sup>15</sup> Prominent in inorganic textbooks,<sup>12, 16</sup> the molecule is often used in advanced MOT courses,<sup>17</sup> with some postgraduate courses even using it as the basis for inorganic octahedral complexes.<sup>33</sup> Chromium hexacarbonyl has an octahedral geometry in which when optimized, the carbonyls are evenly distanced apart, hence the molecule is fully symmetric. Classically the MOs are determined from SALCs. Starting from the carbon’s AOs and the oxygen’s AOs yields MOs of the CO ligand. These MOs are then combined to form SALCs, based on the octahedral symmetry point-group of the  $\text{Cr}(\text{CO})_6$  molecule. SALCs are then matched with the Chromium’s AOs to yield the  $\text{Cr}(\text{CO})_6$  MOs seen in many articles and textbooks.<sup>15, 16, 30, 34</sup> With Chromium hexacarbonyl being such a popular choice in the explanation and teaching of molecular orbitals, it makes it an ideal case study for the development of a framework for this work’s MO deconstruction. The validity of the framework will depend on the comparison of the method to the classical approach of fully interpreting the  $\text{Cr}(\text{CO})_6$  molecular orbital diagram. In this complex, the electron density increases on the metal because of the  $\sigma$ -donor interaction, while the ligand density decreases. The electron density on the metal decreases and increases on the ligand because of the  $\pi$ -accepting nature of the carbonyl ligand.



**Scheme 1. 1.** Charge transfer depictions for the  $\sigma$ -donor and  $\pi$ -acceptor capacity of the carbonyl ligand metal relationship.

We often refer to the carbonyl metal interaction as synergic bonding, because of the overall stabilizing interaction that results. Therefore, as it is apparent, this molecule can be and has been fully described classically. Most of the Fischer carbene complexes comprise a metal centre surrounded by carbonyls, like  $\text{Cr}(\text{CO})_5$ . Keeping most of this backbone makes Fischer carbenes ideal case studies for the framework in studying asymmetric compounds.

Metal-Carbene complexes typically have octahedral symmetry with a metal centre and one of the ligands is a carbon which is doubly bonded. Metal-Carbene complexes are divided into two major categories, namely Fischer and Schrock carbenes, as well as a third category focused around *n*-heterocyclic carbenes. Fischer carbenes are electrophilic and  $\pi$ -donating<sup>35</sup> while Schrock carbenes are nucleophilic and  $\pi$ -neutral. The factors that determines whether a Fischer or Schrock carbene is present highly depends on the substituents, with the metal also playing a role. Fischer Carbenes were first characterized in 1964,<sup>36</sup> with the synthesis of this specific carbene ( $\text{Cr}(\text{CO})_5\{\text{C}(\text{OEt})(\text{Me})\}$ ) only a few years later in 1968.<sup>37</sup> The research emphasis of most Fischer carbene syntheses is on developing a reliable and efficient method of forming carbon-carbon bonds<sup>38</sup> to synthesize the carbene. A typical synthetic process uses Schlenk techniques at inert and low temperatures, where the first lithiation occurs on the group being attached followed by the addition of the metal and finally quenching with an alkoxy or amine salt which is then filtered to remove the lithium to minimize decomposition. However, each individual carbene will have its own synthesis. The application of Fischer carbenes are few, but common in synthetic studies. Fischer carbenes are used in the synthesis of diaryl ethers,<sup>39</sup> in catalysis and have proven electrochemical properties.<sup>40</sup>

The reason why the  $\text{Cr}(\text{CO})_5\{\text{C}(\text{OEt})(\text{Me})\}$  Fischer carbene complex is ideal as a model



compound is because of its simplicity and the available experimental data<sup>37</sup> which can contribute to the overall foundation of the framework. The carbene keeps its pentacarbonyl backbone similar to that of the Cr(CO)<sub>6</sub> complex, and by only changing one ligand, this allows it to break symmetry and keep some original symmetry components. The M—C<sub>carbene</sub> bond forces new orbital combinations, making it an ideal candidate to base the framework model on, however, any carbene could have been chosen as long as it is rudimentary and followed the same rational reasoning for its structure.

### **Problem statement and aims**

The classical interpretation of MOs is an extremely useful and insightful technique to explain chemical phenomena. Unfortunately, interpretation of MOs highly depend on a high degree of symmetry within a molecule, and lower degrees of molecular symmetry and no symmetry leads to generally uninterpretable Mos that will be illustrated later in this work. While some useful information can be gained by focussing on frontier orbitals – the Highest Occupied Molecular Orbitals (HOMO) or the Lowest Unoccupied Molecular Orbitals (LUMO) – disregarding the vast majority of an electronic structure can lead to misinterpretations and inaccurate predictions. Therefore, the restriction of symmetry as required for MO interpretation is a theoretical problem that, if solved, could provide tremendous fundamental understanding of electronic structures.

Density-based methods, such as the general QCT collection of models, provide accurate interpretation of electronic structures regardless of molecular symmetry. However, density-based methods are difficult to use to fully describe and recover molecular-wide properties. In addition, QCT approaches are less chemically intuitive, and does not utilize the same general chemical language developed through MOT.

The recently developed FALDI density decomposition technique provides a bridge between MOT and QCT. FALDI provides atom-based information that is intuitively recognizable by chemists, yet FALDI still recovers the holistic quantum-mechanical wavefunction. As a result, FALDI is an ideal model to provide the utility of MOT without the restriction of symmetry. In particular, preliminary results before the commencement of this project has shown that FALDI's description of atom-localized density contains high degrees of symmetry, even in asymmetrical molecules.

The aim of this work is to further explore the link between FALDI's description of atom-localized and atom-pair delocalized density and MOs. In particular, we aim to investigate the symmetry of FALDI's localized density distributions associated with a central metal within a transition metal complex. We aim to decompose these localized density distributions in terms of MOs which, in turn, should provide symmetry components to the underlying MOs.

We will restrict ourselves to octahedral complexes, and relatively simple Fischer carbene complexes in general. We therefore aim to provide symmetry labels (e.g.  $a_{1g}$ ,  $t_{1u}$ ,  $t_{2g}$  and  $e_g$  characters) to all MOs in these complexes, regardless of the symmetry of a complex. From these assignments, we hope to ultimately obtain  $\sigma$ - and  $\pi$ -information relating to the overlap in terms of bonding, that can describe the whole electronic structure in terms of chemical bonding parameters. Having achieved this level of electronic structure information, theoretically, an asymmetric molecule can then be understood using the same MO-based arguments as for symmetric systems. This allows for a degree of tunability, enabling rational design when changing parameters to achieve specific characteristics.

### **Outline of this dissertation**

This dissertation presents an extension to both the FALDI scheme as well as molecular orbital theory in general. Accordingly, only theoretical results are produced within this work. A short overview is given below for each of the chapters.

**Chapter 2** provides a theoretical background to this work. Quantum chemical topics – such as wavefunction mechanics, density functional theory, basis sets as well as QCT techniques such as QTAIM and FALDI are described. In addition, Chapter 2 contains a full overview of the novel theoretical developments discovered in this work. While this section of the chapter is somewhat repetitive of elements from following chapters, we expect a centralized and accumulated description of novel theoretical developments to be useful to readers.

**Chapter 3** establishes the theoretical framework of the extensions made to FALDI. The novel method are thoroughly applied to two model systems – the symmetrical  $\text{Cr}(\text{CO})_6$  and the asymmetrical and elementary Fischer carbene complex,  $\text{Cr}(\text{CO})_5\{\text{C}(\text{OEt})\text{Me}\}$ .  $\text{Cr}(\text{CO})_6$  is used as validation for the novel FALDI-MO method, which is then tested on the Fischer carbene complex. As a result, the delocalization of electrons between Cr and selected carbon atoms is

fully investigated and interpreted in terms of the full symmetry of the metal – a feat that has, to our knowledge, never been accomplished before.

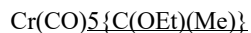
**Chapter 4** extends the FALDI-MO method to the topic of structure-property relationships. In particular, the choice of X-group in Fischer carbene complexes of the general structure  $\text{Cr}(\text{CO})_5\{\text{C}(\text{X})(\text{R})\}$  is particularly important. The X-group provides an important functionality in material design to tweak electronic properties of the complex.<sup>41-43</sup> Two of the most popular X-groups found on Fischer carbenes is dimethylamine ( $\text{NMe}_2$ ) and ethoxy groups (OEt). Elementary Fischer carbene complexes with these two X-groups as well as a wide range of R-groups ( $\text{R} = -\text{H}, -\text{CHCH}_2, -\text{CHCHPh}, -\text{CCH}$ ) are explored using the FALDI-MO method developed in Chapter 3. These varied structures are analyzed in terms of MOs using the FALDI-MO method, and despite the lack of symmetry in their structures. These structures show how FALDI-MO can provide novel insights into the rational design of materials.

**Chapter 5** is the final results chapter, which then takes the application a little further by looking at three different X-groups, namely ethoxy (OEt), dihydrogen amine ( $\text{NH}_2$ ) and dimethylamine ( $\text{NMe}_2$ ) all with a 2-(N-Methyl)pyrrolyl R-group. This chapter aims at incorporating experimental results to the newly developed theoretical method. The synthesis of the compounds in Chapter 5 has been performed previously and experimental data such as crystal structures of those carbenes structures are available and are included in the results and discussion. This chapter illustrates how minor changes vastly affect each system, yet appear so insignificant. The work focus' on rotating the R-group to determine the geometric or electronic effects. The chapter illustrates the effect of geometry but also the effect that the X-group plays in the  $\sigma$ - and  $\pi$ -character, illustrating the importance of the coexisting relationship between the X- and R-group. This theoretical method hopes to predict the electronic system so that before an experiment is performed the electronic structure is fully grasped so that smart synthesis can take place to achieve the desired characteristics. This chapter therefore serves as a final case-study to show the predictive power and general utility of the FALDI-MO approach.

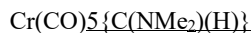
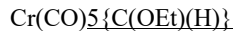
**Chapter 6** provides summaries of the major research outcomes of all the chapters, as well as concluding remarks. This chapter includes a discussion of the future work planned, theoretical developments and experimental verifications from this work.

**Table 1.1.** A list of all the complexes investigated in this work

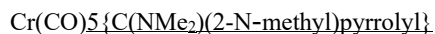
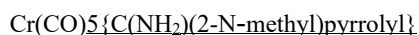
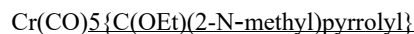
**Chapter 3**



**Chapter 4**



**Chapter 5**



**A note on the structure of results chapters in this dissertation**

Chapters 3, 4 and 5 are written as publications, and we plan to submit each of these chapters for publication in theoretical and inorganic chemistry journals. As such, each chapter contains an introduction and theoretical background section, which redundantly overlaps quite a bit with each other as well as the information contained in Chapter 2. In addition, at the time of writing, Chapter 3 has already been submitted to the Journal of Chemical Theory and Computation, and the chapter is included in its submitted form (i.e. double-columned format).

## References

1. Kohn, W.; Sham, L. J., Self-consistent equations including exchange and correlation effects. *Physical Review* **1965**, *140* (4A), A1133.
2. Hohenberg, P.; Kohn, W., Inhomogeneous electron gas. *Physical Review* **1964**, *136* (3B), B864.
3. Becquerel, M., Mémoire sur les effets électriques produits sous l'influence des rayons solaires. *Comptes Rendus Hebdomadaires des Séances de l'Académie des Sciences* **1839**, *9*, 561-567.
4. Fraas, L. M., History of solar cell development. In *Low-Cost Solar Electric Power*, Springer: 2014; pp 1-12.
5. Chidichimo, G.; Filippelli, L., Organic solar cells: problems and perspectives. *International Journal of Photoenergy* **2010**, *2010*.
6. Okuhara, T.; Mizuno, N.; Misono, M., Catalytic chemistry of heteropoly compounds. In *Advances in Catalysis*, Elsevier: 1996; Vol. 41, pp 113-252.
7. Misono, M., Proc. 10th Int. Congr. Catal. *Budapest* **1992**, 69-103.
8. Misono, M. In *Chem. Uses Molybdenum*, Proc. Int. Conf, 1982; p 289.
9. Misono, M.; Moro-oka, Y.; Kimura, S., *Future opportunities in catalytic and separation technology*. Elsevier: 1990.
10. Mizuno, N., Heterogeneous catalysis. *Chemical Reviews* **1998**, *98* (1), 199.
11. Gerischer, H., Charge transfer processes at semiconductor-electrolyte interfaces in connection with problems of catalysis. *Surface Science* **1969**, *18* (1), 97.
12. Weller, M. D.; Overton, T.; Rourke, J.; Armstrong, F. A., *Inorganic chemistry*. Sixth edition. ed.; Oxford University Press: Oxford, 2014.
13. Albright, T. A.; Burdett, J. K.; Whangbo, M.-H., *Orbital interactions in chemistry*. John Wiley & Sons: 2013.
14. Vincent, A., *Molecular symmetry and group theory : a programmed introduction to chemical applications*. 2nd ed. ed.; Wiley: Chichester, 2000.
15. Schreiner, A. F.; Brown, T. L., A semiempirical molecular orbital model for Cr(CO)<sub>6</sub>, Fe(CO)<sub>5</sub>, and Ni(CO)<sub>4</sub>. *Journal of the American Chemical Society* **1968**, *90* (13), 3366-3374.
16. Dabrowiak, J. C., Metals in Medicine Special Issue. *Inorganica Chimica Acta* **2012**, *393*.
17. Cass, M. E.; Hollingsworth, W. E., Moving beyond the single center-Ways to reinforce molecular orbital theory in an inorganic course. *Journal of Chemical Education* **2004**, *81* (7), 997.
18. Bader, R., Chem. Re V. 1991, 91, 893.(b) Bader, RFW Atoms in Molecules: A Quantum Theory. Oxford University Press: New York: 1990.
19. Popelier, P. L., Quantum chemical topology. In *The Chemical Bond II*, Springer: 2016; pp 71-117.
20. Fradera, X.; Austen, M. A.; Bader, R. F., The Lewis model and beyond. *The Journal of Physical Chemistry A* **1999**, *103* (2), 304-314.
21. Cortés-Guzmán, F.; Bader, R. F., Complementarity of QTAIM and MO theory in the study of bonding in donor-acceptor complexes. *Coordination Chemistry Reviews* **2005**, *249* (5-6), 633-662.
22. Sumar, I.; Cook, R.; Ayers, P. W.; Matta, C. F., AIMLDM: a program to generate and analyze electron localization-delocalization matrices (LDMs). *Computational and Theoretical Chemistry* **2015**, *1070*, 55-67.
23. De Lange, J. H.; Cukrowski, I., Toward deformation densities for intramolecular interactions without radical reference states using the fragment, atom, localized, delocalized,

- and interatomic (FALDI) charge density decomposition scheme. *Journal of computational chemistry* **2017**, *38* (13), 981-997.
24. Ponec, R., Electron pairing and chemical bonds. Chemical structure, valences and structural similarities from the analysis of the Fermi holes. *Journal of Mathematical Chemistry* **1997**, *21* (3), 323-333.
  25. Ponec, R., Electron pairing and chemical bonds. Molecular structure from the analysis of pair densities and related quantities. *Journal of mathematical chemistry* **1998**, *23* (1-2), 85-103.
  26. Ponec, R.; Cooper, D. L., Anatomy of bond formation. Domain-averaged Fermi holes as a tool for the study of the nature of the chemical bonding in Li<sub>2</sub>, Li<sub>4</sub>, and F<sub>2</sub>. *The Journal of Physical Chemistry A* **2007**, *111* (44), 11294-11301.
  27. Kirtley, S. W., Chromium Compounds with η<sup>1</sup>-Carbon Ligands. **1982**.
  28. Mingos, D., Bonding of unsaturated organic molecules to transition metals. **1982**.
  29. Tyndall, G. W.; Jackson, R. L., Excimer laser multiphoton dissociation of Cr(CO)<sub>6</sub>: Evidence for two distinct dissociation processes. *The Journal of Chemical Physics* **1988**, *89* (3), 1364-1377.
  30. Pollak, C.; Rosa, A.; Baerends, E. J., Cr–CO Photodissociation in Cr(CO)<sub>6</sub> : Reassessment of the Role of Ligand-Field Excited States in the Photochemical Dissociation of Metal–Ligand Bonds. *Journal of the American Chemical Society* **1997**, *119* (31), 7324-7329.
  31. Barnes, L. A.; Liu, B.; Lindh, R., Structure and energetics of Cr(CO)<sub>6</sub> and Cr(CO)<sub>5</sub>. *The Journal of Chemical Physics* **1993**, *98* (5), 3978-3989.
  32. Jonas, V.; Thiel, W., Density Functional Study of the Vibrational Spectra of Octahedral Transition-Metal Hexacarbonyls: Neutral Molecules (M = Cr, Mo, W) and Isoelectronic Ions (M = V, Nb, Ta; Mn, Re; Fe, Ru, Os; Co, Rh, Ir; Pt; Au). *Organometallics* **1998**, *17* (3), 353-360.
  33. Tiwari, G., *Inorganic Chemistry-II (For M. Sc. Course for Universities in Uttarakhand)*. S. Chand Publishing.
  34. Johnson, J. B.; Klemperer, W. G., A molecular orbital analysis of electronic structure and bonding in chromium hexacarbonyl. *Journal of the American Chemical Society* **1977**, *99* (22), 7132-7137.
  35. Grubbs, R. H.; Wenzel, A. G.; O'Leary, D. J.; Khosravi, E., *Handbook of metathesis*. Wiley Online Library: 2015; Vol. 2.
  36. Fischer, E. O.; Maasböl, A., On the Existence of a Tungsten Carbonyl Carbene Complex. *Angewandte Chemie International Edition in English* **1964**, *3* (8), 580-581.
  37. Fischer, E. O.; Maasböl, A., Übergangsmetall-carben-komplexe: VII. Über die umlagerung von äthoxymethylcarben zu äthylvinyläther bei der reaktion von äthoxymethylcarben-pentacarbonyl-chrom (0) mit pyridin. *Journal of Organometallic Chemistry* **1968**, *12* (2), P15-P17.
  38. Herndon, J. W., Applications of carbene complexes toward organic synthesis. *Coordination Chemistry Reviews* **2000**, *206*, 237-262.
  39. Kikelj, D., Recent progress in diaryl ether synthesis. *Synthesis* **2006**, *2006* (14), 2271-2285.
  40. Landman, M.; Pretorius, R.; Fraser, R.; Buitendach, B. E.; Conradie, M. M.; van Rooyen, P. H.; Conradie, J., Electrochemical behaviour and structure of novel phosphine- and phosphite-substituted tungsten(0) Fischer carbene complexes. *Electrochimica Acta* **2014**, *130*, 104-118.

41. Jiang, W.; Fuertes, M. J.; Wulff, W. D., Electronic Tuning of Fischer Carbene Complexes in the Preparation of Bicyclo [3.1. 1] heptanones as Taxane A-ring Synthons. *Tetrahedron* **2000**, *56* (15), 2183-2194.
42. Poater, J.; Cases, M.; Fradera, X.; Duran, M.; Solà, M., Electron pairing analysis of the Fischer-type chromium–carbene complexes (CO)<sub>5</sub>Cr-C (X)(R), (X= H, OH, OCH<sub>3</sub>, NH<sub>2</sub>, NHCH<sub>3</sub> and R= H, CH<sub>3</sub>, CH-CH<sub>2</sub>, Ph, C-CH). *Chemical Physics* **2003**, *294* (2), 129-139.
43. Thompson, S.; Wessels, H. R.; Fraser, R.; van Rooyen, P. H.; Liles, D. C.; Landman, M., Computational and experimental structural studies of selected chromium(0) monocarbene complexes. *J. Mol. Struct.* **2014**, *1060*, 111-118.

## **Chapter 2.**

# **Theoretical Background and Developments**



## Introduction

Over the years molecular orbital (MO) theory (MOT) has proved to be extremely useful in characterizing the ground and excited states for small molecules.<sup>1,2</sup> In any molecular study, the principles governing the chemistry is aimed to be understood, the understanding stems from physical and chemical laws, from which MOT developed. While MOT is applicable to any molecular system, interpretation of MOs generally become more difficult with increasing size and complexity of a system. While precise application of group theory can assist in the complete classification of a molecular system's electronic structure in terms of MOs,<sup>3</sup> it generally requires two conditions to be satisfied: (i) the molecule must be small and (ii) the molecule must have a high degree of symmetry. Since the majority of molecules studied in applied chemical fields are often asymmetric, the latter condition is a major focal point of this work.

MOT goes hand in hand with group theory<sup>3</sup> however, its principles can be understood and taught without it (albeit in limited sets of molecular systems<sup>4</sup>). In addition, generation of canonical MOs can be performed using variational computational approaches, regardless of the degree of symmetry present in a molecular system. However, in-depth interpretation of computationally-generated MOs can still be extremely difficult without rigorous application and knowledge of group-theory. This work seeks to use the Fragment, Atomic Localized, Delocalized, Interatomic (FALDI) density decomposition scheme approach<sup>5, 6</sup> to elaborate on the interpretation of computationally-generated MOs – regardless of the degree of symmetry present. The FALDI approach allows a bridging of classical concepts that arise from the application of group theory to MOT – such as symmetry adapted linear combinations (SALCs)<sup>7</sup> of atomic orbitals – to the wide variety of MOs that can be generated using modern computational codes.

This chapter serves as a review of computationally-generated MOs (as produced by electronic structure methods), as well as topological techniques used to analyze the resultant density. In terms of computationally-generated MOs, there are essentially two approaches: the empirical considerations stemmed from Hückels'<sup>8</sup> work which was also extended on<sup>9</sup> and a mathematical formalism approach,<sup>10</sup> also known as the approximate self-consistent field (SCF) theory. The contents of this chapter will focus on the latter, including canonical MOs generated

by Hartree-Fock theory as well as Kohn-Sham orbitals generated by Density Functional Theory.

This chapter is organized in two sections: i) a review of electronic structure methods and subsequent generation of molecular orbitals, and ii) a review of the FALDI scheme and its use in interpreting MOs. The latter section contains all of the theoretical developments introduced in subsequent chapters.

## Canonical Molecular Orbitals

### Hartree-Fock Theory

Hartree-Fock (HF) theory<sup>11, 12</sup> is typically considered to be the cornerstone of computational chemistry, and one of the simplest ways to understand the electronic structure of a system. It has been made famous for its strategy for solving the Schrödinger equation for many-electron systems by reducing it to the approach of a set of single-electron problems. The primary approximation HF makes is to allow electrons within a nuclei field to experience other electrons and their effects in an averaged manner, which assumes paired electrons with the same spin contribution from up and down. Regardless, this allowed chemists to begin modelling and still provides an excellent basis for understanding electronic structures, specifically from teaching introductory courses to computational chemistry.

At the center of HF is the molecular electronic wavefunction,  $\Psi(x_1, x_2, \dots, x_N)$  where  $x_1, x_2, \dots, x_N$  are electronic (spatial and spin,  $x_i = r_i \omega_i$ ) coordinates.  $\Psi(x_1, x_2, \dots, x_N)$  must satisfy certain conditions for it to be valid: it must be single-valued, continuous as well as be differentiable at all points in spin and real-space. While  $\Psi(x_1, x_2, \dots, x_N)$  can be complex, its product with itself must be real. In the HF approximation, the wavefunction is composed of a set of 1-electron functions known as MOs, each dependent on a single spatial orbital and spin function:  $\Psi(x_1, x_2, \dots, x_N) \leftarrow \chi_1(x_1), \chi_2(x_2), \dots, \chi_N(x_N)$ , with  $\chi_i(x_i) = \sigma(\omega_i)\phi(r_i)$ .

The spin functions, as either  $\alpha(\omega_i)$  or  $\beta(\omega_i)$  are normalized to unity:

$$\langle \alpha | \alpha \rangle = \int \alpha(\omega_1) \alpha(\omega_2) d\omega_1 d\omega_2 = 1 \quad (1)$$

where the same applies to  $\langle\beta|\beta\rangle$ . However, different spin functions are orthogonal:

$$\langle\alpha|\beta\rangle = \int \alpha(\omega_1)\beta(\omega_2)d\omega_1d\omega_2 = 0 \quad (2)$$

leading to the orthonormality condition of spin functions, and by extension, MOs:

$$\langle\chi_i|\chi_j\rangle = \int \chi_i(x_1)\chi_j(x_2)dx_1dx_2 = \delta_{i,j} \quad (3)$$

where  $\delta_{i,j}$  is the Kronecker delta expressed as:

$$\delta_{i,j} = \begin{cases} 1 & \text{for } i = j \\ 0 & \text{for } i \neq j \end{cases} \quad (4)$$

with the integral Eq. (4) equalling zero for  $i \neq j$  and one for  $i = j$ . For computational convenience the spatial orbitals are often also set to be orthonormal, therefore:

$$\langle\phi_i|\phi_j\rangle = \int \phi_i(r_1)\phi_j(r_2) dr_1dr_2 = \delta_{i,j} \quad (5)$$

### ***Hartree Product wavefunction***

The discussion in the previous section has touched on the central HF approximation, but not on how an electronic wavefunction is constructed from MOs. One such way is a Hartree Product. The Hartree Product is an eigenfunction of the Schrödinger equation ( $\hat{H}\Psi = E\Psi$ ) for independent electrons and is represented by the product of spin orbitals:

$$\Psi_{HP} = \chi_1(x_1)\chi_2(x_2) \dots \chi_N(x_N) \quad (6)$$

Introducing the one-electron Hamiltonian operator:

$$\hat{H} = \sum_i^N \hat{h}_i = \sum_i^N \left( -\frac{1}{2}\nabla_i^2 - \sum_k^M \frac{Z_k}{r_{ik}} \right) \quad (7)$$

which contains kinetic energy and nuclear-electron attraction. Since the one-electron Hamiltonian operator acts on each spin orbital this applies to the one-electron Schrödinger equation where there is a spin orbital eigenfunction and energy eigenvalue:

$$\hat{h}_i\chi_i = \varepsilon_i\chi_i \quad (8)$$

Therefore, the one-electron Hamiltonian operator can act on the molecular orbital,  $\chi_i$ , to give the orbital energy,  $\varepsilon_i$ . When a Hartree Product is substituted into the many-electron Schrödinger equation,

$$\begin{aligned}
\hat{H} \Psi_{HP} &= \hat{H} \chi_1 \chi_2 \dots \chi_N \\
&= \sum_i^N \hat{h} \chi_1 \chi_2 \dots \chi_N \\
&= \left( \sum_i^N \varepsilon_i \right) \Psi_{HP}
\end{aligned} \tag{9}$$

the molecular energy,  $E$ , is obtained as a sum of orbital energies.

### *Electron-electron repulsion*

Since the one-electron Hamiltonian operator,  $\hat{h}$ , only acts on one electron, it cannot account for electron repulsion ( $V_{ee}$ ) which is dependent on the spin-spatial coordinates of two electrons. This is where the one-electron Fock operator comes into play:

$$\hat{f}_i = -\frac{1}{2} \nabla_i^2 - \sum_k^M \frac{Z_k}{r_{ik}} + V_{HF}(i) \tag{10}$$

with the last term accounting for the Hartree Fock potential,  $V_{HF}(i)$ :

$$V_{HF}(i) = \sum_{j \neq i}^N \int \frac{p_j(r)}{r_{ij}} dr \tag{11}$$

and  $p_j(r) = |\chi_j(r)|^2$ . The function considers repulsion of  $i$  to all other electrons  $j$  and because the electrons are treated like waves, it can be integrated over all space to obtain the average electron-electron repulsion. Through the use of  $V_{HF}$ , the independent electron approximation of HF theory can be mitigated by treating electron repulsion in an average (as opposed to dynamic) manner.

Since the spin orbitals are needed to determine the wavefunction, yet are used in Eqs. 10 and 11 to determine the structure of the wavefunction itself, the process has to be performed iteratively. This process of iteratively solving the wavefunction is known as the *Self-Consistent Field* (SCF) procedure. The process starts with MO coefficients that provide densities and the wavefunction. Molecular orbital energy is then solved for by the secular determinant (shorthand for the Hamiltonian integrals which is overlap integrals) to find the roots of the energy and then these energies are used to get new MO coefficients to repeat the process until the coefficients and energies start remaining constant and hence are known to converge.

### *The antisymmetry of the wavefunction*

Since electrons have spin they have been labelled as fermions with a spin of  $\frac{1}{2}(\alpha)$  or  $-\frac{1}{2}(\beta)$ . The concept of spin is a purely quantum construct with no counterpart in classical physics. The effect of spin can be accounted for by ensuring that the wavefunction is antisymmetric:

$$\psi(x_1, x_2 \dots x_i, x_j \dots x_N) = -\psi(x_1, x_2 \dots x_j, x_i \dots x_N) \quad (12)$$

where  $x_i, x_j$  represent coordinates that can be interchanged and by this fact, any electrons that are swapped will inverse the sign in front of the wavefunction. The Eq. 12 leads to the Pauli Exclusion Principle, for which no two electrons may have the same principal quantum numbers. Thus, as a result, only opposite spin electrons may occupy a single orbital.

### *Slater determinants*

Unfortunately, the Hartree Product wavefunction (Eq. 6) is not antisymmetric since swapping any two electrons does not change the wavefunction sign and therefore cannot be used as a quantum mechanics tool. The Hartree Product functions on electrons being indistinguishable. A modification to the wavefunction which resolves these issues is the introduction of the Slater Determinant, which will result in the wavefunction always being antisymmetric:

$$\Psi_{SD} = \frac{1}{\sqrt{N!}} \begin{vmatrix} \chi_1(x_1) & \dots & \chi_N(x_1) \\ \vdots & \ddots & \vdots \\ \chi_1(x_N) & \dots & \chi_N(x_N) \end{vmatrix} \quad (13)$$

since swapping any two rows or columns of the determinant will change the sign. Satisfying the anti-symmetry requirements. Expanding the Slater determinant for a two-electron wavefunction yields:

$$\Psi_{SD} = \frac{1}{\sqrt{2}} [\phi_a(r_1)\alpha(\omega_1)\phi_b(r_2)\beta(\omega_2) - \phi_a(r_2)\alpha(\omega_2)\phi_b(r_1)\beta(\omega_1)] \quad (14)$$

which clearly illustrates that swapping two electrons will yield  $-\Psi_{SD}$ .

Applying the electron-electron repulsion operator ( $\widehat{V}_{ee}$ ) to the Slater determinant yields two integrals. These terms are the Coulomb integral,  $J_{ab}$ , and the Exchange integral,  $K_{ab}$ . The

Coulomb integral represents classic electrostatic repulsions, whereas the exchange term (which will always be negative in the HF approximation) reduces the total electrostatic repulsion due to the antisymmetry of the wavefunction.

### *The Roothaan equations*

The spin-spatial MOs ( $\chi_j$ ) worked with thus far can be linearly expanded into a set of basis functions,  $\varphi_i$ :

$$\chi_j = \sum_{i=1}^N a_{ij} \varphi_i \quad (15)$$

Eq. 15 can be used, together with a Slater determinant and the one-electron Fock operator (Eq. 10) to iteratively solve the Schrödinger equation through the secular determinant:

$$\begin{vmatrix} F_{11} - ES_{11} & \cdots & F_{1N} - ES_{1N} \\ \vdots & \ddots & \vdots \\ F_{N1} - ES_{N1} & \cdots & F_{NN} - ES_{NN} \end{vmatrix} = 0 \quad (16)$$

where  $F_{ij}$  are Fock matrix elements and  $S_{ij}$  are overlap integrals between the  $i$ th and  $j$ th basis functions. The Fock matrix elements are given by:

$$F_{\mu\nu} = \langle \mu | -\frac{1}{2} \nabla^2 | \nu \rangle - \sum_k^M Z_k \langle \mu | \frac{1}{r_k} | \nu \rangle + \sum_{\lambda\sigma} P_{\lambda\sigma} \left[ (\mu\nu | \lambda\sigma) - \frac{1}{2} (\mu\nu | \nu\sigma) \right] \quad (17)$$

where, for readability, lowercase Greek letters ( $\sigma, \lambda, \mu, \nu$ ) are used as indices for basis functions and lowercase Roman letters ( $i, j, k$ ) are used for MOs. The first two terms of Eq. 17 are related to 1-electron operators (kinetic energy and electron-nuclear attraction), where the last term is related to the Hartree-Fock potential. Describing elements of the Roothaan equations which are simply put HF equations in the AO basis. The whole term is weighted by the density matrix,  $P_{\lambda\sigma}$ , which considers all the molecular orbital coefficients:

$$P_{\lambda\sigma} = 2 \sum_i^{\text{occupied}} a_{\mu i} a_{\nu i} \quad (18)$$

and these elements have  $i$  running over all the occupied molecular orbitals. The contribution that each basis function makes to the density is determined by the diagonal elements of the density matrix, indicating either constructive or destructive density interactions. Summing the entire density matrix, therefore, gives the total number of electrons in the system.

In summary, the Hartree Fock procedure starts with selecting a basis set, followed by guessing a density matrix  $\mathbf{P}$ . Then the  $\mathbf{F}$  and  $\mathbf{S}$  elements of the matrix are calculated which

allows for the secular equation to be solved resulting in MO energy values and the molecular energy value. In turn, new MO coefficients are available which are used for a new density matrix  $\mathbf{P}'$  and the secular equation gets solved iteratively using the new  $\mathbf{P}'$  until convergence is reached.

The Achilles heel of HF theory is the fact that while same spin electrons are allowed to move in a correlated fashion (due to the antisymmetry of the wavefunction), opposite spin electrons are entirely uncorrelated. HF theory therefore accounts for *Fermi correlation*, but not *Coulomb correlation*. For the latter, either perturbative methods (such as Moller-Plesset perturbation theory) or multiple Slater determinants can be employed to approximate general electron-electron dynamics. However, these corrections fall outside of the scope of this chapter.

## Basis sets

Commonly basis sets are used to describe *ab initio* calculations that solve the Schrödinger equation without focusing on fitting experimental data parameters.<sup>13, 14</sup> While any set of real-space functions can be used as a basis set, functions resembling Atomic Orbitals (AO) are often computationally efficient. Typical basis functions that are used in modern computational codes are Slater-Type Orbitals (STOs) and Gaussian-Type Orbitals (GTOs). STOs better resemble AOs, but are more expensive to compute than GTOs.<sup>14</sup> However, multiple GTOs can be combined (“contracted”) in order to resemble a single AO, in multiple different strategies, often indicated using specific notations.

Small basis sets, such as 3-21G, provide accurate results only for very simple systems. The basis set can, however, be expanded by the introduction of various additional basis functions, including polarization and diffuse functions. Polarization functions typically introduces a set of  $p$  functions to each set of  $s$  functions,  $d$  functions to each set of  $p$  functions,  $f$  functions for each  $d$  function, etc. The added higher angular momentum functions permit the electron distribution to be *polarized* in various directions, depending on the weight (coefficients) of each added polarizing set. Usually, polarization functions are indicated through the use of stars (\*) or as added bracketed letters, e.g. 3-21G( $d,p$ ), note this is the People-style. Diffuse functions, on the other hand, are normally used to simulate the behaviour of “expanded” electron clouds for molecules, like anions, electronically excited species, or even

heavier heteroatoms. Finally, the number of basis functions describing each electron can be increased for (generally) increased accuracy, usually referred to as ‘zeta’. For instance, 3-21G is a split-valence basis set – 3 contracted GTOs describe each core electron (single zeta), whereas two sets of basis functions describe each valence electron (double zeta).

Whilst the number of basis functions generally increase the accuracy of a quantum chemical calculation to a limit (HF limit for single determinant methods) dependent on the system size and theory used, it does so at a scaling at  $N^4$  increasing computational cost. For heavier atoms – such as transition metals used in this work – the sheer number of electrons can result in very long calculation times even with small basis sets. However, core electrons of heavier atoms can be excluded from the basis set and rather modelled as static potentials, which are known as effective core potentials (ECPs), thereby reducing computational times at a negligible reduction in accuracy.

This work used the Ahlrichs<sup>14</sup> (also known as Karlsruhe basis sets) def2-sv(p) as the basis set of choice (the keyword in *Gaussian 09*<sup>15</sup> is, curiously, “def2svp”). This basis set is *Split Valence Polarized* (SVP) which is a [3s2p] contraction of a (7s4p) set of primitive functions. The “p” is used to indicate polarization functions and is for the diffuse orbitals. Essentially what this translates to is that all atoms in the def2-svp basis set have polarization functions on all electrons, def2-sv does not have these additional functions, while def2-sv(p) does not have polarization functions on the hydrogen atoms since hydrogen atoms have low polarizability. For our systems this makes sense but a large organic molecule with many hydrogens this basis set is not a good choice. Polarization functions have become almost essential for DFT calculations to be considered accurate. The diffuse functions (which is why def2-sv(p) was chosen even though the name does not imply this) are necessary for looking at weaker interactions like hydrogen bonds which is why they are included in this study as X and R groups interacting on a Fischer carbene are later investigated. Both HF and DFT have used the Karlsruhe basis sets extensively and work well since they are available for much of the periodic table but are also computationally rather efficient.



## Molecular Orbital Theory

The electronic structure in *ab initio* models, at their core, is determined from Hartree-Fock theory. Then stemmed MOT describing an electrons motion as an orbital<sup>16</sup> which can be described by a wavefunction. The wavefunction for an atom with a single electron (*i.e.* the hydrogenic atom) can, however, be solved analytically, and provides a platform for understanding and interpreting MOs from which more complexes systems (multi-electron) can now be modelled.

### Atomic orbitals

Molecular orbitals are commonly approximated by the linear combination of atomic orbitals (LCAO) also known as symmetry-adapted linear combinations (SALCs):

$$\chi_n = \sum_i c_{ni} \phi_i = c_{n1} \phi_1 + c_{n2} \phi_2 + \dots \quad (19)$$

where  $\phi$  are the valence AOs of each atom in a molecule and  $c$  the weighting coefficient of the contribution of each AO to the MO. The coefficients will be nonzero if a specific AO interacts with other AOs to form an MO, and are subject to certain qualitative conditions. Firstly, the AOs must have a similar energy, second, they must have the same symmetry and thirdly must have spatial overlap. To describe the atomic orbitals of the electrons, the spherically symmetric field needs to be considered and is best approached using the polar-coordinates. To have a convenient analytical form of the AO for each type of atom, the one-electron Schrödinger solution equation can be written as:<sup>17</sup>

$$\phi(r, \theta, \phi) = R_{nl}(r)Y_{lm}(\theta, \phi) \quad (20)$$

with radius  $r$  and two angles  $\theta, \phi$ .  $Y_{lm}(\theta, \phi)$  describes the spherical harmonics, which depend on the angular-momentum quantum numbers  $m$  and  $l$ . The quantum number  $m$  ranges from  $-l$  to  $+l$ ; this is the *magnetic* quantum number which determines the orbital angular-momentum vectors' orientation. The *azimuthal* quantum number  $l$  is the total orbital angular momentum. Finally,  $R_{nl}(r)$  is the radial part of the atomic function, which accounts for the radial distance  $r$  multiplied by a decaying exponential called the orbital exponent which includes nuclear charge and principal quantum number. It is also common to see the equation in the simplified form:

$$\phi(r, \theta, \phi) = R(r)Y(\theta, \phi) \quad (21)$$

where  $R(r)$  only depends on the electron distance from the nucleus and the angular information for the wavefunction is described in  $Y(\theta, \phi)$ <sup>18</sup>.

---

**Table 2. 1.** Angular variables without the radial component  $r, \theta$  and  $\phi$  related to the real angular parts of s, p and d atomic orbitals

---

s functions	$l = 0$	$s: \left(\frac{1}{4\pi}\right)^{\frac{1}{2}}$
p functions	$l = 1$	$p_x: \left(\frac{3}{4\pi}\right)^{\frac{1}{2}} \cos \theta$
		$p_y: \left(\frac{3}{4\pi}\right)^{\frac{1}{2}} \sin \theta \cos \phi$
		$p_z: \left(\frac{3}{4\pi}\right)^{\frac{1}{2}} \sin \theta \sin \phi$
d functions	$l = 2$	$d_{z^2}: \left(\frac{5}{16\pi}\right)^{\frac{1}{2}} (3 \cos^2 \theta - 1)$
		$d_{xz}: \left(\frac{15}{4\pi}\right)^{\frac{1}{2}} \sin \theta \cos \theta \cos \phi$
		$d_{yz}: \left(\frac{15}{4\pi}\right)^{\frac{1}{2}} \sin \theta \cos \theta \sin \phi$
		$d_{x^2-y^2}: \left(\frac{15}{8\pi}\right)^{\frac{1}{2}} \sin^2 \theta \cos 2\phi$
		$d_{xy}: \left(\frac{15}{8\pi}\right)^{\frac{1}{2}} \sin^2 \theta \sin 2\phi$

---

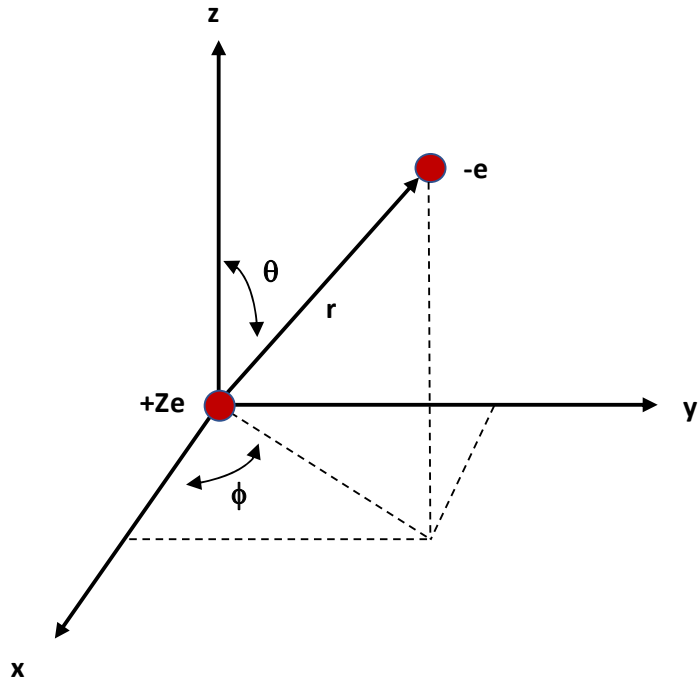


**Figure 2. 1.** Cartesian layout for spherical polar coordinates

The cartesian layout (**Figure 2.1**) for the spherical polar coordinates are describe by:

$$x = r \sin \theta \cos \phi \quad (22)$$

$$y = r \sin \theta \sin \phi$$

$$z = r \cos \theta$$

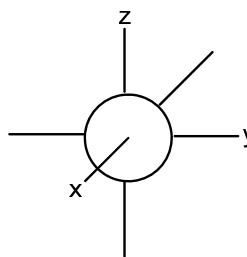
with  $d\tau = dx dy dz$  containing the coordinates translates as:

$$d\tau = r^2 dr \sin \theta d\theta d\phi \quad (23)$$

The atomic orbitals are labeled according to their azimuthal quantum number  $l$ ;  $s$ ,  $p$ ,  $d$  when  $l = 0, 1, 2$ , respectively. Visually these atomic orbitals are well recognised and can be seen in **Figure 2.2** described by the coordinate system of Eq. (22).

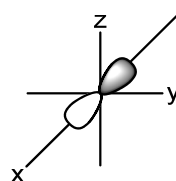
s functions  $l = 0$

s

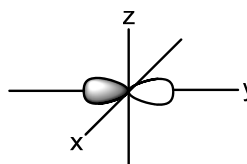


p functions  $l = 1$

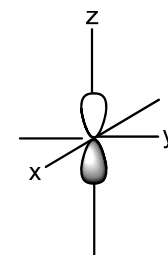
$p_x$



$p_y$

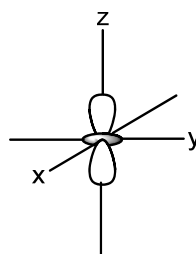


$p_z$

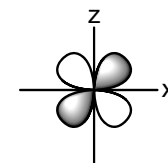


d functions  $l = 2$

$d_{z^2}$



$d_{zx}$



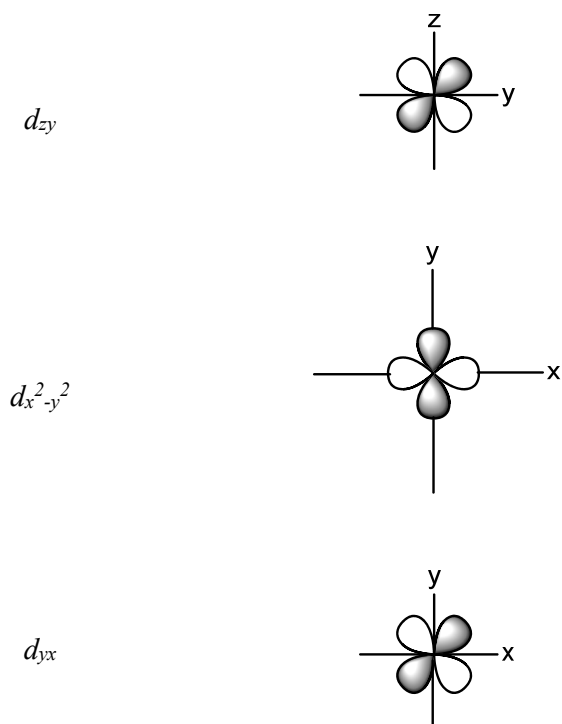


**Figure 2. 2.** A graphic representation of the spherical coordinates of the atomic orbitals.

This  $R_{nl}(r)$  function is often known as the STOs, which is its most popular analytical form for high accuracy atomic or diatomic systems, but not the default of most computational software. This popular function of choice, which is easier to compute, that is normally considered is the GTOs which is similar to the STOs however, the decaying exponential depends on  $r^2$  and not just  $r$ . Therefore, the integration is much easier with the gaussian functions, and for this reason, they are normally used in the polyatomic molecules molecular orbital calculations as already mentioned. Another, yet uncommon function option is the lobe-function which combines spherical and elliptical functions to produce the conventional orbital shapes but this will not be discussed.

### ***Molecular Orbitals***

Molecular orbitals simply approximate the electronic structure of a molecule by considering the wavefunction delocalized across all atoms, which when combined in various sequences of combinations produces the molecular orbitals.<sup>1</sup> These molecular orbitals are used as good approximates of the molecular Schrödinger equation.<sup>19</sup> As already stated, the molecular orbitals in a molecule are usually approximated with LCAO/SALCs, written slightly different as:

$$\psi_i = c_{1i}\chi_1 + c_{2i}\chi_2 + \dots + c_{mi}\chi_m = \sum_{\mu} c_{\mu i}\chi_{\mu} \quad (24)$$

with  $i=1,2,3,\dots,m$  where the sum of the Eq. (24) runs over all the atoms.

The energy of the orbital  $\psi_i$  is specified by the nature of the molecular orbital coefficients ( $c_{\mu i}$ ) the energy is obtained by solving for the eigenvalue using the effective one-electron Hamiltonian associated with the molecular orbital:

$$H^{eff} \psi_i = e_i \psi_i \quad (25)$$

The expectation value of  $H^{eff}$  is the molecular orbital energy which is:

$$e_i = \frac{\int \psi_i H^{eff} \psi_i d\tau}{\int \psi_i^2 d\tau} = \frac{\langle \psi_i | H^{eff} | \psi_i \rangle}{\langle \psi_i | \psi_i \rangle} \quad (26)$$

$$e_i = \langle \psi_i | H^{eff} | \psi_i \rangle$$

If the overlap integral  $S_{\mu\nu}$  describes two atomic orbitals centred on a different atom  $\chi_{\mu}$  and  $\chi_{\nu}$  then:

$$S_{\mu\nu} = \langle \chi_{\mu} | \chi_{\nu} \rangle \quad (27)$$

and when two orbitals have the same sign for the internuclear region there is positive overlap and negative when the signs are opposite for the lobes of the orbital.

$$S_{\mu\nu} = \langle -\chi_{\mu} | -\chi_{\nu} \rangle = \langle \chi_{\mu} | \chi_{\nu} \rangle \quad (28)$$

and

$$-S_{\mu\nu} = \langle -\chi_{\mu} | \chi_{\nu} \rangle = \langle \chi_{\mu} | -\chi_{\nu} \rangle \quad (29)$$

The interaction between orbitals is determined by the extent of this overlap. More intricately the symmetry also plays a role whether this overlap can occur or not, labelled as sigma ( $\sigma$ ) pi ( $\pi$ ) and delta ( $\delta$ ) the orbital overlap integral varies, generally but not always in the order of  $\sigma > \pi > \delta$ . Whether an orbital can overlap with another is due to the angular dependence of the overlap integral (symmetry). The overlap integral can be written as:

$$S_{\mu\nu} = S_{\mu\nu}(\lambda, \tau) f(\text{angular geometry}) \quad (30)$$

The orbital overlap is very sensitive to the internuclear distance between two atoms. This angular geometry dependent term is only dependent on the orbital description (*s*, *p* or *d*) which is dependent on the identity of the atom.<sup>20</sup> For MOs to be formed, the AOs need to fit mathematical conditions for them to combine. Firstly, the orbitals must be in proximity to interact, since the degree to which they combine is inversely proportional to the distance between the atoms. Second, there must be mutual symmetry along an axis, the cosine angle between orbitals is directly proportional to the orbital combination magnitude. Finally, orbitals need to be of similar size and energy, then there can be an orbital combination to produce MOs.

### Summary of the Orbital model

For identical *fermions*, the wavefunction needs to be antisymmetric regarding the exchange of spin-spatial coordinates,<sup>21</sup> since the same spin-spatial coordinate cannot be occupied by two electrons at the same time. Electrons with the same spin coordinate, therefore, avoid each other based on the exchange (Fermi) hole since the wavefunction is continuous – a display of the Pauli Exclusion Principle. When electrons have opposite spin the exchange hole is zero throughout all molecular space as the Pauli Exclusion Principle does not apply. Regardless, due to Coulombic forces, electrons' charge will cause repulsion at any finite distance, and a Coulomb hole will form in order to minimize electrostatic repulsion. However, it has been established that the Fermi hole generally plays a larger determining role in chemical bonding than the Coulomb hole.<sup>22</sup> For a wavefunction that accurately models reality, both the Coulomb and Fermi holes will be reflected.

Hartree-Fock theory fails to capture any details regarding the Coulomb hole (i.e. electrons are uncorrelated due to their charge and irrespective of spin), but models the Fermi hole exactly due to the requirement that the wavefunction be antisymmetric. As a result, the Pauli Exclusion Principle is fully met in Hartree-Fock theory, and consequently spin-orbitals are limited to occupations of two electrons. Spin-orbitals will therefore have known integer occupations. In addition, as long as the Koopmans theorem is kept (all orbitals remain the same when removing an electron<sup>23</sup>) then the energy needed to remove an electron (ionization) in an orbital is the orbital energy.

If the excitation of electrons is considered it is identified as a state with a change in electron occupancy relative to the ground state. Linear mixing of excited and ground states leads to an overall lowering of total molecular electronic energy and is a method for incorporating Coulomb correlation.

The orbital diagram can be conceptually linked to molecular perturbations. For instance, the start of the final molecular diagram describes a chemical reaction. This is where chemical reactions<sup>24, 25</sup> and optical excitations<sup>26</sup> became dependent on symmetry selection rules.

## Density Functional Theory

Density Functional Theory (DFT) follows a very similar conceptual core to Hartree-Fock. While Hartree-Fock theory accounts for Fermi correlation exactly but entirely disregards Coulomb correlation, DFT allows for an approximation of both. Accordingly, many DFT models allow for more accurate electronic structure calculations than Hartree-Fock theory, and often with improved computational times as well. However, unlike Hartree-Fock theory, DFT is not an *ab initio* approach, and care must be taken in the generalized application of DFT results.

Essentially the DFT electronic ground state structure is based on the electron density,  $\rho(r)$ , distribution.<sup>21</sup> The theory was developed relatively early on in the 20<sup>th</sup> century, but only started becoming popular in the 1990s due to better implementations<sup>27</sup> and the development of gradient-corrected functionals.<sup>28</sup> The first effort to define electronic structure based primarily on  $\rho(r)$  was performed by calculating the energy without reference to a wavefunction by the Thomas-Fermi equations, and assumed variational principle applies.<sup>29</sup> The improved scalability of DFT versus the wavefunction based approaches made it popular in the solid-state physics community where modelling massive periodic systems is common; however, early DFT models observed large errors in molecular calculations which did not make it particularly viable in chemistry.<sup>29</sup> However, in 1964 Hohenberg and Kohn proved two crucial theorems: the ***Existence Theorem*** and the ***Variational Theorem***. The density and ground state energy could be determined exactly by a unique functional and they demonstrated the independence of the functional to any particular system, that exact energy is a functional of density  $E(\rho)$  and the minimum energy is at the exact density.<sup>30</sup>



### *The Existence Theorem of Hohenberg-Kohn*

In DFT, electrons are allowed to interact with each other as well as with an ‘external potential’. This external potential is a positive charge uniformly distributed in the uniform electron gas concept that is attracted to the nuclei. The ground-state density is used to determine the Hamiltonian operator from density and the number of electrons can be calculated from the integration of density. Therefore, to fully define the operator only the determination of the external potential is needed. The variational theorem states that the expectation value of  $a$  over  $b$ ’s wavefunction as the expectation value must be higher than  $a$ ’s ground state energy.

$$E_{0,a} < \langle \psi_{0,b} | H_a | \psi_{0,b} \rangle \quad (31)$$

Assume that there are two different external potentials,  $v_a$  and  $v_b$ , both which are non-degenerate with ground-state density  $\rho_0$  and with Hamiltonian operators  $H_a$  and  $H_b$ . The individual Hamiltonian operators can be combined linearly to form the ground state Hamiltonian operator  $H_0$ , associated with the ground-state wavefunction,  $\psi_0$ , and its eigenvalue  $E_0$ . Then Eq. 31 can be written as:

$$E_{0,a} < \langle \psi_{0,b} | H_a + H_b - H_b | \psi_{0,b} \rangle \quad (32)$$

Simplifying Eq 32,

$$\begin{aligned} E_{0,a} &< \langle \psi_{0,b} | H_b | \psi_{0,b} \rangle + \langle \psi_{0,b} | H_a - H_b | \psi_{0,b} \rangle \\ E_{0,a} &< E_{0,b} + \langle \psi_{0,b} | v_a - v_b | \psi_{0,b} \rangle \end{aligned} \quad (33)$$

and combining with ground-state density because of the one-electron operators,  $v$ :

$$E_{0,a} < \int [v_a(\mathbf{r}) - v_b(\mathbf{r})] \rho_0(\mathbf{r}) d\mathbf{r} + E_{0,b} \quad (34)$$

Just as simply  $a$  and  $b$  can be interchanged for each other as no distinctions have been made for them. Thus, adding both options (after interchanging) the result is:

$$E_{0,a} + E_{0,b} < \int [v_a(\mathbf{r}) - v_b(\mathbf{r})] \rho_0(\mathbf{r}) d\mathbf{r} + E_{0,b} + \int [v_b(\mathbf{r}) - v_a(\mathbf{r})] \rho_0(\mathbf{r}) d\mathbf{r} + E_{0,a} \quad (35)$$

Simplifying the equation leaves:

$$E_{0,a} + E_{0,b} < E_{0,a} + E_{0,b} \quad (36)$$

However, the summation of two energies cannot be less than itself otherwise there is an impossibility so the assumption was incorrect, and the external potential must be exactly determined by the non-degenerate ground-state density and the Hamiltonian and ultimately the

wavefunction. However, the Hamiltonian also applies to the excited state and therefore density is condensed with many scientific insights embedded in it.

### ***The Variational Theorem of Hohenberg-Kohn***

In their second theorem, Hohenberg and Kohn showed that a density-based approach, like MOT, follows the variational principle.<sup>22</sup> To postulate: for several electrons,  $N$ , the existence theorem says the density determines a Hamiltonian and candidate wavefunction which then allows expectation energy to be analyzed:

$$\langle \psi_{candidate} | H_{candidate} | \psi_{candidate} \rangle = E_{candidate} \geq E_0 \quad (37)$$

Hence, the densities are varied to lower the energy. The challenge, however, lies in the selection of the candidate densities chosen to lower the energies. This is because of the unknown nature of the functional, as a result, nothing has been suggested in terms of a generic characteristic for the variational equation.

### ***The Ground State Origin***

The variation principle allows for the determination of a minimized energy associated with normalized electronic wavefunctions,  $\psi$ , with  $\hat{T}$  and  $\hat{V}$  being the kinetic and potential energy operators respectively:

$$E(\psi) = \int d\tau \psi \hat{H} \psi = \int d\tau \psi \hat{T} \psi + \int d\tau \psi \hat{V} \psi = T(\psi) + V(\psi) \quad (38)$$

The ground state,  $\psi_g$ , is obtained when the lowest value for  $E$  is reached. Minimizing  $T(\psi) + V(\psi)$  therefore determines the shape of  $\psi_g$ .

Contracting  $\psi$  closer to the nuclei intuitively lowers the negative potential energy integral  $V$ . The kinetic energy integral  $T$  can be written as:

$$T = \int d\tau \psi \hat{T} \psi = -\frac{1}{2} \sum_k \int d\tau \psi (\nabla_k)^2 \psi = +\frac{1}{2} \sum_k \int d\tau (\nabla_k \psi)^2 \quad (39)$$

with all electrons  $k$  being considered in the sum  $\sum_k$  (the kinetic energy can be written in atomic units). Expressing  $\psi$  as natural orbitals  $\psi_n$  with fractional occupation numbers  $N_n$  allows Eq. 39 to be rewritten as:

$$T = -\frac{1}{2} \sum_n N_n \int d\tau (\psi \nabla^2 \psi_n) = \frac{1}{2} \sum_n N_n \int d\tau (\nabla \psi_n)^2 \quad (40)$$

Subsequent analyses and derivations are unbiased as to the gradient form of  $T$  or the Laplacian being used since the interferences only involve the invariant integrated expectation values. However, due to didactic reasons, the gradient form is preferred for appearing as positive kinetic energy in the formulas. The gradient expression in Eq. 40 relates kinetic energy integrals to properties of the wavefunction because each electron  $k$  positively contributes to each volume element,  $d\tau$ . Therefore, each volume element has a positive contribution from every orbital. The gradient form, following the fundamental kinetic energy property, can be deduced. If  $\psi$  represents a single electron wavefunction, then the kinetic energy is simply and uniquely,

$$T = \frac{1}{2} \int d\tau (\nabla \psi)^2 = \frac{1}{2} \int dx \int dy \int dz \left[ \left(\frac{d\psi}{dx}\right)^2 + \left(\frac{d\psi}{dy}\right)^2 + \left(\frac{d\psi}{dz}\right)^2 \right] \quad (41)$$

Evident from this expression is that contracting the space of  $\psi$  will increase  $T$  due to an increase in curvature. So,  $T$  can be increased by localizing  $\psi$ , which will *increase* the molecular energy  $E$ . Electrons, therefore, have tendencies to delocalize due to the nature of the variation principle.

From the statements discussed above regarding  $V$  and  $T$ , it is evident that the wavefunction is required to meet opposing demands in lowering both potential and kinetic energy in order to minimize the total energy. Concentrating the wavefunction on the nuclear centers would minimize potential energy while dispersing the wavefunction would minimize kinetic energy. Thus, compromising between potential and kinetic energy will allow the minimum energy wavefunction  $\psi_g$  to be achieved, through variational competition of the delocalization dilution pressure from the kinetic energy and contraction to localize electrons to the nuclei for the electrostatic potential energy. Summarizing this variational process, the wavefunction of the ground state is determined by how close the nuclei can electrostatically attract electrons based on the resistance received from the kinetic energy. A caveat, however, is that the wavefunction must be antisymmetric when many electrons are considered to account for electron exchange, introducing new restriction parameters. The exclusion principle forces localized electrons to avoid sharing the same space.<sup>31</sup>

### ***Self-consistent Field of Kohn-Sham***

An investigation into the *process* of a DFT calculation starts by examining the Hamiltonian of the non-interacting reference density.<sup>32</sup> This Hamiltonian is, in principle, a set of one-electron operators acting on non-interacting electrons and results in one-electron eigenvalues. Accordingly, a set of one-electron eigenfunctions can be defined and, by analogy to HF theory, is called Kohn-Sham orbitals. This concept of a non-interacting reference system structured from the cornerstone of one-electron functions provides decent accuracy for kinetic energy calculations.<sup>28</sup> Additionally, non-classical contributions are considered to include the unknown contribution electron-electron repulsion due to electron exchange and missing electron correlation. This allows for a great approximate functional that only excludes a small part of the total energy. It is then vital for the initial point of the fictitious (*i.e.* imaginary) system of non-interacting electrons to have the same DFT density as a real system which contains interacting electrons (*i.e.* overall ground state-density). This is then followed by dissecting the energy functional into specific components:

$$E[\rho(\mathbf{r})] = \Delta T[\rho(\mathbf{r})] + \Delta V_{ee}[\rho(\mathbf{r})] + T_{ni}[\rho(\mathbf{r})] + V_{ne}[\rho(\mathbf{r})] + V_{ee}[\rho(\mathbf{r})] \quad (42)$$

These components are the kinetic energy correction based on interacting electrons, the electron-electron repulsion energy correction (all non-classical), kinetic energy of the non-interacting, nuclear-electron interaction and electron-electron repulsion (classical). Since the system has non-interacting electrons the individual kinetic energies give the total kinetic energy. Considering the orbital expression for density the, Eq. (42) can be rewritten as:

$$E[\rho(\mathbf{r})] = \sum_i^N \left( \langle \chi_i | -\frac{1}{2} \nabla_i^2 | \chi_i \rangle - \langle \chi_i | \sum_k^{\text{nuclei}} \frac{Z_k}{|\mathbf{r}_i - \mathbf{r}_k|} | \chi_i \rangle \right) + \sum_i^N \langle \chi_i | \frac{1}{2} \int \frac{p(\mathbf{r}')}{|\mathbf{r}_i - \mathbf{r}'|} d\mathbf{r}' | \chi_i \rangle + E_{xc}[p(\mathbf{r})] \quad (43)$$

with  $N$  the number of the electrons and since the density comes from the precise eigenfunction describing the non-interacting system (Slater-determinantal wavefunction) producing:

$$\rho = \sum_{i=1}^N \langle \chi_i | \chi_i \rangle \quad (44)$$

The  $E_{xc}$  term describes the exchange-correlation energy which encapsulates the  $\Delta T$  and  $\Delta V_{ee}$  terms. Included in this term are electron correlation and the difference in kinetic energy of the real system and the non-interacting fictitious system.

Introducing a classical orbital,  $\chi$ , approach into the Kohn-Sham (KS) methodology, eigenvalues can be obtained when minimizing the energy  $E$ :

$$h_i^{KS} \chi_i = \varepsilon_i \chi_i \quad (45)$$

A new term is then needed,  $V_{xc}$ , which is the functional derivative that describes the one-electron operator giving the expectation value for  $E_{xc}$

$$V_{xc} = \frac{\delta E_{xc}}{\delta \rho} \quad (46)$$

Then including this term in the KS one-electron operator:

$$h_i^{KS} = V_{xc} + \int \frac{p(\mathbf{r}')}{|\mathbf{r}_i - \mathbf{r}'|} d\mathbf{r}' - \frac{1}{2} \nabla_i^2 - \sum_k^{nuclei} \frac{Z_k}{|\mathbf{r}_i - \mathbf{r}_k|} \quad (47)$$

the exact  $E$  is being minimized and the exact density must be given because of the orbitals,  $\chi$ . Additionally, the sum of the Kohn-Sham operators (Slater-determinantal eigenfunction for the non-interacting Hamiltonian ) are form these orbitals:

$$\sum_{i=1}^N h_i^{KS} |\chi_1 \chi_2 \chi_3 \cdots \chi_N\rangle = \sum_{i=1}^N \varepsilon_i |\chi_1 \chi_2 \chi_3 \cdots \chi_N\rangle \quad (48)$$

which provides the Kohn-Sham approach with internal consistency for a non-interacting system which has the density of a real system.

To determine the KS orbitals, they are set within a basis set of functions<sup>33</sup> followed by calculating the coefficients with the slight changes in the secular equations from Hartree Fock such that  $K_{\mu\nu}$  replaces  $F_{\mu\nu}$  which can be written as:

$$K_{\mu\nu} = \langle \phi_\mu | V_{xc} + \int \frac{p(\mathbf{r}')}{|\mathbf{r}_i - \mathbf{r}'|} d\mathbf{r}' - \frac{1}{2} \nabla_i^2 - \sum_k^{nuclei} \frac{Z_k}{|\mathbf{r}_i - \mathbf{r}_k|} | \phi_\nu \rangle \quad (49)$$

in so much that nuclear attraction and kinetic energy components of  $K$  are the same as  $F$ . Since the density comes from the solution of the secular equation, it must be an iterative SCF process for the Kohn-Sham methodology. The difference between DFT and HF are that DFT is exact and all that is needed is  $E_{xc}$  as a function of the density, the problem is that the form of this functional is unknown.<sup>27</sup> As a result, several expressions to approximate  $E_{xc}$  have been produced from the immense research efforts thus far. In essence, DFT is exact but needs to be solved approximately due to this unknown operator.

### ***Functionals for the Exchange-correlation***

The exchange-correlation potential,  $E_{xc}$ , is typically referred to as the ‘junk-yard’ term which includes all the unknowns, including  $T$ . This is the term that makes DFT imperfect.<sup>14</sup> Much research has gone into determining this unknown term, as an approximate solution many different functionals have been developed to calculate this electron correlation. These functionals normally are designed for a specific purpose and describe certain molecules better than others.

Each functional uses different functional form to describe the exchange-correlation potential. A few of these popular functionals are: (i) *GGA*, (ii) *PBEPBE* and (iii) *B3LYP*. Typically, the name of the functional describes the origin. The examples: (i) generalized gradient approximation, (ii) Perdew, Burke and Ernzerhof’s exchange and correlation functionals (PBE) and (iii) Becke’s 3-parameter exchange and Lee, Young and Parr’s correlation.<sup>27</sup> As example is the energy density,  $\varepsilon_{xc}$ , which is dependent on the electron density expressing the exchange-correlation,  $E_{xc}$ :

$$E_{xc}[\rho(\mathbf{r})] = \int \rho(\mathbf{r})\varepsilon_{xc}[\rho(\mathbf{r})]d\mathbf{r} \quad (50)$$

Additionally, the nomenclature does not express clearly that there are two different types of densities involved. The two types are per unit volume density and a per particle density.

Modelling spin unrestricted systems with respect to DFT has also not yet been discussed; however, it can easily be incorporated – all that is needed is to introduce functionals of the  $\alpha$  and  $\beta$  densities. The notation typically reserved for the spin is termed  $\zeta$  (normalized spin polarization) but it is more than a notation, it is a variable in the functional form:

$$\zeta(\mathbf{r}) = \frac{\rho^\alpha(\mathbf{r}) - \rho^\beta(\mathbf{r})}{\rho(\mathbf{r})} \quad (51)$$

Where half of the product for the total density is described by the  $\alpha$  spin density and  $(\zeta+1)$  while the total density and difference of that value describe the  $\beta$  spin densities.

The hybrid functional *B3LYP* – Becke’s 3-parameter exchange functional coupled with Lee, Young and Parr’s correlation functional – was chosen for all electronic structure calculations in this work, due to the massive body of evidence that shows the generalized applicability of B3LYP to molecular systems. *B3LYP* is termed a hybrid functional because it linearly combines Hartree-Fock’s exact, calculated as a sum over all the HF exchange integrals, with the B88 exchange functional.

### *An overview of DFT*

The above sections described generalized DFT approaches in considerable detail; below, a shortened overview using an alternative exposition is given.

The primary strength of DFT for molecular modelling is that only the total electron density needs to be considered. DFT postulates that determining the probability distribution (total electron density,  $\rho(\vec{r})$ ) will allow the energy and associated properties to be calculated.<sup>27</sup> This is proposed using:

$$\rho(\vec{r}_g) = \sum_i^{\text{occupied}} \phi_i^2(\vec{r}_g) \quad (52)$$

The orbitals represented by  $\phi_i$  which is constructed from a linear basis set, and the coordinates in space– which normally uses spherical coordinates. Based on the Hohenberg-Kohn theorems, the molecular energy and its constituents are *functionals* of the electron density:

$$E_{DFT}(\rho(\vec{r})) = T[\rho(\vec{r})] + V_{NE} + J[\rho(\vec{r})] + E_{XC}[\rho(\vec{r})] \quad (53)$$

The only term that is absent is the Hartree-Fock exchange ( $K$ ), this, however, is dependent on the DFT functionals as it is excluded in pure functionals while partially included in hybrid functionals. Hybrid functionals have Hartree-Fock exchange and exchange-correlation functionals normally in some fixed percentages, such as *B3LYP*.

A modified Fock matrix can then be introduced from Eq. (53) which was proposed by Kohn and Sham in 1965:

$$F_{\mu\nu}^{DFT} = H_{\mu\nu}^{\text{core}} + J_{\mu\nu}(P_{\lambda\sigma}) + \sum_g w_g F_{\mu\nu}^{DFT}(\rho(\vec{r}_g)) \quad (54)$$

where the kinetic and nuclear attraction is encapsulated in the one-electron integral giving,  $H^{\text{core}}$ , then the classical electron-repulsion is described by,  $J_{\mu\nu}$ , depending on the density matrix,  $P_{\lambda\sigma}$ , giving the molecular orbitals. Lastly, the electron correlation is introduced (correlation and exchange) which is multiplied by a weighting factor,  $w_g$ , evaluated as the summation over a grid. This, in turn, allows DFT to analyze many-electron (larger) systems.

One of the most popular methods in DFT and our method of choice uses the hybrid functional approach of *B3LYP*, where fixed percentages are always used:

$$E_{XC}^{\text{hybrid}}(\rho(\vec{r})) = c_{DFT} E_{XC}^{\text{pure}}(\rho(\vec{r})) + c_{HF} K \quad (55)$$

where  $c_i$  is a constant of the specific percentages. This, however, is a generalization and Becke's formulation is much more precise, where there are parts that are calculated using the local value of the density and a LDA functional.

$$E_{XC}(\rho(\bar{r})) = c_1 E_X^{HF} + c_2 E_X^{local} + c_3 E_X^{non-local} + c_4 E_X^{local} + c_5 E_X^{non-local} \quad (56)$$

The  $E_X^{component}$  in  $E_{XC}(\rho(\bar{r}))$  has three major components (i) local exchange (ii) non-local exchange and (iii) local and non-local correlation. Each can be described differently for the DFT method chosen; for the original *B3LYP* the components can be broken down into (i) LDA<sup>34</sup> (ii) B88<sup>35</sup> and (iii) PW91<sup>36-38</sup> or more accurately depicted with the constants as:

$$E_{XC}^{B3LYP} = (1 - a) E_X^{LSDA} + a E_X^{HF} + b \Delta E_X^{B88} + (1 - c) E_C^{LSDA} + c E_C^{LYP} \quad (57)$$

which is experimental data was used to fit the parameters  $a$ ,  $b$  and  $c$  with  $a=0.20$ ,  $b=0.72$  and  $c=0.81$  for B3LYP respectively.<sup>14</sup> The coefficients are optimized for each functional and hence cannot be used with different functionals. This is just one of the functionals applied to DFT but the benefit of integrating the Hartree Fock exchange energy gives this method an advantage over other functionals and the accounting for electron correlation makes DFT more applicable to real-world systems that have more than one electron. While DFT is computationally more expensive than HF it is worth the computational effort and has some comparability to experimental data which this project may find useful.<sup>13</sup>

## Wavefunction Analysis

While electronic structure methods such as HF theory or DFT allow for accurate modelling of a molecular geometry and electronic wavefunction, their results are often quite difficult to interpret – especially in conceptual chemical terms. Various approaches, tools and theories have been developed to analyse and deconstruct molecular electronic wavefunctions in more chemically relevant terms. Below, the Quantum Theory of Atoms in Molecules as well as the Fragment, Atomic, Localized, Delocalized and Interatomic density decomposition scheme are discussed in-depth. The latter approach is the key and central analyses applied in this work, and has been expanded in this work as well.

## QTAIM

Richard Bader and co-workers' Quantum Theory of Atoms in Molecules (QTAIM) is a comprehensive, *ab initio* theory and definition of open quantum subsystems (i.e. *atoms*) within a generally closed quantum system (i.e. *molecules*).<sup>39-43</sup> An atom in a molecule is defined as a



bound atom, which allows the average properties to be obtained. Due to physical continuity, this average corresponds to the isolated atom from quantum mechanics. Therefore, the atomic values must consider the entire molecule for a molecule average to be given for a property.

The virial theorem is important in molecular mechanisms governing the kinetic and potential energies of a molecule. This has been transformed, by Bader, from a global statement (over the molecule as a whole) to a local statement in real-space.<sup>44</sup> In essence, the local distributions for kinetic energy density and kinetic energy density as a function of electron density.<sup>42, 44</sup> The term “atomic virial theorem” then gave rise to the ability to obtain “atomic energy”. Additionally, Bader’s work on molecular electron density distributions coincided with the DFT work that came about in 1964-1965.

The applicability of QTAIM has now become extremely versatile and is routine practice in many computations, giving rise to useful information following from the interpretation of the topology of the electron density. The application of QTAIM has become particularly useful to crystallographers by bridging the gap between crystallography and chemical theory.<sup>45-48</sup> The popularity of QTAIM originates from the physical insight it provides to chemistry making it an extremely powerful technique.

### *Electron density topology*

The electron density (ED) topology is determined by attractive forces from the nuclei, which is a local maximum at the nucleus. As a result, electron density distribution is determined by the forces which neighbouring nuclei exert until the forces are balanced out in a region of space. Atoms in molecules are defined in QTAIM by this ED topology.

A term strongly related to QTAIM is a critical point (CP) which is when first derivative of the density is zero. A CP at a coordinate  $r_c$ , where this first derivative has vanished, is either a local minimum, maximum or saddle point.

$$\nabla\rho = i\frac{d\rho}{dx} + j\frac{d\rho}{dy} + k\frac{d\rho}{dz} \rightarrow \begin{cases} \vec{0} & (\text{Critical points and } \infty) \\ \text{Normally } \neq \vec{0} & (\text{All other points}) \end{cases} \quad (58)$$

where each term in the gradient operator,  $\nabla$ , is zero, as indicated by the zero vector, not the sum. The maximum at the nucleus is a critical point called the nuclear critical point (NCP). Atomic nuclei size (finite) is neglected, which causes cusps in electron density and potential at the nucleus. At the nucleus, the electron density derivative is not defined (not truly a critical point).

The partial second derivative differentiates between the saddle point, local minimum or

local maximum. The Hessian matrix is comprised of the nine of these partial second derivatives for  $\rho(r)$  and is written at a CP located at  $r_c$ :

$$A(r_c) = \begin{pmatrix} \frac{\partial^2 \rho}{\partial x^2} & \frac{\partial^2 \rho}{\partial x \partial y} & \frac{\partial^2 \rho}{\partial x \partial z} \\ \frac{\partial^2 \rho}{\partial y \partial x} & \frac{\partial^2 \rho}{\partial y^2} & \frac{\partial^2 \rho}{\partial y \partial z} \\ \frac{\partial^2 \rho}{\partial z \partial x} & \frac{\partial^2 \rho}{\partial z \partial y} & \frac{\partial^2 \rho}{\partial z^2} \end{pmatrix}_{r=r_c} \quad (59)$$

and because the Hessian matrix is symmetric and real, it can be diagonalized. Rotation of the coordinate system is the same as diagonalization which superimposes the rotated axes with the critical points principal curvature axes. So, a unitary transformation (coordinate system rotation)  $r' = rU$  and  $U$  the unitary matrix yields three eigenvalue equations  $Au_i = \lambda_i u_i$  with  $i=1, 2$  and  $3$  where  $u_i$  is an eigenvector in  $U$ . Simple linear algebra allows the diagonal form  $U^{-1}AU = \Lambda$  to be achieved

$$A(r_c) = \begin{pmatrix} \frac{\partial^2 \rho}{\partial x'^2} & 0 & 0 \\ 0 & \frac{\partial^2 \rho}{\partial y'^2} & 0 \\ 0 & 0 & \frac{\partial^2 \rho}{\partial z'^2} \end{pmatrix}_{r=r_c} = \begin{pmatrix} \lambda_1 & 0 & 0 \\ 0 & \lambda_2 & 0 \\ 0 & 0 & \lambda_3 \end{pmatrix}, \quad (60)$$

where the eigenvalues,  $\lambda$ , represent the curvatures of the density with regards to the rotated axes  $x', y', z'$ . The eigenvector is the algebraic sum of the signs that indicate if the electron density is a local minimum, maximum or saddle point. Respectively a positive and negative eigenvalue corresponds to a local maximum and minimum. A key feature, however, is that the trace is invariant to coordinate rotations. The Laplacian of the density is the trace of the Hessian  $[\nabla^2 \rho(r)]$  so  $x=x'$  and when forth, note the primes have now been dropped:

$$\nabla^2 \rho(r) = \nabla \cdot \nabla^2 \rho(r) = \frac{\partial^2 \rho(r)}{\partial x^2} + \frac{\partial^2 \rho(r)}{\partial y^2} + \frac{\partial^2 \rho(r)}{\partial z^2} \quad (61)$$

$$\lambda_1 \quad \lambda_2 \quad \lambda_3$$

The CPs have a *rank* ( $\omega$ ) which is the number of curvatures of the density at the CP and a *signature* ( $\sigma$ ) which is the algebraic sum of signs of the curvatures, so the CPs can be characterized as  $(\omega, \sigma)$ . A change in the topology of density occurs in the molecular structure when the rank is less than three. Due to these parameters, there are four CPs that are stable with three non-zero eigenvalues. These stable points are  $(3, +3)$   $\rho$  a local minimum,  $(3, +1)$   $\rho$  a minimum in the plane and a maximum on the perpendicular third axes,  $(3, -3)$  where  $\rho$  is a local maximum,  $(3, -1)$   $\rho$  a maximum in the plane and a minimum along the perpendicular third

axis. Elements of the chemical structure are linked to these CP's: (3, +3) is a cage critical point (CCP), (3, +1) ring critical point (RCP), (3, -3) nuclear critical point (NCP) and (3, -1) bond critical point (BCP). The CP type and number can coexist abiding by the topological relationship:

$$n_{RCP} - n_{CCP} + n_{NCP} - n_{BCP} = \begin{cases} 1 & \text{(Poincare - Hopf relationship)} \\ 0 & \text{Morse equation} \end{cases} \quad (62)$$

with the number of the CPs as  $n$ . In the case of the Poincare-Hopf relationship,<sup>43</sup> it applies to isolated molecules while the Morse equation<sup>45</sup> applies to infinite crystals. A “characteristic set” is the term used to describe the left-hand side. If Eq. 62 is violated, then a CP has been excluded, but the opposite may also not be used to indicate the completeness.

CPs at nuclear positions (3, -3) and CCPs, RCPs and BCPs at several internuclear separations result in space being naturally partitioned into subspaces,  $\Omega$ , which are labelled an atomic basin for which only a single nucleus is contained in the basin. The gradient vector field of the ED describes the surfaces separating the atomic basins.

$$\nabla\rho(r) \cdot n(r) = 0 \quad (63)$$

the points on the surface are described by Eq. 63 resulting in a surface  $S(\Omega)$  with the above condition, with  $r$  on this surface and  $n(r)$  a unit vector which is normal to  $S(\Omega)$ .

### *Atomic Overlap Matrix*

Topological analysis of either experimental or theoretical electron densities forms the basis of QTAIM.<sup>46, 49, 50</sup> Accordingly, functions other than the electron density can be integrated over QTAIM-defined atomic volumes in order to obtain useful quantitative information. In particular, and especially important for this work, is the localization indices [LI,  $\lambda(A)$ ] and delocalization indices [DI,  $\delta(A, B)$ ] that can be obtained for atoms and atom pairs showing electrons localized to a given atom or delocalized over an atom-pair.<sup>51,52, 53</sup>

Cioslowki and Mixon used<sup>54</sup> QTAIM atomic volumes to derive a model for bond orders. They used the atomic overlap matrix (AOM) to relate useful information contained in orbitals across the entire molecule to atom-centric quantities. Likewise, AOMs play a central role in FALDI analysis and accordingly is quite important to this work, particularly with respect to interpreting and deconstructing LIs and DIs.

One approach to determine the AOMs is to use Mulliken population analysis, as proposed by Pipek and Mezey<sup>55</sup> but this achieves arbitrary partitioning of the AOMs in terms

of basis functions. Other approaches also exist such as generalized atomic polar tensor (GAPT) population analysis<sup>56, 57</sup> but the most elegant definition of the AOMs comes from Bader's definition.<sup>58</sup> The definition is independent of the basis set used, so true molecular properties are reflected in the AOMs. This means numerical integration can be used to calculate atomic contributions for arbitrary properties. Specifically, an element of the AOM associated with atom  $A$ , usually given the symbol  $S^A$ :

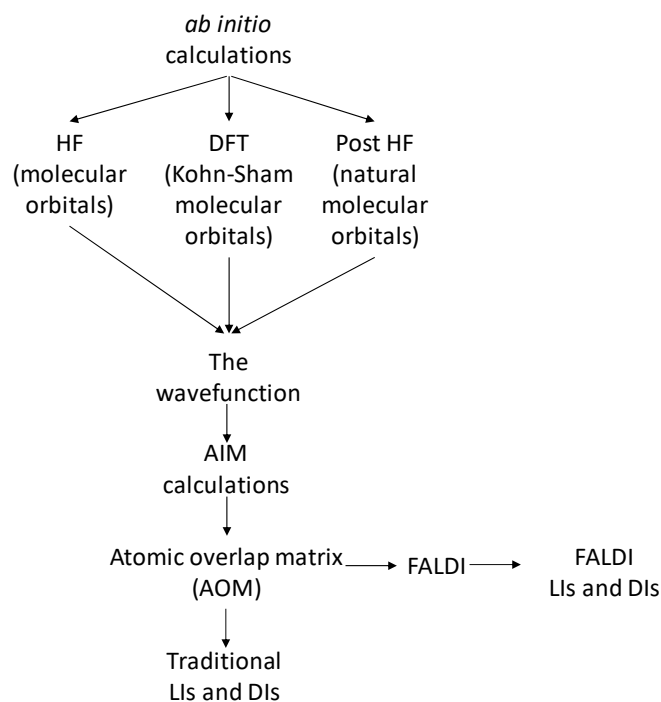
$$\langle i|j\rangle_A = S_{ij}^A = \int_{\text{over basin of } A} \sqrt{v_i v_j} \chi_i^*(r) \chi_j(r) dr \quad (64)$$

where  $\chi$  is a natural orbital with occupation  $v$ .  $\langle i|j\rangle_A$  therefore gives the overlap of the  $i$ th and  $j$ th MOs over the QTAIM-defined atomic basin of atom  $A$ ,  $\Omega(A)$ . The diagonal terms of an AOM (when  $i=j$ ) relates the contribution of each MO to an atom's electron population,  $N(A)$ , or the number of electrons found, on average, in  $\Omega(A)$ ,

$$N(A) = \sum_i^{N_{MO}} \langle i|i\rangle_A = \int_A \rho(r) dr \quad (65)$$

which is equivalent to integrating the total electron density over the same volume.

Once atomic overlap matrices (AOM) elements have been calculated, multiple other QTAIM and FALDI-based indices can be derived relatively simply. In addition, the accuracy of these indices rely inherently on the numerical accuracy of the integration in Eq. 64 as well as the accuracy of the MOs, as based on the underlying electronic structure model. The computational process that were used in this work therefore starts with an *ab initio* calculation to obtain the wavefunction which is needed for the AOM, the AOM can then be decomposed to obtain the LIs and DIs illustrated in **Scheme 2.1** which has been adapted from Wang and Werstuijk.<sup>51</sup>



**Scheme 2. 1.** The process of obtaining localized and delocalized indices.

In the atomic basin, the degree of localization or delocalization of electrons can be found using the AOMs off-diagonal elements which describe the second-order density distribution across the atom.<sup>59</sup> This describes how the MOs interact with each other in the basin. To start, consider, how electrons are localized to *a single basin*:

$$\lambda(A) = \sum_{ij} \int_A dr_1 \int_A dr_2 \sqrt{v_i v_j} \{ \chi_i^*(r_1) \chi_j(r_1) \chi_j^*(r_2) \chi_i(r_2) \} \quad (66)$$

or in terms of AOM elements:

$$\lambda(A) = \sum_{ij} \sqrt{v_i v_j} S_{ij}^A S_{ij}^A \quad (67)$$

This is for the atomic basin  $\Omega(A)$  where  $\lambda(A)$  is the LI for atom A.<sup>60, 61</sup> The degree of localization or delocalization can be calculated by simultaneously integrating across two domains the pair density for electrons in each basin. The total electron delocalization is calculated similarly:

$$\delta(A, B) = 2 \sum_{ij} \int_A dr_1 \int_B dr_2 \sqrt{v_i v_j} \{ \chi_i^*(r_1) \chi_j(r_1) \chi_j^*(r_2) \chi_i(r_2) \} \quad (68)$$

or in terms of AOMs:

$$\delta(A, B) = 2 \sum_{ij} \sqrt{v_i v_j} S_{ij}^A S_{ij}^B \quad (69)$$

The well-known DI is the  $\delta(A, B)$  term<sup>60, 61</sup> for atom pair A and B. The factor 2 in Eq. 69 is introduced for if the integrations are swapped, which will result in the same number of electrons found on  $\Omega(A)$  which are delocalized to  $\Omega(B)$  and vice versa.

Both the LIs and DIs give indications of where the electrons are, either localized to a specific basin or shared across two atomic basins through delocalization. Having both the LI and DI the total atomic electron population can be determined through:

$$N(A) = \lambda(A) + \sum_{A \neq B}^{M-1} 0.5 \delta(A, B) \quad (70)$$

where the number of atomic basins for the molecule indicated by  $M$ . The first term in the equation indicates the electrons localized to the basin and the second term (now halved) the delocalized electrons and when summed together produce the average number of electrons in the atomic basin  $\Omega(A)$ . Both these LI and DI terms carry significant weight in this project as they form part of the basis of the symmetry classification method of the MOs and the quantification where the DI traditionally relates to the bond order.

### ***Domain averaged Fermi Holes***

Ponec and co-workers developed the Domain Averaged Fermi Hole (DAFH)<sup>62, 63</sup> approach which allows for a visualization and molecular-wide distribution of an atom's electron population,  $N(A)$  (Eq. 65). The concept revolves around taking a specific domain in real space and averaging one of the coordinates (spinless XC (exchange-correlation)-hole definition). Any domain can be chosen but meaningful results are obtained using QTAIM based atomic domains<sup>64</sup> and everything subsequent refers to this QTAIM domain. For a chosen atomic basin, the central quantity  $g_A(\mathbf{r})$ :

$$g_A(r_1) = \int_A \rho(r_2) \rho^{Hole}(r_1; r_2) dr_2 \quad (71)$$

where the electron-hole is averaged (integrated) over the spatial coordinates. Due to the XC effects for the average electrons in  $\Omega(A)$ , the electrons excluded at  $\mathbf{r}$  is the  $g_A(\mathbf{r})$  value. At  $\mathbf{r}$  the full decomposition of electron density can therefore be obtained in terms of atomic contributions:

$$\rho(r) = \sum_A^M g_A(r) \quad (72)$$

where  $M$  is the number of atoms. There are many useful and interesting relationships<sup>65</sup> which DAFHs  $g_A(r)$  and QTAIM populations have, but are outside the scope of this work. Unfortunately, the calculation of  $g_A(r)$  is computationally extremely costly due to a second-order density matrix.  $g_A(r)$  can, however, be calculated (exactly for HF and DFT wavefunctions, but approximately for higher order wavefunctions) through the use of AOM elements:

$$g_A(r) = \sum_{ij} \sqrt{v_i} \sqrt{v_j} \chi_i^*(r) \chi_j(r) S_{ji}^A \quad (73)$$

In this form, it is also quite clear  $g_A(r)$  can be written as a matrix,  $\mathbf{G}^A$ , which itself can be further manipulated using linear algebra techniques. For instance,  $\mathbf{G}^A$  can be diagonalized, resulting in one electron domain natural functions with the atomic basin's respective occupations. Other modifications are available such as those which Cioslowski introduced like isopycnic transformations<sup>54</sup> which Ponec, Kohout and Cooper<sup>66</sup> used, but this work focuses on the general DAFH function and not the modifications, except in the light of FALDI.

### **FALDI Density Decomposition scheme**

The Fragment, Atomic, Localized, Delocalized and Interatomic (FALDI) density decomposition scheme is a relatively new approach that calculates real-space distributions of atom-centric, (de)localized electron densities. In this manner FALDI provides chemical insight that fully recovers the holistic, molecular-wide nature of the wavefunction and its MOs whilst adhering to the chemically intuitive atomistic molecular structure hypothesis. A method of exhaustive molecular ED decomposition was presented as the FALDI density decomposition scheme, which isolates any coordinate  $\mathbf{r}$  in real space about all domains of  $M$ .<sup>5</sup> The molecular systems are defined by QTAIM to describe these domains with atomic basins.<sup>64</sup> FALDI allows for the calculation of any domain-specific electron population in terms of real-space distributions. In the case of the total electron population the count of electrons found, on average, in atomic basin  $\Omega_A$ :

$$N(A) = \int_{\Omega_A} \rho(r) dr \quad (74)$$

$$= \int_{\infty} g_A(r) dr$$

$N(A)$  can be obtained by integrating the spin-independent electron density over an atomic domain, or it can be obtained by integrating an *atom*-ED distribution ( $g_A(r)$ ) over the entire molecular space. The *atom*-ED distribution is therefore a real-space distribution of  $N(A)$ , taking into account how the delocalization averaged over all electrons in  $\Omega_A$  is delocalized across the molecule.  $g_A(r)$  is borrowed from DAFH analysis, although further decomposed in FALDI.  $g_A(r)$  is commonly calculated by approximating Eq. 71 by applying a one-electron approximation to simplify finding  $\rho_{xc}(\mathbf{r}_1; \mathbf{r}_2)$  in terms of AOMs:

$$\begin{aligned} g_A(\mathbf{r}) &= \sum_{ij} \sqrt{v_i v_j} \chi_i(\mathbf{r}) \chi_j(\mathbf{r}) S_{ji}^A \\ &= \sum_{ij} G_{ji}^A S_{ji}^A \end{aligned} \quad (75)$$

so that  $S_{ij} = \sum_A \int \chi_i^*(r) \chi_j(r) dr$  (Eq. 64) and  $N(A) = tr(S^A)$  (Eq. 65). Notably, in Hartree-Fock and DFT wavefunctions, the matrix  $\mathbf{G}^A$  is equivalent to an AOM weighted by MO populations.

FALDI also calculates real-space distributions of atom-localized electrons and electrons delocalized over atom-pairs. The latter is known as *loc*-ED distributions:

$$\mathcal{L}_A(\mathbf{r}) = \sum_{ij} \chi_i(\mathbf{r}) \chi_j(\mathbf{r}) (\mathbf{G}^A \mathbf{S}^A)_{ji} \quad (76)$$

where the matrix product  $\mathbf{G}^A \mathbf{S}^A$  is a localized overlap matrix (LMAT), and quantifies how MOs and MO-interference leads to a localization of electrons to an atom. Integrating  $\mathcal{L}_A(\mathbf{r})$  over all molecular space yields the QTAIM-defined LI (localization index),  $LI = \lambda(A) = \int_{\infty} \mathcal{L}_A(\mathbf{r}) dr$ . Therefore,  $\mathcal{L}_A(\mathbf{r})$  is a real-space distribution of LI and can be used to visualize and quantify electrons localized to a specific atom.

A *deloc*-ED distribution can be similarly defined,

$$\mathcal{D}_{A,B}(\mathbf{r}) = \sum_{ij} \chi_i(\mathbf{r}) \chi_j(\mathbf{r}) (\mathbf{G}^A \mathbf{S}^B + \mathbf{S}^B \mathbf{G}^A)_{ji} \quad (77)$$

where the sum  $\mathbf{G}^A \mathbf{S}^B + \mathbf{S}^B \mathbf{G}^A$  ensures a symmetric delocalized overlap matrix (DMAT), and quantifies how MOs and MO-interference leads to a delocalization of electrons across two atomic basins.  $\mathcal{D}_{A,B}(\mathbf{r})$  calculates the contribution that electrons shared by two atoms make to the total electron density at  $\mathbf{r}$ . The QTAIM-defined DI can also be recovered by integration



over molecular space for any *deloc*-ED distribution.  $DI = \delta(A, B) = \int_{\infty} D_{A,B}(\mathbf{r})d\mathbf{r}$ .  $D_{A,B}(\mathbf{r})$  are extremely useful distributions which can illustrate how any two atoms of a molecule – regardless of whether they are bonded, or the distance between them – shares electrons throughout all molecular space.

Note that, for simplicity, the matrix product  $\mathbf{G}^A\mathbf{S}^A$  will henceforth be referred to as  $\mathbf{G}^{AA}$ , indicating the localized overlap matrix of atom A. Similarly, the sum  $\mathbf{G}^A\mathbf{S}^B + \mathbf{S}^B\mathbf{G}^A$  will be referred to as  $\mathbf{G}^{AB}$ , or the delocalized overlap matrix of atom-pair A and B. Doing so allows for simpler matrix manipulations, described below.

### Natural Density functions

The matrices  $\mathbf{G}^A$ ,  $\mathbf{G}^{AA}$  and  $\mathbf{G}^{AB}$ , associated with *atom*-, *loc*- and *deloc*-ED distributions, respectively, can be manipulated using linear algebra in order to reveal additional chemical insight. Natural density functions (NDFs) are sets of orthogonal functions which can be generated from diagonalizing these matrices. The procedure for producing NDFs are generally the same, irrespective of which matrix was used; as an example, the LMAT  $\mathbf{G}^{AA}$  will be used.

$\mathbf{G}^{AA}$  contains MO contributions to LI(A) (diagonal elements) as well as MO-interferences in real-space with respect to electron localization. While MOs are (usually) orthogonal, they often exhibit non-zero overlap in a specific domain – such as an atomic basin  $\Omega_A$  – making local MO-based analysis quite difficult. However, orthogonal, MO-based distributions of atom-localized density can be generated by diagonalizing  $\mathbf{G}^{AA}$ :

$$\mathbf{G}^{AA}\mathbf{U}^{AA} = \boldsymbol{\lambda}^{AA}\mathbf{U}^{AA} \quad (78)$$

where  $\mathbf{U}^{AA}$  is a unitary transformation matrix. This procedure results in a set of eigenvalues (contained in diagonal matrix  $\boldsymbol{\lambda}^{AA}$ ) and eigenvectors (column vectors of  $\mathbf{U}^{AA}$ ), and with  $LI(A) = \sum \lambda_i^{AA}$ . The resulting Eq. producing eigenvalues which sum up to the LI,  $LI(A) = \sum \lambda_i^{AA}$ . The occupation for the eigenvalues  $\lambda_i^{AA}$  can be calculated by:

$$\lambda_i^{AA} = \sum_t^{N_{MO}} U_{jt}^{AA} G_{kj}^{AA} U_{kt}^{AA} \quad (79)$$

Finally, the original *loc*-ED distribution can then be written in terms of its eigenvalues:

$$\mathcal{L}_A(r) = \sum_i^{N_{MO}} \lambda_i^{AA} [\phi_i^{AA}(r)]^2 \quad (80)$$

where  $\phi_i^{AA}(r)$  is known as a *loc*-NDF and is defined in terms of MOs and the eigenvectors of  $\mathbf{G}^{AA}$ ,

$$\phi_i^{AA}(r) = \sum_j^{N_{MO}} \chi_j(r) U_{ji}^{AA} \quad (81)$$

Similarly, by diagonalizing  $\mathbf{G}^{AB}$ , a set of *deloc*-NDFs with occupations  $\delta_i^{AB}$  can be constructed:

$$\mathcal{D}_{A,B}(r) = \sum_i^{N_{MO}} \delta_i^{AB} [\phi_i^{AB}(r)]^2 \quad (82)$$

where

$$\phi_i^{AB}(r) = \sum_j^{N_{MO}} \chi_j(r) U_{ji}^{AB} \quad (83)$$

NDFs are quite interesting in that they represent orthogonal functions of atom-centric (de)localized density. Due to the Pauli Exclusion Principle, NDFs are never occupied by more than 2 electrons (even though the condition is never enforced throughout the FALDI procedures), and often reveal the underlying electronic structure in a considerably more localized and atomistic form than MOs. For instance, *loc*-NDFs commonly take forms similar to atomic orbitals, *e.g.*  $1s$ ,  $2s$ ,  $3sp^2$ ... whereas *deloc*-NDFs commonly take diatomic symmetries such as  $\sigma$ -,  $\pi$ - and  $\delta$ -modes of bonding. NDFs and their analysis play a central role in this work, and examples of NDFs are given throughout.

### **Determination of approximated molecular symmetries through NDF-analysis**

The next section represents original contributions to FALDI, and is primarily explored in Chapter 3 in this thesis.

The *loc*-NDFs of a metal centre often carefully resemble its atomic orbitals, regardless of whether the metal is in a bound or unbound state, and regardless of the total point-group symmetry of the molecule it forms a part of. In addition, since *loc*-NDFs are constructed from MO distributions (Eq 81), each MO can be fully decomposed into *loc*-NDFs and their occupations. Therefore, *loc*-NDFs can be used to assign partial symmetry terms to electronic structure components, such as MOs, of an asymmetrical complex.

To do so, the eigenvalue equation diagonalizing  $\mathbf{G}^{AA}$  is first manipulated by isolating the eigenvalues:

$$(\mathbf{U}^{AA})^\dagger \mathbf{G}^{AA} \mathbf{U}^{AA} = \boldsymbol{\lambda}^{AA} \mathbf{U}^{AA} (\mathbf{U}^{AA})^\dagger \quad (84)$$

then

$$\boldsymbol{\lambda}^{AA} = (\mathbf{U}^{AA})^\dagger \mathbf{G}^{AA} \mathbf{U}^{AA} \quad (85)$$

where  $(\mathbf{U}^{AA})^\dagger$  is the conjugate transpose of  $\mathbf{U}^{AA}$  and a unitary matrix is by definition positive definite.

The eigenvectors (column vectors of  $\mathbf{U}^{AA}$ ) themselves are square normalizable to unity. In addition, these eigenvectors are in a basis of MOs. Therefore, each element  $[U_{ij}^{AA}]^2$  provides the relative, fractional contribution of the  $i$ th MO to the  $j$ th *loc*-NDF associated with atom A. Alternatively, each MO can be fully decomposed into all NDFs of the molecule. Since the symmetry of each *loc*-NDF can usually be determined through visual inspection, that means an approximated symmetry can be assigned to any given MO based on the square-normalized eigenvectors,  $[U_{ij}^{XX}]^2$ .

Alternatively, a specific NDF can be decomposed in terms of its constituent MOs. As mentioned above and explored in Chapter 3, *loc*-NDFs of a metal centre correspond to all of its occupied atomic orbitals. For instance, a chromium metal centre in a prototypical complex such as  $\text{Cr}(\text{CO})_6$  is expected to have 14 significantly occupied *loc*-NDFs. Of these, 9 should be fully occupied and correspond to the electron configuration of  $[\text{Ar}] = 1s^2 2s^2 2p^6 3s^2 3p^6$  and the remaining 5 should correspond to various 3d orbitals in an octahedral ligand field, i.e. 3  $t_{2g}$  and 2  $e_g$  orbitals. with occupations significantly less than 2. Amazingly, *loc*-NDFs tend to be very similar in distribution regardless of environment, and only their occupations significantly differ. In other words, the set of *loc*-NDFs is expected to be qualitatively the same for  $\text{Cr}(\text{CO})_6$  (a symmetrical complex with well-defined MO symmetries) as for  $\text{Cr}(\text{CO})_5\text{CH}_2$  (an asymmetrical complex with MOs of pure identity symmetries). The fractional contributions of  $[U_{ij}^{XX}]^2$  and symmetries of *loc*-NDFs of a metal centre allows for effective determination of approximate MO symmetries in asymmetrical metal complexes. Specifically, a particular MO  $\chi_i$  can be classified in terms of symmetry-labelled *loc*-NDFs associated with the central metal atom. This is done by evaluating  $[U_{ij}^{XX}]^2$  after the  $j$ th *loc*-NDF has been labelled as  $\sum_j [U_{ij}^{XX}]^2 = 1$ .  $j_n$  is used to indicate the weight of the  $j$ th *loc*-NDF to the  $i$ th MO:

$$\sum_j^{N_{MO}} j n_i^M = 1 \quad (86)$$

where M is used to indicate the metal-centre. Since multiple *loc*-NDFs can have the same symmetry,  $j n_i^M$  contributions can be grouped by symmetry label. This procedure is explained in detail below for octahedral metal complexes.

Octahedral ( $O_h$ ) metal complexes are the primary focus, as proof of concept of this work. MOs in complexes with  $O_h$  symmetry can consist of  $a_{1g}$ ,  $t_{1u}$ ,  $e_g$  and  $t_{2g}$  symmetries. A specific MO can be classified based on the symmetries of the *loc*-NDF associated with the metal centre of an  $O_h$  complex, as the grouped version of Eq. 86:

$$^{a1g}n_i^M + ^{t1u}n_i^M + ^{t2g}n_i^M + ^{eg}n_i^M + ^{NL}n_i^M = 1 \quad (87)$$

The final term  $^{NL}n_i^A$  refers to non-localized symmetry concerning the metal and encapsulates ligand-centred orbitals such as  $t_{2u}$  and  $t_{1g}$  which are not directly related to the metal. Each *loc*-NDF is therefore classified in terms of symmetry, and its MO constituents gain a degree of symmetry character through the classification process.

Just as each *loc*-NDF can be classified in terms of symmetry, so can each *deloc*-NDF be decomposed in terms of symmetry-labelled MOs. The limitation on this being linked to the symmetry terms defined by the eigenvalue. Not every MO symmetry term can be defined by looking at one atoms symmetry (in this work the metal centre) and hence unknown symmetries arise such as the NL terms. The NL terms are present as a result of the ligands and need to be separately classified, which is left for future work.

MO contributions to a *deloc*-NDF can be obtained as the total number of electrons delocalized between the metal and any other atom B,  $DI(M, B)$  through the diagonal values of the associated DMAT,  $G_{ii}^{MB}$ , with  $DI(M, B) = \sum G_{ii}^{MB}$ . Based on the *loc*-NDFs classifications (Eq. 87) the MO contributions can be filtered and corresponded such that:

$$DI(M, B) = \sum_i^{N_{MO}} G_{ii}^{MB} [^{a1g}n_i^M + ^{t1u}n_i^M + ^{t2g}n_i^M + ^{eg}n_i^M + ^{NL}n_i^M] \quad (88)$$

so that the symmetries can be weighted using their  $DI(M, B)$  contribution. Clarity of the method shines in the examples discussed in the coming Chapters and supplementary information that depict how the mathematical terms are linked pictorially for a better grasp of the concept. The result of using the LMAT as the symmetry labelling process allows us to classify MOs and then quantify them due to the DMAT that corresponds to the now labelled MOs.

## FALDI Fragments

All the FALDI interactions discussed so far are based on either atomic or diatomic interactions. This is a limiting factor when molecular wide interactions are considered like MOs, for this reason, fragments are introduced. FALDI fragments group atom and atom-pair components of FALDI together, to result in a collective distribution that when integrated can be interpreted. To describe the operation of FALDI fragments; take two fragments,  $\mathcal{F}1$  and  $\mathcal{F}2$  for example, and by summing the FALDI *atom*-ED distributions for a fragment, the total density contribution for any coordinate  $\mathbf{r}$  can be obtained:

$$g_{\mathcal{F}1}^{total}(\mathbf{r}) = \sum_A^{M_{\mathcal{F}1}} g_A(\mathbf{r}) \quad (89)$$

For fragment,  $\mathcal{F}1$ ,  $M_{\mathcal{F}1}$  represents the number of atoms. The total fragment electronic population,  $N^{total}(\mathcal{F}1)$ , can then be obtained by integrating Eq. 96 over all molecular space. The total electronic contribution of  $\mathcal{F}1$  to the molecule can also be visualized by considering the 3D-isosurface of  $g_{\mathcal{F}1}^{total}(\mathbf{r})$ . This  $g_{\mathcal{F}1}^{total}(\mathbf{r})$  term is a compounded term that includes localized electrons to each fragment and the delocalized electrons between the other atoms/fragments and  $\mathcal{F}1$ .

For each fragment the atom-localized electronic contribution is obtained by:

$$\mathcal{L}_{\mathcal{F}1}(\mathbf{r}) = \sum_A^{M_{\mathcal{F}1}} \mathcal{L}_A(\mathbf{r}) \quad (90)$$

where for each atom of the fragment the electrons are localized to the contribution at  $\mathbf{r}$ . For each atom in the fragment, the term includes the core and non-bonded electrons. This term on its own does not describe the full picture and therefore the intra-fragment delocalized electronic contribution is introduced:

$$\mathcal{D}_{\mathcal{F}1}^{intra}(\mathbf{r}) = \sum_A^{M_{\mathcal{F}1}-1} \sum_{B=A+1}^{M_{\mathcal{F}1}} \mathcal{D}_{A,B}(\mathbf{r}) \quad (91)$$

which describes the delocalization of electrons between atoms within the same fragment at  $\mathbf{r}$ . This describes strongly delocalized (covalent) and weakly delocalized electrons. The total intra-fragment electron distribution can then be obtained by the summation of Eq. 90 and 91 to give:

$$g_{\mathcal{F}1}^{intra}(\mathbf{r}) = \mathcal{L}_{\mathcal{F}1}(\mathbf{r}) + \mathcal{D}_{\mathcal{F}1}^{intra}(\mathbf{r}) \quad (92)$$

therefore, both atom-localized and intra-atomic delocalized electrons between diatomic interactions of the fragment are described by electrons localized to  $\mathcal{F}1$  by the contribution at  $\mathbf{r}$ . The sum of the LIs and DIs for atoms in the fragment can then be obtained by integrating over all molecular space, which is defined as the total intra-fragment population,  $N^{intra}(\mathcal{F}1) = \int g_{\mathcal{F}1}^{intra}(\mathbf{r})d\mathbf{r} = \sum_A LI(A) + \sum_{A, B} DI(A, B)$ , where  $A, B \in \mathcal{F}1$ .

For two different fragments, the *deloc*-ED distribution can be determined to give the inter-fragment delocalization:

$$\mathcal{D}_{\mathcal{F}1, \mathcal{F}2}^{inter}(\mathbf{r}) = \sum_A \sum_B^{M_{\mathcal{F}1} M_{\mathcal{F}2}} \mathcal{D}_{A, B}(\mathbf{r}) \quad (93)$$

where the delocalized distribution of electrons between the two fragments are described by  $\mathcal{D}_{\mathcal{F}1, \mathcal{F}2}^{inter}(\mathbf{r})$ . Integrating over all molecular space thus produces the inter-fragment delocalization index  $DI(\mathcal{F}1, \mathcal{F}2) = \int \mathcal{D}_{\mathcal{F}1, \mathcal{F}2}^{inter}(\mathbf{r}) d\mathbf{r} = \sum_{A, B} DI(A, B)$ , where  $A \in \mathcal{F}1$  and  $B \in \mathcal{F}2$ .

Coming back to Eq. 96 the  $g_{\mathcal{F}1}^{total}(\mathbf{r})$  can be fully described by the summation of Eq. 92 and 93 to give:

$$g_{\mathcal{F}1}^{total}(\mathbf{r}) = g_{\mathcal{F}1}^{intra}(\mathbf{r}) + \sum_X^{\mathcal{M}} \frac{1}{2} \mathcal{D}_{\mathcal{F}1, \mathcal{F}X}^{inter}(\mathbf{r}) \quad (94)$$

Thus, the fragments are defined with the total number of fragments represented as  $\mathcal{M}$  and based on the atomic basin overlap approach which is known to be orthodox (QTAIM), everything in this work is performed under orthodox conditions in FALDI terms.

Lastly, the FALDI fragments need to be linked to the FALDI MO analysis. The FALDI MO analysis has described the origin of the symmetry terms, resulting from the *loc*-NDFs of the metal centre. The fragments are defined based on the atoms of interest and their respective LIs and DIs can be calculated and visualized using a 3D-isosurface. The DI of fragments can therefore be correlated and weighted by the *loc*-NDFs of the metal as was done for an atomic or diatomic DI. This yields an equation similar to Eq. 88:

$$DI(\mathcal{F}1, \mathcal{F}2) = \sum_i^{N_{MO}} d_i^{\mathcal{F}1, \mathcal{F}2} \left[ {}^{a_1g}n_i^M + {}^{t_{1u}}n_i^M + {}^{t_{2g}}n_i^M + {}^{eg}n_i^M + {}^{NL}n_i^M \right] \quad (95)$$

which describes the DI between fragments, providing the MO contributions with symmetry classifications based on the metal *loc*-NDFs. This method has been used extensively in Chapter 4 and 5 to classify and quantify symmetry in multiple fragment interactions.

## Perspectives

Computational chemistry is a fast-growing research field that requires constant review and updates. Describing electronic structure, shape, charge distribution and interpreting synthetic processes are just some of the tasks of this field and the computational method should look at the molecule in a multiscale, multiperspective way. Avoiding case-by-case scenarios is where the true power of the computational field lies by zooming out and identifying the electronic reasons for the chemistry. The field is finally at a place where the hardware can handle most of the theory, which is thanks to Moore's Law<sup>67</sup> stating processing power virtually doubles every two years, which has led progress to leaps and bounds being achieved in recent years, making computations that would take decades in the past run in minutes. With computational hardware advancements making studies like this possible. Some of the topics discussed above just brush the surfaces of quantum mechanics and acts as a preview into the world of computational chemistry. One of the important aspects that can be concluded thus far is that the toolset varies. The tasks differ for each level of theory or basis set which it can handle and will most likely depend on the system with which one works. It has become the norm that DFT is typically the go-to level of theory for most chemists and rightly so since it is a very well-rounded theory. Still, the downfalls and strengths of each theory need to be considered before blindly applying the method. Likewise, Molecular Orbital theory in all its glory is an excellent and powerful theory but like everything is not perfect and hence this work tries to build on the powerful MOT in the coming chapters by providing a new approach at interpreting MOs. The FALDI work aims to contribute to how the symmetry terms, specifically for asymmetric molecules, can be classified. The work also intends to add quantification to justify scientific conclusions. Thankfully there is an excellent starting foundation to build from and improvements just need to be discovered.

## References

1. Ballhausen, C. A.; Gray, H. B., *Molecular orbital theory: an introductory lecture note and reprint volume*. WA Benjamin, Inc.: 1965.
2. Pople, J. A.; Beveridge, D. L., *Molecular orbital theory*. NY **1970**.
3. Vincent, A., *Molecular symmetry and group theory : a programmed introduction to chemical applications*. 2nd ed. ed.; Wiley: Chichester, 2000.
4. Cass, M. E.; Hollingsworth, W. E., Moving beyond the single center-Ways to reinforce molecular orbital theory in an inorganic course. *Journal of Chemical Education* **2004**, *81* (7), 997.
5. De Lange, J. H.; Cukrowski, I., Toward deformation densities for intramolecular interactions without radical reference states using the fragment, atom, localized, delocalized, and interatomic (FALDI) charge density decomposition scheme. *Journal of computational chemistry* **2017**, *38* (13), 981-997.
6. de Lange, J. H.; van Niekerk, D. M. E.; Cukrowski, I., FALDI-based criterion for and the origin of an electron density bridge with an associated (3,-1) critical point on Bader's molecular graph. *J. Comput. Chem.* **2018**, *39* (27), 2283-2299.
7. Cotton, F. A., *Chemical applications of group theory*. 3rd ed. ed.; Wiley: New York, 1990.
8. Streitwieser, A.; Salzberg, H., *Molecular orbital theory for organic chemists*. *Journal of The Electrochemical Society* **1962**, *109* (4), 116C-117C.
9. Pople, J. A.; Segal, G. A., Approximate self-consistent molecular orbital theory. II. Calculations with complete neglect of differential overlap. *The Journal of Chemical Physics* **1965**, *43* (10), S136-S151.
10. Pople, J. A., Electron interaction in unsaturated hydrocarbons. *Transactions of the Faraday Society* **1953**, *49*, 1375-1385.
11. Fock, V., Näherungsmethode zur Lösung des quantenmechanischen Mehrkörperproblems. *Zeitschrift für Physik* **1930**, *61* (1-2), 126-148.
12. Fock, V., "Self-consistent" field with interchange for sodium. *Z. Phys* **1930**, *62*, 795-805.
13. Lewars, E., *Computational chemistry. Introduction to the theory and applications of molecular and quantum mechanics* **2003**, 318.
14. Jensen, F., *Introduction to computational chemistry*. John wiley & sons: 2017.
15. M. J. Frisch, G. W. T., H. B. Schlegel, G. E. Scuseria, M. A. Robb, J. R. Cheeseman, G. Scalmani, V. Barone, G. A. Petersson, H. Nakatsuji, X. Li, M. Caricato, A. V. Marenich, J. Bloino, B. G. Janesko, R. Gomperts, B. Mennucci, H. P. Hratchian, J. V. Ortiz, A. F. Izmaylov, J. L. Sonnenberg, D. Williams-Young, F. Ding, F. Lipparini, F. Egidi, J. Goings, B. Peng, A. Petrone, T. Henderson, D. Ranasinghe, V. G. Zakrzewski, J. Gao, N. Rega, G. Zheng, W. Liang, M. Hada, M. Ehara, K. Toyota, R. Fukuda, J. Hasegawa, M. Ishida, T. Nakajima, Y. Honda, O. Kitao, H. Nakai, T. Vreven, K. Throssell, J. A. Montgomery, Jr., J. E. Peralta, F. Ogliaro, M. J. Bearpark, J. J. Heyd, E. N. Brothers, K. N. Kudin, V. N. Staroverov, T. A. Keith, R. Kobayashi, J. Normand, K. Raghavachari, A. P. Rendell, J. C. Burant, S. S. Iyengar, J. Tomasi, M. Cossi, J. M. Millam, M. Klene, C. Adamo, R. Cammi, J. W. Ochterski, R. L. Martin, K. Morokuma, O. Farkas, J. B. Foresman, and D. J. Fox, Gaussian, Inc., Wallingford CT, 2016., gaussian 09, Revision d. 01, Gaussian. Inc., Wallingford CT **2009**, 201.
16. Sherrill, C. D., An introduction to Hartree-Fock molecular orbital theory. *School of Chemistry and Biochemistry Georgia Institute of Technology* **2000**.



17. Pauling, L.; Wilson, E. B., *Introduction to quantum mechanics with applications to chemistry*. Courier Corporation: 2012.
18. Albright, T. A.; Burdett, J. K.; Whangbo, M.-H., *Orbital interactions in chemistry*. John Wiley & Sons: 2013.
19. Schrödinger, E., An undulatory theory of the mechanics of atoms and molecules. *Physical Review* **1926**, 28 (6), 1049.
20. Burdett, J. K., *Molecular shapes: theoretical models of inorganic stereochemistry*. John Wiley & Sons: 1980.
21. Leszczynski, J.; Kaczmarek-Kedziera, A.; Puzyn, T.; Papadopoulos, M. G.; Reis, H.; Shukla, M., *Handbook of computational chemistry. Volume 2*. Second edition. ed.; Springer: Cham, Switzerland, 2017.
22. Pielak, L., *Ideas of quantum chemistry*. Elsevier: 2013.
23. Koopmans, T., Über die Zuordnung von Wellenfunktionen und Eigenwerten zu den einzelnen Elektronen eines Atoms. *Physica* **1934**, 1 (1-6), 104-113.
24. Woodward, R. B.; Hoffmann, R., Selection rules for sigmatropic reactions. *Journal of the American Chemical Society* **1965**, 87 (11), 2511-2513.
25. Fukui, K.; Fujimoto, H., An MO-theoretical Interpretation of the Nature of Chemical Reactions.: I. Partitioning Analysis of the Interaction Energy. In *Frontier Orbitals and Reaction Paths: Selected Papers of Kenichi Fukui*, World Scientific: 1997; pp 257-265.
26. Cotton, F. A., *Chemical applications of group theory*. John Wiley & Sons: 2003.
27. Foresman, J. B.; Frisch, E., *Exploring chemistry with electronic structure methods*. 3 ed.; Gaussian: Wallingford, Conn., 2015.
28. Koch, W.; Holthausen, M. C., *A chemist's guide to density functional theory*. John Wiley & Sons: 2015.
29. Cramer, C. J., *Essentials of computational chemistry: theories and models*. John Wiley & Sons: 2013.
30. Hohenberg, P.; Kohn, W., Inhomogeneous electron gas. *Physical Review* **1964**, 136 (3B), B864.
31. Frenking, G.; Shaik, S. S., *The chemical bond : fundamental aspects of chemical bonding*. First edition. ed.; Wiley-VCH Verlag: Weinheim, 2014.
32. Kohn, W.; Sham, L. J., Self-consistent equations including exchange and correlation effects. *Physical Review* **1965**, 140 (4A), A1133.
33. Bachler, V., A quantum chemical calculation on Fe(CO)<sub>5</sub> revealing the operation of the Dewar–Chatt–Duncanson model. *Journal of Computational Chemistry* **2012**, 33 (24), 1936-1947.
34. Slater, J. C., *The self-consistent field for molecules and solids*. McGraw-Hill: 1974; Vol. 4.
35. Russo, T. V.; Martin, R. L.; Hay, P. J., Density functional calculations on first-row transition metals. *The Journal of chemical physics* **1994**, 101 (9), 7729-7737.
36. Perdew, J. P., Unified theory of exchange and correlation beyond the local density approximation. *Electronic Structure of Solids' 91* **1991**, 11.
37. Perdew, J. P.; Chevary, J. A.; Vosko, S. H.; Jackson, K. A.; Pederson, M. R.; Singh, D. J.; Fiolhais, C., Atoms, molecules, solids, and surfaces: Applications of the generalized gradient approximation for exchange and correlation. *Physical Review B* **1992**, 46 (11), 6671.
38. Perdew, J. P.; Chevary, J.; Vosko, S.; Jackson, K. A.; Pederson, M. R.; Singh, D.; Fiolhais, C., Erratum: Atoms, molecules, solids, and surfaces: Applications of the generalized gradient approximation for exchange and correlation. *Physical Review B* **1993**, 48 (7), 4978.

39. Bader, R., Binding regions in polyatomic molecules and electron density distributions. *Journal of the American Chemical Society* **1964**, *86* (23), 5070-5075.
40. Bader, R.; Jones, G., Electron-Density Distributions in Hydride Molecules. The Ammonia Molecule. *Canadian Journal of Chemistry* **1963**, *41* (3), 586-606.
41. Bader, R.; Jones, G., Electron-Density Distributions in Hydride Molecules. The Ammonia Molecule. *The Journal of Chemical Physics* **1963**, *38* (12), 2791-2802.
42. Bader, R. F., Vibrationally induced perturbations in molecular electron distributions. *Canadian Journal of Chemistry* **1962**, *40* (6), 1164-1175.
43. Bader, R. F., Atoms in molecules. *Accounts of Chemical Research* **1985**, *18* (1), 9-15.
44. Bader, R.; Bandrauk, A., Molecular charge distributions and chemical binding. III. The isoelectronic series N<sub>2</sub>, CO, BF, and C<sub>2</sub>, BeO, LiF. *The Journal of Chemical Physics* **1968**, *49* (4), 1653-1665.
45. Coppens, P., *X-ray charge densities and chemical bonding*. International Union of Crystallography: 1997.
46. Koritsanszky, T. S.; Coppens, P., Chemical applications of X-ray charge-density analysis. *Chemical Reviews* **2001**, *101* (6), 1583-1628.
47. Gatti, C., Chemical bonding in crystals: new directions. *Zeitschrift für Kristallographie-Crystalline Materials* **2005**, *220* (5/6), 399-457.
48. Macchi, P.; Sironi, A., Chemical bonding in transition metal carbonyl clusters: complementary analysis of theoretical and experimental electron densities. *Coordination Chemistry Reviews* **2003**, *238*, 383-412.
49. Bader, R., Chem. Re V. 1991, 91, 893.(b) Bader, RFW Atoms in Molecules: A Quantum Theory. Oxford University Press: New York: 1990.
50. Bader, R. F., A quantum theory of molecular structure and its applications. *Chemical Reviews* **1991**, *91* (5), 893-928.
51. Wang, Y. G.; Werstiuk, N. H., A practical and efficient method to calculate AIM localization and delocalization indices at post-HF levels of theory. *Journal of Computational Chemistry* **2003**, *24* (3), 379-385.
52. Bader, R. F.; Matta, C. F., Bonding to titanium. *Inorganic Chemistry* **2001**, *40* (22), 5603-5611.
53. Werstiuk, N. H.; Wang, Y.-G., An atoms in molecules and electron localization function computational study on the molecular structure of the 6-tricyclo [3.2. 1.02, 4] octyl cation. *The Journal of Physical Chemistry A* **2001**, *105* (51), 11515-11523.
54. Cioslowski, J.; Mixon, S. T., Covalent bond orders in the topological theory of atoms in molecules. *Journal of the American Chemical Society* **1991**, *113* (11), 4142-4145.
55. Pipek, J.; Mezey, P. G., A fast intrinsic localization procedure applicable for abinitio and semiempirical linear combination of atomic orbital wave functions. *The Journal of Chemical Physics* **1989**, *90* (9), 4916-4926.
56. Cioslowski, J., General and unique partitioning of molecular electronic properties into atomic contributions. *Physical Review Letters* **1989**, *62* (13), 1469.
57. Cioslowski, J., Partitioning of the orbital overlap matrix and the localization criteria. *Journal of mathematical chemistry* **1991**, *8* (1), 169-178.
58. Bader, R.; Nguyen-Dang, T. T.; Tal, Y., A topological theory of molecular structure. *Reports on Progress in Physics* **1981**, *44* (8), 893.
59. Cortés-Guzmán, F.; Bader, R. F., Complementarity of QTAIM and MO theory in the study of bonding in donor-acceptor complexes. *Coordination Chemistry Reviews* **2005**, *249* (5-6), 633-662.

60. Bader, R. F.; Stephens, M. E., Spatial localization of the electronic pair and number distributions in molecules. *Journal of the American Chemical Society* **1975**, *97* (26), 7391-7399.
61. Daudel, R.; Bader, R.; Stephens, M.; Borrett, D., The electron pair in chemistry. *Canadian Journal of Chemistry* **1974**, *52* (8), 1310-1320.
62. Ponec, R., Electron pairing and chemical bonds. Chemical structure, valences and structural similarities from the analysis of the Fermi holes. *Journal of Mathematical Chemistry* **1997**, *21* (3), 323-333.
63. Ponec, R., Electron pairing and chemical bonds. Molecular structure from the analysis of pair densities and related quantities. *Journal of mathematical chemistry* **1998**, *23* (1-2), 85-103.
64. Bultinck, P.; Cooper, D. L.; Ponec, R., Influence of atoms-in-molecules methods on shared-electron distribution indices and domain-averaged fermi holes. *The Journal of Physical Chemistry A* **2010**, *114* (33), 8754-8763.
65. De Lange, J. H.; Van Niekerk, D. M. E.; Cukrowski, I., FALDI-based decomposition of an atomic interaction line leads to 3D representation of the multicenter nature of interactions. *Journal of Computational Chemistry* **2018**, *39* (16), 973-985.
66. Cooper, D. L.; Ponec, R.; Kohout, M., Are orbital-resolved shared-electron distribution indices and Cioslowski covalent bond orders useful for molecules? *Molecular Physics* **2015**, *113* (13-14), 1682-1689.
67. Schaller, R. R., Moore's law: past, present and future. *IEEE spectrum* **1997**, *34* (6), 52-59.

## Chapter 3.

# Development of a theoretical FALDI-based framework for the symmetry classifications of Molecular Orbitals in asymmetric Fischer Carbenes.

*Submitted to the Journal of Chemical Theory and Computation for consideration.*

*The chapter is presented here as the submitted manuscript.*

# Development of a theoretical FALDI-based framework for the symmetry classifications of Molecular Orbitals in asymmetric Fischer Carbenes.

Brent Nel, Jurgens Hendrik de Lange\*

Department of Chemistry, Faculty of Natural and Agricultural Sciences, University of Pretoria, Lynnwood Road, Hatfield, Pretoria 0002

*KEYWORDS Symmetry, Group Theory, FALDI, Fischer Carbene, Molecular Orbitals and DFT*

---

A novel approach to define symmetry terms in octahedral inorganic molecules is discussed. While the concept of group theory stands strong, only symmetric molecules are well accounted for. Classically the Molecular Orbitals (MOs) define symmetry through SALC's while this work introduces a DFT study with a Fragment, Atomic, Localised, Delocalized and Interatomic (FALDI) electron density decomposition approach that isolates an atom in terms of its orthodox localized electron density (loc-ED) and presents its Natural Density Functions (NDF's) to recovers classical symmetry terms with 3D representation. This classical symmetry defined through the NDF is linked to the corresponding MO's to fully recover the symmetry, stemmed from Molecular Orbital Theory with the addition of quantification allowing the determination of symmetry contributions. Verification was performed using the case study of (i)  $\text{Cr}(\text{CO})_6$  as the symmetric baseline and then expanded to the asymmetric Fischer Carbene of (ii)  $\text{Cr}(\text{CO})_5\text{C}(\text{OEt})(\text{Me})$ . The framework recovers a holistic symmetry definition for both cases, providing comprehensive an electronic definition for asymmetric molecules.

---

## Introduction

The relationship between the electronic structure and nuclear geometry of a molecule is an interesting and highly correlated one, even within the confines of the Born-Oppenheimer approximation: The nuclear geometry give rise to a potential field which lends structure to an otherwise uniform electron gas, but the distribution of electrons determines the degree to which nuclear-nuclear repulsion is shielded by nuclear-electron attraction.<sup>1</sup> This relationship between electronic and nuclear distributions can be very difficult to study, beyond obvious patterns of critical points in the topology of electron density. However, and perhaps luckily, the presence of molecular symmetry simplifies this relationship tremendously – group symmetry provides a description of both electronic and nuclear structure. In fact, the identification of symmetry in the nuclear geometries of molecules opened up the study of electronic structure within the approximation of the many-electron wavefunction into one-electron functions (orbitals).<sup>2</sup> For instance, in crystal field theory, identification of the point group symmetry of a transition metal complex often allows a surprisingly accurate description of the allowable electronic states of a molecule, which is easily extrapolated to orbital nomena.<sup>3,4</sup> The study of molecular symmetry, together with early pioneering in quantum chemistry, led to the development of one of the most useful interpretive theories in all of chemistry

– Molecular Orbital Theory (MOT).<sup>5</sup> Many new developments have been made since in the field of MOT<sup>6-9</sup>, whether experimental, theoretical or even pedagogical. In particular, with the advent of computational chemistry as a means to solving the Schrödinger equation variationally, molecular orbitals (MOs) can be fully determined for symmetrical as well as asymmetrical systems. Calculation does not necessarily mean comprehension, however, and the interpretation of MOs is still highly dependent on symmetry.

MOT is taught as *par of the course* in most undergraduate chemistry degrees,<sup>10</sup> in addition to (and often as the fundamentals of) many other advanced chemical concepts – such as Fischer Carbene complexes.<sup>11</sup> However, MOT in undergraduate courses are often restricted to simple and highly symmetrical systems. This stems from the complexity, as complex asymmetrical systems exponentially increase the complexity of MOs. In the classroom, MOT is usually introduced through the concept of Symmetry Adapted Linear Combinations of Atomic Orbitals (SALC-AOs) or, more simply, as Linear Combinations of Atomic Orbitals (LCAO).<sup>10</sup> SALCs link hydrogenic atomic orbitals (AO) to molecular-wide MOs, through the application of molecular symmetry. The underlying principle of LCAO is that atomic orbitals of a particular symmetry will have constructive overlap with other AOs of the same symmetry. The resultant MOs are therefore fully interpretable, as they stem from chemically-intuitive

atoms, functional groups and AOs. The MOs can then be used to interpret and explain many fundamental experimental results, such as UV spectra, reactivity and magnetism. The fundamental reliance of SALC-MOs on symmetry makes it a perfect model of electronic structure for chemistry students as well as experimental research chemists, as no advanced knowledge of quantum mechanics is required.

What then, of asymmetrical systems, such as the aforementioned Fischer carbene complexes? If SALC-MOs are fully determined by molecular symmetry, then the extreme interpretive and predictive power of MOT must be limited to only molecules with a significant degree of symmetry. Luckily, advances in quantum chemistry have allowed for the calculation of MOs variationally, usually through a self-consistent field (SCF). SCF-MOs can be generated for any molecular structure, regardless of symmetry. However, unlike SALC-MOs, SCF-MOs *cannot* be directly decomposed to atoms, functional groups and AOs. While many techniques exist which can aid the interpretation of SCF-MOs (including decomposing MOs into their underlying basis function contributions), none of these have the same transparency and ease of interpretation as SALC-MOs. Accordingly, experimentalists utilizing SCF-MOs often *roughly* classify MOs via visual inspection and attempt to apply the same principles of SALC-MOs for interpretation. This approach can be very misleading, as will be shown successively throughout this work.

SCF-MOs would reach the same level of utility as SALC-MOs if they could be classified in the same manner. In this proof-of-concept work, we introduce a novel method to classify SCF-MOs of transition metal complexes to allow them the same interpretation as for SALC-MOs. By doing so, the predictive power and ease-of-use of SALC-MOs are extended to computationally generated SCF-MOs, but without the massive limitation of symmetry. Our quantum chemical approach, based on the recently developed Fragment, Atomic, Localized, Delocalized and Interatomic (FALDI) electron density decomposition scheme,<sup>12,13</sup> are tested on two transition metal complexes – a well-studied symmetrical octahedral complex as well as an asymmetrical Fischer carbene complex.

## Computational Details

All structures were optimized using restricted B3LYP, with def2svp(p) basis set in Gaussian 09.<sup>24</sup> Atomic overlap matrices and Atomic populations were computed using AIMAll v. 17.01.25.<sup>25</sup> FALDI distributions were calculated using in-house software with the orthodox overlap algorithm. Isosurface visualization was performed with VMD 1.9.3.<sup>26</sup>

## Theoretical Background and Development

### *The FALDI density decomposition scheme.*

The FALDI scheme<sup>12, 13</sup> provides an exhaustive electron density (ED) decomposition at any coordinate  $\mathbf{r}$  into chemically relevant, atomistic components. Using concepts explored during the development of Domain Averaged Fermi Holes (DAFH)<sup>REF</sup>, FALDI quantifies pseudo-second-order electronic contributions that allows for insights into molecular-wide electron (de)localization patterns. FALDI is inherently dependent on a definition of an atomic basin, and, as for DAFH,

QTAIM’s atomic basins provides physically and chemically intuitive atomistic descriptions<sup>14</sup>. A brief discussion of the FALDI terms follows.

The exchange-correlation hole associated with an atomic basin  $\Omega_A$  can be found by integrating the well-defined electron hole over an atomic volume:

$$g_A(\mathbf{r}_1, \mathbf{r}'_1) = \int_{\substack{\Omega_A \\ \mathbf{r}_2 = \mathbf{r}'_2}} \rho_{xc}(\mathbf{r}_1, \mathbf{r}'_1; \mathbf{r}_2, \mathbf{r}'_2) d\mathbf{r}_2 \quad (1)$$

For simplicity, we will henceforth assume that  $\mathbf{r}_i = \mathbf{r}'_i$ , and we will drop the accented coordinates. The DAFH,  $g_A(\mathbf{r})$ , provides a molecular-wide distribution of the electrons localized to (when  $\mathbf{r} \in \Omega_A$ ) or delocalized with (when  $\mathbf{r} \notin \Omega_A$ ) the domain of atom A.  $g_A(\mathbf{r})$  is borrowed from DAFH-analysis, and is known as an *atom-ED* distribution in FALDI. Integration of  $g_A(\mathbf{r})$  over all molecular space provides a count of the total number of electrons found on average in  $\Omega_A$  – the atomic electron population  $N(A)$ :

$$\begin{aligned} N(A) &= \int_{\Omega_A} \rho(\mathbf{r}) d\mathbf{r} \\ &= \int_{\infty} g_A(\mathbf{r}) d\mathbf{r} \end{aligned} \quad (2)$$

Considering the difficulty in finding  $\rho_{xc}(\mathbf{r}_1; \mathbf{r}_2)$  for larger molecular systems and wavefunctions, a convenient one-electron approximation<sup>27</sup> can be utilized,

$$\begin{aligned} g_A(\mathbf{r}) &= \sum_{ij} \sqrt{v_i v_j} \chi_i(\mathbf{r}) \chi_j(\mathbf{r}) S_{ji}^A \\ &= \sum_{ij} G_{ji}^A S_{ji}^A \end{aligned} \quad (3)$$

where  $\chi(\mathbf{r})$  is a natural orbital with occupation  $v$ .  $S_{ji}^A$  is an element of the atomic overlap matrix (AOM) associated with  $\Omega_A$ :

$$S_{ji}^A = \sum_{ij} \int_{\Omega_A} \chi_i^*(\mathbf{r}) \chi_j(\mathbf{r}) d\mathbf{r} \quad (4)$$

which satisfies  $N(A) = \text{tr}(\mathbf{S}^A)$ . The one-electron approximation is exact in closed-shell restricted Hartree-Fock wavefunctions (with  $v = 2$ ), and has been recently<sup>28</sup> shown to be fairly accurate in correlated wavefunctions as well.

Localization and delocalization indices (LI and DI, respectively) are QTAIM-defined quantities<sup>28</sup> that provide useful insights into atomic and molecular electronic structures. In the same fashion that *atom-ED* distributions provide real-space representations of  $N(A)$ , so does FALDI also provide real-space distributions of LIs and DIs. Specifically, and still within the one-electron approximation in terms of AOMs, a *loc-ED* distribution,

$$\mathcal{L}_A(\mathbf{r}) = \sum_{ij} \chi_i(\mathbf{r}) \chi_j(\mathbf{r}) (\mathbf{G}^A \mathbf{S}^A)_{ji} \quad (5)$$

quantifies the contribution to the total ED at  $\mathbf{r}$  due to electrons localized to  $\Omega_A$ . Integration of any *loc-ED* distribution over all molecular space recovers the LI,  $\int_{\infty} \mathcal{L}_A(\mathbf{r}) d\mathbf{r} = \lambda(A)$ .

Similarly, a *deloc*-ED distribution can be defined as

$$D_{A,B}(\mathbf{r}) = \sum_{ij} \chi_i(\mathbf{r})\chi_j(\mathbf{r})(\mathbf{G}^A\mathbf{S}^B + \mathbf{S}^B\mathbf{G}^A)_{ji} \quad (6)$$

$D_{A,B}(\mathbf{r})$  provides the contribution to the total ED at  $\mathbf{r}$  due to electrons delocalized between basins  $\Omega_A$  and  $\Omega_B$ . Integration of any *deloc*-ED distribution over all molecular space recovers the DI,  $\int_{\infty} D_{A,B}(\mathbf{r})d\mathbf{r} = \delta(A,B)$ .

#### Natural Density Functions

Sets of orthogonal functions known as natural density functions (NDFs) can be generated by diagonalizing matrix products ( $\mathbf{S}^A\mathbf{S}^A$ ) and ( $\mathbf{S}^A\mathbf{S}^B + \mathbf{S}^B\mathbf{S}^A$ ). These matrix products are known as localized and delocalized matrices (LMAT and DMAT, respectively). The procedure described below illustrates the generation of NDFs for decomposing a *loc*-ED distribution, but the procedure is identical for decomposing *deloc*-ED distributions as well. Solving the eigenvalue problem for one of these matrix products,

$$\mathbf{G}^A\mathbf{S}^A\mathbf{U}^{AA} = \lambda^{AA}\mathbf{U}^{AA} \quad (7)$$

yields a set of eigenvalues that sum up to LI,  $LI(A) = \sum \lambda_i^{AA}$  and a collection of eigenvectors,  $\mathbf{U}^{AA}$ . The *loc*-ED distribution for atom A can then be decomposed,

$$\mathcal{L}_A(\mathbf{r}) = \sum_i^{N_{MO}} \lambda_i^{AA} [\phi_i^{AA}(\mathbf{r})]^2 \quad (8)$$

where  $\phi_i^{AA}(\mathbf{r})$  is known as an NDF:

$$\phi_i^{AA}(\mathbf{r}) = \sum_j^{N_{MO}} \chi_j(\mathbf{r})U_{ji}^{AA} \quad (9)$$

NDFs generated from an LMAT gives a set of  $N_{MO}$  localized functions (*loc*-NDFs) with occupation numbers  $\lambda_i^{AA}$ . The *loc*-NDFs with large occupation numbers (typically close to 2) closely resemble localized atomic orbitals, e.g.  $1s$ ,  $2p_z$  functions. Similarly, NDFs generated from a DMAT gives a set of  $N_{MO}$  delocalized functions (*deloc*-NDFs) with occupation numbers  $\delta_i^{AB}$ , with the largest occupied functions resembling typical bonding and antibonding MOs e.g.  $\sigma$  and  $\pi$  bonds.

#### MO classification

The shapes and occupation numbers of NDFs can provide very useful insights into the localization and delocalization patterns within a molecule, while remaining strictly atomistic in their interpretation. However, in this work, we are particularly interested in further analyzing the eigenvector matrices,  $\mathbf{U}^{AX}$ . Specifically, the eigenvectors of each LMAT or DMAT represents an MO basis through which the NDFs are expressed. Since NDFs provide highly localized functions that can describe chemical concepts such as atomic orbitals or bonding patterns, investigation of each NDF's MO composition provides insight into the nature of a specific MO.

The sum of squares of each column and row of  $\mathbf{U}^{AX}$  is equal to unity. Therefore, the relative contributions of each MO to the  $i$ th *loc*-NDF of atom A can be found by investigation of  $[U_{ji}^{AA}]^2$ . Conversely, the manner of how the  $i$ th MO is distributed over all *loc*-NDFs of atom A can be found by investigation of  $[U_{ij}^{AA}]^2$ . The same approach can be performed for the eigenvectors of a given DMAT as well.

The focus of this work revolves around classification of MOs in symmetric and asymmetric hexacoordinate metal complexes. Our general approach to do so follows. The *loc*-NDFs of a metal describes electrons found in typical atomic orbitals, and can be easily classified, through visual inspection of isosurfaces, in terms of electronic shells and subshells or  $O_h$  point-group symmetry classes. The *loc*-NDFs with occupation numbers close to 2 describe core electrons, whereas *loc*-NDFs with intermediate quantum numbers (between 0.5 and 1.5) describe valence electrons, which are only partially localized to the metal center. Once the *loc*-NDFs of the metal atom have been classified,  $[U_{ji}^{AA}]^2$  elements can be used to assign a weight to each MO relative to each NDF classification. Therefore, each MO can be fully classified in terms of how it contributes to electrons localized in various metallic atomic orbitals or  $O_h$  symmetry classes. In this work we are primarily focused on classifications based on  $O_h$  symmetry species, *i.e.*  $a_{1g}$ ,  $t_{1u}$ ,  $e_g$  and  $t_{2g}$ :

$$a_{1g}n_i^M + t_{1u}n_i^M + t_{2g}n_i^M + e_gn_i^M + N^Ln_i^M = 1 \quad (10)$$

where  $N^Ln_i^A$  captures the weights of MOs that does not localize electrons to atom A – *loc*-NDFs with negligible occupation numbers – and the superscript ‘M’ specifically refers to the metal atom.

The above approach can then be further extrapolated to diatomic delocalized ED. The total number of electrons delocalized between the metal atom and any other atom,  $DI(M,B)$ , can be easily decomposed in terms of various MO contributions through the DMAT,

$$d_i^{M,B} = \sum_j^{N_{MO}} (\mathbf{G}^A\mathbf{S}^B + \mathbf{S}^B\mathbf{G}^A)_{ij} \quad (11)$$

with  $DI(M,B) = \sum d_i^{M,B}$ . Each MO contribution can then be effectively filtered through the classification scheme based on the metal's *loc*-NDFs,

$$DI(M,B) = \sum_i^{N_{MO}} d_i^{A,B} [a_{1g}n_i^M + t_{1u}n_i^M + t_{2g}n_i^M + e_gn_i^M + N^Ln_i^M] \quad (12)$$

providing the contributions of each symmetry class to  $DI(M,B)$ .

## Results and Discussion

### Symmetrical – $Cr(CO)_6$

$Cr(CO)_6$  is a model compound for the study of electronic structure, which makes it an ideal case study for the development of a framework for MO deconstruction.  $Cr(CO)_6$  has 54 canonical MOs (many of which are fully delocalized across the all atomic basins) and no unpaired electrons. MOs can be classified using Symmetry Adapted Linear Combinations (SALCs) of atomic and ligand orbitals, and based on the  $O_h$  symmetry<sup>15</sup> in  $Cr(CO)_6$ . The six CO ligands' valence orbitals form sets of SALCs with  $a_{1g}$ ,  $t_{1u}$  and  $e_g$  symmetries and their unoccupied orbitals form SALCs with  $t_{2g}$  symmetries. The metal ion's occupied valence AOs have  $e_g$  and  $t_{2g}$  symmetries,

while the lowest unoccupied AOs are  $a_{1g}$  and  $t_{1u}$  orbitals – in line with classical interpretations.<sup>16-18</sup>

The completed conceptual MO diagram (MOD) of  $\text{Cr}(\text{CO})_6$  is shown in Figure 1, together with isosurfaces of SCF-MOs as 3D representations. Ligand SALCs and Cr AOs that share a symmetry species couple to form bonding and antibonding MO-pairs. In general, ligand SALCs with  $a_{1g}$  and  $e_g$  are lower in energy than the corresponding Cr  $4s$  and  $3d$  ( $e_g$ ) AOs, and the resulting MOs are therefore ligand-centred with  $\sigma$ -characters (i.e.  $\sigma$ -donating orbitals). On the other hand,  $3d$  ( $t_{2g}$ ) orbitals on the metal overlap with unoccupied  $\pi^*$  ligand SALCs, resulting in metal-centred MOs with  $\pi$ -characters (i.e.  $\pi$ -accepting

orbitals).<sup>17</sup> Finally, unoccupied  $4p$  Cr AOs can form  $\sigma$ - and  $\pi$ -MOs with  $t_{1u}$  ligand orbitals. Lower energy orbitals (i.e. core orbitals) are usually assumed to be non-bonding in the SALC model, as are  $t_{1g}$  and  $t_{2u}$  ligand orbitals for which no corresponding Cr AOs are present.

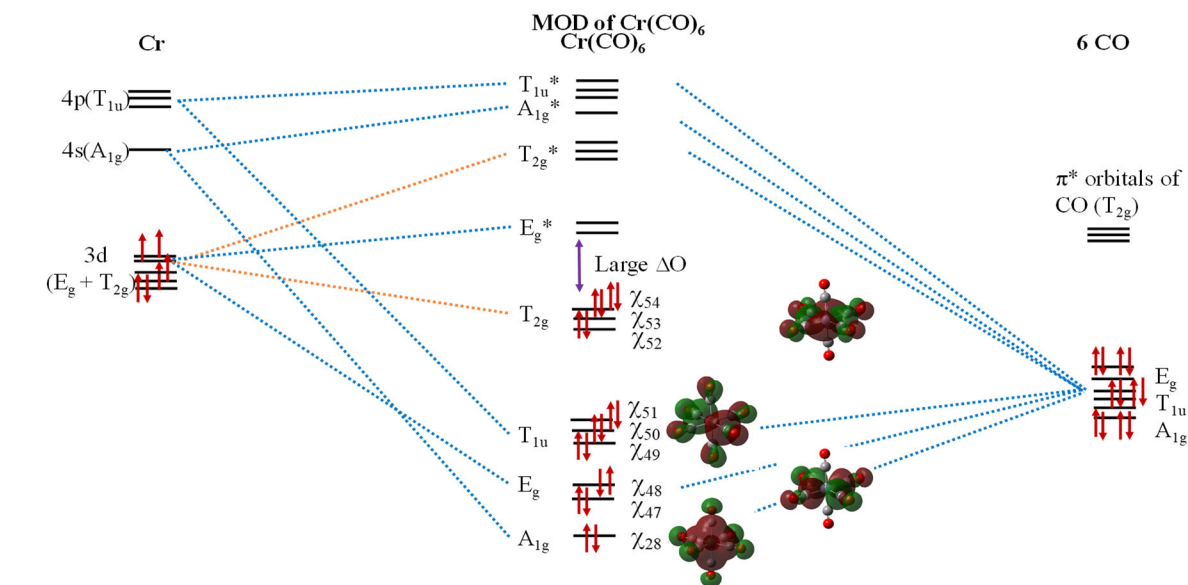


**Figure 1.** Reduced Molecular Orbital Diagram of  $\text{Cr}(\text{CO})_6$ , illustrating the MOs arising from the SALCs. Selected MO isosurfaces are shown at isovalues of 0.001 au.

orbitals).<sup>17</sup> Finally, unoccupied  $4p$  Cr AOs can form  $\sigma$ - and  $\pi$ -MOs with  $t_{1u}$  ligand orbitals. Lower energy orbitals (i.e. core orbitals) are usually assumed to be non-bonding in the SALC model, as are  $t_{1g}$  and  $t_{2u}$  ligand orbitals for which no corresponding Cr AOs are present.

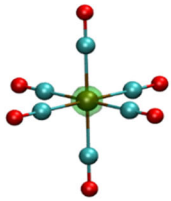
The symmetry present in the complex therefore allows for a full characterization of the canonical MOs and allows for strong insights into the complex's electronic structure, stability, photophysical behavior and reactivity. Each MO can be clearly labelled, and the associated bonding mode (e.g.  $\sigma$  or  $\pi$ ) can be easily recovered. The computationally-generated SCF-MOs are also exactly equivalent to group-theory-generated SALC-MOs. We will now apply the method discussed in the Theoretical Background and Development on the symmetrical  $\text{Cr}(\text{CO})_6$  complex. A set of FALDI-defined, *loc*-NDFs associated with the Cr atom can be generated through diagonalization of Cr's LMAT and is illustrated in Figure 2. Due to the *loc*-NDF's orthogonality, each *loc*-NDF is associated with a metal AO and can be characterized based on its symmetry in an  $O_h$  field. Therefore, the same symmetry terms as found in the conceptual AOs of Cr (Figure 1) apply to the *loc*-NDFs, but without the need to fragment the complex and consider the metal as a free atom. In addition, and as we shall show later, the *loc*-NDFs retain their symmetries even in asymmetrical complexes. The occupation value of each *loc*-NDF (as shown on Figure 2,  $\lambda^i$ )

predominantly involved in bonding. Finally, *loc*-NDFs 15 to 18 correspond to  $4s_{\text{Cr}}$  and  $4p_{\text{Cr}}$  AOs, and their almost 0.0 occupation values correspond with the accepting nature of these orbitals.

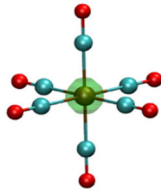
The NDF's are related to MOs through Eq. 9. The MO constituents of a single *loc*-NDF can be calculated, and an example is shown in Figure 3: *loc*-NDF 10 of the Cr atom, of  $t_{2g}$  symmetry, is primarily composed of  $\chi_{53}$ , also of  $t_{2g}$  symmetry (as classified by the SALC approach). Another example is given in Figure 4, where *loc*-NDF 15 (associated with the  $4s_{\text{Cr}}$  AO) is composed of almost two equal  $a_{1g}$  MOs. Conversely, the contributions of a single MO to all FALDI distributions (*loc*- and *deloc*-EDs, as well as their NDFs) can also be calculated. In this manner, each MO in a metal complex can be classified based on its contributions to the *loc*-NDFs of the metal, even in asymmetric complexes. Doing so for  $\text{Cr}(\text{CO})_6$  exactly recovers the MOD given in Figure 1.

Furthermore, a classification of MOs can then be used to investigate and characterize the MOs that contribute to electrons involved in a specific chemical bond or diatomic interaction. We will now demonstrate this approach on a Cr-C bond in  $\text{Cr}(\text{CO})_6$ .

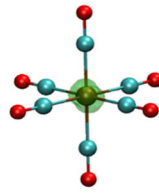




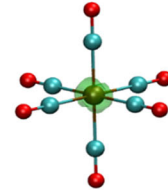
*loc*-NDF1<sup>a</sup> (*1s*)  
 $\lambda^1(\text{Cr1}) = 2.00$



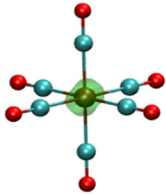
*loc*-NDF2<sup>a</sup> (*2s*)  
 $\lambda^2(\text{Cr1}) = 2.00$



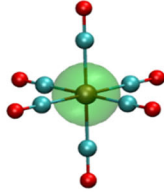
*loc*-NDF3<sup>a</sup> (*2p*)  
 $\lambda^3(\text{Cr1}) = 2.00$



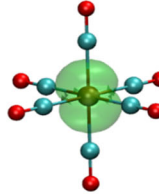
*loc*-NDF4<sup>a</sup> (*2p*)  
 $\lambda^3(\text{Cr1}) = 2.00$



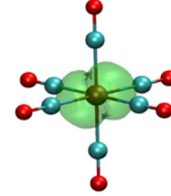
*loc*-NDF5<sup>a</sup> (*2p*)  
 $\lambda^5(\text{Cr1}) = 2.00$



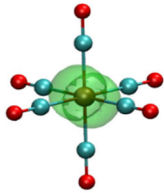
*loc*-NDF6<sup>b</sup> (*3s*)  
 $\lambda^6(\text{Cr1}) = 1.99$



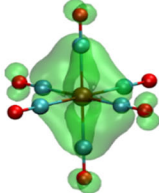
*loc*-NDF7<sup>b</sup> (*3p*)  
 $\lambda^7(\text{Cr1}) = 1.96$



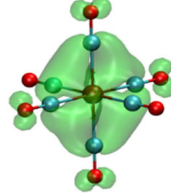
*loc*-NDF8<sup>b</sup> (*3p*)  
 $\lambda^8(\text{Cr1}) = 1.96$



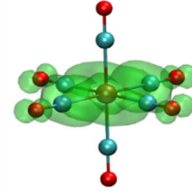
*loc*-NDF9<sup>b</sup> (*3p*)  
 $\lambda^9(\text{Cr1}) = 1.96$



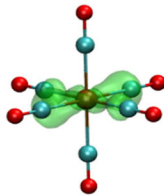
*loc*-NDF10<sup>b</sup> (*t<sub>2g</sub>*)  
 $\lambda^{10}(\text{Cr1}) = 0.60$



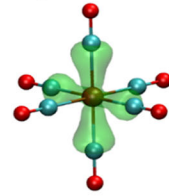
*loc*-NDF11<sup>b</sup> (*t<sub>2g</sub>*)  
 $\lambda^{11}(\text{Cr1}) = 0.60$



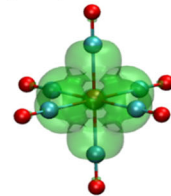
*loc*-NDF12<sup>b</sup> (*t<sub>2g</sub>*)  
 $\lambda^{12}(\text{Cr1}) = 0.60$



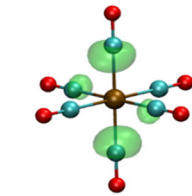
*loc*-NDF13<sup>b</sup> (*e<sub>g</sub>*)  
 $\lambda^{13}(\text{Cr1}) = 0.11$



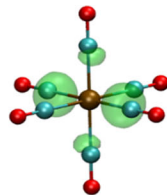
*loc*-NDF14<sup>b</sup> (*e<sub>g</sub>*)  
 $\lambda^{14}(\text{Cr1}) = 0.11$



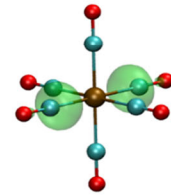
*loc*-NDF15<sup>b</sup> (*a<sub>1g</sub>*)  
 $\lambda^{15}(\text{Cr1}) = 0.03$



*loc*-NDF16<sup>b</sup> (*t<sub>1u</sub>*)  
 $\lambda^{16}(\text{Cr1}) = 0.01$



*loc*-NDF17<sup>b</sup> (*t<sub>1u</sub>*)  
 $\lambda^{17}(\text{Cr1}) = 0.01$



*loc*-NDF18<sup>b</sup> (*t<sub>1u</sub>*)  
 $\lambda^{18}(\text{Cr1}) = 0.01$

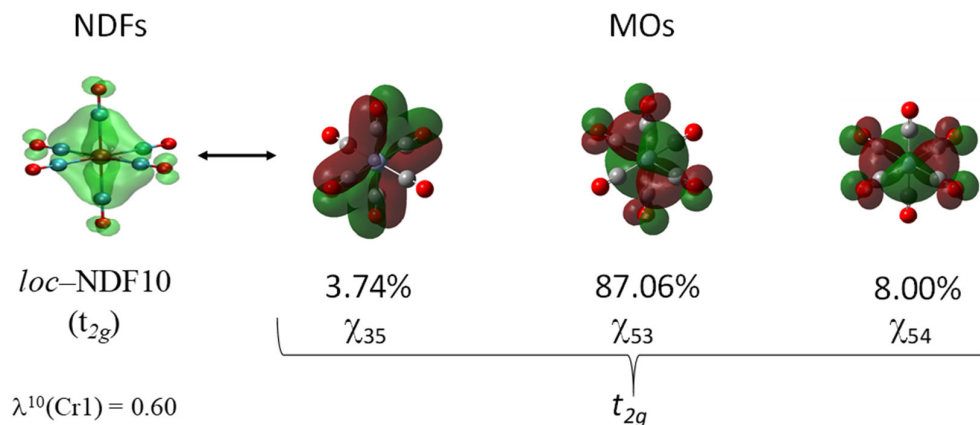


**Figure 3.** The Natural Density Functions corresponding to their respective Molecular Orbitals with their contributions. Illustrating the tenth NDF which represents  $t_{2g}$  symmetry on the Cr linked to the contributing occupied MOs.

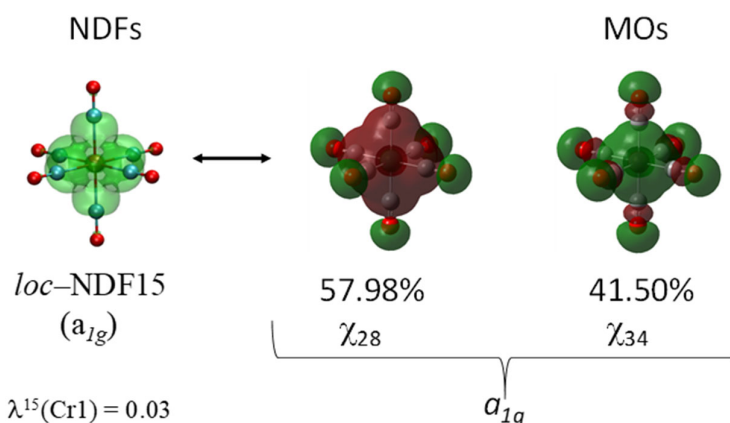


**Figure 4.** The Natural Density Functions corresponding to their respective Molecular Orbitals with their contributions. Illustrating the fifteenth NDF which represents  $a_{1g}$  symmetry on the Cr linked to the contributing occupied MOs.

**Table 1.** The total FALDI-classified symmetry composition of the Cr1–C2 bond in  $\text{Cr}(\text{CO})_6$

<i>FALDI-classified Symmetry<sup>a</sup></i>	Contribution to DI(Cr,C)	Relative MO contribution to DI(Cr1,C2)
$a_{1g}$	0.041	5.0%
$t_{1u}$	0.090	11.0%
$t_{2g}$	0.322	39.2%
$e_g$	0.189	23.0%
NL	0.180	21.9%
<i>Total</i>	<i>0.822</i>	

In order to classify the electrons associated with the Cr–C bond, we proceeded with the following procedure: First, we classified each canonical MO based on its contributions to Cr's *loc*-NDFs, as discussed above and illustrated in Figures 3 and 4. Then, the contributions of each MO to the delocalization index of a Cr–C bond was calculated, as  $\text{DI}(\text{Cr}, \text{C}) = \sum d_i^{\text{Cr,C}}$  (Eqn. 11). Finally, the contributions to  $\text{DI}(\text{Cr1}, \text{C2})$  was grouped into FALDI-classified symmetry groups, based on the *loc*-NDF classifications (Eqn. 12); the results are shown in Table 1. The total  $\text{DI}(\text{Cr1}, \text{C2})$  is 0.822, indicating a *covalent* bond order of slightly less than a single bond and excluding the electronic contributions from dative-covalent electrons. Of the total number of electrons shared, the majority (39.2%) is shared through MOs classified as  $t_{2g}$  character, which corresponds to  $\pi$ -backbonding. MOs with  $e_g$ ,  $a_{1g}$  and  $t_{1u}$  character make up  $\sigma$ -bonds, contributing small amounts individually but summed to a total of 39.0% of the shared electrons. Therefore, in the well-studied  $\text{Cr}(\text{CO})_6$  molecule, our results correspond perfectly with previously reported valence-bond results<sup>21</sup> that suggest equal  $\sigma$ - and  $\pi$ -

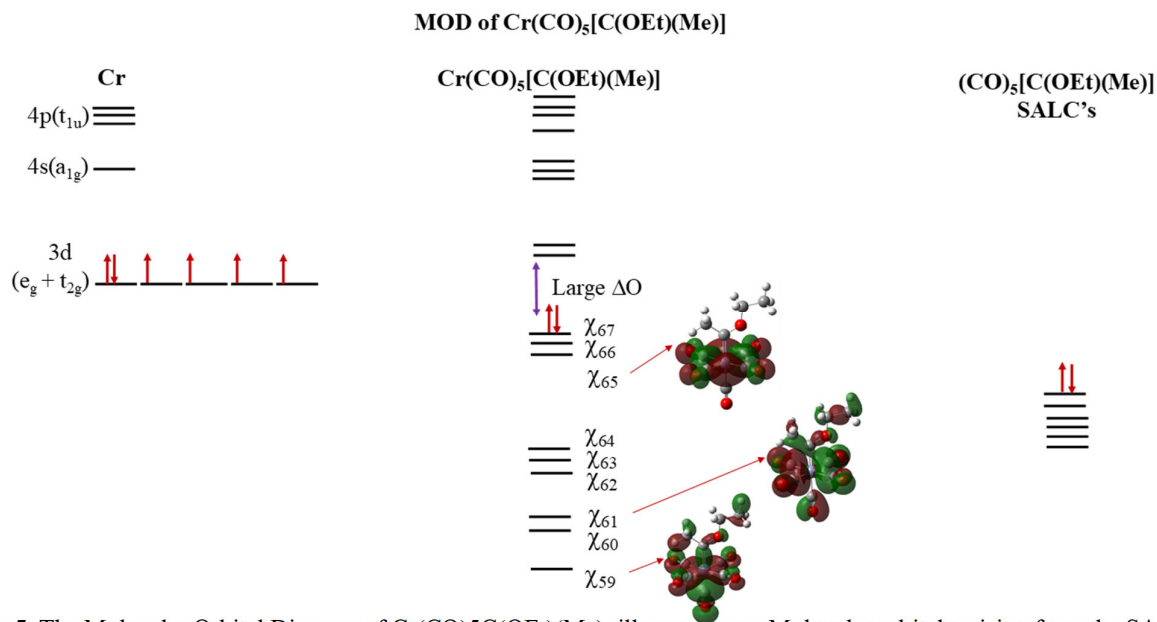


**Figure 5.** The Molecular Orbital Diagram of Cr(CO)<sub>5</sub>C(OEt)(Me), illustrating the Molecular orbitals arising from the SALCs. A single Molecular Orbital (59, 61 and 65) are illustrated to show mixed and non-degenerate orbitals are present.

characters. Furthermore, the remaining 21.9% of the total number of electrons shared are classified as ‘NL’ or MOs ‘non-localized’ to the metal. These MOs typically are fully delocalized across the ligand system, and their substantial contribution to DI(Cr,C) suggests multi-centric effects.

The fact that our method exactly recovered the SALC-defined MOD, with identical classification, as well as contemporary experiments related to the Cr–C bond shows that the FALDI classification is fully corroborating of the symmetry-based model. Next, we investigate and interpret what SALC-MOs cannot do – an asymmetrical metal complex.

#### *Asymmetrical – Cr(CO)<sub>5</sub>C(OEt)(Me)*

Replacing one of the carbonyl ligands in Cr(CO)<sub>6</sub> with a alkoxy-carbene group (:C(OR)R') yields a very simple Fischer carbene complex. We consider here the

structure with R=OEt and R'=Me. Many of the SALCs of the Fischer carbene remain qualitatively comparable to the SALCs of Cr(CO)<sub>6</sub> due to the pentacarbonyl metal cluster. However, unlike Cr(CO)<sub>6</sub>, Cr(CO)<sub>5</sub>C(OEt)(Me) only has C<sub>1</sub> symmetry – no symmetry operations beyond the identity operation. Therefore, none of the SALCs can be accurately classified in terms of an octahedral field – rather, formal group theory classifies every MO simply as *a*. While symmetry for some of the MOs can be assumed,<sup>1</sup> doing so removes any accurate or quantitative insight regarding the physical and chemical properties of the molecule.

The conceptual MOD of Cr(CO)<sub>5</sub>C(OEt)(Me), with isosurfaces of selected SCF-MOs included, is shown in Figure 5. Figure 5 is bland in comparison to Figure 1 and much less information can be retrieved, and no direct link to Cr AOs or ligand SALCs can be made. The best attempt at symmetry labels is a “shotgun”

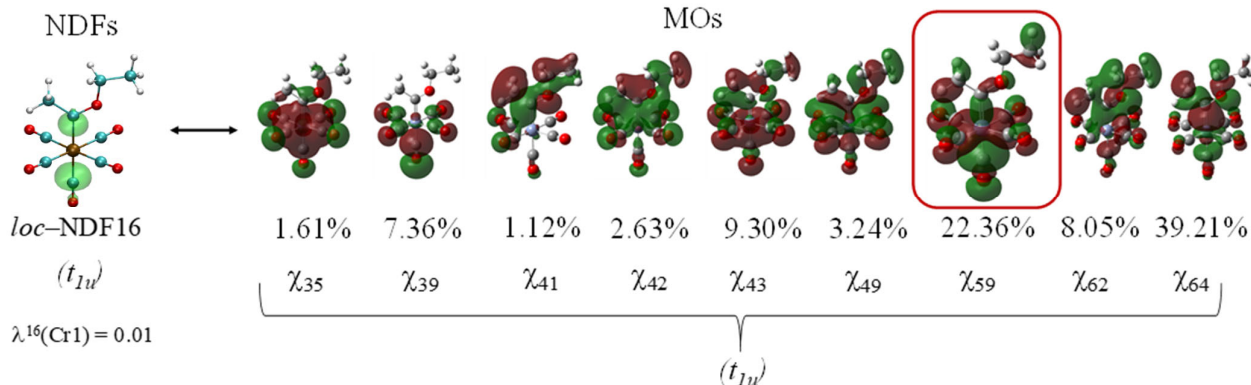


**Figure 6.** The Natural Density Functions corresponding to their respective Molecular Orbitals with their contributions. Illustrating the thirteenth NDF which represents E<sub>g</sub> symmetry on the Cr linked to the contributing occupied MO's.

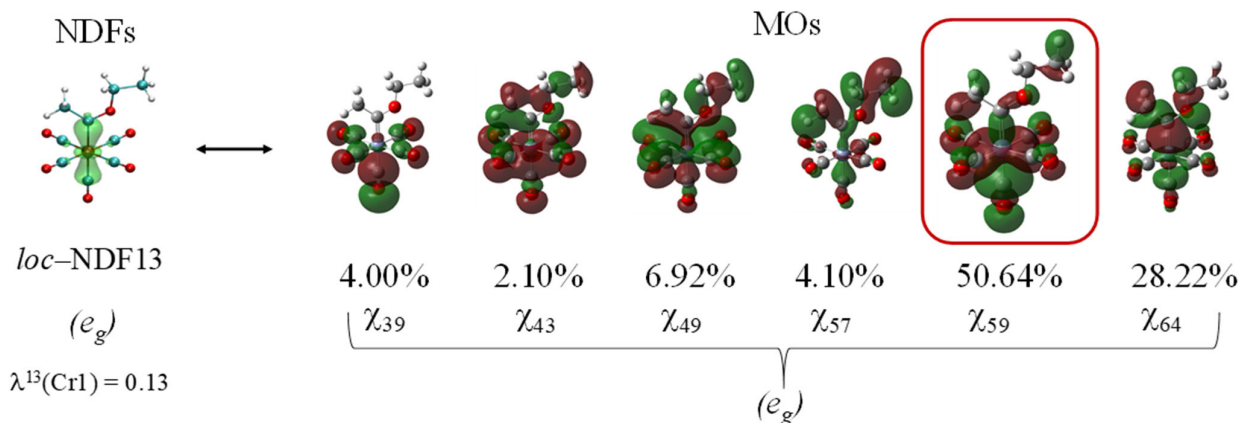


**Figure 7.** The Natural Density Functions corresponding to their respective Molecular Orbitals with their contributions. Illustrating the sixteenth NDF which represents  $T_{1u}$  symmetry on the Cr linked to the contributing occupied MO's.

approach of guessing the symmetry and then linking the SALCs to the MOs. For instance, consider the isosurface of  $\chi_{59}$  in Figure 5. This MO looks to involve the  $3d_{z^2}$  AO on Cr, which would give it  $e_g$  character. However, it is easy to argue that the same MO contains significant  $t_{1u}$  character as well. With no known method to accurately quantify the MOs, interpreting MOs based on their visual character remains a very inaccurate guessing game. We attempt to remove the need for guesses next, using our FALDI approach to classify MOs in the Fischer carbene complex.

Classified *loc*-NDFs of Cr in  $\text{Cr}(\text{CO})_5(\text{OEt})(\text{Me})$  are shown in Figure S2 of the SI, as the analogy of Figure 2 for  $\text{Cr}(\text{CO})_6$ . Importantly, while individual *loc*-NDFs occupation values as well as ordering might differ between the two molecules, the general symmetry and shapes of the NDFs remain identical. Therefore, the same underlying AOs for the Cr atom are recovered by FALDI's *loc*-NDFs for both symmetrical and asymmetrical complexes.

Figures 6 and 7 illustrate the decomposition of two classified *loc*-NDFs into sets of MOs. Due to the asymmetry in the molecule, same MOs are now contributing to multiple NDFs. For instance,  $\chi_{59}$  (blocked in Figures 6 and 7) contributes to both NDF 13 (50.64%) and 16 (22.36%), and the remaining 27.00% is distributed over a variety of other MOs. Therefore, it is fitting to say approximately half of  $\chi_{59}$  is made up of contributions with  $e_g$  symmetry and a quarter is  $t_{1u}$  – accurately answering the question stated above regarding the nature of this MO. The decomposition of all MOs is significantly more complex for the asymmetrical system and must be performed algorithmically; however, this valuable information allows for a much deeper conceptual understanding of the electronic structure of the molecule. MOs can be classified based on dominant contributions, or the partial symmetry of each MO can be retained during further analysis. After classification MOs can be interpreted in the same manner in an asymmetrical complex as for a symmetrical complex.

As illustration, we again decompose the Cr–C<sub>CO</sub> bond, as well as the Cr=C<sub>carbene</sub> bond in terms of classified MO symmetries. Specifically, decomposition of the DMAT allows for MO contributions to the  $\text{DI}(\text{Cr},\text{C})$  or count of covalently shared electrons. Table 2 captures the decomposition of  $\text{DI}(\text{Cr1},\text{C2})$  – the Cr–C<sub>CO</sub> bond *trans* to the carbene fragment. A total of  $0.817 e^-$  are shared between Cr and the *trans* CO's carbon atom – of which 42.3% is contributed by MOs classified by our approach as  $t_{2g}$  symmetry ( $\pi$ -backbonding). MOs classified as  $a_{1g}$ ,  $t_{1u}$  and  $e_g$  contribute a total of 29% to  $\text{DI}(\text{Cr1},\text{C2})$ . Therefore, the *trans* Cr–C<sub>CO</sub> bond in the Fischer carbene complex, while associated with a similar total number of electrons shared as a Cr–C<sub>CO</sub> bond in  $\text{Cr}(\text{CO})_6$ , show quite a significantly different MO decomposition. Specifically, in the Fischer carbene complex, the Cr–C<sub>CO</sub> bond has a much larger  $t_{2g}$  character but smaller  $\sigma$ -character ( $a_{1g}$ ,  $t_{1u}$  and  $e_g$ ). These associations can be directly traced to the underlying classified MOs for further, in-depth analysis, especially with similarly classified MOs in  $\text{Cr}(\text{CO})_6$ . It also illustrates the *trans*-effect, showing the larger degree of  $\pi$ -bonding in the ligand *trans* to the carbene carbon.

Table 3, on the other hand, shows the decomposition of  $\text{DI}(\text{Cr1},\text{C12})$  – the electrons delocalized across the Cr–C<sub>carbene</sub> bond. A slightly smaller (relative to the Cr–C<sub>CO</sub> bond) total number of electrons are shared ( $0.705 e^-$ ), with a considerably smaller  $\pi$ -character ( $t_{2g}$ -classified MOs only contribute 26.9%) but much larger  $\sigma$ -character ( $e_g$ ,  $a_{1g}$  and  $t_{1u}$ -classified MOs contribute a sum of 41.1%). Furthermore, the non-localized contributions contribute a considerable 32.0% to  $\text{DI}(\text{Cr1},\text{C12})$ , indicating a significant multi-centric character to the Cr–C<sub>carbene</sub> bond. While other quantum chemical approaches arrived<sup>2</sup> to much the same conclusion regarding the nature of the Cr–C<sub>carbene</sub> bond, our approach is – to our knowledge – the first to do so from a fully MO point of view.

**Table 2.** The total FALDI-classified symmetry composition of the Cr1–C<sub>CO</sub> bond in Cr(CO)<sub>5</sub>C(OEt)(Me)

<i>FALDI-classified Symmetry<sup>a</sup></i>	Contribution to DI(Cr,C)	Relative MO contribution to DI(Cr1,C2)
a <sub>1g</sub>	0.018	2.2%
t <sub>1u</sub>	0.081	9.9%
t <sub>2g</sub>	0.346	42.3%
e <sub>g</sub>	0.138	16.9%
NL	0.235	28.7%
<i>Total</i>	<i>0.817</i>	

**Table 3.** The total FALDI-classified symmetry composition of the Cr1–C<sub>carbene</sub> bond in Cr(CO)<sub>5</sub>C(OEt)(Me)

<i>FALDI-classified Symmetry<sup>a</sup></i>	Contribution to DI(Cr,C)	Relative MO contribution to DI(Cr1,C2)
a <sub>1g</sub>	0.067	9.5%
t <sub>1u</sub>	0.130	18.4%
t <sub>2g</sub>	0.190	26.9%
e <sub>g</sub>	0.093	13.2%
NL	0.225	32.0%
<i>Total</i>	<i>0.705</i>	

## Conclusion

Molecular Orbital Theory provides a fantastic insight into the electronic structure of transition metal complexes, and is fully derivable from both first-principled quantum mechanics or conceptual group theory. While MOs can be generated computationally for any metal complex, exact interpretation of MOs are generally restricted to symmetrical systems.

The FALDI-based framework developed in this work fully recovers MO symmetries (a<sub>1g</sub>, t<sub>1u</sub>, e<sub>g</sub> and t<sub>2g</sub>) in symmetrical, octahedral metal complexes. Each MO is classified based on its contribution to the central metal ion's atomic electronic structure, determined through first-principle quantum mechanics in the form of FALDI's *loc*-NDFs. However, our approach was also applied to an asymmetrical structure – that of a simple Fischer carbene complex. Still, our approach could classify as well as quantify the relative symmetry contribution of each MO, thereby allowing full interpretation of the electronic structure in terms of MOs.

As proof of concept, we illustrated how the density delocalized among the Cr atom and its neighbouring carbon atoms can be decomposed into symmetry-classified MO groups. In this regard, we fully recovered existing models describing Cr–C<sub>CO</sub> or Cr–C<sub>carbene</sub>, but without the need for unphysical fragmentation or appeal to classical chemical theory. Rather, our approach is (to our knowledge) the first to fully describe the underlying electronic structure of any

given diatomic interaction in terms of fully interpretable MOs, regardless of the nuclear geometry.

While our approach is currently implemented and developed for mono-metallic transition metal complexes, we do not foresee any reason why the approach cannot be extrapolated to any chemical compound. The development of such an approach could provide a universal MOT that is fully interpretable, quantifiable, chemically intuitive and without any restrictions imposed by symmetry.

## AUTHOR INFORMATION

Corresponding Author

*Jurgens Hendrik de Lange*

*E-mail: jurgens.delange@up.ac.za*

## Present Addresses

Department of Chemistry, Faculty of Natural and Agricultural Sciences, University of Pretoria, Lynnwood Road, Hatfield, Pretoria 0002, South Africa.

## Author Contributions

The manuscript was written through contributions of all authors.

## REFERENCES

1. Popelier, P.; Aicken, F.; O'Brien, S., Atoms in molecules. *Chemical Modelling: Applications and Theory* 2000, 1, 143-198.
2. McNaught, A.; Wilkinson, A.; NIC, M., Iupac. Compendium of Chemical Terminology,(the " Gold Book"). 2006. International Union of Pure and Applied Chemistry.
3. Vincent, A., Molecular symmetry and group theory : a programmed introduction to chemical applications. 2nd ed; Wiley: Chichester, 2000.
4. Gryn'ova, G.; Coote, M. L.; Corminboeuf, C., Theory and practice of uncommon molecular electronic configurations. *Wiley Interdisciplinary Reviews: Computational Molecular Science* 2015, 5 (6), 440-459.
5. Pople, J. A.; Beveridge, D. L., Molecular orbital theory. C0., NY 1970.
6. Serrano-Andrés, L.; Merchán, M.; Nebot-Gil, I.; Lindh, R.; Roos, B. O., Towards an accurate molecular orbital theory for excited states: Ethene, butadiene, and hexatriene. *The Journal of chemical physics* 1993, 98 (4), 3151-3162.
7. Brown, D. A.; Chambers, W.; Fitzpatrick, N., Molecular orbital theory of transition metal complexes. *Inorganica Chimica Acta Reviews* 1972, 6, 7-30.
8. Hehre, W. J.; Radom, L.; Schleyer, P. v. R.; Pople, J. A., *AB initio molecular orbital theory*. Wiley: New York, 1990.
9. Tsaparlis, G., Atomic orbitals, molecular orbitals and related concepts: Conceptual difficulties among chemistry students. *Research in Science Education* 1997, 27 (2), 271.

10. Cass, M. E.; Hollingsworth, W. E., Moving beyond the single center-Ways to reinforce molecular orbital theory in an inorganic course. *Journal of Chemical Education* 2004, 81 (7), 997.
11. Montgomery, C. D., Fischer and Schrock Carbene Complexes: A Molecular Modeling Exercise. *Journal of Chemical Education* 2015, 92 (10), 1653-1660.
12. De Lange, J. H.; Cukrowski, I., Toward deformation densities for intramolecular interactions without radical reference states using the fragment, atom, localized, delocalized, and interatomic (FALDI) charge density decomposition scheme. *Journal of computational chemistry* 2017, 38 (13), 981-997.
13. Bultinck, P.; Cooper, D. L.; Ponec, R., Influence of atoms-in-molecules methods on shared-electron distribution indices and domain-averaged fermi holes. *The Journal of Physical Chemistry A* 2010, 114 (33), 8754-8763.
14. Savin, A.; Nesper, R.; Wengert, S.; Fässler, T. F., ELF: The electron localization function. *Angewandte Chemie International Edition in English* 1997, 36 (17), 1808-1832.
15. de Lange, J. H.; Cukrowski, I., Exact and exclusive electron localization indices within QTAIM atomic basins. *Journal of Computational Chemistry* 2018, 39 (20), 1517-1530.
16. Foresman, J. B.; Frisch, A., *Exploring chemistry with electronic structure methods*. 3 ed. ed.; Gaussian: Wallingford, Conn., 2015.
17. Rydberg, P., The accuracy of geometries for iron porphyrin complexes from density functional theory. *Journal of Physical Chemistry A*, The 2009, 113 (43), 11949.
18. Pollak, C.; Rosa, A.; Baerends, E. J., Cr-CO Photodissociation in Cr(CO)<sub>6</sub>: Reassessment of the Role of Ligand-Field Excited States in the Photochemical Dissociation of Metal-Ligand Bonds. *Journal of the American Chemical Society* 1997, 119 (31), 7324-7329.
19. Schreiner, A. F.; Brown, T. L., A semiempirical molecular orbital model for Cr(CO)<sub>6</sub>, Fe(CO)<sub>5</sub>, and Ni(CO)<sub>4</sub>. *Journal of the American Chemical Society* 1968, 90 (13), 3366-3374.
20. Johnson, J. B.; Klemperer, W. G., A molecular orbital analysis of electronic structure and bonding in chromium hexacarbonyl. *Journal of the American Chemical Society* 1977, 99 (22), 7132-7137.
21. Pauling, L., The chromium-carbon bond length in chromium hexacarbonyl. *Acta Crystallographica Section B* 1968, 24 (7), 978-979.
22. Wang, C.-C.; Wang, Y.; Liu, H.-J.; Lin, K.-J.; Chou, L.-K.; Chan, K.-S., Bond characterization of chromium-fischer carbene complexes: a combined study of experiment and theory. *The Journal of Physical Chemistry A* 1997, 101 (47), 8887-8901.
23. Darensbourg, M. Y.; Darensbourg, D. J., Spectroscopic studies of some carbene pentacarbonyl complexes of chromium(0) and tungsten(0). *Inorganic Chemistry* 1970, 9 (1), 32-39.
24. Frisch, M.; Trucks, G.; Schlegel, H. B.; Scuseria, G. E.; Robb, M. A.; Cheeseman, J. R.; Scalmani, G.; Barone, V.; Mennucci, B.; Petersson, G., *Gaussian 09, Revision d. 01*, Gaussian, Inc., Wallingford CT 2009, 201.
25. Keith, T. A., *AIMAll (Version 17.01. 25). TK Gristmill Software, Overland Park KS, USA 2017*.
26. Humphrey, W.; Dalke, A.; Schulten, K., VMD: visual molecular dynamics. *Journal of molecular graphics* 1996, 14 (1), 33-38.
27. Müller, A. *Phys. Lett. A* 1984, 105, 446-452.
28. Cooper, D. L.; de Lange, J. H.; Ponec, R. Comparison of DAFH and FALDI-like approaches, *Theoretical Chemistry Accounts*, 2020, 139, 1-14.

## **Chapter 4.**

**FALDI Molecular Orbital Fragment  
Analysis to identify bonding modes in  
various Fischer carbene complexes.**

## Abstract

The Fragment, Atomic, Localized, Delocalized and Interatomic (FALDI) electron density decomposition scheme coupled with molecular orbital (MO) analysis is used to investigate eight Fischer carbene complexes. The FALDI-MO approach is further expanded to provide MO characterization of the interactions of molecular fragments. The approach is illustrated on various Fischer carbene complexes with a  $\text{Cr}(\text{CO})_5\{\text{C}(\text{X})(\text{R})\}$  skeleton where the X-group is  $\text{X}=\text{OEt}$  or  $\text{NMe}_2$  and the R-groups are  $\text{R}=\text{-H}$ ,  $\text{-CCH}$ ,  $\text{-CHCH}_2$ ,  $\text{-CHCHPh}$ . We investigated the effects of various geometric and electronic variables with rigorous decomposition focusing on the bonding and interactions in terms of MOs. Our approach recovers inter-fragment bonding modes such as  $\sigma$ - and  $\pi$ -character, accounting for the electronic effects that are caused by changing the X- or R-group in the complex. Changing the X- or R-group clearly affects the electronic structure, and we identify the exact MO effect using the FALDI MO analysis.

## Introduction

One of the primary applications of Fischer carbene complexes is catalyzing organic transformations under mild reaction conditions.<sup>1</sup> However, their applications have been expanding recently to fields such as bioorganometallics,<sup>2</sup> material chemistry<sup>3</sup> and sugar-derived gelators,<sup>4</sup> and one of the unique uses of Fischer carbenes is that they can undergo almost any kind of cycloaddition.<sup>5-8</sup> The electronic structure of Fischer carbene complexes are also quite unique, and can offer fundamental insights to conceptual chemical models. As such, Fischer carbenes are often studied theoretically using quantum chemical methods. The focus of most theoretical studies on Fischer carbene complexes to date has been on the metal–carbene double bond, mostly due to the fact that many Fischer carbene reactions typically depend on breaking the  $\text{M}\cdots\text{C}_{\text{carbene}}$  bond. However, Fischer carbene complexes exhibit very interesting electronic structures, and their chemical and physical properties highly depend on the nature of the ligands bonded to the metal.

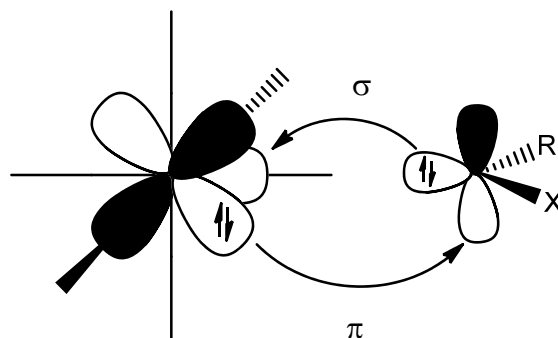
Pentacarbonyl(metal) carbene complexes have become well known for their electron-withdrawing ability – causing the Lewis acid complexed character which is common in push-pull systems –<sup>9</sup> which can display non-linear optical (NLO) properties.<sup>10</sup> These electronic properties of carbenes are the determining factors used to label the carbene in terms of electrophilicity. There are many factors which affect this electrophilic property of the carbene, but this sensitive parameter



also provides the opportunity to tune the carbene to achieve the desired characteristics. In a typical pentacarbonyl(metal) carbene complex  $[\text{CO}]_5\text{M}=\text{C}(\text{X})(\text{R})$ , the nature of X and R functional groups (attached to the carbene carbon) primarily determines the electronic properties of the complex for a given metal. Choice of X- and R-groups allows for a wide-range of tunability in regard to the complex's electronic structure and therefore desired physical properties and chemical reactivity.<sup>11, 12</sup>

The effect of changing the X- and R-groups is seen primarily in the electron density distribution affecting the  $\text{M}\cdots\text{C}_{\text{carbene}}$  bond. Usually, the electron density is discussed in terms of the MO composition of the complex and, in particular, with regard to the  $p$  orbitals of the  $\text{C}_{\text{carbene}}$ . The polarization of  $\pi$ -electrons associated with the bond between  $\text{C}_{\text{carbene}}$  and the donor fragment (typically the X-group) results from the electron-accepting nature of the  $(\text{CO})_5\text{M}=\text{C}$  fragment and makes NLO studies popular.<sup>13</sup> Conclusions have been drawn that the X-group has a dominant electronic effect over the electronic effect that is introduced by changing the R-group in the electronic structure, with experimental data proving the electrophilic nature<sup>14-16</sup> of the C atoms of the carbene ligand. However, the underlying electronic mechanism behind these conclusions remains a mystery.

We can gain some insight into the electronic structure of Fischer carbene complexes through the investigation of electronic transitions, thermodynamics and kinetics. The ligand-field (LF) bands experience strong redshifts with  $\pi$ -donor groups while the opposite is seen with  $\pi$ -acceptor groups, but this was not seen for the metal-ligand charge transfer (MLCT) band.<sup>10</sup> In addition, work by Berasconi and co-workers found that when the carbene has weaker  $\pi$ -donor groups an increase in the thermodynamic acidity is seen, there has also been work showing the kinetics of the reaction is affected.<sup>16</sup> There are many studies showing how the substituents attached to the carbene affect the molecule kinetically and thermodynamically in reactions.<sup>15-18</sup> These types of studies illustrate the importance of understanding the electronic structure of Fischer carbenes. A popular model (taught in university) to explain the metal-carbene bond is known as  $\pi$ -back-bonding and illustrated in **Scheme 4. 1**.



**Scheme 4. 1.** Back-bonding in a Fischer carbene

The metal-carbene bond has  $\pi$ -bond character and has been postulated as a 3-centre 4-electron bond (3c-4e).<sup>19,20</sup> For this reason, due to the  $\pi$ -bond character it is believed that the X-group affects the metal-carbene bond the most, which will be on elaborated shortly. Typically, the metal-carbene bond is described by the Dewar-Chatt-Duncanson (DCD) model<sup>21</sup> as a synergistic  $\sigma$ -donation into the empty metal d( $\sigma$ ) orbital from the carbon's lone pair with  $\pi$ -back-donation coming from the metal d( $\pi$ ) orbital which donates electrons to an empty carbene p( $\pi$ ) orbital<sup>22</sup> (**Scheme 4.1**) and seems to be rather sensitive to the X-substituents.<sup>23</sup> The effect of different X- and R-groups on the degrees of  $\sigma$ -donation and the  $\pi$ -back-donation has been of much interest.<sup>22, 24-27</sup> Typically, the  $\pi$ -donating X-group has an electronic stabilization effect on the electron-deficient carbene carbon (likely due to the  $\pi$ -donating/accepting character) while the low valent metal is stabilized by  $\pi$ -accepting groups like carbon monoxide.<sup>22</sup>

The work of Poater and co-workers<sup>28</sup> found that out of the Fischer carbenes they tested, varying the X- and R-group influenced the bonding in the molecule, especially in the  $M \cdots C_{\text{carbene}}$  bond. The X-substituent is of particular interest because of the effect it has on the metal-carbene bond, or as other work has showed also metal-cumulene bonds.<sup>23</sup> Poater *et al.* noted the  $\pi$ -back-donation between the  $\text{Cr}(\text{CO})_5$  fragment and the carbene fragment is generally weaker than the carbene fragment  $\sigma$ -donation to the  $\text{Cr}(\text{CO})_5$  fragment.<sup>28</sup> They also noted that more  $\pi$ -back-donation was seen when the X-group had a smaller  $\pi$ -donor character. Therefore, an X-group with more  $\pi$ -donor character caused more electrons to be shared between the  $C_{\text{carbene}}$  and X fragment, but fewer electrons shared between the Cr and  $C_{\text{carbene}}$ .

Fischer carbenes similar to this work can be found in Montserrat *et al.*, which used Kohn-Sham (KS) orbitals on the carbenes with a  $\text{Cr}(\text{CO})_5$  fragment<sup>22</sup> and some other ligands similar to

the ones in this work. They discussed three topics; first, the Fischer carbene geometries and the bond dissociation energies, followed by the metal–carbene bond through a decomposition analysis of charge and energy, and finally they discussed electrophilicity. We will highlight the first two points of their discussion; namely molecular geometries and the charge decomposition analysis (CDA). First, they found that certain geometries increased steric repulsion while others reduce it; they found that when a certain conformation is adopted by the carbene ligand, steric repulsion is reduced, which affects the Cr(CO)<sub>5</sub> HOMO overlap with the carbene's LUMO.<sup>22</sup> The conformation is, however, a balance between both the steric repulsion and orbital interaction.<sup>24</sup> Considering the second point; in the CDA, they found that the carbene's donation to the metal (i.e.  $\sigma$ -donation) was mostly twice as large as the  $\pi$ -back-donation (metal donating to the carbene). However, when R= -CCH they found it to be  $\sigma$ -withdrawing.<sup>22, 29</sup> They also found that decreasing the  $\pi$ -donor X-group caused  $\pi$ -back-donation in the R-group to increase. The unexpected result of their publication was when the R-group consisted of an alkyne group (R= -CCH) the  $\pi$ -accepting nature increased and  $\sigma$ -donation was reduced, showing that this system hinders the back-donation mechanism. Moving on to the energy decomposition analysis they found that for a given R-group the decomposition energy increased with decreasing  $\pi$ -donor character of the X-group such that H > OR' > NHR'.

This work focuses on the in-depth investigation of various interactions within Fischer carbene complexes, such as the metal interacting with the carbene carbon or the metal interacting with the R-group. We hope to shed new light onto the interpretability and quantification of 3c-4e interactions in Cr-containing Fischer carbene complexes. In order to do so, we utilize the recently developed Fragment, Atomic, Localized, Delocalized and Interatomic (FALDI) density decomposition scheme,<sup>30, 31</sup> coupled with molecular orbital analysis (henceforth referred to as the FALDI-MO approach). The FALDI-MO analysis allows for a holistic description of bonding (as for traditional investigation of MOs) yet is able to capture details in atomistic resolution (as for atoms-in-molecules approaches). In addition, the FALDI-MO approach is able to characterize MOs in terms of symmetry, even in asymmetrical complexes, without requiring rigorous and successive perturbations<sup>32</sup> or fragmentation of the molecule into unchemical fragments.<sup>33, 34</sup>

The question of the effects that the X- and R-groups have on the electronic structure of Fischer carbene complexes is revisited in this work, from the perspective of the novel FALDI-MO

approach. A set of small, asymmetric Fischer carbene complexes was selected as model compounds in order to show the level of insight and quantification that the FALDI-MO approach can offer. Notably, whereas Chapter 3 established the FALDI-MO approach, here we expand the approach with the inclusion of chemical fragments.

## Theoretical Background and Development

The FALDI density decomposition scheme<sup>30,31</sup> provides an exhaustive electron density (ED) decomposition for any coordinate  $\mathbf{r}$ . The premise of FALDI is based on the definition of the atomic basin, for which QTAIM-based atomic definitions are used. This definition enables FALDI to describe the electron density of not only a single atom or diatomic interactions but collections of atoms, which have been appropriately labelled as fragments ( $\mathcal{F}$ ).

The recently developed FALDI-MO analysis method (Chapter 3) illustrates how classical symmetry terms can be assigned to asymmetric MOs from a metal's perspective, and is briefly reviewed below. In addition, in this chapter we expand the FALDI-MO method to include chemical *fragments*, which aids interpretation tremendously through reduction of variables. The FALDI-MO method decomposes an MO's contribution to the density at a coordinate  $\mathbf{r}$  in terms of atom-localized ED (*loc*-ED) and atom-pair-delocalized ED (*deloc*-ED). For the former:

$$\mathcal{L}_A(\mathbf{r}) = \sum_{ij} \chi_i(\mathbf{r})\chi_j(\mathbf{r})(\mathbf{G}^A\mathbf{S}^A)_{ji} \quad (1)$$

where  $\mathbf{G}^A\mathbf{S}^A$  is a localized overlap matrix (LMAT), of which the diagonal elements  $(\mathbf{G}^A\mathbf{S}^A)_{ii}$  provide the contribution of the  $i$ th MO to the atom-localized ED at  $\mathbf{r}$ .  $\mathcal{L}_A(\mathbf{r})$  recovers Localized indices (LIs) after being integrated of all molecular space. The LI is used to obtain the metal centres localized Natural Density Functions (NDFs) known as  $\phi_i^{AA}(\mathbf{r})$ :

$$\phi_i^{AA}(\mathbf{r}) = \sum_j^{N_{MO}} \chi_j(\mathbf{r})U_{ji}^{AA} \quad (2)$$

where  $U_{ji}^{AA}$  is an element of the eigenvector matrix of  $\mathbf{G}^A\mathbf{S}^A$ . These *loc*-NDFs of the metal centre translate extremely well into classical symmetry terms like  $a_{1g}$ ,  $t_{1u}$ ,  $t_{2g}$  and  $e_g$  (in an octahedral field), with non-localized (NL) describing the unclassified symmetries not described by the metal.

The delocalized indices (DI) can be similarly obtained from the *deloc*-ED distribution:

$$\mathcal{D}_{A,B}(\mathbf{r}) = \sum_{ij} \chi_i(\mathbf{r})\chi_j(\mathbf{r})(\mathbf{G}^A\mathbf{S}^B + \mathbf{S}^B\mathbf{G}^A)_{ji} \quad (3)$$

where the matrix-product sum  $\mathbf{G}^A\mathbf{S}^B + \mathbf{S}^B\mathbf{G}^A$  describes a delocalized overlap matrix (DMAT).  $\mathcal{D}_{A,B}(\mathbf{r})$  calculates the contribution to the ED at  $\mathbf{r}$  that arises from electrons delocalized (shared) between atomic basins  $\Omega_A$  and  $\Omega_B$ . Integrating the *deloc*-ED distribution over all molecular space results in the QTAIM-defined DI.

*Loc*- and *deloc*-ED distributions are defined for individual atoms, and can be summed with respect to a single atom to provide an atom-ED distribution,  $g_A(\mathbf{r})$ . However, multiple atomic basins can be combined in a superatom, or, in chemical terms, a fragment ( $\mathcal{F}$ ):

$$g_{\mathcal{F}I}^{total}(\mathbf{r}) = \sum_A^{M_{\mathcal{F}I}} g_A(\mathbf{r}) \quad (4)$$

where  $M_{\mathcal{F}I}$  is the total number of atoms in fragment  $\mathcal{F}I$ .  $g_{\mathcal{F}I}^{total}(\mathbf{r})$ , when integrated over all molecular space, yields the total average electron count associated with the fragment,  $N^{total}(\mathcal{F}I)$ . The  $g_{\mathcal{F}I}^{total}(\mathbf{r})$  term encapsulates electrons delocalized between all fragments and  $\mathcal{F}I$  as well as electrons localized to each fragment are included in this term.

The contribution to the ED at  $\mathbf{r}$  due to electrons localized to each atom of the fragment can be described, in analogy to Eq. 4, by summing the individual *loc*-ED distributions:

$$\mathcal{L}_{\mathcal{F}I}(\mathbf{r}) = \sum_A^{M_{\mathcal{F}I}} \mathcal{L}_A(\mathbf{r}) \quad (5)$$

This term includes the non-bonded and core electrons within the fragment for each atom. The electrons delocalized between atoms *within* the fragment can also be obtained, as a contribution to the ED at  $\mathbf{r}$ , by

$$\mathcal{D}_{\mathcal{F}I}^{intra}(\mathbf{r}) = \sum_A^{M_{\mathcal{F}I}-1} \sum_{B=A+1}^{M_{\mathcal{F}I}} \mathcal{D}_{A,B}(\mathbf{r}) \quad (6)$$

and is known as *intra*-fragment *delocalized* electrons. Considering both the localized and delocalized electrons in Eqs. 5 and 6 yields the total intra-fragment electron distribution:

$$g_{\mathcal{F}I}^{intra}(\mathbf{r}) = \mathcal{L}_{\mathcal{F}I}(\mathbf{r}) + \mathcal{D}_{\mathcal{F}I}^{intra}(\mathbf{r}) \quad (7)$$

Both the inter-atomic delocalized and atom-localized electrons between atom-pairs of the fragment are included in the  $g_{\mathcal{F}1}^{intra}(\mathbf{r})$  term at  $\mathbf{r}$  for electrons localized to  $\mathcal{F}1$ . The total intra-fragment electron population can also be obtained by simply integrating  $g_{\mathcal{F}1}^{intra}(\mathbf{r})$  over all molecular space, which is the sum of the LIs and DIs of the fragments.

$$N^{intra}(\mathcal{F}1) = \int g_{\mathcal{F}1}^{intra}(\mathbf{r}) d\mathbf{r} = \sum_A \text{LI}(A) + \sum_{A,B} \text{DI}(A,B) \quad (8)$$

where  $A, B \in \mathcal{F}1$ . Looking at the *deloc*-ED distribution between two fragments,  $\mathcal{F}1$  and  $\mathcal{F}2$ , allows the inter-fragment delocalization to be obtained:

$$\mathcal{D}_{\mathcal{F}1,\mathcal{F}2}^{inter}(\mathbf{r}) = \sum_A \sum_B^{M_{\mathcal{F}1} M_{\mathcal{F}2}} \mathcal{D}_{A,B}(\mathbf{r}) \quad (9)$$

which describes the distribution of the delocalized electrons across the two fragments. The inter-fragment DI can then be obtained by integrating over all space:

$$\begin{aligned} \text{DI}(\mathcal{F}1, \mathcal{F}2) &= \int \mathcal{D}_{\mathcal{F}1,\mathcal{F}2}^{inter}(\mathbf{r}) d\mathbf{r} \\ &= \sum_{A,B} \text{DI}(A,B) \end{aligned} \quad (10)$$

with  $A \in \mathcal{F}1$  and  $B \in \mathcal{F}2$ . Then summing Eq. 7 and 9 yields the total of  $g_{\mathcal{F}1}^{total}(\mathbf{r})$  (Eq 4).

$$g_{\mathcal{F}1}^{total}(\mathbf{r}) = g_{\mathcal{F}1}^{intra}(\mathbf{r}) + \sum_X^M \frac{1}{2} \mathcal{D}_{\mathcal{F}1,\mathcal{F}X}^{inter}(\mathbf{r}) \quad (11)$$

Lastly, the metal-based classification scheme, *loc*-NDFs,<sup>31</sup> can be linked to the inter-fragment delocalized electrons contributions to obtain:

$$\text{DI}(\mathcal{F}1, \mathcal{F}2) = \sum_i^{N_{MO}} d_i^{\mathcal{F}1, \mathcal{F}2} \left[ {}^{a1g}n_i^M + {}^{t1u}n_i^M + {}^{t2g}n_i^M + {}^{eg}n_i^M + {}^{NL}n_i^M \right] \quad (6)$$

providing the MO contributions in fragments for the DI ( $\mathcal{F}1, \mathcal{F}2$ ) with symmetry classifications based on the metal *loc*-NDFs.

## Computational Details

All structures were optimized using DFT in Gaussian 09<sup>35</sup> with B3LYP as exchange-correlation functional and a basis set of def2-SV(P) in implicit *n*-hexane solvent model. The spin state was kept as a singlet, as is expected of Fischer carbenes. All ground state single-point calculations were performed using the optimized structure but using CAM-B3LYP in order to

more accurately model long-range interactions. QTAIM analyses, using AIMALL 17.01.25<sup>36</sup>, was the result of single-point calculations to generate atomic overlap matrices necessary for FALDI analysis. FALDI was performed with orthodox (de)localization, using in-house codes. The NDFs generated were then used to visualize the symmetry classification in VMD 1.9.3.<sup>37</sup>

### Structures

We used the following Fischer carbene structures in the FALDI MO decomposition analysis:

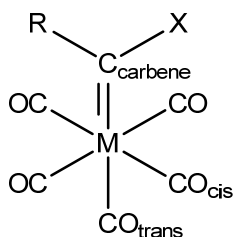


**Figure 4. 1.** The skeleton structure of all the Fischer carbenes.

**Table 4. 1.** The combinations of  $C_{\text{carbene}}$  substituents (X- and R-groups) on Fischer carbenes complexes.

X-Group	R-Group			
	R=H	R=CHCH <sub>2</sub>	R=CHCHPh	R=CCH
X=OEt	<b>4a</b>	<b>4b</b>	<b>4c</b>	<b>4d</b>
X=NMe <sub>2</sub>	<b>4e</b>	<b>4f</b>	<b>4g</b>	<b>4h</b>

We supply the Cartesian coordinates of each structure in **Table B 1. 1. to B 1. 8.** in **Appendix B**, respectively accompanied by the optimized molecules' electronic energies.

### Fragments

We allocated several fragments to every molecule considered in order to look at specific bonds and interactions. Notably, molecular structures were kept intact – no bonds were dissociated in order to perform FALDI-MO analysis. The FALDI-MO analysis assigns symmetry labels

determined by the metal centre which can be used to describe different interactions. The interactions are found in the selected fragments ( $[M]\cdots C_{\text{carbene}}$ ,  $[M]\cdots[X]$ ,  $[M]\cdots[R]$ ,  $[X]\cdots[R]$  and the  $[M]\cdots[L]$  where L is the entire carbene ligand) which are used for the comparison when changing either the X-group or R-group on the various Fischer carbene structures illustrated in **Figure 4. 2.**

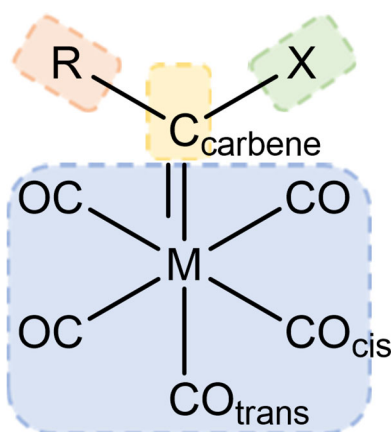


**Figure 4. 2.** Generalized fragments used for FALDI Fragments MO analysis. The fragments are  $[M]\cdots C_{\text{carbene}}$ ,  $[M]\cdots[X]$ ,  $[M]\cdots[R]$ ,  $[X]\cdots[R]$  and  $[M]\cdots[L]$ , where  $[M]\cdots[L]$  interaction refers to the metal cluster ( $[M]$ , metal and pentacarbonyl) interacting with the entire carbene ligand ( $[L]$  which is the  $C_{\text{carbene}}$ , X-group and R-group).

**Figure 4. 2.** illustrates the general fragmentation as a pictorial example. The metal cluster  $[M]$  is defined as the metal and the five carbonyls, in blue, the carbene carbon as yellow, the R-group as orange and the X-group as green. These are the fragments used in the comparisons and classifications for the specific bonds or interactions investigated. Through the FALDI-MO analysis, we can assign any MO symmetry labels, and the bonding character ( $\sigma$ - and  $\pi$ -character) to the fragment. However, because of the nature of the symmetry assignment, the method is limited to using metal-based fragments as the metal provides the symmetry term used in the comparison.



For this reason, the  $[X]\cdots[R]$  fragment interaction can provide delocalized electron data but cannot be assigned symmetry terms like the metal counterparts.

## Results and Discussion

In this study, the electronic structures of various X- and R-group combinations in a general Fischer carbene complex skeleton,  $\text{Cr}(\text{CO})_5\{\text{C}(\text{X})(\text{R})\}$ , are investigated using the FALDI-MO approach. When comparing the various Fischer carbene structures, a few variables need to be noted that may affect the physical and chemical properties of the complexes. Changing X- and R-groups result in both electronic and geometric changes within a complex; the latter can introduce additional electronic structure rearrangements, especially through steric considerations. For instance, and as illustrated in **Figure 4. 3.**, when  $\text{X}=\text{OEt}$  (**4c**), R- and X-groups are perfectly planar relative to each other in the optimized structure, which is not the case when  $\text{X}=\text{NMe}_2$  (**4g**). In attempt to isolate the electronic effect that the choice of X-group imposes, we have also selected structures with  $\text{R}=\text{-CCH}$  – as illustrated in **Figure 4. 4.**

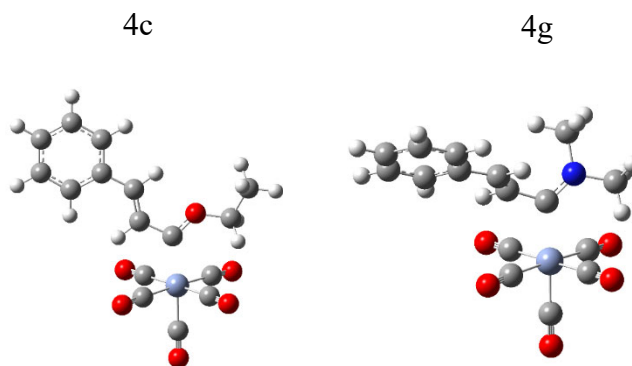


**Figure 4. 3.** The geometric effects of changing the X-group whilst the R-group stays the same, using **4c** and **4g** to show the planarity disruption between the X- and R-group.

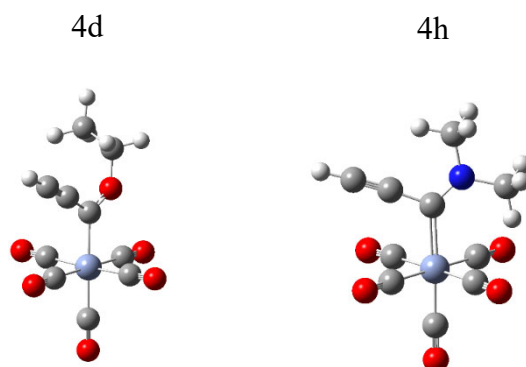


**Figure 4. 4.** The geometric effects of changing the X-group when the R= -CCH forcing planarity between the X- and R-group illustrated by **4d** and **4h**.

With these guidelines set in place, the molecules can be fragmented, and the geometric and electronic effects compared and related to each other based on the varying X- and R-groups.

#### *Inter-fragment electron delocalization*

The diatomic interaction of the metal and carbene carbon ( $M-C_{\text{carbene}}$ ) is often classically regarded as a double bond, and was briefly explored in Chapter 3. A diatomic interaction is, however, an extremely narrow description of the interaction between a metal, its ligands and an entire carbene ligand. Here, using our novel fragment FALDI-MO approach, we can study the full interaction between the metal cluster ( $[M]$ , defined as the pentacarbonyl metal fragment,  $Cr(CO)_5$ ) and sections of the carbene ligand (carbene carbon,  $C_{\text{carbene}}$ , as well as entire R- and X-groups,  $[R]$  and  $[X]$ , respectively) – as shown in Figure 4.2. FALDI-based interfragment DIs describe the total number of electrons shared – whether through-space or through-bond – between any two fragments, and are summarized in Table 4.2. The sections below will discuss selected interfragment interactions – namely  $[M] \cdots C_{\text{carbene}}$ ,  $[M] \cdots [X]$ ,  $[M] \cdots [R]$  and  $[X] \cdots [R]$  – in detail, as using the FALDI-MO approach.

**Table 4. 2.** Inter-fragment Delocalization comparison of X=OEt and NMe<sub>2</sub>.

Interaction	Delocalized electrons							
	R=H		R=CHCH <sub>2</sub>		R=CHCHPh		R=CCH	
	X=OEt	X=NMe <sub>2</sub>	X=OEt	X=NMe <sub>2</sub>	X=OEt	X=NMe <sub>2</sub>	X=OEt	X=NMe <sub>2</sub>
$[M] \cdots C_{\text{carbene}}$	1.3367	1.1048	1.1463	0.9326	1.1082	0.9273	1.2059	0.9427
$[M] \cdots [X]$	0.2440	0.2866	0.3190	0.2949	0.3085	0.2938	0.2403	0.2959
$[M] \cdots [R]$	0.0601	0.0546	0.2182	0.2200	0.2318	0.2286	0.2441	0.2328
$[M] \cdots [L]$	1.6408	1.4460	1.6835	1.4475	1.6484	1.4497	1.6903	1.4713
$[X] \cdots [R]$	0.1362	0.1455	0.2548	0.3133	0.2759	0.3340	0.2977	0.3453

#### *Analysis of the Metal–Carbene ( $[M] \cdots C_{\text{carbene}}$ ) interaction*

**Table 4. 3.** describes the number of electrons shared between the metal cluster fragment ( $[M]$ ) and the carbene carbon ( $C_{\text{carbene}}$ ). **4a** (X=OEt, R=H) can be considered a ‘baseline’ case for a description of the electronic structure: The total number of electrons shared (total DI( $[M]$ ,  $C_{\text{carbene}}$ )) is equal to 1.336  $e^-$ , suggesting a bond-order slightly greater than 1. Fully understanding the nature

of the shared electrons can be somewhat difficult, in particular due to the lack of symmetry within the complex: a high order of symmetry would have allowed MOs and atomic orbitals that are fully classifiable by group theory, and therefore easily interpretable. Fortunately, our FALDI-MO approach allows the characterization of MOs even in asymmetrical complexes, and the grouped contribution of classified MOs to the delocalized electrons of  $[M]\cdots C_{\text{carbene}}$  are also shown in Table 4.3. For **4a**, we note that shared electrons are predominantly distributed among  $t_{2g}$  orbitals ( $0.424 e^-$ ,  $\pi$ -bonding) and *non-localized* orbitals ( $0.480 e^-$ ) – i.e. MOs that do not involve the metal’s atomic orbitals. However, the  $t_{1u}$  ( $0.226 e^-$ ) and  $e_g$  ( $0.167 e^-$ ) orbitals also contribute significantly, and together with  $a_{1g}$  MOs, form the  $\sigma$ -bond of the interaction. Accordingly, the total  $\sigma$ - and  $\pi$ -contributions are almost equal –  $0.4317$  and  $0.4244 e^-$ , respectively. Our results therefore suggest, for an unmodified alkoxy-carbene complex, that  $\sigma$ -donation and  $\pi$ -backbonding are mostly equal, and that the largest amount of electrons shared are within  $t_{2g}$  orbitals (i.e. involving Cr’s  $3d_{xy}$ ,  $3d_{xz}$  and  $3d_{yz}$  atomic orbitals). Furthermore, the large ‘NL’ contribution indicates a significant degree of multi-centric character associated with the  $[M]\cdots C_{\text{carbene}}$  interaction and resulting from MOs localized to the ligands. To our knowledge, this is the first fully quantified MO-based description of a Fischer carbene complex.

**Table 4. 3.** Symmetry decomposition for  $[M]\cdots C_{\text{carbene}}$  with X=OEt and NMe<sub>2</sub>.

	MO DI Contributions							
	X=OEt				X=NMe <sub>2</sub>			
	$[M]\cdots C_{\text{carbene}}$				$[M]\cdots C_{\text{carbene}}$			
	R=H	R=CHCH <sub>2</sub>	R=CHCHPh	R=CCH	R=H	R=CHCH <sub>2</sub>	R=CHCHPh	R=CCH
$a_{1g}$	0.0379	0.0413	0.0332	0.0306	0.0440	0.0224	0.0174	0.0202
$t_{1u}$	0.2265	0.1929	0.1938	0.1514	0.2886	0.1524	0.1298	0.1802
$t_{2g}$	0.4244	0.3257	0.2502	0.3657	0.2497	0.2021	0.1891	0.2190
$e_g$	0.1673	0.1365	0.1369	0.1046	0.1475	0.0686	0.0614	0.0679
NL	0.4805	0.4499	0.4941	0.5536	0.3750	0.4870	0.5296	0.4554
<b>Total</b>	<b>1.3367</b>	<b>1.1463</b>	<b>1.1082</b>	<b>1.2059</b>	<b>1.1048</b>	<b>0.9326</b>	<b>0.9273</b>	<b>0.9427</b>
$\sigma$	0.4317	0.3707	0.3638	0.2866	0.4801	0.2434	0.2086	0.2683
$\pi$	0.4244	0.3257	0.2502	0.3657	0.2497	0.2021	0.1891	0.2190
NL	0.4805	0.4499	0.4941	0.5536	0.3750	0.4870	0.5296	0.4554

When X- and R-groups change, however, we expect to see dramatic changes in the electronic structure (both directly and indirectly as a result of geometrical changes). When

X=NMe<sub>2</sub> (but keeping R=H), the total DI([M], C<sub>carbene</sub>) decreases significantly by 0.22 e<sup>-</sup> relative to X=OEt, suggesting a weaker metal–carbene bond. We generally observe this trend for all R-groups when comparing X=NMe<sub>2</sub> to X=OEt. Interestingly, *t*<sub>2g</sub> contributions (and therefore π-character) is reduced when X=NMe<sub>2</sub> relative to X=OEt, regardless of the choice of R-group, and is the primary reason for the observed reduced total number of electrons shared. Since nitrogen is less electronegative (implying it is a stronger donor), X=NMe<sub>2</sub> will presumably share more electrons with the carbene carbon and hence fewer electrons are available for the [M]···C<sub>carbene</sub> interaction, which the data affirms. Therefore, the [M]···C<sub>carbene</sub> bond is always stronger with X=OEt for all R-groups.

When the R-group is changed, the [M]···C<sub>carbene</sub> trends follow classical reasoning. When X=OEt, the highest DI for the [M]···C<sub>carbene</sub> interaction is when R= -H, and results in the following ranking CHCHPh<CHCH<sub>2</sub><CCH<H for the sharing of metal–carbene electrons. The styryl group, which has the most conjugation and most π-acceptance, will share the most electrons with the carbene carbon, reducing the ability of the metal to share electrons with the carbene carbon. This is followed by the vinyl group and then the alkyne group, which does not have additional orbitals to accept much more electron density. When X=NMe<sub>2</sub> the same trend is observed with CHCHPh<CHCH<sub>2</sub><CCH<H and the same reasoning can be followed.

Tracking back to the surface level analysis, classically it was stated that the more conjugated the R-group was, the more it would interact (electron donation would increase the electron sharing, whereas acceptance/withdrawal would decrease electron sharing) with the carbene carbon. Accordingly, fewer electrons are available to be shared with the metal, from either C<sub>carbene</sub> or through long-range interactions by [R]. The π-contributions (arising from MOs with *t*<sub>2g</sub> character) follow classical expectations perfectly, with the same trend as above: CHCHPh<CHCH<sub>2</sub><CCH<H for both X-groups. However, a missing piece of the puzzle lies within the classical explanation of the σ-character. When X=OEt the order of σ-character in the [M]···C<sub>carbene</sub> interaction is ranked as follows: CCH<CHCHPh<CHCH<sub>2</sub><H while for X=NMe<sub>2</sub> it is CHCHPh<CHCH<sub>2</sub><CCH<H. Clearly, the σ-character of the [M]···C<sub>carbene</sub> interaction, and therefore involvement of a<sub>1g</sub>, t<sub>1u</sub> and e<sub>g</sub> orbitals, is considerably more variable than the π-character and highly correlated with the choice of both X- and R-groups. For both the X=OEt and X=NMe<sub>2</sub> the most e<sub>g</sub> character is seen for R= -H and X=NMe<sub>2</sub> the most a<sub>1g</sub> character, indicating

geometrically this alignment (visually in 3D space on the same plane) strengthens the interaction. As pointed out in the work of Montserrat<sup>22</sup> for this metal–carbene bond, the  $\sigma$ -donation was twice the  $\pi$ -back-donation, these results in **Table 4. 3.** are very similar. The  $\sigma$ -character is stronger than the  $\pi$ -character for every R- and X-group combination. The exception to this observation is for the R= -CCH: when X=OEt, showing the  $\sigma$ -withdrawing behaviour identified in previous work,<sup>22, 29</sup> this was not the case for the X=NMe<sub>2</sub>, however, it was not specified in the list used by Montserrat.

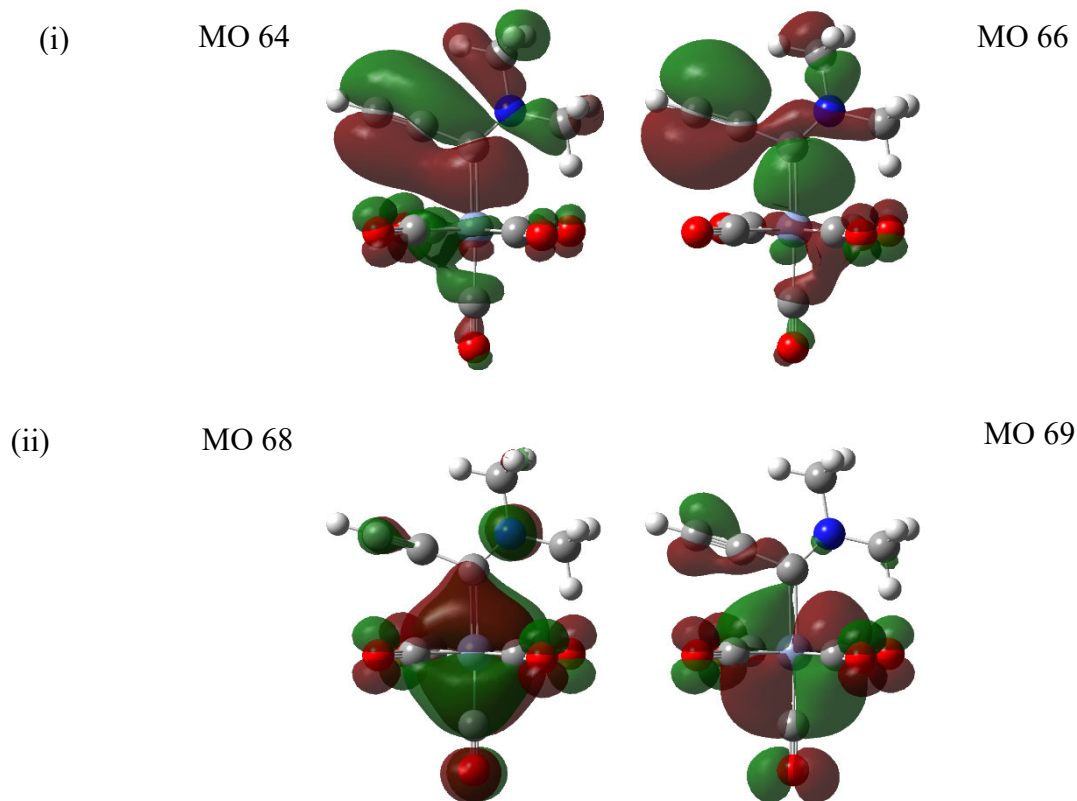


**Figure 4. 5.** The molecular orbitals of  $\text{Cr}(\text{CO})_5\{\text{C}(\text{NMe}_2)(\text{CCH})\}$  displaying the  $[\text{M}] \cdots \text{C}_{\text{carbene}}$  interaction for (i)  $\sigma$  and (ii)  $\pi$  with an isovalue of 0.02 a.u.

In order to eliminate, as much as possible, the influence of geometry on the electronic structure, we now turn to an in-depth analysis of the structures where R= -CCH. **Table 4. 3.** shows that the total number of electrons shared, and in particular the  $\pi$ -contributions, is considerably greater with X=OEt relative to X=NMe<sub>2</sub>. This shows that the R-group when X=NMe<sub>2</sub> is not necessarily optimally aligned with the metal orbitals, as the  $\pi$ -character ( $t_{2g}$ ) is weaker than the  $\sigma$ -character which is not expected from the less electronegative nitrogen with a high degree of

conjugation in the R-group. It does, however, show that the nitrogen is more of an inductive X-group since the  $\sigma$ -character is strengthened mainly through  $t_{1u}$  which correlates to the  $3p$  atomic orbitals on the metal. We can explain these results in terms of MOs, as the FALDI-MO approach allows for a decomposition of any DI value in terms of the entire list of MOs. Almost 70% of the  $DI([M], C_{\text{carbene}})$  in  $R=CCH$  and  $X=NMe_2$  consists of only four MOs which are MO 64, 66, 68 and 69 with contributions of 20.61%, 24.49%, 15.65% and 7.18% respectively, and shown in **Figure 4.5**. The biggest contributing MOs are 64 and 66, which are both made up of NL and  $t_{1u}$  character meaning 45.10% of the  $[M]\cdots C_{\text{carbene}}$  bond is a combination of  $\sigma$ - and NL character. On the other hand, we classify MOs 68 and 69 as  $t_{2g}$ , which makes up only 22.83%  $\pi$ -character described by these four MOs. This result clarifies that the MOs contributing to the  $[M]\cdots C_{\text{carbene}}$  are stronger in  $\sigma$ -nature and hence the  $\pi$ -character is weaker. If we consider all MOs in the system, the percentage of  $\sigma$ -character is 28.46% (0.2683) and 23.23% for the  $\pi$ -character (0.2190) with the remaining made up of NL character. This result is quite interesting, as more  $\pi$ -character is typically expected in the  $[M]\cdots C_{\text{carbene}}$  bond. From **Figure 4.5**, it can be seen that (i) the  $\sigma$ -orbitals (e.g. MO66) fully overlap between the metal and carbene carbon, while (ii) the  $\pi$ -orbitals (e.g. MO 69) does not overlap fully with the metal and carbene carbon. There is one metal orbital just touching the carbene carbon (poor overlap) which is hindering the synergistic mechanism of back-donation as discussed.<sup>22</sup> Since the p-orbital on the carbon atom has a nodal plane through the atom, we do not expect overlap more than what we see. This visual representation backs the numerical data showing that the  $\sigma$ -interaction is stronger for the  $[M]\cdots C_{\text{carbene}}$  than the  $\pi$ -interaction, when  $X=NMe_2$ .

Classifications of the symmetries are relative to their DI contribution and symmetry decomposition in terms of energy results are shown in **Table B 5.2** in **Appendix B**. The energy contributions of MOs to the  $[M]\cdots C_{\text{carbene}}$  interaction generally follows the same trends as DI values; however, if a specific MO (or set of MOs) are lower in energy relative to its contribution to the DI, the trends do shift somewhat. In particular, the data in **Table B 5.2** show how NL classified orbitals can influence the energetics of the system. For relating the  $X=OEt$  relative to  $X=NMe_2$  with the same R-groups, the energetic trend matches the DI trend: MOs describing the  $[M]\cdots C_{\text{carbene}}$  interaction generally shares more electrons and is lower in energy when  $X=OEt$  than  $X=NMe_2$ , and therefore corresponds to a generally stronger metal–carbene bond. The energy

profile also fits in nicely with the length of the R-group. In this work longer side chains require less molecular energy and this is seen with the R= -CHCHPh group requiring least energy and R= -H the most energy for both X=OEt and X=NMe<sub>2</sub>. The work of Monserrat<sup>22</sup> showed the molecular energy increases when the X-group decreases in  $\pi$ -donor ability and the X=NMe<sub>2</sub> being a stronger donor is lower in energy (stabilized) relative to the X=OEt except when R= -H and R= -CCH. This difference is likely due to the calculation of the energy, as the work of Monserrat is based on the binding energy, where the energy in this study is based on the molecular energy (weighted based on the orbitals and their DI contribution), and warrants further investigation.

In summary, we note that the MOs contributing to the electrons shared between the metal fragment and the carbene carbon are highly correlated with the choice of both X- and R-groups. While MOs with  $\pi$ -character contribute to delocalized electrons in an intuitive fashion, MOs with  $\sigma$ -character are considerably more volatile and highly dependent on the nature of both X- and R-groups simultaneously. In general, however, we have observed that the [M]...C<sub>carbene</sub> interaction is significantly stronger when X=OEt and with smaller R-groups (e.g. R= -H, R= -CCH), due primarily to greater  $\pi$ -contributions from MOs.

*Metal X-group ([M]...[X])*

The long-range interaction between the metal cluster and the X-group is interesting, and often not considered due to the assumption that the X-group does not directly significant share electrons with the metal. FALDI, however, allows for the calculation of delocalized electrons between *any* atoms or fragments – whether considered bonded or not.

**Table 4. 4.** Symmetry decomposition for [M]...[X] interaction with X=OEt and NMe<sub>2</sub>.

	MO DI Contributions							
	X=OEt [M]...[X]				X=NMe <sub>2</sub> [M]...[X]			
	R=H	R=CHCH <sub>2</sub>	R=CHCHPh	R=CCH	R=H	R=CHCH <sub>2</sub>	R=CHCHPh	R=CCH
a <sub>1g</sub>	0.0001	0.00498	0.0037	0.0004	0.0030	0.00368	0.0026	0.0033
t <sub>1u</sub>	0.0257	0.05314	0.0527	0.0187	0.0359	0.02900	0.0263	0.0255
t <sub>2g</sub>	0.1561	0.10738	0.0722	0.1328	0.1404	0.10608	0.0928	0.1244
e <sub>g</sub>	0.0201	0.02256	0.0231	0.0125	0.0217	0.01681	0.0142	0.0154
NL	0.0420	0.13099	0.1567	0.0758	0.0856	0.13934	0.1578	0.1272
<b>Total</b>	<b>0.2440</b>	<b>0.31904</b>	<b>0.3085</b>	<b>0.2403</b>	<b>0.2866</b>	<b>0.29490</b>	<b>0.2938</b>	<b>0.2959</b>
σ	0.0459	0.0807	0.0796	0.0316	0.0606	0.0495	0.0432	0.0442
π	0.1561	0.1074	0.0722	0.1328	0.1404	0.1061	0.0928	0.1244
NL	0.0420	0.1310	0.1567	0.0758	0.0856	0.1393	0.1578	0.1272

Whereas multiple clear trends were observed for the [M]...C<sub>carbene</sub> interaction, [M]...[X] interaction shows fewer direct trends – **Table 4. 4**. As a baseline, consider X=OEt and R= -H: DI([M], [X]) is equal to 0.244 e<sup>-</sup>, indicating a surprisingly large number of shared electrons despite the absence of a formal covalent bond. The interaction forms primarily as a result of MOs with t<sub>2g</sub> character (π-character, 0.156 e<sup>-</sup>), although with a small but significant contribution from σ-MOs as well (0.045 e<sup>-</sup>).

The variation of the [M]...[X] interaction when changing X- or R-groups is quite interesting. When R= -H and -CCH, fewer electrons are shared amongst the [M]...[X] interaction when X=OEt relative to X=NMe<sub>2</sub>; however, the opposite is true when R= -CHCH<sub>2</sub> and -CHCHPh. This observation suggests that for planar geometries (R= -H and -CCH), the X=NMe<sub>2</sub> group interacts more strongly with the metal cluster than the X=OEt group. When the geometry is distorted from planarity (i.e. when R= -CHCH<sub>2</sub> and -CHCHPh in the presence of X=NMe<sub>2</sub>), the



[M]...[X] interaction weakens. Stated differently, even though the [M]...[X] interaction is favoured electronically when X=NMe<sub>2</sub>, the geometric distortion imposed by X=NMe<sub>2</sub> with bulkier R-groups leads to a stronger [M]...[X] interaction in the presence of X=OEt. This result indicates that the geometric effect outweighs the electronic effect. In planar geometries (R= -H and -CCH), MO contributions to DI([M], [X]) with  $\sigma$ -characters as well as NL characters increases significantly when X=NMe<sub>2</sub> relative to X=OEt whereas  $\pi$ -contributions decrease, indicating that the electronic influence on the [M]...[X] interaction imposed by X=NMe<sub>2</sub> is mostly  $\sigma$  in nature. When the planarity is distorted in R= -CHCHPh and -CHCH<sub>2</sub> in the presence of X=NMe<sub>2</sub> the electronic contribution of MOs with  $\sigma$ -character is lost.

If the X-group is kept constant, then when X=OEt DI([M], [OEt]) increases with the R-groups as CCH<H<CHCHPh<CHCH<sub>2</sub>. This result is quite unintuitive, as all the substituents have the same planar geometry and therefore suggests a predominantly electronic effect that influences DI([M], [X]). Interestingly, MOs with  $\sigma$ -contributions to DI([M], [X=OEt]) were observed to contribute more when R= -CHCHPh or -CHCH<sub>2</sub>, whereas dominant  $\pi$ -characters were observed when R= -H or -CCH. We also observed MOs with NL characters to contribute much more to DI([M], [OEt]) when R= -CHCHPh or -CHCH<sub>2</sub> than when R= -H or -CCH. When X=NMe<sub>2</sub>, DI([M], [NMe<sub>2</sub>]) displayed much less variability, and slightly increases with the conjugation of R-groups as H<CHCHPh<CHCH<sub>2</sub><CCH. Interestingly, the  $\pi$ -contributions to DI([M], [NMe<sub>2</sub>]) is smallest with R= -CHCHPh and -CHCH<sub>2</sub>, whereas the NL contributions are greatest with these R-groups. This observation suggests that the nature of the [X]...[R] interaction might be the key to explaining the [M]...[X] interaction, and will be investigated in a following section.

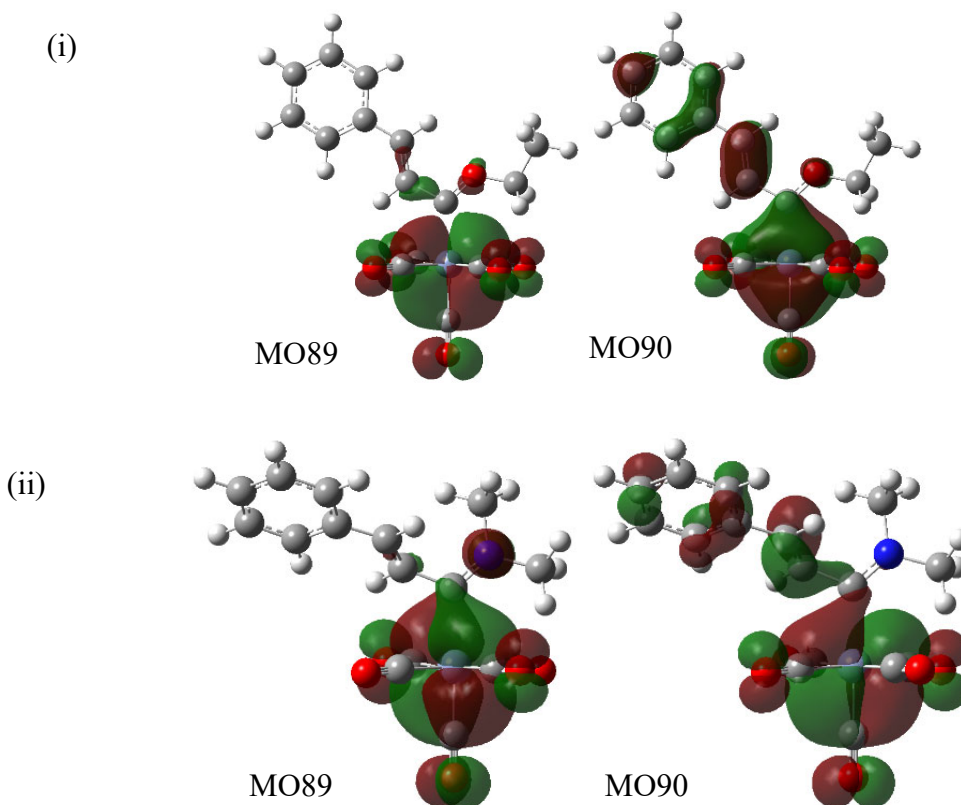


**Figure 4. 6.** The most  $\pi$ -contributing molecular orbitals for  $[M]\cdots[X]$  of  $\text{Cr}(\text{CO})_5\{\text{C}(\text{X})(\text{CHCHPh})\}$  with (i)  $\text{X}=\text{OEt}$  and (ii)  $\text{X}=\text{NMe}_2$  with an isovalue of 0.02 a.u.

The styryl group represents an interesting anomaly. When  $\text{R} = -\text{CHCHPh}$ , the  $\sigma$ -character of the  $[M]\cdots[X]$  interaction is much larger when  $\text{X}=\text{OEt}$  than  $\text{X}=\text{NMe}_2$  and it involves all the symmetry classifications of  $a_{1g}$ ,  $t_{1u}$  and  $e_g$ . The anomaly comes in with the  $\pi$ -character which is expected to be higher when  $\text{X}=\text{OEt}$  (as was observed for all other R-groups) but is, in fact, weaker (**Table 4. 4.**). This is likely due to the geometry, as the styryl-carbene ligand is planar only when  $\text{X}=\text{OEt}$ . For the  $[M]\cdots[X]$  interaction in  $\text{R} = -\text{CHCHPh}$  with  $\text{X}=\text{OEt}$ , two MOs contribute significantly to  $t_{2g}$ , namely MO89 and MO90 (**Figure 4. 6.**), with 6.84% and 13.42% contributions to  $\text{DI}([M], [X])$ . In comparison, when  $\text{R} = -\text{CHCHPh}$  and  $\text{X}=\text{NMe}_2$  there are three MOs which contribute the bulk of the interaction; MO87, 89 and 90 with DI contributions of 8.61%, 22.85% and 5.30% respectively. The reason for the  $\pi$ -character difference between the X-groups is likely because of two MOs namely MO89 and MO90.

From **Figure 4. 6.** and the noted percentages, the main orbital contributing to the  $\pi$ -component of the  $[M]\cdots[X]$  interaction for  $X=OEt$  is MO90 whilst for  $X=NMe_2$  it is MO89. When  $X=OEt$ , this orbital (MO90) is significantly delocalized over the metal cluster and the R-group, with a small contribution to the X-group. On the other hand, when  $X=NMe_2$ , the equivalent orbital (MO89) is not significantly delocalized over the R-group, and is primarily overlapping the metal cluster and X-group. Therefore, from this simple investigation, it can be seen that  $[M]\cdots[X]$  is stronger in  $\pi$ -character when  $X=NMe_2$  because of better  $t_{2g}$  overlap.

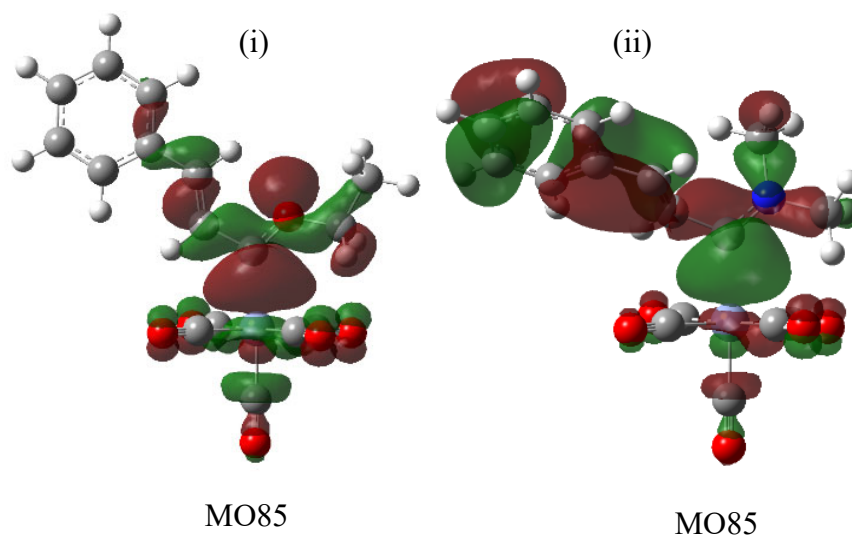


**Figure 4. 7.** The  $\sigma$ -contributing molecular orbitals for  $[M]\cdots[X]$  of  $Cr(CO)_5\{C(X)(CHCHPh)\}$  with (i)  $X=OEt$  and (ii)  $X=NMe_2$  with an isovalue of 0.02 a.u.

For the  $\sigma$ -contribution to the  $[M]\cdots[X]$  interaction,  $X=OEt$  is favoured over  $X=NMe_2$ . For  $X=OEt$ , MO85 is the primary  $\sigma$ -orbital (**Figure 4. 7.**), contributing 22.59% to the total  $DI([M], [X])$  and mainly consisting of  $t_{1u}$  and  $e_g$  characters, while for the  $X=NMe_2$  the main orbital contributing is also MO85, but only contributes 10.95% and consists of NL interactions and  $t_{1u}$  character. It is clear from **Figure 4. 7.** that the planar geometry observed when  $X=OEt$  results in a  $\sigma$ -orbital that is much more concentrated on the metal cluster and X-group than the perpendicular geometry observed when  $X=NMe_2$ , where the  $\sigma$ -orbital is delocalized across the entire carbene ligand. This planar geometry leads to more direct overlap and hence an increase in the sigma interaction when  $X=OEt$ .

The energetics of the  $[M]\cdots[X]$  interaction for  $X=OEt$  relative to  $NMe_2$  (presented in **Table B 5. 2.** of **Appendix B**) display roughly the same trend as the  $DI([M], [X])$  values, for all R-groups. The  $DI([M], [X])$  increases with R-groups as  $CCH < H < CHCHPh < CHCH_2$  for  $X=OEt$  and  $H < CHCHPh < CHCH_2 < CCH$  for  $X=NMe_2$ , whereas the energetic order for  $X=OEt$  is  $H > CCH > CHCHPh > CHCH_2$  (with  $-CHCH_2$  the most stabilized) while for  $X=NMe_2$  it is  $H > CCH > CHCH_2 > CHCHPh$  (with  $-CHCHPh$  the most stabilized). For the  $X=OEt$  DI relative to the energetics, there is a swap between  $R = -CCH$  and  $-H$ , likely because of  $-CCH$  having more NL character interacting with the metal increasing the average energy, while more conjugation lowers the energy for  $X=NMe_2$  because of the involvement of the NL orbitals. In  $X=NMe_2$  the restructuring of the order is because of the NL in  $R = -CHCH_2$  and  $-CHCHPh$  becomes larger (which is expected as the R-group gets larger, with less of the R-group being classified by the metal) even though the  $-H$  and  $-CCH$  have lower  $t_{2g}$  energies.

In summary, the interaction between the metal cluster and the X-group adds a significant number of shared electrons to the entire metal–carbene bond. While the interaction is mostly stabilized by MOs with  $\pi$ -characters for most of the X- and R-group combinations investigated, significant stabilization through  $\sigma$ - and NL MOs was also observed. When  $R = -H$  or  $-CCH$ , the  $[M]\cdots[X]$  interaction is greater when  $X=NMe_2$  than  $X=OEt$  due primarily to stronger overlap of  $\sigma$ -MOs. However, the opposite was observed when  $R = -CHCH_2$  or  $-CHCHPh$ , which was shown to be a result of the non-planar geometry observed with  $X=NMe_2$ .

#### *Metal R-group ( $[M]\cdots[R]$ )*

The interaction between the metal cluster and R-group follows a more familiar trend similar to that of the  $[M]\cdots C_{\text{carbene}}$  bond –  $[M]\cdots[R]$  is stronger when  $X=OEt$  than  $X=NMe_2$  for most R-groups considered, **Table 4. 5.** Similarly,  $DI([M], [R])$  increases with respect to R-groups as  $H < CHCH_2 < CHCHPh < CCH$ , regardless of choice of X-group. This is expected for the metal's long-range interaction with the R-group – we see more electrons are shared as the R-group's conjugation increases.

**Table 4. 5.** Symmetry decomposition for the [M]···[R] interaction with X=OEt and X=NMe<sub>2</sub>.

	MO DI Contributions							
	X=OEt				X=NMe <sub>2</sub>			
	[M]···[R]				[M]···[R]			
	R=H	R=CHCH <sub>2</sub>	R=CHCHPh	R=CCH	R=H	R=CHCH <sub>2</sub>	R=CHCHPh	R=CCH
a <sub>1g</sub>	0.0014	0.00236	0.0025	0.0028	0.0004	0.00263	0.0014	0.0028
t <sub>1u</sub>	0.0169	0.02660	0.0253	0.0219	0.0160	0.02756	0.0202	0.0252
t <sub>2g</sub>	0.0240	0.09914	0.1321	0.1327	0.0204	0.05971	0.0770	0.0765
e <sub>g</sub>	0.0104	0.01469	0.0131	0.0144	0.0077	0.01209	0.0074	0.0118
NL	0.0074	0.07542	0.0588	0.0722	0.0102	0.11800	0.1225	0.1164
<b>Total</b>	<b>0.0601</b>	<b>0.21821</b>	<b>0.2318</b>	<b>0.2441</b>	<b>0.0546</b>	<b>0.21998</b>	<b>0.2286</b>	<b>0.2328</b>
σ	0.0288	0.0437	0.0409	0.0392	0.0240	0.0423	0.0291	0.0398
π	0.0240	0.0991	0.1321	0.1327	0.0204	0.0597	0.0770	0.0765
NL	0.0074	0.0754	0.0588	0.0722	0.0102	0.1180	0.1225	0.1164

The [M]···[R] interaction, in terms of MO-characters, is quite easy to interpret. When R=-H, MOs with t<sub>1u</sub>, e<sub>g</sub> and t<sub>2g</sub> characters contribute predominantly to DI([M], [R]) and results in an interaction of mostly equal σ- and π-characters. When the conjugation of the R-group increases, contributions from MOs with t<sub>2g</sub> character (and therefore π-character) as well as NL character increase accordingly and as classically expected. Generally stronger σ- and π-contributions are observed when X=OEt than X=NMe<sub>2</sub>, although weaker NL contributions are observed. The resulting [M]···[R] interaction, as mentioned above, is strongest when X=OEt and R= -CCH.

Looking at the energies of [M]···[R] in **Table B 5. 3.** it is seen that the energetics don't correlate well with the DI values. The energy is always lower for all R-groups in X=NMe<sub>2</sub> even if the [M]···[R] interaction is not always stronger. Looking at the X=OEt relative to X=NMe<sub>2</sub>, only the R= -CHCH<sub>2</sub> has a weaker DI contribution, while all the other R-groups (-H, -CHCHPh and -CCH) have more DI interaction between the [M]···[R]. This is because of NL contribution, looking at the NL contribution in either **Table 4. 5.** or **Table B 5. 3.** both show that there is more NL contribution with X=NMe<sub>2</sub> and sometimes even up to double, relative to the X=OEt, such as when R= -CHCHPh. Showing how some R-groups are not interacting with the metal, which overall influences the DI weighted energy.

**Table 4. 6.** Symmetry decomposition of [M]...[L] interaction with X=OEt and NMe<sub>2</sub>.

	MO DI Contributions							
	X=OEt				X=NMe <sub>2</sub>			
	[M]...[L]				[M]...[L]			
	R=H	R=CHCH <sub>2</sub>	R=CHCHPh	R=CCH	R=H	R=CHCH <sub>2</sub>	R=CHCHPh	R=CCH
a <sub>1g</sub>	0.0395	0.0486	0.0394	0.0338	0.0474	0.0287	0.0214	0.0263
t <sub>1u</sub>	0.2691	0.2726	0.2718	0.1921	0.3405	0.2090	0.1764	0.2310
t <sub>2g</sub>	0.6045	0.5322	0.4546	0.6313	0.4105	0.3679	0.3589	0.4199
e <sub>g</sub>	0.1978	0.1738	0.1731	0.1315	0.1768	0.0975	0.0830	0.0950
NL	0.5299	0.6563	0.7096	0.7016	0.4708	0.7444	0.8100	0.6991
<b>Total</b>	<b>1.6408</b>	<b>1.6835</b>	<b>1.6484</b>	<b>1.6903</b>	<b>1.4460</b>	<b>1.4475</b>	<b>1.4497</b>	<b>1.4713</b>
σ	0.5064	0.4950	0.4843	0.3574	0.5647	0.3352	0.2808	0.3523
π	0.6045	0.5322	0.4546	0.6313	0.4105	0.3679	0.3589	0.4199
NL	0.5299	0.6563	0.7096	0.7016	0.4708	0.7444	0.8100	0.6991

*Interaction between C<sub>carbene</sub>, X- and R-groups*

In the preceding sections, [M]...C<sub>carbene</sub>, [M]...[X] and [M]...[R] interactions all revealed large changes with respect to the choice of both X- and R-groups. In particular, the [M]...[X] interaction is strongly influenced by the choice of R-group whereas the [M]...[R] interaction is influenced by the choice of X-group. The observations made in the preceding sections therefore suggest that the X- and R-groups have a strongly correlated and non-linear effect on the electronic structure. In this section, C<sub>carbene</sub>...[X], C<sub>carbene</sub>...[R] and [X]...[R] interactions and their influences on the interactions involving the metal cluster will be briefly investigated. Since no classification of the MOs in terms of symmetry-characters can be made (as the FALDI-MO methodology is specific to NDFs centered on the metal ion), we will investigate only the total DI values.

**Table 4. 7.** The total DI of interactions not localized to the metal.

Interaction	Total inter-fragment DI							
	R=H		R=CHCH <sub>2</sub>		R=CHCHPh		R=CCH	
	X=OEt	X=NMe <sub>2</sub>	X=OEt	X=NMe <sub>2</sub>	X=OEt	X=NMe <sub>2</sub>	X=OEt	X=NMe <sub>2</sub>
C <sub>carbene</sub> ...[X]	1.1655	1.4429	1.1101	1.4109	1.0963	1.3981	1.0957	1.3781
C <sub>carbene</sub> ...[R]	0.8946	0.8978	1.1978	1.1754	1.2637	1.2062	1.2265	1.2194
[X]...[R]	0.1362	0.1455	0.2548	0.3133	0.2759	0.3340	0.2977	0.3453

The carbene carbon shares  $\sim 1.1 e^-$  with the X-group, when X=OEt. However, the interaction is consistently stronger when X=NMe<sub>2</sub>, and  $DI(C_{\text{carbene}}, [X]) \sim 1.4 e^-$ . This observation is in-line with classical thinking in that the X=NMe<sub>2</sub> group is a stronger electron donor than X=OEt. In addition, this observation explains, in part, the results in the preceding sections that  $DI([M], C_{\text{carbene}})$  is decreased when X=NMe<sub>2</sub> relative to X=OEt: a stronger  $C_{\text{carbene}} \cdots [X]$  bond results in fewer electrons available for the  $[M] \cdots C_{\text{carbene}}$  bond. Similarly, the carbene carbon shares  $\sim 1.2 e^-$  with the R-groups (with the exception of R= -H). On average,  $DI(C_{\text{carbene}}, [R])$  is greater when X=OEt than X=NMe<sub>2</sub>. In addition,  $DI(C_{\text{carbene}}, [X])$  decreases as the degree of conjugation in the R-group increases. Therefore, the interplay between  $C_{\text{carbene}} \cdots [X]$  and  $C_{\text{carbene}} \cdots [R]$  bonds is clear: as the one interaction strengthens, fewer electrons are available for the other.

The X- and R-groups also interact surprisingly strongly – a significant number of electrons are shared between these groups (up to a maximum of  $0.3453 e^-$  when X=NMe<sub>2</sub> and R= -CCH, **Table 4. 7.**). When X=NMe<sub>2</sub>, the  $[X] \cdots [R]$  interaction is consistently stronger than for X=OEt, for all R-groups considered. This observation provides an intuitive and strong hypothesis for the generally weaker  $[M] \cdots [X]$  and  $[M] \cdots [R]$  interactions observed when X=NMe<sub>2</sub> relative to X=OEt: as more electrons are shared between X- and R-groups, fewer electrons are available to be shared with the metal cluster. In addition,  $DI([X], [R])$  increases with increasing conjugation, in the order  $H < CHCH_2 < CHCHPh < CCH$ , for both X-groups considered. Therefore, increasing the conjugation of the R-group does not result in a linear increase in  $DI([M], [R])$ , as noted in the previous section. Rather, increased conjugation in the R-group results in a general increase in electrons shared between the R-group and all other fragments of the molecule.

*Summary: an overview of the Metal–Ligand ( $[M] \cdots [L]$ ) interaction*

The metal–ligand interaction considers the metal cluster and the ligand group each as a whole. The metal has been consistent throughout the above discussions but here the ligand encapsulates each component that has been discussed into a single fragment namely; the carbene carbon, R-group and X-group to see the overall effect. The preceding sections discussed electron delocalization of each individual interfragment interaction; however, the total delocalization between the metal cluster and the entire carbene ligand ( $[L]$ ) is additive,  $DI([M], [L]) = DI([M], C_{\text{carbene}}) + DI([M],$

[X]) + DI([M], [R]). DI([M],[L]) values are tabulated in Table 4.2, and provide a concise overview of the electronic structure of the molecule.

As an example, consider first **4a**, with X=OEt and R= -H. The total number of electrons shared between the metal cluster and the carbene ligand is  $DI([M], [L]) = 1.6408 e^-$ , and therefore displays an overall bond order between a single and double bond. Of these electrons: i) 81% is shared between the metal cluster and carbene carbon ( $DI([M], C_{\text{carbene}}) = 1.3367 e^-$ ) involving MOs with relatively equal  $\sigma$ -,  $\pi$ - and NL characters; ii) 15% is shared between the metal cluster and X-group ( $DI([M], [X]) = 0.244 e^-$ ) involving MOs with predominantly  $\pi$ -characters; and iii) 4% is shared between the metal cluster and R-group ( $DI([M],[R]) = 0.0601 e^-$ ), involving MOs with relatively equal  $\sigma$ - and  $\pi$ -characters. Overall and in chemical terms, the bond between the metal cluster and carbene ligand for **4a** can therefore be described as primarily a metal–carbene carbon bond with equal  $\sigma$ - and  $\pi$ -character, with minor stabilization through the  $\pi$ -orbitals involving the X-group.

When the R-group is replaced by R= -CHCH<sub>2</sub> (**4b**), a relatively small increase in the total number of electrons shared is seen, relative to R=H ( $\Delta DI([M], [L]) = +0.0427 e^-$ ). However, this change is a result of three competing effects: i) a large increase in the number of electrons shared between the metal cluster and R-group ( $\Delta DI([M], [R]) = +0.1581 e^-$ ), ii) a large decrease in the number of electrons shared between the metal cluster and the carbene carbon ( $\Delta DI([M], C_{\text{carbene}}) = -0.1904 e^-$ ) and iii) a small but significant increase in the number of electrons shared between the metal cluster and the X-group ( $\Delta DI([M], [X]) = +0.0750 e^-$ ). Therefore, even though introducing a conjugated R-group has the expected effect of strengthening the [M]···[R] interaction, various correlated changes occurred simultaneously and result in a much smaller strengthening of the [M]···[L] interaction than would otherwise be anticipated. As discussed in the previous section, these correlated changes are a result of an interplay between  $C_{\text{carbene}}\cdots[R]$  and  $[X]\cdots[R]$  interactions. Note that while the changes in the above-mentioned interactions primarily involved MOs with  $\pi$ -characters, contributions from MOs with  $\sigma$ - and NL characters were also significantly altered. Further increasing the conjugation of the R-group (R= -CHCHPh and -CCH, **4c** and **4d**, respectively) results in an expected linear increase in  $DI([M], [R])$  but variable changes in  $DI([M], [L])$  because of a different interplay of the DI values mentioned above. Finally, the



same general changes were observed when  $X=NMe_2$ , although with some variation due to non-planar geometries.

On the other hand, if the R-group is kept constant (R= -H, **4a**) but the X-group is changed to  $X=NMe_2$  (**4e**), a relatively large decrease is observed in the total number of electrons shared ( $\Delta DI([M], [L]) = -0.1948 e^-$ ). This result is predominantly due to a reduction in the electrons shared between the metal cluster and the carbene carbon ( $\Delta DI([M], C_{\text{carbene}}) = -0.2319 e^-$ ) as a result of reduced contributions from MOs with  $\pi$ - and NL characters. Considerably smaller changes seen in the interactions of the metal cluster with X- or R-groups ( $\Delta DI([M], [X]) = +0.0426 e^-$  and  $\Delta DI([M],[R]) = -0.0055 e^-$ ). Interestingly, the change in  $DI([M], [X])$  was not consistent with  $X=NMe_2$  compared to  $X=OEt$ , and we observed significant variance with respect to the choice of R-group. When the carbene ligand is planar (R= -H or -CCH),  $DI([M], [X])$  increased relative to  $X=OEt$ . This increase was noted to be predominantly as a result of *increased* contributions of MOs with  $\sigma$ - and NL characters, and suggests that  $X=NMe_2$  imposes a stronger  $\sigma$ -donation effect on the metal–ligand bond. On the other hand, when the carbene ligand is non-planar (R= -CHCH<sub>2</sub> or -CHCHPh),  $DI([M], [X])$  decreased relative to  $X=OEt$ . This decrease was a result of *decreased* contributions of MOs with  $\sigma$ -character. In general chemical terms, these observations result in an interesting hypothesis:  $NMe_2$  as an X-group generally reduces the  $\pi$ -character of the metal–carbene bond; however, it can either increase or decrease the total  $\sigma$ -bonding character of the metal–carbene carbon bond depending on the nature and geometry of the R-group.

## Conclusions

Changing the X- and R-groups on a molecule is a common practice in tuning the physical and chemical properties of Fischer carbene complexes. At a conceptual level, a number of assumptions and simplifications lead to a few highly generalized predictions regarding the electronic structure of the complex. We have shown, however, that the electronic structures of Fischer carbene complexes is a result of a highly correlated interplay between the interactions of various fragments. That said, the recently developed FALDI density decomposition scheme coupled with the novel FALDI-MO approach can reliably provide accurate and quantified (albeit complex) insights into the electronic mechanisms at play.

The tool most preferred by experimental and theoretical chemists to evaluate electronic structures remains molecular orbitals. However, the lack of symmetry in Fischer carbene complexes means that MOs cannot be interpreted or quantified to the same level as for symmetrical coordination structures. We have developed and expanded the FALDI-MO scheme to allow for symmetry classification of MOs even in asymmetrical metal complexes. In addition, we illustrated that the FALDI-MO method can fully decompose interfragment electron delocalization in terms of chemically-interpretable classified MOs. This approach was then used to interpret the electronic structures of a series of Fischer carbene complexes, and, for the first time, bonding between the metal cluster and carbene fragments were fully elucidated in terms of MOs. We showed that the metal–ligand bond is primarily constructed from a metal–carbon bond with equal contributions of MOs with both  $\sigma$ - ( $a_{1g}$ ,  $e_g$  and  $t_{1u}$ ) and  $\pi$ -characters ( $t_{2g}$ ). In addition, the metal–ligand bond is further stabilized by a long-range interaction between the metal cluster and the X-group composed of MOs with primarily  $\pi$ -character.

We further considered the modification of Fischer carbenes through two different variables: i) the choice of electron-donating X-group, and ii) the choice of a conjugated R-group. We have shown that a stronger X-group electron donor (*i.e.* X=NMe<sub>2</sub> as opposed to X=OEt) results in a stronger bond between the carbene carbon and the X-group, and consequently, a weaker bond between the metal and the carbene ligand. However, the degree to which the metal–ligand bond weakened was noted to be highly correlated with the choice of R-group. The exact electronic mechanism through which these changes occurred was elucidated, and involves the interplay between delocalized electron density amongst [M]···C<sub>carbene</sub>, [M]···[X], C<sub>carbene</sub>···[X] and [X]···[R] interactions. Furthermore, increasing the conjugation of the R-group was shown to have a surprisingly small increase on the strength of the metal–ligand bond. However, we found that this observation was the result of the cancellation of shared electron increases in long-range [M]···[R] interactions by decreases in the [M]···C<sub>carbene</sub> interaction. Again, however, we note that the extent of the effect imposed by choice of R-group was highly dependent on the choice of X-group. We have also shown how the MO-characters change when either the X- or R-groups are modified. For instance, X=NMe<sub>2</sub> provides considerably more  $\sigma$ -character to the metal–ligand bond (relative to X=OEt) when the ligand is fully planar, yet provides less  $\sigma$ -character when the ligand is non-planar.

We have shown that the FALDI-MO approach can provide immense and quantifiable insights to the interpretation of electronic structures in Fischer carbene complexes. Our approach provides a holistic representation of the electronic structure (involving all atoms and the full electron density distribution) yet does so in a chemically intuitive and atomistic manner. In addition, the FALDI-MO approach not only provides insights with regards to the inter-fragment electron delocalization patterns, but does so in a manner that is fully recoverable in terms of molecular orbital theory. This study shows how decomposing the Fischer carbene with the FALDI MO analysis recovers symmetry labels and in particular  $\sigma$ - and  $\pi$ -character which is extremely useful in classical chemistry and fundamental for fully describing a complex. We expect the FALDI-MO approach to find a valuable spot in the computational chemists' toolbox, whether to provide information on a case-by-case basis or for use in expanding general conceptual chemistry.

## References

1. Wu, Y.-T.; Kurahashi, T.; De Meijere, A., Some recent applications of Fischer carbenometal complexes in organic synthesis. *Journal of Organometallic Chemistry* **2005**, 690 (24-25), 5900-5911.
2. Salmain, M.; Licandro, E.; Baldoli, C.; Maiorana, S.; Tran-Huy, H.; Jaouen, G., Transition metal ('Fischer-type') carbene complexes as protein labelling reagents. *Journal of Organometallic Chemistry* **2001**, 617, 376-382.
3. Robin-Le Guen, F.; Le Poul, P.; Caro, B.; Pichon, R.; Kervarec, N., Synthesis of electron donor-acceptor polyunsaturated methylenepyran Fischer type carbene complexes: dynamic <sup>1</sup>H-NMR study and solvatochromic properties. *Journal of Organometallic Chemistry* **2001**, 626 (1-2), 37-42.
4. Tu, T.; Malineni, J.; Doetz, K. H., A Novel Pyridine-Bridged Bis-benzimidazolylidene Pincer Palladium Complex: Synthesis and Catalytic Properties. *Advanced Synthesis & Catalysis* **2008**, 350 (11-12), 1791-1795.
5. Solà, M.; Duran, M.; Torrent, M., The Dötz Reaction: A Chromium Fischer Carbene-Mediated Benzannulation Reaction. In *Computational Modeling of Homogeneous Catalysis*, Springer: 2002; pp 269-287.
6. Frühauf, H.-W., Metal-assisted cycloaddition reactions in organotransition metal chemistry. *Chemical Reviews* **1997**, 97 (3), 523-596.
7. Barluenga, J.; Martínez, S.; Suárez-Sobrino, A. L.; Tomás, M., New reaction pathways for Fischer carbene complexes:[6+ 3] cycloaddition of chromium alkenyl carbene complexes with fulvenes. *Journal of the American Chemical Society* **2001**, 123 (44), 11113-11114.
8. Barluenga, J.; Tomas, M.; Rubio, E.; López-Pelegrín, J. A.; García-Granda, S.; Priede, M. P., Unusual [1, 2]-and [1, 3]-M (CO)<sub>5</sub> Shifts in Fischer Carbene Complexes:[4+ 3] and [3+ 3] Annulation Reactions of Furan and Pyrrole Rings. *Journal of the American Chemical Society* **1999**, 121 (13), 3065-3071.
9. Fernández, I.; Sierra, M. A.; Cossío, F. P., DFT Study on the diels- alder cycloaddition between alkenyl- m (0)(m= cr, w) carbene complexes and neutral 1, 3-dienes. *The Journal of Organic Chemistry* **2008**, 73 (6), 2083-2089.
10. Chu, G. M.; Fernández, I.; Sierra, M. A., Synthesis, Structure, and Electronic Properties of Extended  $\pi$ -Conjugated Group 6 Fischer Alkoxy-Bis (carbene) Complexes. *Chemistry-A European Journal* **2013**, 19 (19), 5899-5908.
11. Jiang, W.; Fuertes, M. J.; Wulff, W. D., Electronic Tuning of Fischer Carbene Complexes in the Preparation of Bicyclo [3.1. 1] heptanones as Taxane A-ring Synthons. *Tetrahedron* **2000**, 56 (15), 2183-2194.
12. Thompson, S.; Wessels, H. R.; Fraser, R.; van Rooyen, P. H.; Liles, D. C.; Landman, M., Computational and experimental structural studies of selected chromium(0) monocarbene complexes. *J. Mol. Struct.* **2014**, 1060, 111-118.
13. Licandro, E.; Maiorana, S.; Papagni, A.; Hellier, P.; Capella, L.; Persoons, A.; Houbrechts, S., Synthesis and non-linear properties of conjugated poly-unsaturated amino carbene complexes. *Journal of Organometallic Chemistry* **1999**, 583 (1-2), 111-119.
14. Dötz, K. H., Synthesis of the Naphthol Skeleton from Pentacarbonyl-[methoxy (phenyl) carbene] chromium (O) and Tolan. *Angewandte Chemie International Edition in English* **1975**, 14 (9), 644-645.

15. Bernasconi, C. F.; Flores, F. X.; Sun, W., Physical Organic Chemistry of Transition Metal Carbene Complexes. 5. Kinetics and Mechanism of Hydrolysis of  $(\text{CO})_5\text{Cr}:\text{C}(\text{OCH}_3)\text{CH}_3$  and  $(\text{CO})_5\text{Cr}:\text{C}(\text{OCH}_2\text{CH}_3)\text{CH}_3$  in Aqueous Acetonitrile. *Journal of the American Chemical Society* **1995**, *117* (17), 4875-4880.
16. Bernasconi, C. F.; Perez, G. S., Physical Organic Chemistry of Transition Metal Carbene Complexes. 21.1 Kinetics and Mechanism of Hydrolysis of  $(\text{CO})_5\text{M}:\text{C}(\text{SR})\text{Ar}$  (M= Cr and W; R=  $\text{CH}_3$  and  $\text{CH}_3\text{CH}_2\text{CH}_2$ ; Ar=  $\text{C}_6\text{H}_5$  and 3- $\text{ClC}_6\text{H}_4$ ) in Aqueous Acetonitrile. Important Differences Relative to Complexes with Alkoxy Leaving Groups. *Journal of the American Chemical Society* **2000**, *122* (50), 12441-12446.
17. Bernasconi, C. F.; Ali, M., Physical Organic Chemistry of Transition Metal Carbene Complexes. 15.1 Kinetic and Thermodynamic Acidities of (Methylthiomethoxycarbene) pentacarbonyl Complexes of Chromium and Tungsten in Aqueous Acetonitrile. *Journal of the American Chemical Society* **1999**, *121* (13), 3039-3045.
18. Bernasconi, C. F.; Sun, W., Physical Organic Chemistry of Transition Metal Carbene Complexes. 8. 1 Kinetic and Thermodynamic Acidities of Alkoxyalkylcarbene Pentacarbonyl Complexes of Cr, Mo, and W in Aqueous Acetonitrile. Dependence on Metal, Alkyl Group, and Alkoxy Group. *Organometallics* **1997**, *16* (9), 1926-1932.
19. Block, T. F.; Fenske, R. F., A photoelectron spectroscopic study of some pentacarbonylchromium carbene complexes. *Journal of the American Chemical Society* **1977**, *99* (13), 4321-4330.
20. Wang, C.-C.; Wang, Y.; Liu, H.-J.; Lin, K.-J.; Chou, L.-K.; Chan, K.-S., Bond characterization of chromium–fischer carbene complexes: a combined study of experiment and theory. *The Journal of Physical Chemistry A* **1997**, *101* (47), 8887-8901.
21. Dewar, J., A review of the pi-complex theory. *Bulletin de la Societe Chimique de France* **1951**, *18* (3-4), C71-C79.
22. Cases, M.; Frenking, G.; Duran, M.; Solà, M., Molecular Structure and Bond Characterization of the Fischer-Type Chromium–Carbene Complexes  $(\text{CO})_5\text{Cr}-\text{C}(\text{X})(\text{R})$  (X= H, OH,  $\text{OCH}_3$ ,  $\text{NH}_2$ ,  $\text{NHCH}_3$  and R= H,  $\text{CH}_3$ ,  $\text{CH}-\text{CH}_2$ , Ph, CCH). *Organometallics* **2002**, *21* (20), 4182-4191.
23. Marrone, A.; Re, N., Effects of Terminal Substituents on Metallacumulene Complexes: A Density Functional Study on  $(\text{CO})_5\text{Cr}(\text{C})_n\text{X}_2$  (X=F,  $\text{SiH}_3$ ,  $\text{CHCH}_2$ ,  $\text{NH}_2$ ,  $\text{NO}_2$ ). *Organometallics* **2002**, *21* (17), 3562-3571.
24. Jacobsen, H.; Ziegler, T., Trends in Structure and Bonding of Fischer Type Chromium Carbenes and Silylenes. A Density Functional Study. *Organometallics* **1995**, *14* (1), 224-230.
25. Ehlers, A. W.; Dapprich, S.; Vyboishchikov, S. F.; Frenking, G., Structure and Bonding of the Transition-Metal Carbonyl Complexes  $\text{M}(\text{CO})_5\text{L}$  (M= Cr, Mo, W) and  $\text{M}(\text{CO})_3\text{L}$  (M= Ni, Pd, Pt; L= CO, SiO, CS,  $\text{N}_2$ ,  $\text{NO}^+$ ,  $\text{CN}^-$ ,  $\text{NC}^-$ , HCCH, CCH<sub>2</sub>, CH<sub>2</sub>, CF<sub>2</sub>, H<sub>2</sub>). *Organometallics* **1996**, *15* (1), 105-117.
26. Torrent, M.; Duran, M.; Sola, M., Density Functional Study on the Preactivation Scenario of the Dötz Reaction: Carbon Monoxide Dissociation versus Alkyne Addition as the First Reaction Step. *Organometallics* **1998**, *17* (8), 1492-1501.
27. Vyboishchikov, S. F.; Frenking, G., Structure and Bonding of Low-Valent (Fischer-Type) and High-Valent (Schrock-Type) Transition Metal Carbene Complexes. *Chemistry–A European Journal* **1998**, *4* (8), 1428-1438.

28. Poater, J.; Cases, M.; Fradera, X.; Duran, M.; Solà, M., Electron pairing analysis of the Fischer-type chromium-carbene complexes  $(CO)_5Cr-C(X)(R)$ , ( $X=H, OH, OCH_3, NH_2, NHCH_3$  and  $R=H, CH_3, CH-CH_2, Ph, C-CH$ ). *Chemical Physics* **2003**, *294* (2), 129-139.
29. Topsom, R. D., Contribution of theoretical chemistry to an understanding of electronic substituent effects. *Accounts of Chemical Research* **1983**, *16* (8), 292-298.
30. De Lange, J. H.; Cukrowski, I., Toward deformation densities for intramolecular interactions without radical reference states using the fragment, atom, localized, delocalized, and interatomic (FALDI) charge density decomposition scheme. *Journal of computational chemistry* **2017**, *38* (13), 981-997.
31. de Lange, J. H.; van Niekerk, D. M. E.; Cukrowski, I., FALDI-based criterion for and the origin of an electron density bridge with an associated (3,-1) critical point on Bader's molecular graph. *J. Comput. Chem.* **2018**, *39* (27), 2283-2299.
32. Albright, T. A.; Burdett, J. K.; Whangbo, M.-H., *Orbital interactions in chemistry*. John Wiley & Sons: 2013.
33. Dapprich, S.; Frenking, G., Investigation of donor-acceptor interactions: a charge decomposition analysis using fragment molecular orbitals. *The Journal of Physical Chemistry* **1995**, *99* (23), 9352-9362.
34. Dapprich, S.; Frenking, G., CDA 2.1, Marburg, Germany, 1994. *The program is available via anonymous ftp server: ftp.chemie.unimarburg.de/pub/cda*.
35. M. J. Frisch, G. W. T., H. B. Schlegel, G. E. Scuseria, M. A. Robb, J. R. Cheeseman, G. Scalmani, V. Barone, G. A. Petersson, H. Nakatsuji, X. Li, M. Caricato, A. V. Marenich, J. Bloino, B. G. Janesko, R. Gomperts, B. Mennucci, H. P. Hratchian, J. V. Ortiz, A. F. Izmaylov, J. L. Sonnenberg, D. Williams-Young, F. Ding, F. Lipparini, F. Egidi, J. Goings, B. Peng, A. Petrone, T. Henderson, D. Ranasinghe, V. G. Zakrzewski, J. Gao, N. Rega, G. Zheng, W. Liang, M. Hada, M. Ehara, K. Toyota, R. Fukuda, J. Hasegawa, M. Ishida, T. Nakajima, Y. Honda, O. Kitao, H. Nakai, T. Vreven, K. Throssell, J. A. Montgomery, Jr., J. E. Peralta, F. Ogliaro, M. J. Bearpark, J. J. Heyd, E. N. Brothers, K. N. Kudin, V. N. Staroverov, T. A. Keith, R. Kobayashi, J. Normand, K. Raghavachari, A. P. Rendell, J. C. Burant, S. S. Iyengar, J. Tomasi, M. Cossi, J. M. Millam, M. Klene, C. Adamo, R. Cammi, J. W. Ochterski, R. L. Martin, K. Morokuma, O. Farkas, J. B. Foresman, and D. J. Fox, Gaussian, Inc., Wallingford CT, 2016., gaussian 09, Revision d. 01, Gaussian. Inc., Wallingford CT **2009**, 201.
36. Keith, T. A., AIMAll (Version 17.01. 25). *TK Gristmill Software, Overland Park KS, USA* **2017**.
37. Humphrey, W.; Dalke, A.; Schulten, K., VMD: visual molecular dynamics. *Journal of Molecular Graphics* **1996**, *14* (1), 33-38.

## **Chapter 5.**

### **The Ground State Molecular Orbital**

### **Fragment Analysis of Experimental Fischer**

### **Carbenes with X=OEt, NH<sub>2</sub> and NMe<sub>2</sub> and**

### **R= 2-(N-Methyl)pyrrolyl**

## Abstract

The choice of substituents in Fischer carbene complexes provides a large range of chemical functionality through electronic and geometrical effects. In particular, amino X-groups are thought to stabilize Fischer carbene complexes relative to ethoxy X-groups. The origin of amino groups' stabilizing effect is intuitively ascribed to their strong  $\pi$ -donating characters. However, the electronic structures of Fischer carbene complexes are notoriously difficult to elucidate, due to asymmetric molecular orbitals (MOs), correlated geometrical features and multi-centre bonding. The recently-developed Fragment, Atomic, Localized, Delocalized, Interatomic (FALDI) MO analysis allows for a classification of MOs based on a central metal's localized electron population. Such a classification can then be further used for decomposition of delocalized electrons for the quantification of MO contributions and recovery of  $\sigma$ - and  $\pi$ -characters. This work shows a case-study of the FALDI-MO approach on a small subset of Fischer carbene complexes commonly encountered in research laboratories. Our approach provides an in-depth interpretation of the electronic structure, as well as decouples electronic and geometric effects of various substituents.

## Introduction

The preceding chapters 3 and 4 have revolved around obtaining molecular orbital (MO) symmetry terms from asymmetric systems such as Fischer-type carbenes and then quantifying and recovering useful parameters such as  $\sigma$ - and  $\pi$ -character. The structures investigated, however, were predominantly chosen for their simplicity, rather than chemical applicability in an experimental laboratory. The current chapter aims to investigate the electronic structure, through the FALDI-MO approach of real, synthesized Fischer carbene complexes and compare with existing experimental results.<sup>1</sup>

Although many experimental and theoretical studies<sup>1-5</sup> of Fischer-type monocarbenes, bimetallic and even multi-metal carbenes complexes have been performed, in-depth theoretical investigations of their electronic structures are scarce. The dominant conceptual theory describing bonding in Fischer carbene complexes is the Dewar-Chatt-Duncanson (DCD) donor-acceptor model.<sup>6</sup> Unfortunately, DCD depends on atomic orbital (AO) and MO symmetries for exact



interpretation and quantification<sup>7</sup> – which, in turn, is only well-defined in a molecule with a high degree of symmetry. For the precise, rational design of novel materials, exact and quantifiable metrics are required, which necessitates a very comprehensive and *ab initio* understanding of electronic structures. This is particularly true if specific molecular properties – such as catalytic activity – are to be tuned through step-wise modification of molecular moieties – such as the choice of R- or X-groups in a Fischer carbene complex.

Computational studies on Fischer carbene complexes have mainly focussed on the steric and electronic effects within the framework of DCD – such as the degree to which the donor/acceptor atoms are affected.<sup>8</sup> A significant amount of experimental and computational work has been done on these heteroatom-stabilized Fischer carbene complexes.<sup>1, 9, 10, 11</sup> The majority of these works focus on alkoxy and amino substituents paired with group (VI) metals.<sup>12</sup> The alkoxy and amino groups (OR and NR<sub>2</sub>) substituents are found in most Fischer carbenes because of their stabilizing  $\pi$ -donor ability when paired with a low oxidation state metal like chromium.<sup>13</sup> While synthetic studies<sup>12</sup> and characterization methods<sup>14</sup> have taken forefront, little has been published regarding the 3D conformations<sup>1</sup> or their fundamental electronic structures.<sup>15</sup>

Since the 1970s heteroaromatic substituents have been studied in mononuclear Fischer carbenes of the form Cr(CO)<sub>5</sub>{C(X)(R)} where the heteroatomic substituents form the X-group (ethoxy, amino) and the heteroaromatic (R-group) substituent are 2-(N-methyl)pyrrolyl and (2-furyl,2-thienyl). Fischer carbene complex studies typically focus on the synthesis, spectroscopic and electronic properties of the complex, with the focus being the diatomic M–C<sub>carbene</sub> bond.<sup>16-18</sup> The M–C<sub>carbene</sub> interaction shows large variances in bond-length and ascribed  $\sigma$ - and  $\pi$ -bonding characters. Results that have stemmed from these studies have led to conclusions that if the R-group stays the same in the system Cr(CO)<sub>5</sub>{C(X)(R)} then typically the Cr⋯C<sub>carbene</sub> bond length is longer when the X-group is a stronger  $\pi$ -electron donor substituents.<sup>9</sup> As such, amino substituents are often better at stabilizing the carbene bond than ethoxy substituents.<sup>5</sup> Considering the X-group and the  $\pi$ -donor strength, it has been found that the alkoxy groups are softer donor groups than the amino groups.<sup>15</sup> This result is often reflected in the bond lengths, where alkoxy carbene complexes display larger bond lengths between the X-group and the carbene carbon than amino counterparts.<sup>1, 19-22</sup> Conversely, an amino group as X-substituent causes the Cr–C<sub>carbene</sub> bond to lengthen and the C<sub>carbene</sub>–X bond to shorten. This is because the X-group is a strong electron

donor which, supposedly, causes the metal to donate less electron density back to the carbene carbon through  $\pi$ -backbonding. In turn, the metal's back donation to the CO groups increases so the Cr-CO<sub>trans</sub> bond is expected to shorten – as observed in crystal structures.<sup>19, 20, 23</sup> The electronic effects of the X-group therefore clearly affect bond length which relates to  $\sigma$ -,  $\pi$ -character making the electronic structure crucial to understand. The X-group may also change the molecular geometry because of hybridization of the heteroatom, which has 3D implications on the system because of steric effects even though the electronic structure may be the same.

Spectroscopic studies<sup>16, 17</sup> are typically used to investigate the electronic properties of the various substituents and their effects by using techniques such as NMR, UV-visible and IR spectral studies to observe effects of electron density delocalized from the X- and R-group into the carbene carbon's empty *p* orbital. The work of Connor<sup>16</sup> concluded that the heteroaromatic substituent causes stabilization by releasing conjugated electrons. The carbene carbon's electronic character was found, by NMR studies,<sup>17</sup> to be the most influenced by the X-group over either the R-group or the metal. The same conclusion was obtained by Montserrat and co-workers<sup>9</sup> – that the Cr-C<sub>carbene</sub> bond is more affected by the X-group than the R-group. While it was originally expected that there would be specific  $\pi \rightarrow p$  donation (i.e. from the X-group to C<sub>carbene</sub>), evidence pointed instead towards the R-group delocalizing electrons through conjugation.<sup>1</sup> This is an interesting result with electrons being shared throughout the system in a multi-centric fashion, rather than through specific electron delocalization. However, electron (de)localization is a notoriously difficult concept to study due to the correlated nature of electrons, and further proof for these conjectures have not been found yet.

The chemical reactivity of Fischer carbene complexes is also mostly influenced by electrophilicity of the ligands, which is determined and controlled by the X- and R-substituents on the carbene.<sup>9</sup> As a result, many coordination chemists look at tuning and controlling the specific reactivity of a system through careful modification. For instance, there are Fischer carbenes with 2-thienyl groups which show potential in organic synthesis reactions<sup>24-26</sup> while other R-groups still need investigation.<sup>1</sup> A plethora of photochemical and thermal reactions are typically also associated with chromium carbene complexes and they have proven to be useful in organic chemistry as synthons<sup>27, 28</sup> but their overall uses in material chemistry are rather limited. Systematically testing each chemical modification is a time-consuming process and such 'bulk

screening' approaches to material design are highly inefficient – unless accelerated by predictive computational models. Unfortunately, such models do not exist yet, and requires more fundamental understanding of the electronic structure to be effective.

A potential avenue of relating the computational results and the experimental systems is to look at the electrochemistry. Many Fischer carbene complexes have been electrochemically studied in order to investigate the electronic effects caused by various ligands.<sup>1, 29</sup> It was observed that the  $\pi$ -acceptor/ $\sigma$ -donor ratio of ligands reflected trends for the half-wave potential ( $E_{1/2}$ ) of oxidation. Much older work, however, showed that although the  $\pi$ -acceptor/ $\sigma$ -donor ratio closely followed the molecular orbital calculations, the carbene substituents' (X- and R-groups) influence on the redox orbitals are indirect.<sup>29</sup> Regardless, other studies have revealed that the electrochemical properties of N-methylpyrrol derivatives differ slightly from other heterocycles in Fischer systems because of the methyl substituents' steric influence which can affect orbital overlap.<sup>30</sup>

Clearly, the bridging of experimental results and fundamental electronic structure theories is a challenging yet very important task. In this work we provide novel insights into this task, using the recently-developed Fragment, Atomic, Localized, Delocalized and Interatomic (FALDI) density decomposition scheme. In particular, we utilize the FALDI-MO scheme, which allows for an in-depth and symmetry-based interpretation of MOs with respect to interacting fragments of a molecule. The conceptual component of this chapter is an excellent example of how FALDI simplifies the bonding into visual components. Specifically, we will analyze experimental trends of the selected Fischer carbene complexes and attempt to correlate these patterns with FALDI-based insights of the electronic structure.

## Theoretical Background and Development

The FALDI density decomposition scheme<sup>31, 32</sup> provides an exhaustive electron density (ED) decomposition for atomic and diatomic interactions for any coordinate  $\mathbf{r}$ . The postulate of FALDI is defined by the atomic basin from QTAIM. This is the orthodox definition of FALDI. We have further expanded FALDI through the FALDI-MO method (Chapters 3 and 4), which recovers classical symmetry terms from octahedral asymmetric metal centred systems. MOs are decomposed into their distributions in terms of localized electron density (*loc*-ED):

$$\mathcal{L}_A(\mathbf{r}) = \sum_{ij} \chi_i(\mathbf{r})\chi_j(\mathbf{r})(\mathbf{G}^A \mathbf{S}^A)_{ji} \quad (1)$$

The *loc*-ED is specifically focused on the metal centre and localized indices (LIs) can be recovered after integrating Eq. 1 over all molecular space. The LI is used to obtain the metal centres Natural Density Functions (NDFs) which when visualized as 3D-isosurfaces represents the classical symmetry terms such as  $a_{1g}$ ,  $t_{1u}$ ,  $t_{2g}$  and  $e_g$ . Mathematically the NDFs are known as  $\phi_i^{AA}(\mathbf{r})$ :

$$\phi_i^{AA}(\mathbf{r}) = \sum_j^{N_{MO}} \chi_j(\mathbf{r})U_{ji}^{AA} \quad (2)$$

the classical symmetry terms described by the *loc*-NDFs of the metal are mostly recovered except for the non-localized (NL) term which is used to label symmetries that are not defined by the metal.

Similarly, the delocalized indices (DI) can be described by *deloc*-ED distribution:

$$D_{A,B}(\mathbf{r}) = \sum_{ij} \chi_i(\mathbf{r})\chi_j(\mathbf{r})(\mathbf{G}^A \mathbf{S}^B + \mathbf{S}^B \mathbf{G}^A)_{ji} \quad (3)$$

with  $D_{A,B}(\mathbf{r})$  providing the contribution at  $\mathbf{r}$  and describing the total ED between atomic basin  $\Omega_A$  and  $\Omega_B$ . Integrating the *deloc*-ED then yields the DI, which describes electrons delocalized diatomically between atoms.

Atomic and diatomic interactions however do not describe the entire molecule. This work focuses on MOs, which are molecular wide and therefore multiple diatomic interactions occurring molecular wide need to be considered. For this reason, FALDI fragments are introduced which is essentially a summation of diatomic interactions, these fragments are labelled ( $\mathcal{F}$ ).

To accommodate the fragments (multiple diatomic interactions) the *deloc*-ED distribution can be adapted. If two fragments are considered,  $\mathcal{F}1$  and  $\mathcal{F}2$ , with the sum of the FALDI *atom*-ED distributions, then the total density contribution of a fragment contributing at any coordinate  $\mathbf{r}$  can be found:

$$g_{\mathcal{F}1}^{total}(\mathbf{r}) = \sum_A^{M_{\mathcal{F}1}} g_A(\mathbf{r}) \quad (4)$$

where  $M_{\mathcal{F}1}$  represents the number of atoms within the fragment  $\mathcal{F}1$ . The total electronic population,  $N^{total}(\mathcal{F}1)$ , of the fragment can then be obtained by integrating  $g_{\mathcal{F}1}^{total}(\mathbf{r})$  over all molecular space.

The electrons localized for each fragment and the delocalized electrons between fragments are found in the  $g_{\mathcal{F}1}^{total}(\mathbf{r})$  term.

The contribution of the localized electrons to each fragment at  $\mathbf{r}$  is described by:

$$\mathcal{L}_{\mathcal{F}1}(\mathbf{r}) = \sum_A^{M_{\mathcal{F}1}} \mathcal{L}_A(\mathbf{r}) \quad (5)$$

and each atom in the fragment contains core and non-bonded electrons which are described by this term. Similarly, the electrons which are delocalized between fragments (intra-delocalization) can be determined at the coordinate  $\mathbf{r}$ ,

$$\mathcal{D}_{\mathcal{F}1}^{intra}(\mathbf{r}) = \sum_A^{M_{\mathcal{F}1}-1} \sum_{B=A+1}^{M_{\mathcal{F}1}} \mathcal{D}_{A,B}(\mathbf{r}) \quad (6)$$

The localized and delocalized electrons in Eq. 5 and 6 can then be combined to produce the total intra-fragment electron distribution:

$$g_{\mathcal{F}1}^{intra}(\mathbf{r}) = \mathcal{L}_{\mathcal{F}1}(\mathbf{r}) + \mathcal{D}_{\mathcal{F}1}^{intra}(\mathbf{r}) \quad (7)$$

The  $g_{\mathcal{F}1}^{intra}(\mathbf{r})$  term includes both atom-localized and intra-atomic delocalized electrons localized to  $\mathcal{F}1$  at coordinate  $\mathbf{r}$ . Integrating  $g_{\mathcal{F}1}^{intra}(\mathbf{r})$  over all molecular space produces the total intra-fragment electron population, which is equivalent to the sum of the LIs and DIs for the fragments,

$$N^{intra}(\mathcal{F}1) = \int g_{\mathcal{F}1}^{intra}(\mathbf{r}) d\mathbf{r} = \sum_A LI(A) + \sum_{A,B} DI(A,B) \quad (8)$$

for which  $A, B \in \mathcal{F}1$ . The inter-fragment delocalization can be obtained by considering the *deloc-ED* distribution between fragments  $\mathcal{F}1$  and  $\mathcal{F}2$ ,

$$\mathcal{D}_{\mathcal{F}1,\mathcal{F}2}^{inter}(\mathbf{r}) = \sum_A^{M_{\mathcal{F}1}} \sum_B^{M_{\mathcal{F}2}} \mathcal{D}_{A,B}(\mathbf{r}) \quad (9)$$

describing the delocalized electron distribution for the two fragments. Integrating the inter-fragment delocalization over all molecular space yields the inter-fragment DI,

$$DI(\mathcal{F}1, \mathcal{F}2) = \int \mathcal{D}_{\mathcal{F}1, \mathcal{F}2}^{\text{inter}}(\mathbf{r}) \, d\mathbf{r} \quad (10)$$

where  $A \in \mathcal{F}1$  and  $B \in \mathcal{F}2$ . Coming back to Eq. 4 the total of  $g_{\mathcal{F}1}^{\text{total}}(\mathbf{r})$  can be obtained by the summation of Eq. 7 and 9.

$$g_{\mathcal{F}1}^{\text{total}}(\mathbf{r}) = g_{\mathcal{F}1}^{\text{intra}}(\mathbf{r}) + \sum_X \frac{1}{2} \mathcal{D}_{\mathcal{F}1, \mathcal{F}X}^{\text{inter}}(\mathbf{r}) \quad (11)$$

Finally, linking the FALDI MO analysis to the fragments for quantification is rather straightforward. Just as the FALDI MO analysis would be linked to the atomic or diatomic DI the same can be done with the inter-atomic DI. The metal-based classification scheme depends on the *loc*-NDFs of the metal for the symmetry term, which is then weighted by the inter-fragment delocalized electrons:

$$DI(\mathcal{F}1, \mathcal{F}2) = \sum_i^{N_{MO}} d_i^{\mathcal{F}1, \mathcal{F}2} \left[ a_{1g} n_i^M + t_{1u} n_i^M + t_{2g} n_i^M + e_g n_i^M + N_L n_i^M \right] \quad (12)$$

The result is quantified MO contributions of the defined fragment with symmetry classifications determined by the *loc*-NDFs of the metal. These symmetry classifications allow the recovery of bonding modes such as  $\sigma$  ( $a_{1g}$ ,  $t_{1u}$  and  $e_g$ ) and  $\pi$  ( $t_{2g}$ ) which can be quantified allowing for more holistic interpretations of the electronic structure.

## Computational Details

Crystal structures of the three Fischer carbenes **5a-c** (Figure 5. 1.) were obtained from a colleague, and single complexes were isolated as input structures. A series of structures were generated for each of **5a-c** by varying the Cr-C<sub>carbene</sub>-C<sub>pyrrole</sub>-N<sub>pyrrole</sub> dihedral angle of the R-group in ten-degree increments between 90° and 180° whilst keeping the remainder of the molecule frozen. All the structures were then optimized (subject to the above-mentioned constraint) using DFT in Gaussian 09<sup>33</sup> with B3LYP<sup>7</sup> and a basis set of def2-SV(P) in an implicit solvent model of *n*-hexane. The spin state was kept as a singlet, as is expected of Fischer Carbenes. The optimized structures were

used, and ground state single-point calculations were performed using these structures and the perpendicular and planar frozen dihedrals ( $90^\circ$  and  $180^\circ$ ) optimized structure with CAM-B3LYP, nosymm (no symmetry) in a solvent of n-hexane. The wavefunctions used in AIMAll v. 17.01.25.<sup>34</sup> were generated from the single point calculations using Gaussian 09. FALDI were performed using the QTAIM data calculated with orthodox overlap matrices. The NDFs generated in FALDI was visualized in VMD 1.9.3<sup>35</sup> in order to confirm symmetry assignments. In-house software was used to calculate the LMAT, label symmetries and the FALDI fragments which were used for the quantification cross-linked to the symmetries and shared electrons analysis.

## Structures

The following structures were used in the FALDI MO decomposition and fragment analysis:

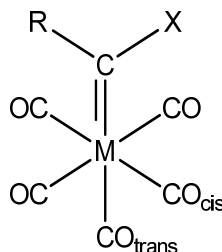


**Figure 5. 1.** The Fischer Carbene labelling, with the X-group representing the electron-donating group. Where  $M=Cr$ , 5a is  $X=OEt$  and  $R=2-(N\text{-Methyl})\text{pyrrolyl}$ , 5b is  $X=NH_2$  and  $R=2-(N\text{-Methyl})\text{pyrrolyl}$  and 5c is  $X=NMe_2$  and  $R=2-(N\text{-Methyl})\text{pyrrolyl}$

We supply the Cartesian coordinates of the crystal input structures in Table C 1. 1. to C 1. 12. of Appendix C, accompanied by the molecules' molecular energies.

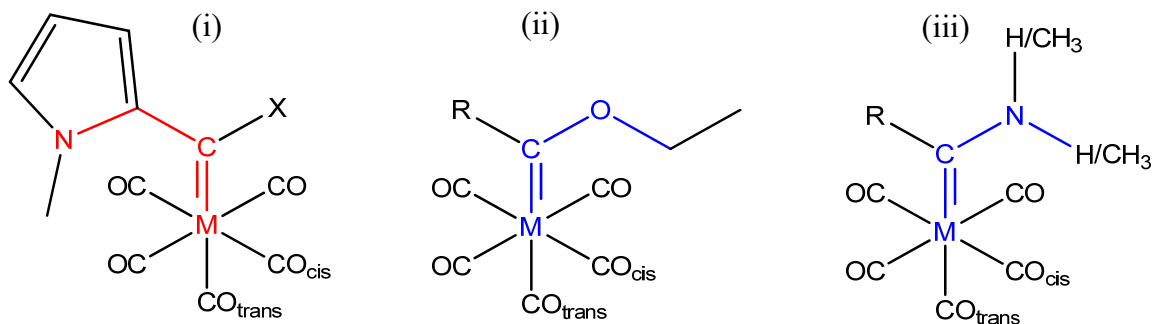


**Figure 5. 2.** The dihedral angles of the three Fischer carbenes selected for constrained optimizations. The red lines show the dihedral angle ( $\text{Cr-C}_{\text{carbene}}\text{-C}_{\text{pyrrole}}\text{-N}_{\text{pyrrole}}$ ) that were frozen for the R-group in (i) while the blue lines represent the X-groups dihedral angle ( $\text{Cr-C}_{\text{carbene}}\text{-O/N-H/C}$ ) that were set to zero at the start of each optimization calculation for the three different X-groups (ii) and (iii).

We optimized each of the three structures nine times, changing the  $\text{Cr-C}_{\text{carbene}}\text{-C}_{\text{pyrrole}}\text{-N}_{\text{pyrrole}}$  dihedral from  $180^\circ$  to  $90^\circ$  (in ten-degree increments). The X-group  $\text{Cr-C}_{\text{carbene}}\text{-X-C/H}$  dihedral (in blue for Figure 5. 2. (ii) and (iii)) were set to 0 degrees at the start of each optimization and left unfrozen.

## Fragmentations

For the purposes of fragment-based FALDI-MO analyses, chemical fragments need to be defined. The fragmentation scheme used is displayed in Figure 5.3, and contains the metal and pentacarbonyl ligands, [M], carbene carbon atom,  $\text{C}_{\text{carbene}}$ , and R- and X-groups, [R] and [X], respectively. The carbene ligand as a whole was also considered, with  $[\text{L}] = \text{C}_{\text{carbene}} + [\text{R}] + [\text{X}]$ . Various interfragment interactions will be considered and discussed throughout this manuscript, i.e. the notation  $[\text{M}]\cdots[\text{R}]$  implies the long-range interaction between the metal fragment and the R-group.

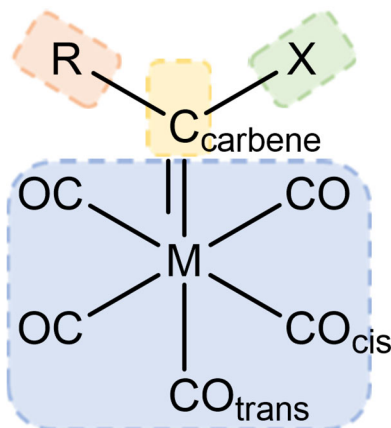




**Figure 5. 3.** Generalized fragments used for FALDI Fragments Molecular Orbital Analysis. Blue: Metal and pentacarbonyl ligands, [M]. Yellow: C<sub>carbene</sub>; Orange: R-group, [R]; and Green: X-group, [X]. The carbene ligand as a whole, [L] = C<sub>carbene</sub> + [R] + [X].

Figure 5. 3. illustrates the general fragmentation of the molecule in a pictorial format, the X-group was the only parameter changed. The metal cluster, [M], is defined as the metal and the five carbonyls, indicated in blue, the carbene carbon as yellow, the R-group as orange and the X-group as green. These are the fragments used in the comparisons and classifications for the specific bonds or interactions investigated. Through FALDI, any fragment can be assigned and analysed.

## Results and Discussion

### *Investigation of structural parameters*

All structures were optimized by constraining the dihedral angle of Cr, C<sub>carbene</sub>, C<sub>pyrrole</sub>, and N<sub>pyrrole</sub>, henceforth referred to as DA(Cr,C,C,N). The dihedral angles were scanned in steps of 10°, and the lowest energy structures for **5a**, **5b** and **5c** corresponded to DA(Cr,C,C,N) of 170°, 150° and 110°, respectively.

Selected computational structural parameters are compared to those from crystallographic data in Table 5. 1. Absolute comparisons of bond lengths and dihedral angles is irrelevant in this study due to very different environmental factors (i.e. crystal-packing and solvation factors). Important, however, is that our computational modelling predicts the same trends with respect to **5a**, **5b** and **5c** as is observed in the crystal structures. Indeed, lowest-energy structures predict the same trends in dihedral and torsional angles, as well as M...X<sub>1</sub> and M...R<sub>1</sub> distances (X<sub>1</sub> and R<sub>1</sub> being the first atom of the fragment). The M...C<sub>carbene</sub> bond length trend, however, is not reproduced by B3LYP, nor by B3LYP with Grimme's empirical dispersion or even MP2 optimization (Table 5. 2.) with a def2-SV(P) basis set. However, the variation of the experimental M...C<sub>carbene</sub> bond length is extremely small (2.108 and 2.103 in **5a** and **5b**, respectively) and is possibly due to crystal packing and/or solvation factors.

**Table 5. 1.** Comparison of the crystal structures to lowest energy-optimized structures, where the dihedral (N<sub>pyrrole</sub>-C<sub>pyrrole</sub>-C<sub>carbene</sub>-X) and torsion angle (R-C<sub>carbene</sub>-X) represent the angle between the X- and R-groups.

	Frozen	Structure	Dihedral Angle (°)	Torsion Angle (°)	Bond Length (Å)		
	Dihedral Angle (°)				M···C <sub>carbene</sub>	M···X	M···R
Experimental	none	5a	0.000	107.657	2.108	3.104	3.152
	none	5b	29.307	114.458	2.103	2.990	3.164
	none	5c	80.252	112.004	2.104	3.127	3.086
B3LYP	170	5a	-7.465	108.244	2.137	3.119	3.192
	150	5b	-27.093	114.697	2.131	3.021	3.203
	110	5c	-68.176	113.156	2.139	3.165	3.104

The X-group can drastically affect the character of the Fischer carbene complex, and specifically so the Cr···C<sub>carbene</sub>, C<sub>carbene</sub>···X and Cr···CO<sub>trans</sub> bondlengths.<sup>19, 20, 23</sup> Based on the  $\pi$ -donating ability of the X-group, these bond lengths are predicted to change. The expected  $\pi$ -donating ability<sup>36</sup> for the X-groups in this study is OEt<NH<sub>2</sub><NMe<sub>2</sub> or **5a**<**5b**<**5c**. Conceptually weaker donors should cause longer C<sub>carbene</sub>···X bonds but this, in turn, should cause the Cr···C<sub>carbene</sub> bond to shorten due to increased  $\pi$ -back-bonding from the metal. Consequentially, the Cr···CO<sub>trans</sub> bond should then lengthen because of the *trans*-effect.<sup>19, 20</sup> The *trans* effect is however difficult to see in carbonyl complexes, as the minor changes in bond length are often lost in their standard deviation.<sup>19</sup>

**Table 5. 2.** The crystal structures bond lengths when the X-group changes<sup>a</sup>

		Bond lengths (Å)			
	Structure	Cr···C <sub>carbene</sub>	C <sub>carbene</sub> ···X	C <sub>carbene</sub> ···R	Cr···CO <sub>trans</sub>
Experimental	<b>5a</b>	2.108	1.330	1.433	1.874
	<b>5b</b>	2.103	1.313	1.448	1.871
	<b>5c</b>	2.104	1.314	1.496	1.865
B3LYP	<b>5a</b>	2.137	1.328	1.447	1.881
	<b>5b</b>	2.131	1.334	1.452	1.880
	<b>5c</b>	2.139	1.330	1.487	1.881
B3LYP with D3 Grimme's	<b>5a</b>	2.137	1.328	1.447	1.881
	<b>5b</b>	2.131	1.334	1.452	1.880
	<b>5c</b>	2.139	1.330	1.487	1.881
MP2	<b>5a</b>	2.029	1.323	1.444	1.828
	<b>5b</b>	2.026	1.329	1.449	1.824
	<b>5c</b>	2.032	1.323	1.477	1.825

<sup>a</sup>The computational structures are the lowest energy structures

The conceptual model described above seems to predict experimental and computational bond lengths fairly well: the C<sub>carbene</sub>···X bond is shortest in the amines (stronger  $\pi$ -donating ability). These effects are however of an *electronic* origin. In addition, we also expect several geometric or steric effects, such as Coulombic attraction or steric repulsion between various functional groups within the complex. For instance, when X=NH<sub>2</sub> (**5b**) is replaced by X=NMe<sub>2</sub> (**5c**), we expect the bulkier methyl groups to influence the position and orientation of the pyrrole R-group.

Of particular importance is then the DA(Cr,C,C,N), Figure 5.2(i). When X=OEt, DA(Cr,C,C,N) = 170° (computational) and 0° (experimental), and the entire carbene ligand is therefore expected to be close to planar. On the other hand, when X=NMe<sub>2</sub>, DA(Cr,C,C,N) = 110° (computational) and 99.748° (experimental), and the pyrrole ligand is therefore expected to be almost perpendicular with respect to the carbene ligand. While it is tempting to ascribe the

observed DA(Cr,C,C,N) values to steric effects, it is unclear how much of an effect the electronic influence of the X-group has on DA(Cr,C,C,N).

It is clear from the above discussion that the choice of X-group imposes both a steric (geometric) and an electronic effect. The structure that is observed (whether experimentally or computationally) is the net result of both geometric and electronic effects. In order to gauge the extent to which both these effects influence the final structure, we will now conduct further analysis using two different approaches: (i) the geometric effect will be investigated by keeping the X-group constant and systematically changing the DA(Cr,C,C,N), and (ii) the electronic effect will be investigated by changing the X-group for a constant (Cr,C<sub>carbene</sub>,C<sub>pyrrole</sub>,N<sub>pyrrole</sub>) dihedral angle. We will analyze these effects using both the FALDI-MO analysis (as discussed in Chapters 3 and 4) approach and a full FALDI fragment population analysis. For FALDI-MO analyses, we will primarily focus on the MO classification and decomposition of the electrons shared across the entirety of the metal cluster's interaction with the ligand, [M]...[L] and its associated delocalization index, DI([M],[L]). This index measures the total number of electrons delocalized (shared) between all atoms, including the electrons shared by Cr and C<sub>carbene</sub> as well as between CO<sub>trans</sub> and the R- and X-groups.

### *The geometric effect imposed by choice of X-group*

We investigated all structures **5a–5c** at three different dihedral angles: DA(Cr,C,C,N) equal to 180°, 90° and the DA corresponding to the optimized geometry (170°, 150° and 110° for **5a**, **5b** and **5c**, respectively). To ease discussion, we will primarily focus on the changes occurring within **5a**, and will only discuss the changes occurring within **5b** and **5c** in a comparative fashion.

MOs are often used to interpret and understand electronic and steric effects within a metal complex. The MOs in **5a** remain qualitatively similar when the DA(Cr,C,C,N) is changed, however. Given the large number of occupied MOs present in the structure, correlating near imperceptible MO changes with a change in DA(Cr,C,C,N) is therefore impossible when visually inspecting MO isosurfaces. In addition, the lack of symmetry in the molecule excludes exact quantification and interpretation using group theory. The FALDI-MO method, however, provides concise answers regarding specific metal–ligand interactions while taking into account the full list

of occupied MOs. MOs describing the entire metal–ligand interaction **5a** in (X=OEt) were first classified in terms of symmetry labels (i.e.  $t_{2g}$  and  $e_g$ ) and then grouped accordingly as  $\sigma$ - and  $\pi$ -contributions. This procedure was discussed briefly in the Theoretical Background, as well as extensively in previous chapters.

Table 5. 3. shows the FALDI-MO results for the [M]...[L] interaction – the interaction between the full metal–carbonyl cluster and the entire carbene ligand – in **5a**. At  $DA(\text{Cr,C,C,N}) = 180^\circ$ , the total number of electrons shared between [M] and [L] fragments is  $DI([\text{M}], [\text{L}]) = 1.5733 e^-$ . Of these electrons,  $\sigma$ -MOs contribute  $0.4810 e^-$  (30.57%) whereas  $\pi$ -MOs contribute  $0.3720 e^-$  (23.64%). The remaining 45.78% arises from non-localized (NL) MOs that do not involve metal-centered atomic orbitals (AOs) directly, but contribute to shared density through polarization, inductive or multicentric effects. As the  $DA(\text{Cr,C,C,N})$  is changed to  $90^\circ$ , the total number of shared electrons increases to  $1.7953 e^-$ . Of these electrons, the  $\sigma$ -MOs' contributions decrease (to 24.46%) whereas the  $\pi$ -MOs' contributions increase (to 30.80%). We observe similar trends in **5b** and **5c** (Tables C 3. 2. and C 3. 3. in Appendix C).

**Table 5. 3.** The FALDI MO analysis of X=OEt (**5a**) for various dihedrals  $DA(\text{Cr,C,C,N})$  considering the [M]...[L] interaction.

Frozen						
Dihedral Angle ( $^\circ$ )	180		170		90	
	Contribution	%	Contribution	%	Contribution	%
$\sigma$	0.4810	30.57	0.4788	30.41	0.4032	22.46
$\pi$	0.3720	23.64	0.3798	24.12	0.5530	30.80
NL	0.7203	45.78	0.7162	45.48	0.8391	46.74
$\sigma$ & $\pi$	0.8530	54.22	0.8586	54.52	0.9562	53.26
<i>Total</i>	<i>1.5733</i>		<i>1.5748</i>		<i>1.7953</i>	

These trends are quite surprising and unintuitive – a *decrease* in both total number of electrons shared as well as  $\pi$ -MOs' contributions might have been expected because of the break

in planarity when  $DA(\text{Cr,C,C,N}) = 90^\circ$  relative to  $180^\circ$ , yet an *increase* is observed. Furthermore, minor change would be expected for the  $\sigma$ -MOs' contributions because of the symmetry of the  $\sigma$ -MOs, yet a large change was observed. From a synthetic design perspective, these trends illustrate that a geometrical change alone has a significant impact on the distribution of both  $\sigma$ - and  $\pi$ -delocalized electrons.

**Table 5. 4.** The FALDI fragment population for  $X=\text{OEt}$ , **5a**.

Structure	Frozen Dihedral Angle ( $^\circ$ )	Total Electron Population, $N([\text{A}])$				Total intra-fragment population $N^{\text{intra}}([\text{A}])$			
		[M]	$\text{C}_{\text{carbene}}$	[X]	[R]	Metal	$\text{C}_{\text{carbene}}$	[X]	[R]
5a	90	94.03	5.52	25.50	42.95	92.27	3.79	24.66	42.14
5a	170	94.14	5.53	25.53	42.81	92.43	3.81	24.65	41.80
5a	180	94.14	5.53	25.53	42.81	92.43	3.81	24.64	41.80

To provide some additional insight to these trends, a FALDI fragment-based population analysis was performed using the fragmentation scheme shown in Figure 5. 3. Table 5. 4. contains the fragment electronic populations for **5a** for the three selected values of  $DA(\text{Cr,C,C,N})$  whereas Table 5. 5. shows the changes in inter-fragment electron delocalization counts. Most notably, the total number of electrons found, on average, in the metal cluster is given by  $N([\text{M}])$  in Table 5. 4. and is referred to as the total electron population.  $N([\text{M}])$  decreases significantly (by  $\sim 0.11 e^-$ ) when  $DA(\text{Cr,C,C,N}) = 90^\circ$  relative to  $180^\circ$ , whereas the electron population of the pyrrole group,  $N([\text{R}])$ , increases significantly (by  $\sim 0.14 e^-$ ). While  $N([\text{M}])$  includes all electrons within the metal cluster (including electrons delocalized between fragments), the total intra-fragment population ( $N^{\text{intra}}([\text{M}])$ , Table 5. 4.) counts electrons that are only localized to the metal cluster itself.  $N^{\text{intra}}([\text{M}])$  also decreases whereas  $N^{\text{intra}}([\text{R}])$  also increases as the  $DA(\text{Cr,C,C,N})$  changes from  $180^\circ$  to  $90^\circ$ . The observed changes in  $N$  and  $N^{\text{intra}}$  therefore indicate a *transfer of charge* from the metal cluster to the pyrrole group in the perpendicular relative to planar structure. Comparatively minor changes are observed for the carbene carbon and X-group electron populations.

**Table 5. 5.** The FALDI inter-fragment electron delocalization for X=OEt, 5a.

Structure	Frozen Dihedral Angle (°)	Electrons shared DI([A], [B])					
		[M]...C <sub>carbene</sub>	[M]...[X]	[M]...[R]	C <sub>carbene</sub> ...[X]	C <sub>carbene</sub> ...[R]	[R]...[X]
5a	90	1.1855	0.3280	0.2818	1.1390	1.1312	0.2209
5a	170	0.9927	0.3062	0.2758	1.0785	1.3685	0.3720
5a	180	0.9874	0.3068	0.2791	1.0785	1.3711	0.3760

Charge-transfer, however, does not explain the trends observed for  $\sigma$ - and  $\pi$ -MOs' contributions to shared density (Table 5. 3.). The inter-fragment delocalization index  $\{DI([M], [C_{\text{carbene}}])\}$ , Table 5. 5., counts the number of electrons shared between the metal cluster and the carbene carbon. When  $DA(\text{Cr,C,C,N}) = 180^\circ$ , 0.9874 electrons are shared between the [M] and C<sub>carbene</sub> fragments. As  $DA(\text{Cr,C,C,N})$  changes to  $90^\circ$ ,  $DI([M], C_{\text{carbene}})$  increases to 1.1855  $e^-$  (+0.1981  $e^-$ ), indicating that the metal–carbene bond (and carbonyl...carbene interactions) strengthened significantly in the perpendicular structure. The other notable trends as  $DA(\text{Cr,C,C,N})$  changes from  $180^\circ$  to  $90^\circ$  are: i) a significant decrease of the electrons shared between C<sub>carbene</sub> and the pyrrole [R] fragment ( $-0.2399 e^-$ ), ii) a significant increase in the electrons shared between pyrrole [R] and ethoxy [X] fragments (+0.1551  $e^-$ ) and, to a lesser extent, iii) an increase in the electrons shared between C<sub>carbene</sub> and the ethoxy [X] fragment (+0.0605  $e^-$ ).

Each of the terms in Table 5. 4. and Table 5. 5. can also be visualized. Selected FALDI isosurfaces, are shown in Figure 5. 4. The manner through which electrons are shared between C<sub>carbene</sub> and the [R] fragment, as well as between [X] and [R] fragments, is considerably different (and more) when  $DA(\text{Cr,C,C,N}) = 180^\circ$  than  $90^\circ$ . For instance, the [X]...[R] interaction involves the methyl group on the pyrrole at  $180^\circ$  but not at  $90^\circ$ . While the [M]...C<sub>carbene</sub> and [M]...[X] interactions seem to involve more  $\pi$ -character when  $DA(\text{Cr,C,C,N}) = 90^\circ$  than  $180^\circ$ . Interestingly, inspection of FALDI isosurfaces also revealed a different manner of electron sharing between the [R] fragment and the carbonyl groups in the metal cluster, with respect to the DA. This is just an observation and for this reason these results are shown, and discussed, in Section 4 and Section 5 of Appendix C under Table C 4. 1. to Table C 4. 3. and Table C 5. 1. to Table C 5. 3. illustrating greater  $\pi$ -character at  $90^\circ$  than at  $180^\circ$  for [M]...C<sub>carbene</sub> and [M]...[X] respectively.

## Interfragment electron delocalization

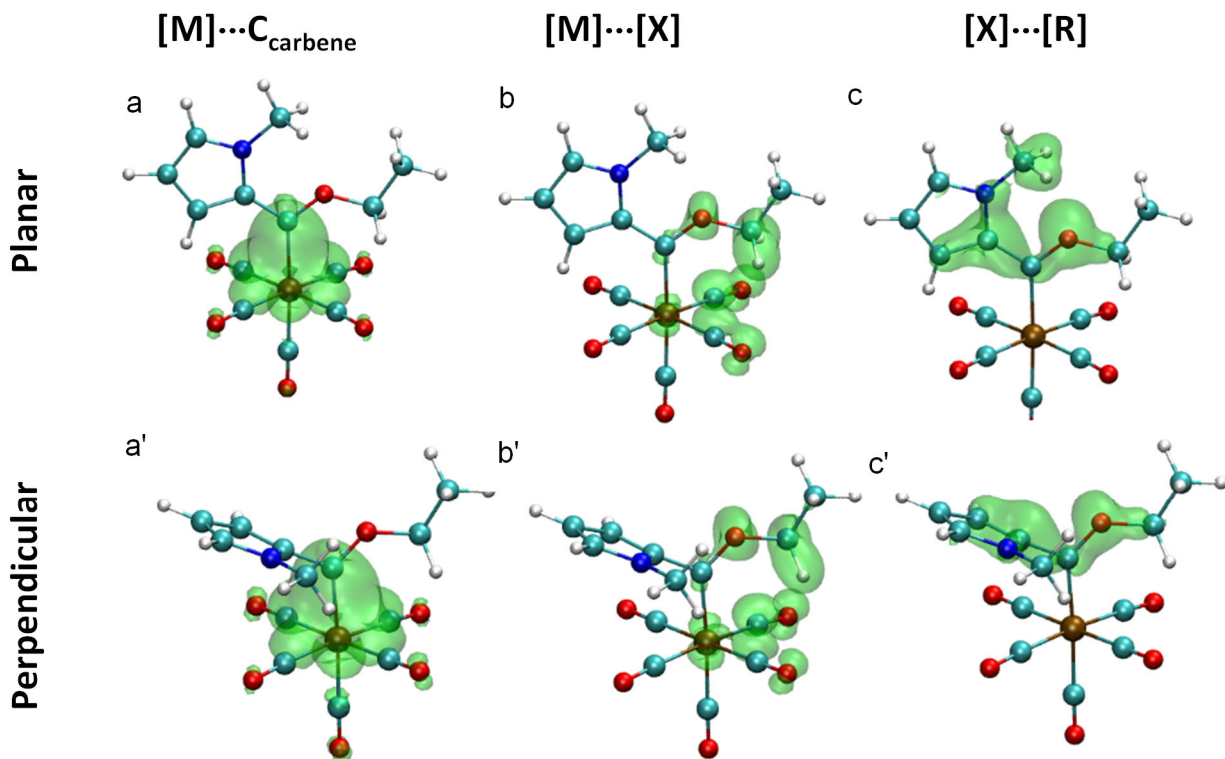


**Figure 5. 4.** The interfragment interaction where the X=OEt (**5a**) is compared at dihedral angle, DA(Cr,C,C,N), of  $180^\circ$  (a) and  $90^\circ$  (a'). The electrons are shared between fragments (a)  $[M]\cdots C_{\text{carbene}}$ , (b)  $[M]\cdots [X]$  (c)  $[X]\cdots [R]$ . All the isovalues are shown at 0.001 a.u.

In summary, regarding the geometric effect in **5a**: changing DA(Cr,C,C,N) from  $180^\circ$  (planar) to  $90^\circ$  (perpendicular) results in a considerable increase in contributions from  $\pi$ -MOs and a decrease in contributions from  $\sigma$ -MOs. At DA(Cr,C,C,N) =  $90^\circ$ , both the carbene carbon and ethoxy X-group shares considerably fewer electrons with the pyrrole R-group. Correspondingly, more electrons are localized on the R-group and an overall increase in electronic population is observed. On the other hand, the carbene carbon shares more electrons with both the ethoxy X-group and the metal cluster as a whole at  $90^\circ$  than at  $180^\circ$ . Correspondingly, fewer electrons are localized in the metal cluster and we observe an overall decrease in electronic population. Overall, as the DA(Cr,C,C,N) is changed from  $180^\circ$  to  $90^\circ$ , the manner through which the [R] fragment shares electrons with the rest of the molecule becomes noticeably different and significantly less. Our results suggest that the weaker  $[R]\cdots C_{\text{carbene}}$  and  $[R]\cdots [X]$  interactions lead to stronger



[M]...C<sub>carbene</sub> and [M]...[X] interactions with greater  $\pi$ -characters, and an overall increase in the number of electrons shared between the metal cluster and the carbene ligand as a whole.

Very similar trends are obtained when the  $DA(\text{Cr,C,C,N})$  is varied for structures **5b** and **5c**; FALDI-MO and FALDI population analyses are provided for these structures in Section 7 of Appendix C. We can therefore conclude that the geometric effect of changing the  $DA(\text{Cr,C,C,N})$  is similar, regardless of the nature of the X-group. In all three structures, the largest number of electrons shared between [M] and the entire carbene ligand [L] was consistently noted when  $DA(\text{Cr,C,C,N}) = 90^\circ$ . Our model, however, only regards the (de)localization of electrons, and does not take Coulombic attraction or steric repulsion into account. The preferred  $DA(\text{Cr,C,C,N})$  of each structure is therefore a balance between stabilizing electron (de)localization patterns and steric effects. It is important to note again that **5a**, **5b** and **5c** display different values of  $DA(\text{Cr,C,C,N})$  in their respective crystal structures or when optimized to their lowest energy conformers. When  $X=\text{OEt}$  (**5a**), the optimized optimal  $DA(\text{Cr,C,C,N}) \approx 170^\circ$  which indicates that the steric effects are more influential than the (de)localization patterns in controlling the optimized structure. On the other hand, when  $X=\text{NMe}_2$  (**5c**), the optimized  $DA(\text{Cr,C,C,N}) \approx 110^\circ$  and the opposite seems to be the case – a greater influence from the (de)localization patterns than steric effects.

In the next section, the X-group will be varied whilst keeping  $DA(\text{Cr,C,C,N})$  constant in order to investigate the electronic effect that the X-group exerts and provides additional insight on the structural trends of **5a**, **5b** and **5c** observed above.

#### *The electronic effect imposed by varying the X-group*

In the preceding section, focus was placed on the rotation of the R-group for a given X-group. Here, we analyze the transpose effect – for a given constant geometry, how does the nature of the X-group affect the electronic structure of the molecule? Specifically, we focus on varying the X-group between  $X=\text{OEt}$ ,  $\text{NH}_2$  and  $\text{NMe}_2$  at a constant  $DA(\text{Cr,C,C,N})$  to investigate the electronic effect. Comparing the different X-groups at fixed dihedral angles of the R-group minimizes the geometric effect so that mostly the electronic effects are highlighted. When we varied the  $DA(\text{Cr,C,C,N})$  in the geometric analysis we considered the total population of the fragments, in this electronic analysis the total population is not as significant because of the different X-groups with different populations. The electron populations can therefore be found tabulated in the

Appendix C under Section 8 in Tables C 8. 1., C 8. 2. and C 8. 3. Instead, the electrons shared amongst the various fragments are much more significant and can be compared relative to each other in Table 5. 8.

**Table 5. 6.** The electrons shared between fragments for the various dihedrals DA(Cr,C,C,N).

Electrons shared DI([A], [B])							
Structure	Frozen						
	Dihedral Angle (°)	[M]...C <sub>carbene</sub>	[M]...[X]	[M]...[R]	C <sub>carbene</sub> ... [X]	C <sub>carbene</sub> ... [R]	[X]...[R]
5a	90	1.1855	0.3280	0.2818	1.1390	1.1312	0.2209
5b	90	1.0647	0.2226	0.2305	1.3070	1.1426	0.2406
5c	90	0.9518	0.3052	0.2804	1.4197	1.1466	0.3446

Electrons shared DI([A], [B])							
Structure	Frozen						
	Dihedral Angle (°)	[M]...C <sub>carbene</sub>	[M]...[X]	[M]...[R]	C <sub>carbene</sub> ... [X]	C <sub>carbene</sub> ... [R]	[X]...[R]
5a	170	0.9927	0.3062	0.2758	1.0785	1.3685	0.3720
5b	150	0.9675	0.2093	0.2247	1.2516	1.3057	0.3311
5c	110	0.9662	0.3056	0.2594	1.3979	1.1660	0.3843

Electrons shared DI([A], [B])							
Structure	Frozen						
	Dihedral Angle (°)	[M]...C <sub>carbene</sub>	[M]...[X]	[M]...[R]	C <sub>carbene</sub> ... [X]	C <sub>carbene</sub> ... [R]	[X]...[R]
5a	180	0.9874	0.3068	0.2791	1.0785	1.3711	0.3760
5b	180	0.9029	0.2117	0.2452	1.2511	1.3498	0.3502
5c	180	0.8472	0.3061	0.2722	1.3265	1.3374	0.4824

As in the preceding geometric effect analysis, the inter-fragment delocalization index  $\{DI([M], [C_{\text{carbene}}])\}$ , Table 5. 8., counts the number of electrons shared between the metal cluster and the carbene carbon. When  $DA(\text{Cr,C,C,N}) = 90^\circ$ ,  $1.1855 e^-$  are shared between  $[M]$  and  $C_{\text{carbene}}$  fragments for **5a** followed by  $1.0647 e^-$  for **5b** and  $0.9518 e^-$  for **5c**. At the  $DA(\text{Cr,C,C,N}) = 180^\circ$ , the  $DI([M], C_{\text{carbene}})$  follows the same trend where **5a** shares  $0.9874 e^-$  with **5b** and **5c** sharing  $0.9029 e^-$  and  $0.8472 e^-$  respectively. We also see this trend at the approximate lowest energy conformers. Clearly, the metal–carbene bond (and associated  $[CO] \cdots C_{\text{carbene}}$  interactions) weakens considerably in the series  $X=\text{OEt} > \text{NH}_2 > \text{NMe}_2$ , regardless of the geometry of the R-group.

Interestingly, the trend regarding electrons shared between  $C_{\text{carbene}}$  and  $[X]$  is the inverse of the  $[M] \cdots C_{\text{carbene}}$  interaction, at all dihedrals  $DA(\text{Cr,C,C,N})$ :  $DI(C_{\text{carbene}}, [X])$  increases in the order  $X=\text{OEt} < \text{NH}_2 < \text{NMe}_2$ . Since this trend is observed at all geometries investigated, it is clear that it is electronic rather than geometric in nature. Furthermore, this trend confirms the electronic role that the X-group plays in the stability of carbene complexes: As the carbene carbon's bond with the X-group strengthens, its bond with the metal cluster weakens.

We found that the  $[M] \cdots [X]$  and  $[M] \cdots [R]$  interactions also follow a constant trend throughout all the dihedral angles investigated. Consider the  $[M] \cdots [X]$  interaction when  $DA(\text{Cr,C,C,N}) = 90^\circ$ : we see that **5a** shares the most electrons ( $0.3062 e^-$ ) which is followed by **5c** ( $0.3056 e^-$ ) and then **5b** ( $0.2226 e^-$ ). The  $[M] \cdots [X]$  interaction for ethoxy and dimethylamine X fragments are very similar ( $0.0228 e^-$  maximum difference) while the dihydrogen amine differs by a magnitude of  $\sim 0.1 e^-$  for all dihedrals. The difference between the ethoxy (**5a**) X fragment and dimethylamine (**5c**) is therefore minuscule compared to the dihydrogen amine (**5b**) and this trend with similar ratios are carried throughout all the dihedrals  $DA(\text{Cr,C,C,N})$ . More interestingly, perhaps, is how the  $[M] \cdots [R]$  interaction is affected by choice of X-group.  $DI([M], [R])$  follows the same general pattern as  $DI([M], [X])$  – comparable values for  $X=\text{OEt}$  and  $X=\text{NMe}_2$ , and considerably smaller for  $X=\text{NH}_2$  – for all dihedral angles. This is a remarkable result since the R-group does not change, and indicates the remarkable *electronic* effect that choice of X-group has on the entire molecule.

Considering the  $[X]$  and  $[R]$  group interaction, there is no visible trend across all the dihedrals  $DA(\text{Cr,C,C,N})$ . The number of electrons shared between the  $[X]$  and  $[R]$  fragments is also considerably different at the different dihedrals. For all X-groups, electrons shared between

[X] and [R] are greatest when  $DA(\text{Cr,C,C,N}) = 180^\circ$  but least when  $DA(\text{Cr,C,C,N}) = 90^\circ$ , which suggests conjugative interactions when the R-group is planar. It is therefore likely that the [X]...[R] interaction plays an electronically stabilizing role that favours the planar structure, but is balanced against steric factors. The FALDI isosurfaces for electrons shared in the [X]...[R] interaction at  $DA(\text{Cr,C,C,N}) = 180^\circ$  to  $90^\circ$  visually describing the manner in which the electrons are shared can be found in Figure C 9. 2., Figure C 10. 1. and Figure C 10. 2. of Appendix C.

The last parameter that we looked at was the  $\sigma$ - and  $\pi$ -character from the FALDI-MO analysis. Table 5. 10. shows the FALDI-MO results for the [M]...[L] interaction – the interaction between the full metal carbonyl cluster and the entire carbene ligand – for each of the X-groups at the lowest energy  $DA(\text{Cr,C,C,N})$ .

**Table 5. 7.** FALDI-MO analysis of the [M]...[L] interaction for various X-groups at the lowest energy  $DA(\text{Cr,C,C,N})$ .

Structure	<b>5a</b>		<b>5b</b>		<b>5c</b>	
Frozen Dihedral Angle ( $^\circ$ )	170		150		110	
	<i>Contribution</i>	<i>%</i>	<i>Contribution</i>	<i>%</i>	<i>Contribution</i>	<i>%</i>
DI([M], [L])	1.5747		1.4015		1.5313	
$\sigma$	0.4788	30.41	0.4936	35.22	0.3755	24.52
$\pi$	0.3798	24.12	0.3420	24.41	0.4008	26.17
NL	0.7162	45.48	0.5659	40.38	0.7550	49.31
$\sigma$ & $\pi$	0.8586	54.52	0.8356	59.62	0.7763	50.69

At the beginning of this chapter, it was stated that we expect the dimethylamine (**5c**) to be the best electron donor followed by the dihydrogen amine (**5b**) and finally the ethoxy (**5a**) X-group. At the lowest energy dihedrals ( $DA(\text{Cr,C,C,N}) = 170^\circ$ ,  $150^\circ$  and  $110^\circ$  for **5a**, **5b**, and **5c**, respectively) we observe that the total number of electrons shared between the [M] and [L] fragments is  $DI([M], [L]) = 1.5747 e^-$ ,  $1.4015 e^-$  and  $1.5313 e^-$  for **5a**, **5b**, and **5c** respectively. MOs with  $\sigma$ -symmetry contributes 30.41%, 35.22% and 24.52% of the total  $DI([M],[L])$ , whereas

MOs with  $\pi$ -symmetry contributes 24.12%, 24.41% and 26.17% for **5a**, **5b**, and **5c**, respectively. The remaining 45.48%, 40.38% and 49.31% (of **5a**, **5b**, and **5c** respectively) stems from the NL MOs that contribute to shared density through polarization and multicentric effects. This result recovers classically what we expect with regard to the  $\pi$ -character:  $\pi$ -MOs contribute the most to the [M]...[L] interaction in **5c**, but the least in **5a**. The  $\sigma$ -contribution is more difficult to interpret, as the chapter has already shown how the geometry affects the orbitals aligning and, specifically, the [X]...[R] interaction. Clearly, and perhaps surprisingly, changing the X-group has a significant effect on how electrons are shared in  $\sigma$ -bonds. The  $\sigma$ -contribution is often overlooked and the trend not as straightforward as the  $\pi$ -character. There is a ~5% difference in the  $\sigma$ -contribution when varying the X-group, with dihydrogen amine (**5b**) contributing the most  $\sigma$ -character and dimethylamine (**5c**) the least. This is an interesting result in that the only difference between them is two hydrogens are exchanged for two methyl groups, yet there is ~10% change in the  $\sigma$ -contribution. In addition, while the presence of methyl groups could suggest inductive effects, the overall  $\sigma$ -contribution from MOs to [M]...[L] is greater for X=NH<sub>2</sub> than for X=NMe<sub>2</sub>. Using CDA, Cases et al. found (Table 3) that the  $\sigma$ -donation in C (X=NHCH<sub>3</sub>, R=H) is 0.511, compared to D (X=NH<sub>2</sub>, R=H) where it is 0.501. However, for H (X=NHCH<sub>3</sub>, R=CH<sub>3</sub>) it is 0.524 whereas for I (X=NH<sub>2</sub>, R=CH<sub>3</sub>) it is 0.527 hence literature supports the trend we see. However, it is clear that additional investigation is necessary in order to elucidate this phenomenon

Finally, we are interested in exploring the diatomic Cr-C<sub>carbene</sub> bond (i.e. without carbonyl ligands, R- and X-groups) from a FALDI-MO point of view as well. Table 5.11 lists the DI(Cr,C<sub>carbene</sub>) decomposed in symmetry-grouped MOs, for the lowest energy structures of **5a-5c**. The fragmentation for this separation can be found in Figure C 9. 1. of Appendix C.

**Table 5. 8.** The  $\sigma$ - and  $\pi$ -contribution of the different X groups for Cr $\cdots$ C<sub>carbene</sub> bond

Structure	<b>5a</b>		<b>5b</b>		<b>5c</b>	
Frozen Dihedral Angle (°)	170		150		110	
	<i>Contribution</i>	<i>%</i>	<i>Contribution</i>	<i>%</i>	<i>Contribution</i>	<i>%</i>
DI([Cr], [C <sub>carbene</sub> ])	0.5934		0.5692		0.5768	
$\sigma$	0.2318	38.99	0.2540	44.52	0.1874	32.47
$\pi$	0.1162	19.54	0.1147	20.09	0.1325	22.96
NL	0.2454	41.47	0.2005	35.40	0.2569	44.57
$\sigma$ & $\pi$	0.3480	58.53	0.3686	64.60	0.3199	55.43

We see the same trend is followed with respect to  $\sigma$ - and  $\pi$ - contribution for the diatomic Cr–C<sub>carbene</sub> bond (Table 5. 11.) as was found for the total [M] $\cdots$ [L] interaction (Table 5. 10). The computational bond lengths for the Cr $\cdots$ C<sub>carbene</sub> bond is 2.137 Å, 2.131 Å, 2.139 Å for **5a**, **5b**, and **5c** respectively (X= OEt, NH<sub>2</sub> and NMe<sub>2</sub>). Typically, the stronger the bond the shorter the bond length, what this then translates to is that shorter bonds are expected to have more  $\sigma$ - and  $\pi$ -character than longer bonds. We see this classical interpretation in the FALDI MO results of Table 5. 11. Considering **5b** we see it has the most  $\sigma$ - and  $\pi$ -character, sitting at total of 64.60%, matching the shortest bond length of 2.131 Å, structure **5a** follows with 58.53% and the second shortest bond length of 2.137 Å and finally we have **5c** with the least  $\sigma$ - and  $\pi$ -character of 55.43% and the longest bond length of 2.139 Å. This result is significant as it is not reflected in the  $\pi$ -donation of the X-group, which we expect to be NMe<sub>2</sub>>NH<sub>2</sub>>OEt and is matched by the  $\pi$ -contribution in Table 5. 11. Rather, the result shows how the  $\sigma$ -contribution is often underappreciated and shows the significant contribution it can make, especially when combined with the  $\pi$ -contribution to explain experimental results like the bond length.

In summary, the section above described evidence for the nature of the X-group's *electronic* influence on the electronic structure of the molecule, which we reported by keeping the

DA(Cr,C,C,N) constant but varying the X-groups. Notably, from dihydrogen amine to ethoxy and dimethylamine (**5b**, **5a** and **5c**) there is a *decrease* in  $\sigma$ -MOs for the lowest energy structures (150°, 170° and 110° respectively). On the other hand, for **5a**, **5b** and **5c** the  $\pi$ -MOs were seen to *increase* at a constant DA(Cr,C,C,N) for the lowest energy structures (170°, 150° and 110° respectively). Correspondingly, the  $\pi$ -MO result affirms the classical expectation that dimethylamine will donate the most  $\pi$ -electrons and ethoxy the least. The  $\sigma$ -MOs are however far more complicated, and the trend is unintuitive with dihydrogen amine sharing the most electrons and dimethylamine the least. Combining the  $\sigma$ - and  $\pi$ -MOs yielded an overview perspective that correlated to the computational bond lengths between chromium and the carbene carbon, the result being that dimethyl amine had the shortest bond and dimethylamine the longest. Combining the  $\sigma$ - and  $\pi$ - character therefore provides a much more holistic view of the bonding situation between atoms and helps explain uncommon trends in bond lengths. Our results suggest that the increasing electrons shared for the  $C_{\text{carbene}}\cdots[X]$  interaction from **5a**, **5b** to **5c** for each dihedrals leads to *decreasing* the  $[M]\cdots C_{\text{carbene}}$  interaction with *decreasing*  $\pi$ -character from **5a**, **5b** to **5c**. This trend was observed for all dihedral angles considered, except for **5c** at DA(Cr,C,C,N) = 110° – which suggests that geometric in addition to electronic features play an important role in determining the lowest energy structure of **5c**.

### Binding energies

Finally, one of the most useful experimental and theoretical measures of bond strength is the binding energy. The binding energy of a *specific bond* within a molecule is calculated by taking the molecular energy and subtracting the fragments of interest. For instance, the binding energy between the metal cluster  $\{[M]=M(\text{CO})_5\}$  and the carbene ligand  $\{[L]=:C(\text{R})(\text{X})\}$  can be calculated as  $\Delta E_{\text{binding}} = E_{\text{M}(\text{CO})_5\text{L}} - E_{[M]} - E_{[L]}$ , where  $E_{\text{M}(\text{CO})_5\text{L}}$  is the molecular electronic energy of the molecule, and  $E_{[M]}$  and  $E_{[L]}$  energies of isolated fragments. The binding energy therefore represents the energy required to separate two fragments ( the fragments frozen as in the complex) into separate species. The interaction energy between  $[M]$  and  $[L]$  is represented by  $\Delta E_{\text{binding}}$ , and it is therefore tempting to directly compare  $\Delta E_{\text{binding}}$  to the FALDI-based count of delocalized electrons, DI( $[M],[L]$ ). However,  $\Delta E_{\text{binding}}$  includes energetic stabilization due to

electron delocalization and electrostatics, as well as includes electronic reorganization, polarization and dispersion. On the other hand,  $DI([M],[L])$  only includes a count of electron delocalization. That said, comparison of the two indices – as shown in Table 5.12 for **5a** – **5c** and over three different dihedral angles – can provide some interesting insights.

**Table 5. 9.** The binding energy of the different X-groups calculated using single point calculations at B3LYP.

	Frozen Dihedral Angle (°)	$DI([M],[L])$	Binding energy
Structure	<b>5a</b>	( $e^-$ )	( $kcal/mol$ )
	90	1.7953	-332.72
	170	1.5747	-329.41
	180	1.5733	-329.36
Average		1.6478	-330.50
Structure	<b>5b</b>		
	90	1.5178	-301.30
	150	1.4015	-301.18
	180	1.3598	-299.47
Average		1.4264	-300.65
Structure	<b>5c</b>		
	90	1.5374	-328.54
	110	1.5313	-329.38
	180	1.4255	-324.85
Average		1.4981	-327.59

It is clear from Table 5.9. that the *average* number of electrons shared between [M] and [L] increases in the order of **5b** < **5c** < **5a**. In addition, the difference is quite significant: an average of  $DI([M],[L]) = 1.648 e^-$  for **5a** as opposed to  $1.426 e^-$  for **5b**. The same trend is observed for the average binding energy which decreases (i.e. more stabilizing) in the order of **5b** < **5c** < **5a**, with  $\Delta E_{binding}$  stronger by  $-29.85 kcal\cdot mol^{-1}$  in **5a** relative to **5b**. Clearly, the choice of X-group rather than geometry is a deciding factor on the stability and strength of the bond between the metal cluster and carbene ligand. In addition, this result suggests that our FALDI-MO decomposition of



the electronic structure, as discussed in detail throughout this chapter, provides valid results that correspond to the well-known binding energy and can also be found in the work of Outeiral *et al.*<sup>37</sup>

No other significant and consistent trends are observed in the data in Table 5.9. For instance, neither  $DI([M],[L])$  nor  $\Delta E_{binding}$  are maximized/minimized for the lowest energy conformers of each structure (i.e.  $DA(Cr,C,C,N) = 170^\circ, 150^\circ$  and  $110^\circ$  for **5a**, **5b** and **5c**, respectively). It is clear that the electronic structure – which determines the molecular energy and geometry – cannot be sufficiently described by a single *bonding* metric such as  $\Delta E_{binding}$ . Rather, our systematic exploration of various interacting elements of the molecule (such as investigation of  $[M]\cdots[X]$ ,  $[M]\cdots[R]$  and  $[R]\cdots[X]$ ) allows for a piecewise and comprehensive description of the electronic structure, especially when decomposed with the FALDI-MO approach.

## Conclusions

Fischer carbene complexes, and especially the structures investigated in this work, are relatively small molecules in a science accustomed to bio- and nanostructures. However, by systematically changing only two variables in a Fischer carbene complex – that of the choice of X-group and the rotation of the R-group – we observed an immense variation in the electronic structure.

The case-study investigated within this chapter stands as a fully formed proof-of-concept of the FALDI-MO approach, developed and discussed in the preceding chapters. With this approach we were able to perform an extremely in-depth and detailed analysis of the electronic structures of all complexes considered. Accordingly, a number of important observations were made with respect to the geometrical or electronic effects on the molecular electronic structure.

We investigated the geometric effect by keeping the X-group constant, but systematically rotating the pyrrolic R-group. Rotating the R-group from a planar to a perpendicular structure resulted in weaker intra-ligand interactions –  $[R]\cdots C_{carbene}$  and  $[R]\cdots[X]$ . However, we found that weaker intra-ligand interactions then lead to stronger metal-ligand interactions,  $[M]\cdots C_{carbene}$  and  $[M]\cdots[X]$ . In particular, our MO decomposition revealed that the changes in these interactions were driven primarily by changing  $\pi$ -characters, as would be intuitively expected.

On the other hand, we investigated the electronic effect imposed by the X-group by varying it while keeping the geometry of the remainder of the molecule constant. We showed that the effect of changing the X-groups is mostly electronic, as the trends remained constant across all dihedral angles. We found in the optimized structure the [X]...[R] interaction plays an important role and that there is an inverse relationship between the strength of [M]...C<sub>carbene</sub> and the C<sub>carbene</sub>...[X] interactions. The FALDI MO analysis revealed that the  $\pi$ -contributions matched the classical expectation based on the strength of the  $\pi$ -donor X-group. Our result also shows how significant the  $\sigma$ -contribution can be when considering bond length, which is often overlooked. Combining the  $\sigma$ - and  $\pi$ -character provides a much more holistic view of the bonding situation between atoms and helps explain trends in bond lengths.

The interplay of these two variables – choice of X-group and rotation of the R-group – showed a significant effect on how MOs were distributed across the molecule. In particular, we note that the  $\sigma$ - and  $\pi$ - characters of the [M]...C<sub>carbene</sub> interaction is quite dependent on both variables. Clearly, the choice of X- and R-groups, as well as incorporation of steric factors affecting geometry, is a choice that cannot be made independently of one another. Rather, the degree to which these variables were correlated and their effects on the electronic structure are quite remarkable.

Finally, it is evident that our FALDI-MO approach can produce clear insights into difficult electronic structure problems, whilst recovering classical and intuitive notions. The results obtained in this chapter illustrate the proof of concept and the potential of this method to obtain the information needed to tune Fischer carbenes to display certain characteristics (like optimizing molecular structure for maximized  $\pi$ -character). The conceptual component of this FALDI analysis is probably the most powerful, whereby the gap between computational/theoretical chemistry and classical chemistry could be bridged by relaying the results visually and making it appealing to the experimental chemist.

While this chapter is a testament to the complexity of chemistry, we hope that our FALDI-MO approach introduces a kernel of order. Through confirmation, repetition and perturbation, fundamentals of electronic structure can be elucidated. After all, a set of observations in this chapter can form part of a trend in future work, trends become a hypothesis, hypotheses become theories and eventually contribute to our general and conceptual chemical intuition.

## References

1. Thompson, S.; Wessels, H. R.; Fraser, R.; van Rooyen, P. H.; Liles, D. C.; Landman, M., Computational and experimental structural studies of selected chromium(0) monocarbene complexes. *J. Mol. Struct.* **2014**, *1060*, 111-118.
2. Bezuidenhout, D. I.; van der Watt, E.; Liles, D. C.; Landman, M.; Lotz, S., Steric and Electronic Effects of Metal-Containing Substituents in Fischer Carbene Complexes of Chromium. *Organometallics* **2008**, *27* (11), 2447-2456.
3. Gövdeli, N.; Karakaş, D., Quantum chemical studies on hypothetical Fischer type Mo(CO)<sub>5</sub>[C(OEt)Me] and Mo(CO)<sub>5</sub>[C(OMe)Et] carbene complexes. *J. Mol. Struct.* **2018**, *1163*, 94-102.
4. Wang, C.-C.; Wang, Y.; Liu, H.-J.; Lin, K.-J.; Chou, L.-K.; Chan, K.-S., Bond characterization of chromium–fischer carbene complexes: a combined study of experiment and theory. *The Journal of Physical Chemistry A* **1997**, *101* (47), 8887-8901.
5. Poater, J.; Cases, M.; Fradera, X.; Duran, M.; Solà, M., Electron pairing analysis of the Fischer-type chromium–carbene complexes (CO)<sub>5</sub>Cr-C (X)(R), (X= H, OH, OCH<sub>3</sub>, NH<sub>2</sub>, NHCH<sub>3</sub> and R= H, CH<sub>3</sub>, CH-CH<sub>2</sub>, Ph, C-CH). *Chemical Physics* **2003**, *294* (2), 129-139.
6. Dewar, J., A review of the pi-complex theory. *Bulletin de la Societe Chimique de France* **1951**, *18* (3-4), C71-C79.
7. Jensen, F., *Introduction to computational chemistry*. John wiley & sons: 2017.
8. Bezuidenhout, D. I.; Lotz, S.; Liles, D. C.; Van der Westhuizen, B., Recent advances in the field of multicarbene and multimetal carbene complexes of the Fischer-type. *Coordination Chemistry Reviews* **2012**, *256* (5-8), 479-524.
9. Cases, M.; Frenking, G.; Duran, M.; Solà, M., Molecular Structure and Bond Characterization of the Fischer-Type Chromium–Carbene Complexes (CO)<sub>5</sub>Cr-C (X)(R) (X= H, OH, OCH<sub>3</sub>, NH<sub>2</sub>, NHCH<sub>3</sub> and R= H, CH<sub>3</sub>, CH-CH<sub>2</sub>, Ph, CCH). *Organometallics* **2002**, *21* (20), 4182-4191.
10. Licandro, E.; Maiorana, S.; Papagni, A.; Hellier, P.; Capella, L.; Persoons, A.; Houbrechts, S., Synthesis and non-linear properties of conjugated poly-unsaturated amino carbene complexes. *Journal of Organometallic Chemistry* **1999**, *583* (1-2), 111-119.
11. Montgomery, C. D., Fischer and Schrock Carbene Complexes: A Molecular Modeling Exercise. *Journal of Chemical Education* **2015**, *92* (10), 1653-1660.
12. Barluenga, J.; Santamaria, J.; Tomás, M., Synthesis of heterocycles via group VI Fischer carbene complexes. *Chemical Reviews* **2004**, *104* (5), 2259-2284.
13. Frenking, G.; Solà, M.; Vyboishchikov, S. F., Chemical bonding in transition metal carbene complexes. *Journal of Organometallic Chemistry* **2005**, *690* (24-25), 6178-6204.
14. Gövdeli, N.; Karakaş, D., Quantum chemical studies on hypothetical Fischer type Mo(CO)<sub>5</sub>[C(OEt)Me] and Mo(CO)<sub>5</sub>[C(OMe)Et] carbene complexes. *J. Mol. Struct.* **2018**, *1163*, 94-102.
15. Lage, M. L.; Fernández, I.; Mancheño, M. a. J.; Sierra, M. A., Electronic structure of alkoxychromium (0) Carbene complexes: A joint TD-DFT/experimental Study. *Inorganic Chemistry* **2008**, *47* (12), 5253-5258.
16. Connor, J.; Jones, E., Stabilisation of nucleophilic carbenes co-ordinated to transition metals. *Journal of the Chemical Society A: Inorganic, Physical, Theoretical* **1971**, 1974-1979.
17. Connor, J. A.; Jones, E. M.; Randall, E. W.; Rosenberg, E., The <sup>13</sup>C nuclear magnetic resonance spectra of carbene and isonitrile complexes of chromium and tungsten and a

- reinvestigation of the  $^1\text{H}$  nuclear magnetic resonance spectra of phenyl carbene complexes. *Journal of the Chemical Society, Dalton Transactions* **1972**, (22), 2419-2424.
18. Connor, J. A.; Jones, E. M., Reactions of [acetoxy(2-furyl)carbene]pentacarbonylchromium. *Journal of the Chemical Society A: Inorganic, Physical, Theoretical* **1971**, (0), 3368-3372.
  19. Schubert, U., Structural consequences of bonding in transition metal carbene complexes. *Coordination Chemistry Reviews* **1984**, 55 (3), 261-286.
  20. Hafner, A.; Hegedus, L. S.; DeWeck, G.; Hawkins, B.; Doetz, K. H., Chromium-53 nuclear magnetic resonance studies of pentacarbonylchromium carbene complexes. *Journal of the American Chemical Society* **1988**, 110 (25), 8413-8421.
  21. Cardin, D.; Cetinkaya, B.; Lappert, M., Transition metal-carbene complexes. *Chemical Reviews* **1972**, 72 (5), 545-574.
  22. Darensbourg, M. Y.; Darensbourg, D. J., Spectroscopic studies of some carbene pentacarbonyl complexes of chromium(0) and tungsten(0). *Inorganic Chemistry* **1970**, 9 (1), 32-39.
  23. Dötz, K. H.; Fischer, E. O., *Transition metal carbene complexes*. Verlag Chemie: 1983.
  24. Dötz, K.; Tiriliomis, A.; Harms, K., Phosphahydroquinones and oxaphospholes via carbene annulation and cycloaddition reactions of chromium carbonyl carbene complexes and phosphalkynes. *Tetrahedron* **1993**, 49 (25), 5577-5597.
  25. Aumann, R.; Kuckert, E.; Heinen, H., 3-Aminoindole, Imidazolidine und Oxazolidine aus Isocyaniden und Carbenkomplexen durch metallinduzierte [4+ 2]-bzw.[3+ 2]-Cycloadditionen. *Angewandte Chemie* **1985**, 97 (11), 960-962.
  26. Aumann, R.; Hinterding, P.; Krüger, C.; Goddard, R., Organische Synthesen mit Übergangsmetall-Komplexen LXX. Aldehyde durch Hydrolyse der M-C-Bindung von Alkoxy-carben-Chromkomplexen mit Wasser/Urotropin. Ein zweikerniger verbrückter ( $\beta$ -Amino) vinylcarben-Chromkomplex durch Fragmentierung von Urotropin. *Journal of Organometallic Chemistry* **1993**, 459 (1-2), 145-149.
  27. Dötz, K.; Tomuschat, P., Annulation reactions of chromium carbene complexes: scope, selectivity and recent developments. *Chemical Society Reviews* **1999**, 28 (3), 187-198.
  28. Hegedus, L. S., Photoinduced Reactions of Metal Carbenes in Organic Synthesis. In *Metal Carbenes in Organic Synthesis*, Springer: 2004; pp 157-201.
  29. Lloyd, M. K.; McCleverty, J. A.; Orchard, D. G.; Connor, J. A.; Hall, M. B.; Hillier, I. H.; Jones, E. M.; McEwen, G. K., Electrochemical oxidation of organometallic complexes. Carbene and Lewis base complexes of chromium, molybdenum, and tungsten carbonyls. *Journal of the Chemical Society, Dalton Transactions* **1973**, (17), 1743-1747.
  30. Metelková, R.; Tobrman, T. s.; Kvapilová, H.; Hoskovcová, I.; Ludvík, J. i., Synthesis, characterization and electrochemical investigation of hetaryl chromium(0) aminocarbene complexes. *Electrochimica Acta* **2012**, 82.
  31. De Lange, J. H.; Cukrowski, I., Toward deformation densities for intramolecular interactions without radical reference states using the fragment, atom, localized, delocalized, and interatomic (FALDI) charge density decomposition scheme. *Journal of computational chemistry* **2017**, 38 (13), 981-997.
  32. de Lange, J. H.; van Niekerk, D. M. E.; Cukrowski, I., FALDI-based criterion for and the origin of an electron density bridge with an associated (3,-1) critical point on Bader's molecular graph. *J. Comput. Chem.* **2018**, 39 (27), 2283-2299.

33. M. J. Frisch, G. W. T., H. B. Schlegel, G. E. Scuseria, M. A. Robb, J. R. Cheeseman, G. Scalmani, V. Barone, G. A. Petersson, H. Nakatsuji, X. Li, M. Caricato, A. V. Marenich, J. Bloino, B. G. Janesko, R. Gomperts, B. Mennucci, H. P. Hratchian, J. V. Ortiz, A. F. Izmaylov, J. L. Sonnenberg, D. Williams-Young, F. Ding, F. Lipparini, F. Egidi, J. Goings, B. Peng, A. Petrone, T. Henderson, D. Ranasinghe, V. G. Zakrzewski, J. Gao, N. Rega, G. Zheng, W. Liang, M. Hada, M. Ehara, K. Toyota, R. Fukuda, J. Hasegawa, M. Ishida, T. Nakajima, Y. Honda, O. Kitao, H. Nakai, T. Vreven, K. Throssell, J. A. Montgomery, Jr., J. E. Peralta, F. Ogliaro, M. J. Bearpark, J. J. Heyd, E. N. Brothers, K. N. Kudin, V. N. Staroverov, T. A. Keith, R. Kobayashi, J. Normand, K. Raghavachari, A. P. Rendell, J. C. Burant, S. S. Iyengar, J. Tomasi, M. Cossi, J. M. Millam, M. Klene, C. Adamo, R. Cammi, J. W. Ochterski, R. L. Martin, K. Morokuma, O. Farkas, J. B. Foresman, and D. J. Fox, Gaussian, Inc., Wallingford CT, 2016., gaussian 09, Revision d. 01, Gaussian. Inc., Wallingford CT **2009**, 201.
34. Keith, T. A., AIMAll (Version 17.01. 25). *TK Gristmill Software, Overland Park KS, USA* **2017**.
35. Humphrey, W.; Dalke, A.; Schulten, K., VMD: visual molecular dynamics. *Journal of Molecular Graphics* **1996**, *14* (1), 33-38.
36. Smith, J. G., *Organic chemistry*. 4th ed. ed.; McGraw-Hill: New York, NY, 2014.
37. Outeiral, C.; Vincent, M. A.; Martín Pendás, Á.; Popelier, P. L. A., Revitalizing the concept of bond order through delocalization measures in real space. *Chemical Science* **2018**, *9* (25), 5517-5529.

## **Chapter 6.**

### **Summary and conclusions**

## Summary

The major contribution of this work revolves around implementing the Fragment, Atomic, Localized, Delocalized and Interatomic (FALDI) electron density decomposition scheme for decomposing and analysing Molecular Orbital (MO) distributions in Fischer carbene complexes. The resultant FALDI-MO method uses the atom-centric and density-based backbone of FALDI to apply octahedral symmetry labels to any MO based on the symmetry of electrons localized to the metal. The method provides point group symmetry labels to both symmetric and asymmetric systems and allows for quantification of interatomic delocalized density in terms of chemically intuitive labels.

Embedded in the electronic structure (usually described as a MO diagram) are all the electronic and chemical properties of a molecular system. However, MOs in polyatomic molecules can be quite difficult to interpret, and borders on impossible in asymmetric complexes. The aim of this project revolved around improving our fundamental knowledge of the electronic structure of a molecular system. We achieved this aim by extending the FALDI density decomposition scheme based with an MO analysis and decomposition technique that takes a classical approach of understanding MOs (i.e. symmetry terms) and extends it to asymmetric systems. The classical symmetry terms (such as  $a_{1g}$ ,  $t_{1u}$ ,  $e_g$  and  $t_{2g}$  in symmetric octahedral complexes) have been expanded from being limited to symmetrical systems, to a technique that applies these labels to asymmetric Fischer carbene systems. For symmetric molecules, we can take a first principles approach to derive the symmetry adapted linear combinations (SALCs) of atomic orbitals and construct the MOs from scratch. SALCs allow an exact interpretation of MOs, and links MO symmetries and energy levels to parameters like the stabilizing or destabilizing effects of  $t_{2g}$  or  $e_g$  orbitals and even ranking ligands on a spectrochemical series from the octahedral splitting parameter to be determined. Such an exact interpretation significantly opens up the rational design of novel materials. For instance, a symmetric molecular system can be tuned for more  $\pi$ -acceptor or  $\pi$ -donating ability, based on the desired needs. This has not been possible for asymmetric systems but, theoretically, our FALDI-MO method brings a similar level of first principle chemistry to the asymmetric systems.

Three different topics were covered in this manuscript using the FALDI-MO analysis technique. First, in Chapter 3 the foundation of the method was established and carefully illustrated from where the metal symmetry terms are obtained and how this translates into useable information. The mathematical relationship of how FALDI's localized distributions' eigenvalues can be linked to the MOs was derived. The localization indices (LIs)<sup>1, 2</sup>, which can be obtained from the Quantum Theory of Atoms in Molecules (QTAIM)<sup>3</sup>, have previously been proven to be problematic in their chemical interpretations.<sup>4</sup> This is where FALDI has provided an alternative and more effective approach. Since FALDI allows the visualization of localized electron density (*loc*-ED) it was shown that, to an extent, there are delocalized electrons in QTAIM-defined LIs which is problematic. Therefore, FALDI-defined LIs have been used to obtain the true localization about the metal centre and then through visualization, the classical symmetry terms were labelled. The symmetry term is determined from FALDI's localized overlap matrices (LMATs) after being square normalized – a process which has been automated to provide reliable results. The symmetry labelling process is manual and based on visualizing the symmetry terms and assigning them. In **Appendix A** the details of the symmetry labelling process are provided alongside the method in Chapter 2 and 3. This analysis is purely based on the metal centre providing clean visual images which can easily be classified as typical symmetry terms.

The labelling process relies on visual inspection mainly because of technical parameters, which could be automated in future work. Second, the MO overlap was quantified based on the delocalized indeces (DIs) which were recovered from FALDI. This was done using FALDI's unique approach of exclusively calculating the delocalized electrons which can be linked to the localized electron labelling process in the first part. From this, an atom-centric and a density-based set of information can be recovered. We can focus the method on one or multiple atoms that can also be visualized to obtain  $\sigma$ - and  $\pi$ -distributions between not only two atoms but entire fragments within the molecule (*i.e.* multiple diatomic interactions). Finally, the combination of symmetry labels and the analytical quantification was applied to real-world experimental systems for which experimental crystal data is available. This showed the importance of the X- and R-groups interactions in Fischer carbenes and the level at which they interact, highly depending on the geometry of the molecule which affects the overall stabilization of the system. Classical electron counts are recovered from FALDI in which the core, non-bonded and valence electrons can be found to help explain these trends and phenomena in simple terms. We can correlate this type of



classification to conceptual molecular orbital theory and the quantum chemical topology (QCT).<sup>5</sup> The FALDI MO analysis therefore allows for a better understanding of diatomic interactions involving the metal on the electronic level by relating to classical symmetry terms.

Chapter 4 is a bridging chapter between pure theory and application. This chapter explores how the information generated by the FALDI-MO method can be used to answer questions related to chemical modifications. To do so, we introduced chemical *fragments* to the FALDI-MO method. Fragments reduce the number of variables that need to be analyzed without losing any information, thereby greatly increasing the utility of the FALDI-MO approach. Information such as the  $\sigma$ - and  $\pi$ -characters of density delocalized between different fragments of the molecule, based on FALDI-classified symmetries of MOs, can be obtained through this method. This information can be localized about any bond and even more so used to look at molecular fragments and fragments interacting with each other for a more holistic approach. Chapter 5 followed a similar approach, with the difference being that the systems analyzed have been synthesized and crystal structure data is available for comparison. We performed a geometric study on the Fischer carbenes where the R-group's dihedral angle was rotated in ten-degree increments from 180° to 90°, thereby studying the effects of a planar or perpendicular conjugated R-group have on the electronic structure of the complex. The relative lowest energy structures of the rotations were compared with different X-groups and compared at 90° and 180°. This study revealed the importance of the choice of the X- and R-groups within Fischer carbenes and how small changes in geometry affects energy and bond strength. From the FALDI MO analysis, in **Appendix C** we found an interesting (but relatively weak interaction when compared to  $[M]\cdots C_{\text{carbene}}$ ) interaction between the carbonyls on the metal and the R-group, mainly interacting through  $\pi$ -interactions, which highly depended on the conformation (DA(Cr,C,C,N)). Equally, the interaction between the X- and R-group depended on the conformation of the R-group, there was often significant interaction between these two groups at the lowest energy structures.

These interactions are difficult to study with existing methods, and FALDI provides quantifiable and visual results that are insightful for interpreting these long-range interactions. From this, we expect the tunability of Fischer carbene complexes to increase by homing in on the intramolecular interactions that can be manipulated to produce the desired characteristics in almost any octahedral inorganic complex.

## Chapter Breakdown

There are three experimental chapters in this manuscript Chapters 3, 4 and 5. **Chapter 3** focused on the method development of the FALDI-MO analysis technique by explaining the mathematical manipulation taking place and where this picks up from and builds on FALDI.<sup>4,6</sup> Two systems are taken as case studies: i) a symmetric system as the ‘baseline’ or ‘golden standard’ which can be fully explained in terms of MOs conceptually and ii) an asymmetric system, namely a Fischer carbene that keeps the pentacarbonyl skeleton and only one branch of the octahedral symmetry is broken. Breaking symmetry drastically alters the MO composition and muddles their interpretations. The symmetric model system was chosen as  $\text{Cr}(\text{CO})_6$  which has been well documented and researched over the years and forms part of teaching MOs in advanced MO theory.<sup>7,8</sup> This system is ideal because of its ‘simplicity’ and can be described from the ground up using SALCs. Once this symmetric baseline was fully explained and recovered using the FALDI based method, we applied the same method to the asymmetric system. The asymmetric system was a classic Fischer carbene  $\text{Cr}(\text{CO})_5\{\text{C}(\text{OEt})(\text{OMe})\}$  that only slightly changed the symmetric system, keeping most of the symmetric backbone. The FALDI-MO method was able to fully recover classic MO theory in the symmetric system, and provide the same information in the asymmetric system. In addition, the method could provide additional quantification regarding MOs and their  $\sigma$ -,  $\pi$ -characteristics for both symmetric and asymmetric systems. This chapter formed the cornerstone for the rest of this manuscript and laid the groundwork regarding the method.

**Chapter 4** expanded this ideology of labelling asymmetric systems with classical symmetry terms by looking at multiple asymmetric molecules. There are eight structures which we looked at, consisting of two different X-groups (ethoxy,  $\text{X}=\text{OEt}$  and dimethylamine,  $\text{X}=\text{NMe}_2$ ) and the four R-groups which varied in the level of conjugation (hydrogen,  $\text{R}=\text{-H}$ , vinyl,  $\text{-CHCH}_2$ , styryl,  $\text{-CHCHPh}$  and an alkyne,  $\text{-CCH}$  group). These eight structures made a decent test pool for FALDI-MO analysis to test certain parameters and the robustness of the method. This pool of structures presented challenges and complications concerning interpreting the MOs because of the distinction between geometric and electronic effects, this led to the development of a quantification method which recovers  $\sigma$ - and  $\pi$ -character of bonds. As such, quantification developed past just the diatomic level which is in Chapter 3 and multiple diatomic interactions were considered, giving

us the ability to consider fragment interactions. We considered fragments such as the whole X-group and whole R-group and how they interact with the metal cluster (chromium pentacarbonyl). This provided an interesting case study that encouraged an application chapter (Chapter 5) beyond the purely theoretical study that has taken place in Chapter 4. The different R-groups that we tested in Chapter 4 had a variety of effects on geometry from -H and -CCH having planarity between the X- and R-groups whilst the vinyl and styryl group broke planarity (i.e. non-planar). We found that a significant number of electrons is shared in the metal–carbene bond as a result of the metal cluster and X-group. The metal–carbene bond is typically considered to be  $\pi$ -stabilized (which our results found) but there is also considerable stabilization from the  $\sigma$ - and non-localized MOs. The X-group also particularly influenced the different R-groups and the  $[M]\cdots[X]$  interaction. When R= -H or -CCH, the  $[M]\cdots[X]$  interaction is favoured when X=NMe<sub>2</sub> over X=OEt due primarily to better overlap of  $\sigma$ -MOs. However, the opposite was observed when R= -CHCH<sub>2</sub> or -CHCHPh, showing the effect that the X-groups' conformation plays. The results in Chapter 4 confirmed a QTAIM-based study performed by Poater and co-workers showing that when the X-group contributes more to  $\pi$ -donation, then the metal and carbene carbon shares less electrons.<sup>9</sup> This result showed promising possibilities for this analytical technique. The study also revealed that we often overlook the geometric effect, yet it has a significant impact on the system and causes trends or classical expectations to change. The results showed that the metal–carbene carbon bond could be described primarily with equal  $\sigma$ - and  $\pi$ -character, where the X-group added minor stabilization through the  $\pi$ -orbitals, specifically for X=OEt. For X=NMe<sub>2</sub> the metal–carbene carbon bond had less  $\pi$ -character and the  $\sigma$ -character depended on the R-group overall geometry. Finally, a stronger electron donating X-group (i.e. X=NMe<sub>2</sub> as opposed to X=OEt) was correlated to a weaker bond between the metal and the carbene ligand. However, the degree to which the metal–ligand bond weakened was noted to be highly correlated with the choice of R-group. Chapter 4 therefore paved the way for the technique as an example of holistically recovering the electronic structure (for all atoms and with a full electron density distribution) but in a chemically intuitive manner.

In the final experimental chapter (Chapter 5), the analytical possibilities of the FALDI-MO approach were explored, and the geometric effect was further investigated. Three Fischer carbene complexes – for which crystal structures are available – were analyzed at different geometries. These synthesized Fischer carbenes retained similarity in having a 2-(N-

Methyl)pyrrolyl R-group and the X-group which varied between ethoxy (OEt), dihydrogen amine (NH<sub>2</sub>) and dimethylamine (NMe<sub>2</sub>). The study started with freezing and manipulating the dihedral angle  $DA(\text{Cr}, \text{C}_{\text{carbene}}, \text{C}_{\text{pyrrole}}, \text{N}_{\text{pyrrole}})$  to determine the lowest energy of the theoretical structures and correlate the results with the crystal data. The R-group's dihedral angle ( $DA(\text{Cr}, \text{C}, \text{C}, \text{N})$ ) was the only angle which was frozen and rotated, while the X-group started at the same position for each optimization. We froze the dihedral  $DA(\text{Cr}, \text{C}, \text{C}, \text{N})$  in ten-degree increments from 180° to 90° and optimized each structure subject to this constraint. The experimental data aligned with the computational results having the dihedral within ten degrees variance. The bond lengths however varied between experiment and computation because of possible environmental factors such as crystal packing, however, the small basis set may also be at play.

An interesting yet unexpected result was that the lowest energy structure did not necessarily have the shortest (strongest) Chromium–carbene carbon bond, hence the geometric investigation. Taking this study deeper and applying the FALDI MO analysis, we looked at the results from two perspectives, first where the X-group is kept constant at the different dihedrals  $DA(\text{Cr}, \text{C}, \text{C}, \text{N})$  and secondly looking at where the X-group changed and the same dihedrals  $DA(\text{Cr}, \text{C}, \text{C}, \text{N})$  were compared. The constant X-group analysis revealed that the  $\sigma$ -contribution decreased and the  $\pi$ -contribution increased when changing the dihedral from 180° to 90° when looking at the  $[\text{M}] \cdots \text{C}_{\text{carbene}}$  bond and the  $[\text{M}] \cdots [\text{L}]$  interaction. Our results suggest that the weaker  $[\text{R}] \cdots \text{C}_{\text{carbene}}$  and  $[\text{R}] \cdots [\text{X}]$  interactions lead to stronger  $[\text{M}] \cdots \text{C}_{\text{carbene}}$  and  $[\text{M}] \cdots [\text{X}]$  interactions with greater  $\pi$ -characters, and an overall increase in the number of electrons shared between the metal cluster and the carbene ligand as a whole. In **Appendix C** we also made a hypothesis; that the rotation of the R-group caused the carbonyls of the metal to interact with the R-group due to orbitals obtaining the correct symmetry (this interaction is however weak compared to the  $[\text{M}] \cdots \text{C}_{\text{carbene}}$  or other interactions discussed in Chapter 5). By separating the metal cluster ( $\text{Cr}(\text{CO})_5$ ) into chromium and pentacarbonyl the hypothesis was found to be indeed correct, as there were long-range interactions between the fragments that could be visualized and quantified. The geometric investigation illustrated that there is likely an energetic competition between the X- and R-group interacting and the carbonyl and R-group interaction. This is due to their inverse relationship, as the  $[\text{X}] \cdots [\text{R}]$  interaction increased the  $[\text{CO}] \cdots [\text{R}]$  interaction decreased but the lowest energy structures favoured the  $[\text{X}] \cdots [\text{R}]$  interaction. The varied X-group analysis revealed that the FALDI MO

analysis matches the classical expectation of the  $\pi$ -donor X-group based on the calculated  $\sigma$ - and  $\pi$ -contributions. Combining the  $\sigma$ - and  $\pi$ -MOs yielded an overview perspective that correlated to the computational bond lengths between chromium and the carbene carbon, the result being that dihydrogen amine X-group had the shortest  $[M]\cdots C_{\text{carbene}}$  bond and dimethylamine X-group the longest. Significant emphasis was also put on the contribution that the  $\sigma$ -character makes to meet the classical expectation, since excluding the  $\sigma$ -character meant the classical interpretation of how shared electrons influence bond length could not be used. This result shows how significant the  $\sigma$ -contribution can be in influencing the bond length, where the  $\sigma$ -MOs are often overlooked.

The geometric effect also remained mostly constant throughout the different dihedrals  $DA(\text{Cr},\text{C},\text{C},\text{N})$  which showed that the effect seen in our results was therefore mainly electronic because of changing the X-group. Lastly, the binding energies were looked at. The binding energies matched the crystal data for the  $\text{Cr}\cdots\text{C}_{\text{carbene}}$  bond. The electrons shared calculated with FALDI matched the binding energies extremely well as did the  $\sigma$ -,  $\pi$ - and NL contributions. For the lowest energy structure we combined the  $\sigma$ -,  $\pi$ - and NL contributions (*i.e.* total DI,  $1.5747e^- > 1.5313e^- > 1.4015e^-$ ) and found that it matched the binding energy trend ( $-329.408 \text{ kcal/mol} > -329.382 \text{ kcal/mol} > -301.183 \text{ kcal/mol}$ ) for  $\text{OEt} > \text{NMe}_2 > \text{NH}_2$  (or **5a**, **5c**, **5b**) respectively. With these small experimentally consistent trends, we gained confidence in the FALDI MO method and we are excited to see how much it could still relate to other experimental results.

## Future Studies

Currently, this new FALDI MO analysis method is limited to the metal centre being the source of the symmetry classification. Ideally, this method should be expanded to any atom, so that any atom in the system could be labelled, enabling organic systems to be investigated. This would better define and open alternative possibilities and avenues for describing the NL term, which has been used to describe orbitals that are not defined by the metal. The NL term carries a lot of information and is significant when considering the contribution it makes in some fragments. Better characterized and interpreted data like the NL term could shed light into some unanswered trends which may be observed in chemical systems.

Chapter 4 focused on the ground state MO analysis of Fischer carbenes, but future work may include looking at the excited states of these complexes, thereby extending the FALDI-MO method into analysis of excited states and time-dependent electronic structure analysis. It is common knowledge that the  $X=OEt$  complexes typically have a redshift relative to  $X=NMe_2$ ,<sup>10</sup> but we do not see the strong redshifts as prominent for the MLCT band. This work may provide the toolset needed to investigate this result. It is also worth noting that chromium(0) and tungsten(0) have remarkably different positions for the MLCT band, which is because of the tungsten(0) pentacarbonyl having a lower acceptor capacity.<sup>10</sup> This observation indicates that the chromium(0) pentacarbonyl is more accepting and has a lower  $\pi$ -backdonation ability.

Carbonyls are also unique and display some interesting properties, and as such some metal carbonyl complexes are often dubbed “nonclassical carbonyls”.<sup>11,12</sup> Typically, free carbonyls have a stretching frequency of  $2143\text{cm}^{-1}$  but these non-classical carbonyls have C–O modes smaller than the free carbonyls. This phenomena is usually explained by  $\pi$ -backdonation from the metal to the CO into the  $\pi^*$ -bonding orbital of CO weakening the C–O bond. Strangely, this changes with  $Os(CO)_6^{2+}$  and  $Ir(CO)_6^{3+}$  where  $\nu(C-O) > 2143\text{cm}^{-1}$  and these complexes break the trend.<sup>13</sup> This has been investigated before using CDA analysis, where C–O bond length change is explained by the  $M \rightarrow CO$   $\pi$ -back-donation and  $M \leftrightarrow CO$  repulsive polarization using a CDA analysis.<sup>14</sup> For  $Ir(CO)_6^{3+}$  the repulsive polarization seems to be more important than the  $\pi$ -back-donation. The application of the FALDI MO analysis presented in this work may shed light on these types of burning questions, providing a heuristic way of understanding and interpreting the complexes on the electronic level.

Having a method to label symmetry for the non-metal atoms would allow characterizing the very interesting X- and R-group interactions that have become so prominent, in Chapter 5 and any other atom. So far FALDI recovers the nature of the X- and R-group interaction but not how they interact. The data from changing the dihedral angles ( $DA(Cr,C,C,N)$ ) suggests X- and R-group interact in a  $\sigma$ -fashion and the visualization seems to confirm this. However, the result would be much more impactful if the symmetry was recovered by the MOs of these interacting groups. More information about these fragments is still locked within the deeper electronic structure. Ideally, the FALDI method will expand to any atom or interaction.

Chapter 5 correlated extremely well with classical reasoning, but the crystal data results did not correlate in a quantifiable manner. The bond lengths of the chromium carbene carbon bond came close to the crystal data, but not acceptable for high accuracy. The level of theory may be to blame for this, but is likely also because of only optimizing to the lowest energy within the ten degree increments of the dihedral. Unfortunately, the MP2 calculations were also unsatisfactory, tilting the result only to the other side of the spectrum relative to B3LYP. Ideally, this study would be repeated but with different electronic structure models in order to generate geometries with more similarity to the crystal data. Suggested levels of theory that could obtain this level of similarity include PM3 as has been used in other Fischer carbene studies<sup>15</sup>, however PM3 is not recommended when good quality hybrid DFT or double hybrid DFT methods exist. Fortunately, the FALDI MO analysis results are independent to the level of theory. This indicates that the analysis should be able to just be repeated and the interpretation should be similar. A full energy decomposition analysis of the structures is recommended to test the [X]···[R] interaction relative to the [CO]···[R] interaction and how their relationship affects the energetics of the system, which can confirm/reject the speculation that the [X]···[R] interaction stabilizes the system.

The current MO labelling and quantification process within the FALDI-MO method is a very manual and tedious process. Ideally, the process will become automated using software so that an interpretable result can be obtained much faster and more reliably, not prone to human error.

Finally, while working on this project, considerations were made. If there is an R-group which is to be used for subsequent electron transfer reactions by exciting a molecule to transfer electrons from the metal into the R-group and then once the electrons are in the R-group transfer the electrons are transferred again to a different group. This a process used in solar cells and begs the thought of possible tuning or optimization opportunities. It then raises a few questions around this topic. If the [M]···[R] interaction is maximised does excitation of electrons occur more easily or when the electrons are transferred, are they still more delocalized? Will this information then help tune a molecule to achieve the desired characteristics? Can a rational design process be used? For example, using the amine or ethoxy to force a specific geometry that maximizes the interaction between the Metal and R-group. Does this maximize electron transfer? Organic solar cells have become a new high-interest research field because of how expensive metals are, but they are so far

relatively inefficient<sup>16</sup> and a tuning method like this would greatly influence the progress of this field. These are a few of the interests that have arisen whilst developing this work and the potential applications that may arise.

The main and future focus of this work is how to apply the information obtained through these FALDI methods and optimize the process so that the tunability of a system can be obtained accurately and within a reasonable time frame. We hope this tool will develop further beyond this study, becoming more detailed, visually orientated and even commercially viable so that molecular systems can become holistically understood at the electronic level.



## References

1. Bader, R. F.; Stephens, M. E., Spatial localization of the electronic pair and number distributions in molecules. *Journal of the American Chemical Society* **1975**, *97* (26), 7391-7399.
2. Daudel, R.; Bader, R.; Stephens, M.; Borrett, D., The electron pair in chemistry. *Canadian Journal of Chemistry* **1974**, *52* (8), 1310-1320.
3. Bader, R. F., Atoms in molecules. *Accounts of Chemical Research* **1985**, *18* (1), 9-15.
4. de Lange, J. H.; van Niekerk, D. M. E.; Cukrowski, I., FALDI-based criterion for and the origin of an electron density bridge with an associated (3,-1) critical point on Bader's molecular graph. *J. Comput. Chem.* **2018**, *39* (27), 2283-2299.
5. Popelier, P. L., Quantum chemical topology. In *The Chemical Bond II*, Springer: 2016; pp 71-117.
6. De Lange, J. H.; Cukrowski, I., Toward deformation densities for intramolecular interactions without radical reference states using the fragment, atom, localized, delocalized, and interatomic (FALDI) charge density decomposition scheme. *Journal of computational chemistry* **2017**, *38* (13), 981-997.
7. Dabrowiak, J. C., Metals in Medicine Special Issue. *Inorganica Chimica Acta* **2012**, *393*.
8. Schreiner, A. F.; Brown, T. L., A semiempirical molecular orbital model for Cr(CO)<sub>6</sub>, Fe(CO)<sub>5</sub>, and Ni(CO)<sub>4</sub>. *Journal of the American Chemical Society* **1968**, *90* (13), 3366-3374.
9. Poater, J.; Cases, M.; Fradera, X.; Duran, M.; Solà, M., Electron pairing analysis of the Fischer-type chromium–carbene complexes (CO)<sub>5</sub>Cr-C (X)(R), (X= H, OH, OCH<sub>3</sub>, NH<sub>2</sub>, NHCH<sub>3</sub> and R= H, CH<sub>3</sub>, CH-CH<sub>2</sub>, Ph, C-CH). *Chemical Physics* **2003**, *294* (2), 129-139.
10. Chu, G. M.; Fernández, I.; Sierra, M. A., Synthesis, Structure, and Electronic Properties of Extended  $\pi$ -Conjugated Group 6 Fischer Alkoxy–Bis (carbene) Complexes. *Chemistry–A European Journal* **2013**, *19* (19), 5899-5908.
11. Lupinetti, A. J.; Frenking, G.; Strauss, S. H., Nonclassical metal carbonyls: appropriate definitions with a theoretical justification. *Angewandte Chemie International Edition* **1998**, *37* (15), 2113-2116.
12. Lupinetti, A. J.; Strauss, S. H.; Frenking, G., Nonclassical metal carbonyls. *Progress in Inorganic Chemistry* **2001**, *49*, 1-112.
13. Frenking, G.; Shaik, S. S., The chemical bond : chemical bonding across the periodic table. Wiley-VCH Verlag GmbH & Co: Weinheim, Germany, 2014.
14. Szilagyí, R. K.; Frenking, G., Structure and Bonding of the Isoelectronic Hexacarbonyls [Hf(CO)<sub>6</sub>]<sup>2-</sup>, [Ta(CO)<sub>6</sub>]<sup>-</sup>, W(CO)<sub>6</sub>, [Re(CO)<sub>6</sub>]<sup>+</sup>, [Os(CO)<sub>6</sub>]<sup>2+</sup>, and [Ir(CO)<sub>6</sub>]<sup>3+</sup>: A Theoretical Study. *Organometallics* **1997**, *16* (22), 4807-4815.
15. Montgomery, C. D., Fischer and Schrock Carbene Complexes: A Molecular Modeling Exercise. *Journal of Chemical Education* **2015**, *92* (10), 1653-1660.
16. Chidichimo, G.; Filippelli, L., Organic solar cells: problems and perspectives. *International Journal of Photoenergy* **2010**, *2010*.

# **Appendix A**

## **Supplementary Information for Chapter 3**

# Development of a theoretical FALDI-based framework for the symmetry classifications of Molecular Orbitals in asymmetric Fischer Carbenes.

*Brent Nel, Jurgens Hendrik de Lange\**

Department of Chemistry, Faculty of Natural and Agricultural Sciences, University of Pretoria, Lynnwood Road, Hatfield, Pretoria 0002

Correspondence to : Jurgens de Lange (E-mail: [jurgens.delange@up.ac.za](mailto:jurgens.delange@up.ac.za) )

## ELECTRONIC SUPPORTING INFORMATION

### Table of Contents

<u>Section 1: Cartesian Coordinates and Energy of All Molecules Studied.</u>	<u>148</u>
<u>Section 2: Localized Matrix of Cr1 of All Molecules Studied Corresponding the Eigenvalues to Molecular Orbitals.</u>	<u>150</u>
<u>Section 3: Delocalization Matrix Summary for All Molecules Studied Corresponding the Symmetry Terms of Molecular Orbitals Obtained in the Localized Matrix.</u>	<u>155</u>
<u>Section 4: Cr(CO)<sub>6</sub> Natural Density Functions corresponded to the Molecular Orbitals</u>	<u>158</u>
<u>Section 5: Cr(CO)<sub>5</sub>[C(OEt)(Me)] Natural Density Functions</u>	<u>162</u>
<u>Section 6: Cr(CO)<sub>5</sub>[C(OEt)(Me)] Natural Density Functions corresponded to the Molecular Orbitals</u>	<u>163</u>

Section 1: Cartesian Coordinates and Energy of All Molecules Studied.

**Table S1.** Cartesian coordinates of Cr(CO)<sub>6</sub> at B3LYP/dev2svp(p) level.

Atom	X	Y	Z
Cr1	0.000000	0.000000	0.000000
C2	0.000000	0.000000	1.917895
O3	0.000000	0.000000	3.062340
C4	0.000000	1.917895	0.000000
O5	0.000000	3.062340	0.000000
C6	0.000000	0.000000	-1.917895
O7	0.000000	0.000000	-3.062340
C8	0.000000	-1.917895	0.000000
O9	0.000000	-3.062340	0.000000
C10	-1.917895	0.000000	0.000000
O11	-3.062340	0.000000	0.000000
C12	1.917895	0.000000	0.000000
O13	3.062340	0.000000	0.000000

Molecular Energy of Cr(CO)<sub>6</sub>: -1723.92369060 a.u.

**Table S2.** Cartesian coordinates of Cr(CO)<sub>5</sub>[C(OEt)Me] at B3LYP/dev2svp(p) level.

Atom	X	Y	Z
Cr1	0.785497	-0.091149	-0.000009
C2	2.509582	-0.909647	0.000227
O3	3.547014	-1.404139	0.000326
C4	1.346721	1.130202	-1.348567
O5	1.682678	1.870564	-2.161682
C6	0.160865	-1.308585	-1.331607
O7	-0.232785	-2.037547	-2.126077
C8	0.160392	-1.308283	1.331640
O9	-0.233530	-2.036955	2.126265
C10	1.346246	1.130238	1.348722
O11	1.681896	1.870586	2.161970
C12	-1.037487	0.777613	-0.000279
C13	-1.320440	2.259359	-0.000340
H14	-1.915756	2.547693	-0.889395
H15	-1.915452	2.547773	0.888886
H16	-0.394206	2.848418	-0.000525
O17	-2.111839	0.011873	-0.000260
C18	-3.483988	0.478246	-0.000278
H19	-3.652327	1.101532	-0.895497
H20	-3.652236	1.101929	0.894676
C21	-4.377024	-0.746706	0.000043
H22	-4.190618	-1.364842	0.894594
H23	-5.437295	-0.439356	0.000025
H24	-4.190710	-1.365254	-0.894241

Molecular energy of Cr(CO)<sub>5</sub>C(OEt)(Me): -1842.89166103 a.u

Section 2: Localized Matrix of Cr1 of All Molecules Studied Corresponding the Eigenvalues to Molecular Orbitals.

**Table S3.** Sorted and Square normalized Localized Matrix of Cr1 for Cr(CO)<sub>6</sub>.

Molecular Orbitals	Square normalized Localized Density of Cr1			
MO1	0.91			0.09
MO2	0.09			0.91
MO3		0.47	0.07	0.46
MO4		0.04	0.93	0.03
MO5		0.49		0.51
MO6				
MO7				
MO8				
MO9				
MO10				
MO11				
MO12				
MO13				
MO14				
MO15				
MO16				
MO17				
MO18			1.00	
MO19			0.68	0.20 0.11
MO20			0.27	0.14 0.58
MO21			0.04	0.65 0.30
MO22				
MO23				
MO24				
MO25				
MO26				

**Table S3. continued**

MO27																			
MO28															0.58				
MO29																0.10	0.03		
MO30																0.03	0.10		
MO31																		0.14	
MO32													0.03	0.06					
MO33													0.06	0.03					
MO34															0.42				
MO35									0.04										0.85
MO36										0.04									
MO37											0.04								0.10
MO38																0.05	0.15		
MO39																		0.20	
MO40																0.15	0.05		
MO41																			
MO42																			
MO43																			
MO44																			
MO45																			
MO46																			
MO47													0.63	0.28					
MO48													0.28	0.63					
MO49																0.50	0.16		
MO50																		0.65	
MO51																0.16	0.50		
MO52											0.06	0.90							
MO53										0.87	0.06	0.02							0.04
MO54										0.08	0.84	0.04							

Cr1	EV54	EV50	EV51	EV52	EV53	EV49	EV46	EV47	EV48	EV45	EV44	EV43	EV42	EV41	EV40	EV39	EV38	EV37	EV36
Eigenvalues	2.00	2.00	2.00	2.00	2.00	1.99	1.96	1.96	1.96	0.60	0.60	0.60	0.11	0.11	0.03	0.01	0.01	0.01	0.00
	NDF1	NDF2	NDF3	NDF4	NDF5	NDF6	NDF7	NDF8	NDF9	NDF10	NDF11	NDF12	NDF13	NDF14	NDF15	NDF16	NDF17	NDF18	NDF19

**Table S4.** Sorted and Square normalized Localized Matrix of Cr1 for Cr(CO)<sub>5</sub>[C(OEt)(Me)].

Molecular Orbitals	Square normalized Localized Density of Cr1			
MO1	0.91		0.09	
MO2	0.09		0.03	0.87
MO3		1.00		
MO4		0.41	0.58	
MO5		0.58	0.38	0.04
MO6				
MO7				
MO8				
MO9				
MO10				
MO11				
MO12				
MO13				
MO14				
MO15				
MO16				
MO17				
MO18				
MO19				
MO20				
MO21			0.99	
MO22				0.99
MO23				0.99
MO24			0.98	
MO25				
MO26				
MO27				
MO28				
MO29				



**Table S4. continued**

MO30																				0.01				
MO31																								
MO32																				0.10				
MO33																			0.01	0.03				
MO34																			0.03					
MO35																			0.46	0.02				
MO36																				0.07	0.06			
MO37																				0.06	0.07			
MO38																			0.08					
MO39																			0.04	0.07				
MO40																								
MO41																				0.01	0.01	0.35		
MO42																				0.14	0.03			
MO43																			0.02	0.26	0.09	0.03		
MO44																			0.04			0.02		
MO45																				0.03				
MO46																				0.02		0.06	0.05	0.22
MO47																					0.07	0.09		
MO48																					0.03	0.02	0.16	
MO49																				0.07	0.04	0.03		
MO50																								
MO51																								
MO52																								
MO53																								
MO54																								
MO55																							0.01	
MO56																							0.86	
MO57																				0.04				
MO58																							0.05	0.01
MO59																				0.51		0.22		
MO60																							0.26	0.31
MO61																							0.34	0.28

**Table S4. continued**

MO62																			0.08	0.03	0.02	
MO63																				0.04	0.05	
MO64														0.28		0.04	0.39					0.01
MO65																					0.96	
MO66																						0.96
MO67																						0.96

Cr1	EV67	EV63	EV64	EV65	EV66	EV62	EV61	EV60	EV59	EV58	EV57	EV56	EV55	EV54	EV53	EV52	EV51	EV50	EV49
Eigenvalues	2.00	2.00	2.00	2.00	2.00	1.99	1.97	1.96	1.96	0.67	0.56	0.49	0.13	0.11	0.03	0.01	0.01	0.01	0.00
	NDF1	NDF2	NDF3	NDF4	NDF5	NDF6	NDF7	NDF8	NDF9	NDF10	NDF11	NDF12	NDF13	NDF14	NDF15	NDF16	NDF17	NDF18	NDF19

The data in **Tables S3** and **S4** allow for the allocation of Molecular orbitals to specific eigenvalues, which relates to a Natural Density function that can be visualized to assign the symmetry term. Each column and row add to a value of 1.00, the rows however will not total as not all the columns are illustrated in these tables.

Section 3: Delocalization Matrix Summary for All Molecules Studied Corresponding the Symmetry Terms of Molecular Orbitals Obtained in the Localized Matrix.

**Table S5.** Sorted Summary of the Delocalized Matrix for Cr1-C2 of Cr(CO)<sub>6</sub> where NL depicts symmetry not defined by the Cr1 Localized Matrix.

Molecular Orbitals	Delocalized Contribution	Percentage (%)	Rolling	Symmetry
MO48	0.19	23%	22.59%	e <sub>g</sub>
MO53	0.16	19%	41.62%	t <sub>2g</sub>
MO52	0.16	19%	60.64%	t <sub>2g</sub>
MO51	0.08	9%	69.88%	t <sub>1u</sub>
MO28	0.04	5%	75.32%	a <sub>1g</sub>
MO35	0.03	4%	79.02%	t <sub>2g</sub>
MO36	0.03	4%	82.71%	t <sub>2g</sub>
MO32	0.03	4%	86.32%	e <sub>g</sub>
MO34	0.03	3%	89.47%	a <sub>1g</sub>
MO30	0.02	2%	91.89%	t <sub>1u</sub>
MO38	0.02	2%	93.88%	t <sub>1u</sub>
MO21	0.02	2%	95.80%	t <sub>1u</sub>
MO54	0.01	1%	97.04%	t <sub>2g</sub>
MO47	0.00	1%	97.59%	e <sub>g</sub>
MO39	0.00	0%	98.01%	t <sub>1u</sub>
MO40	0.00	0%	98.42%	t <sub>1u</sub>
MO18	0.00	0%	98.74%	a <sub>1g</sub>
MO19	0.00	0%	98.93%	t <sub>1u</sub>
MO20	0.00	0%	99.12%	t <sub>1u</sub>
MO50	0.00	0%	99.22%	t <sub>1u</sub>
MO49	0.00	0%	99.33%	t <sub>1u</sub>
MO37	0.00	0%	99.44%	t <sub>2g</sub>
MO31	0.00	0%	99.54%	t <sub>1u</sub>
MO29	0.00	0%	99.65%	t <sub>1u</sub>
MO33	0.00	0%	99.74%	e <sub>g</sub>
MO25	0.00	0%	99.83%	NL
MO22	0.00	0%	99.90%	NL
MO26	0.00	0%	99.93%	NL

**Table S6.** Sorted Summary of the Delocalized Matrix for Cr1-C12 (Cr-Carbene) of Cr(CO)<sub>5</sub>[C(OEt)(Me)] where NL depicts symmetry not defined by the Cr1 Localized Matrix.

Molecular Orbitals	Delocalized Contribution	Percentage (%)	Rolling	Symmetry				Sum
				a <sub>1g</sub>	t <sub>1u</sub>	t <sub>2g</sub>	e <sub>g</sub>	
MO64	0.27	36%	35.56%	0.04	0.39		0.28	0.71
MO66	0.19	25%	60.53%			0.96		0.96
MO67	0.05	6%	67.00%	0.96				0.96
MO42	0.04	5%	72.24%	0.14	0.03			0.16
MO59	0.03	4%	76.73%		0.22		0.51	0.73
MO62	0.03	3%	80.15%		0.13381			0.13
MO45	0.02	3%	83.21%			0.03		0.03
MO41	0.02	3%	86.09%	0.01	0.01			0.03
MO24	0.01	2%	87.68%		0.98			0.98
MO33	0.01	1%	89.01%	0.01				0.01
MO34	0.01	1%	90.20%	0.03				0.03
MO65	0.01	1%	91.33%			0.96		0.96
MO35	0.01	1%	92.27%	0.46	0.02			0.47
MO57	0.01	1%	93.17%				0.04	0.04
MO31	0.01	1%	94.07%	NL				0.00
MO49	0.01	1%	94.91%	0.04	0.03		0.07	0.14
MO60	0.01	1%	95.68%		0.571069			0.57
MO63	0.01	1%	96.44%		0.085412			0.09
MO43	0.01	1%	97.11%	0.26	0.09		0.02	0.37
MO40	0.00	1%	97.72%	NL				0.00
MO32	0.00	1%	98.31%	NL				0.00

The data in **Table S6** can only provide total symmetry information for symmetries obtained from the Cr1 analysis therefore this data need to be normalized to obtain a summary as presented in the article.

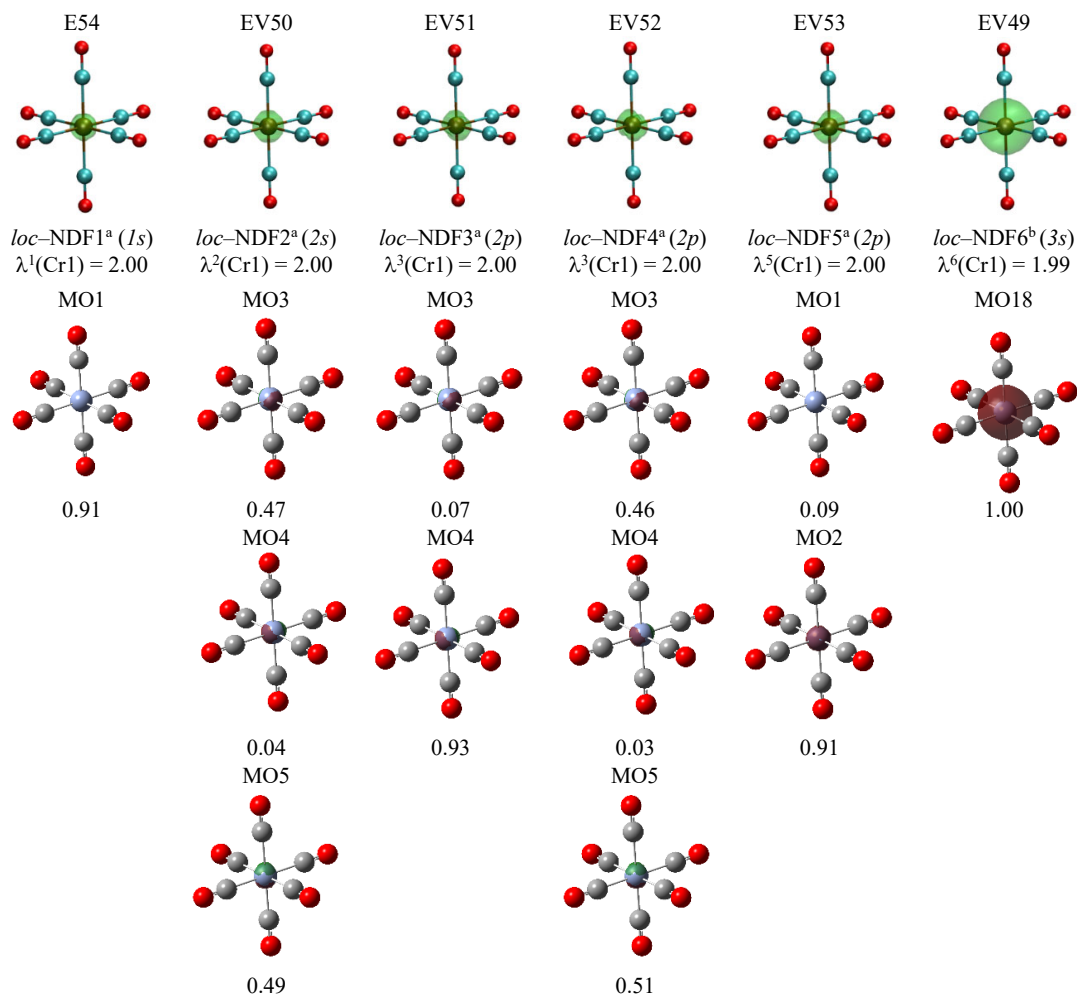
**Table S7.** Sorted Summary of the Delocalized Matrix for Cr1-C2 (Cr-Trans to the Carbene) of Cr(CO)<sub>5</sub>[C(OEt)(Me)] where NL depicts symmetry not defined by the Cr1 Localized Matrix.

Molecular Orbitals	Delocalized Contribution	Percentage (%)	Rolling	Symmetry				Sum
				a <sub>1g</sub>	t <sub>1u</sub>	t <sub>2g</sub>	e <sub>g</sub>	
MO59	0.28	32%	32.06%		0.22		0.51	0.73
MO67	0.20	24%	55.83%			0.96		0.96
MO66	0.14	17%	72.63%			0.96		0.96
MO39	0.06	7%	79.32%		0.07		0.04	0.11
MO35	0.03	3%	82.74%	0.46	0.02			0.47
MO46	0.03	3%	86.12%		0.10	0.02		0.12
MO43	0.02	2%	88.19%	0.26	0.09		0.02	0.37
MO49	0.02	2%	90.14%	0.04	0.03		0.07	0.14
MO24	0.02	2%	92.00%		0.98			0.98
MO57	0.01	2%	93.55%				0.04	0.04
MO47	0.01	1%	94.99%		0.16			0.16
MO45	0.01	1%	96.40%			0.03		0.03
MO65	0.01	1%	97.56%			0.96		0.96
MO53	0.01	1%	98.16%	NL				0.00
MO48	0.00	0%	98.60%		0.05			0.05
MO50	0.00	0%	99.03%	NL				0.00

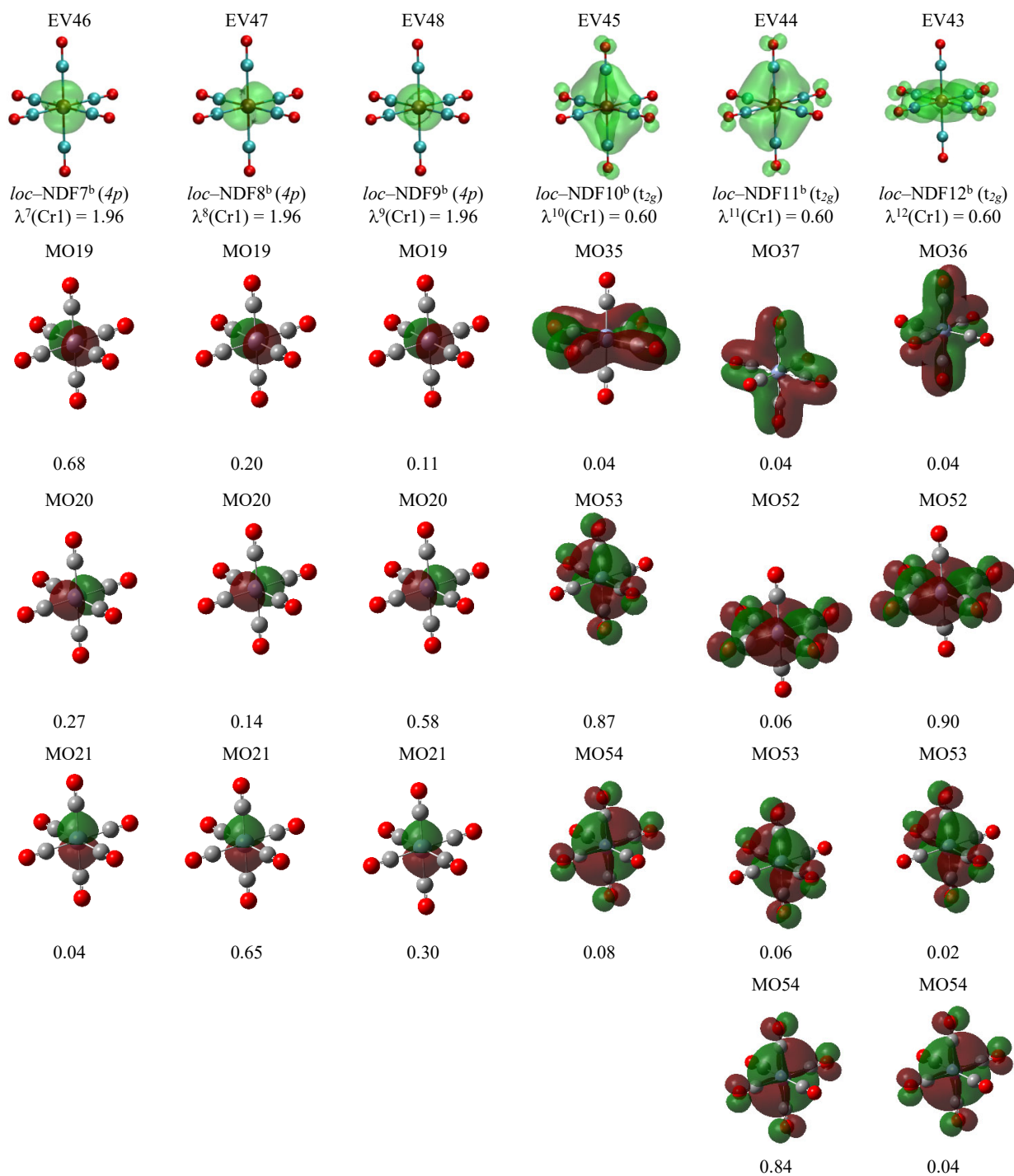
The data in **Table S7** can only provide total symmetry information for symmetries obtained from the Cr1 analysis therefore this data need to be normalized to obtain a summary as presented in the article.

## Section 4: Cr(CO)<sub>6</sub> Natural Density Functions corresponded to the Molecular Orbitals

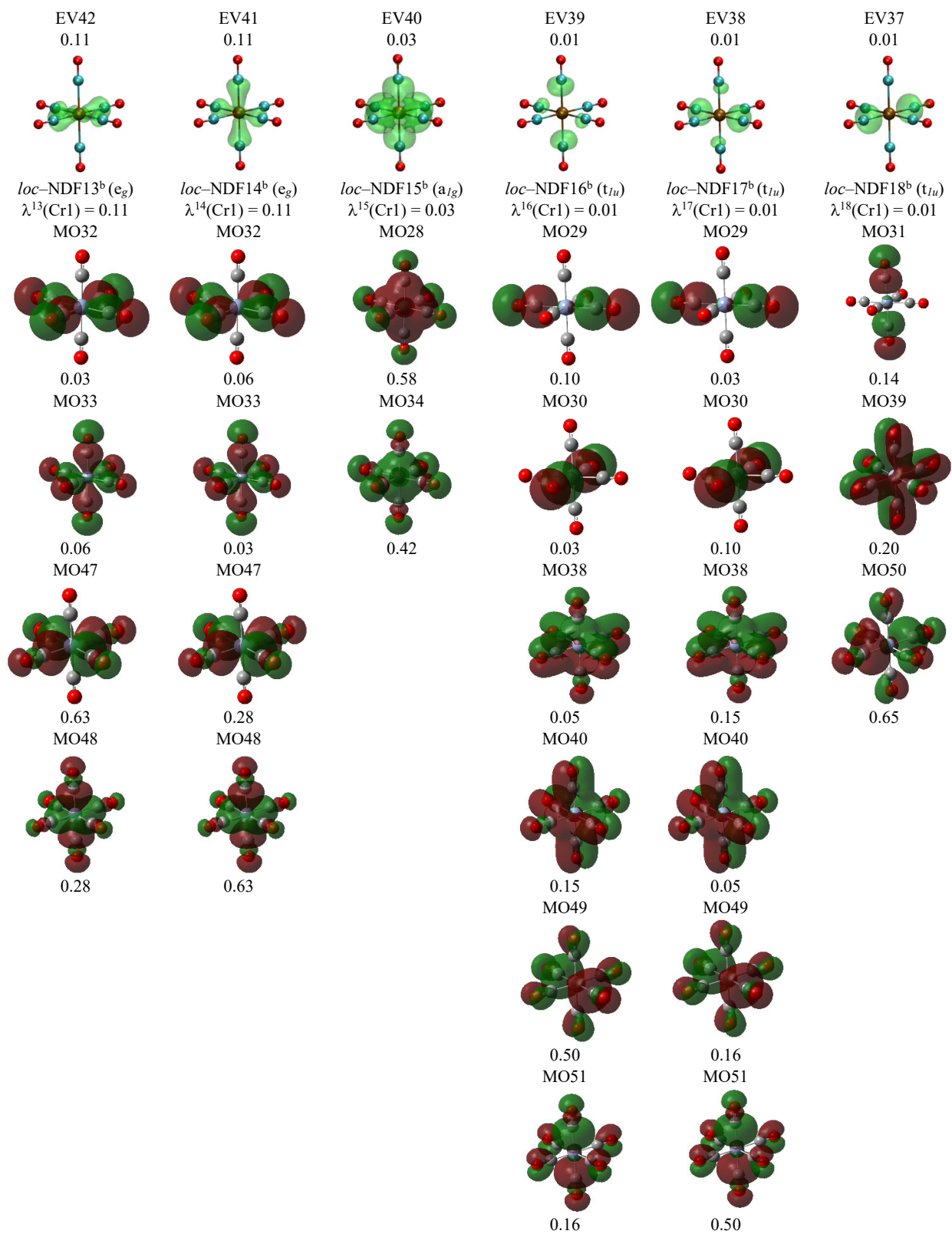
This supporting information is mainly comprised of the full decomposition of the Molecular orbitals derived from the determined eigen values and assigned via the natural density function describe in the article. The Molecular orbitals have been assigned with 99% accuracy from the eigenvalues. The larger the  $\lambda$  value the more metal centred the delocalization while the lower values are ligand centred. All Molecular orbitals are not classified with this approach as only the metal is used to define the orbitals, for a symmetry definition of every orbital ligands will also need to be considered.



**Figure S1-1:** The full compilation of Molecular orbitals through the NDF analysis for Cr(CO)<sub>6</sub> with isovalues of a=0.0001au and b=0.001au and EV=Eigenvalue

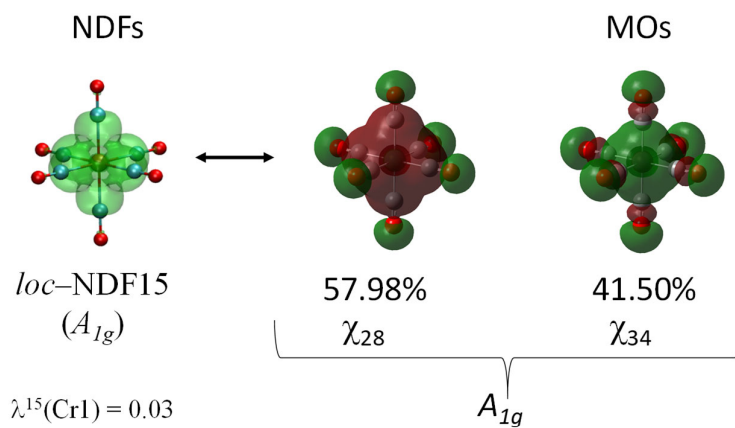


**Figure S1-2:** The full compilation of Molecular orbitals through the NDF analysis for Cr(CO)<sub>6</sub> with isovalues of a=0.0001au and b=0.001au and EV=Eigenvalue



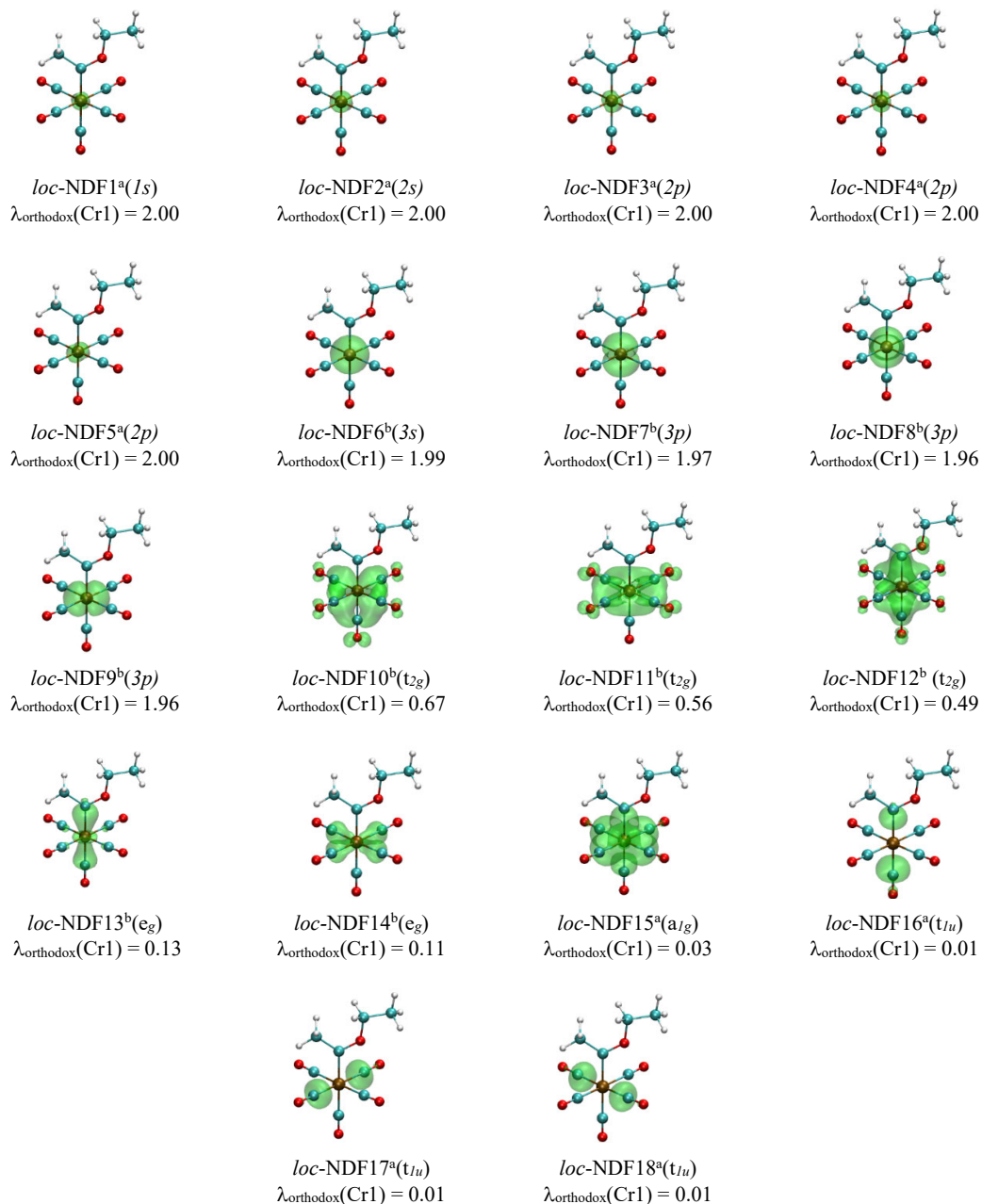
**Figure S1-3:** The full compilation of Molecular orbitals through the NDF analysis for  $\text{Cr}(\text{CO})_6$  with isovalues of  $a=0.0001\text{au}$  and  $b=0.001\text{au}$  and EV=Eigenvalue





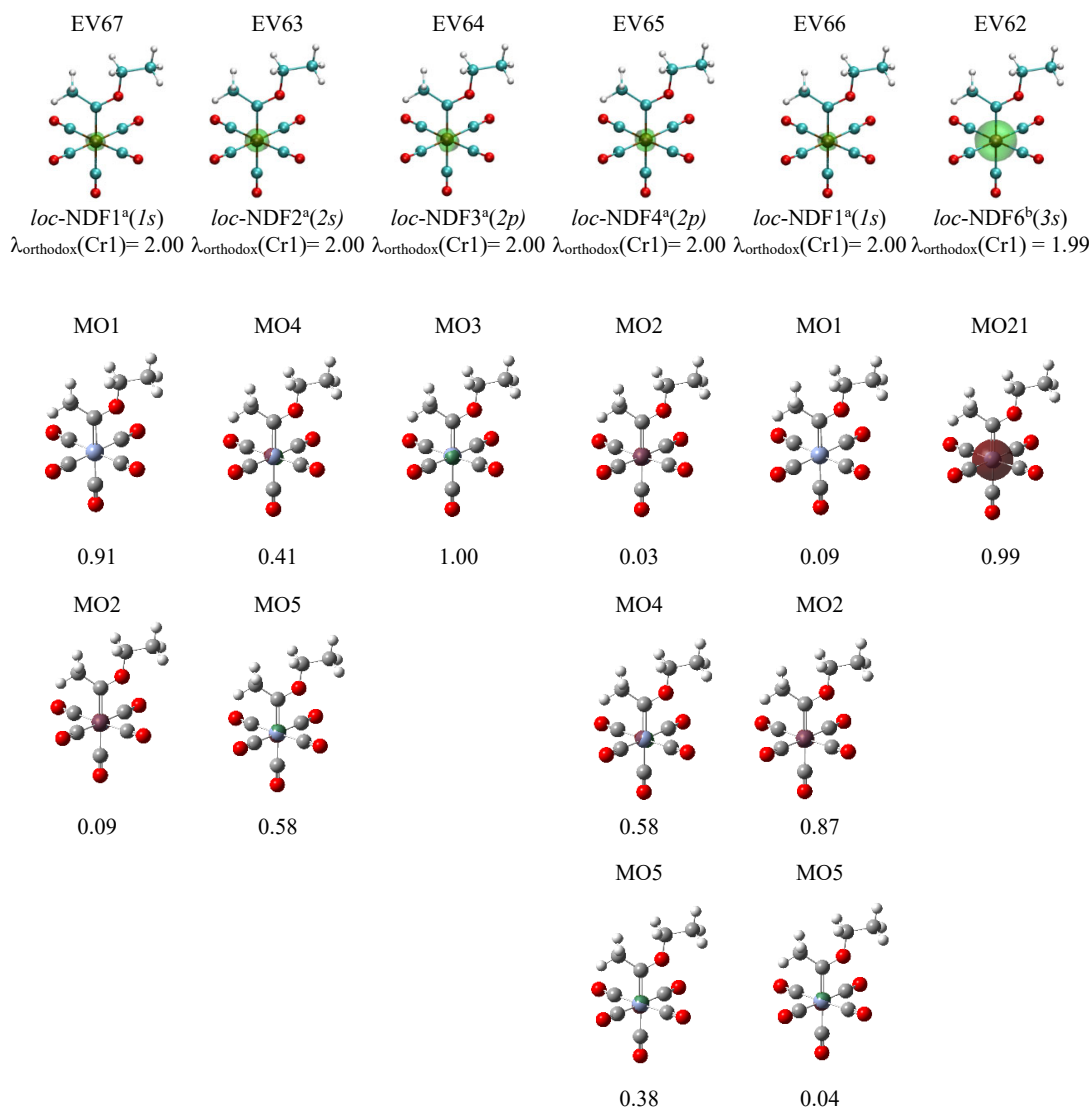
**Figure S1-4:** The Natural Density Functions corresponding to their respective Molecular Orbitals with their contributions. Illustrating the fifteenth NDF which represents  $A_{1g}$  symmetry on the Cr linked to the contributing occupied MO's.

Section 5: Cr(CO)<sub>5</sub>[C(OEt)(Me)] Natural Density Functions

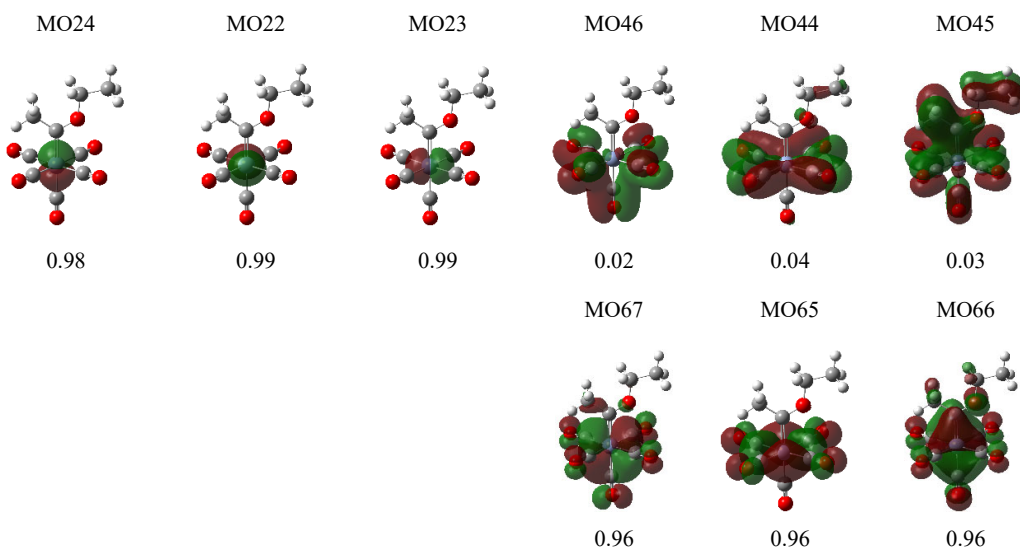
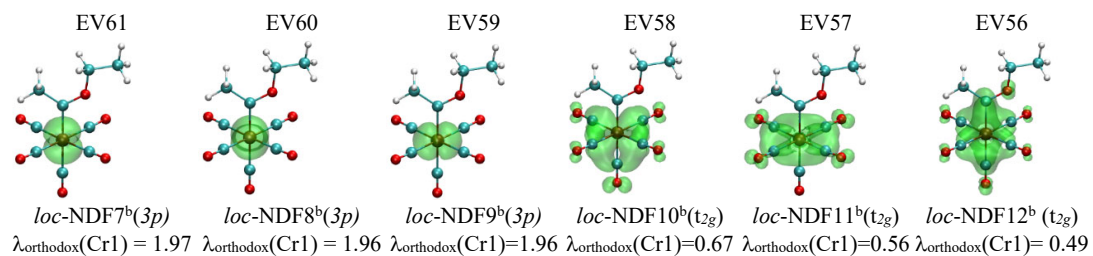


**Figure S2:** The Localized (*loc*) Natural Density Functions (NDF's) of Cr(CO)<sub>5</sub>[C(OEt)(Me)] centered on the Chromium atom. The Isovalues are indicated as a = 0.0001 au and b = 0.001 au while  $\lambda^{\text{number}}$  refers to the eigenvalue retrieved from the Orthodox Localised Matrix.

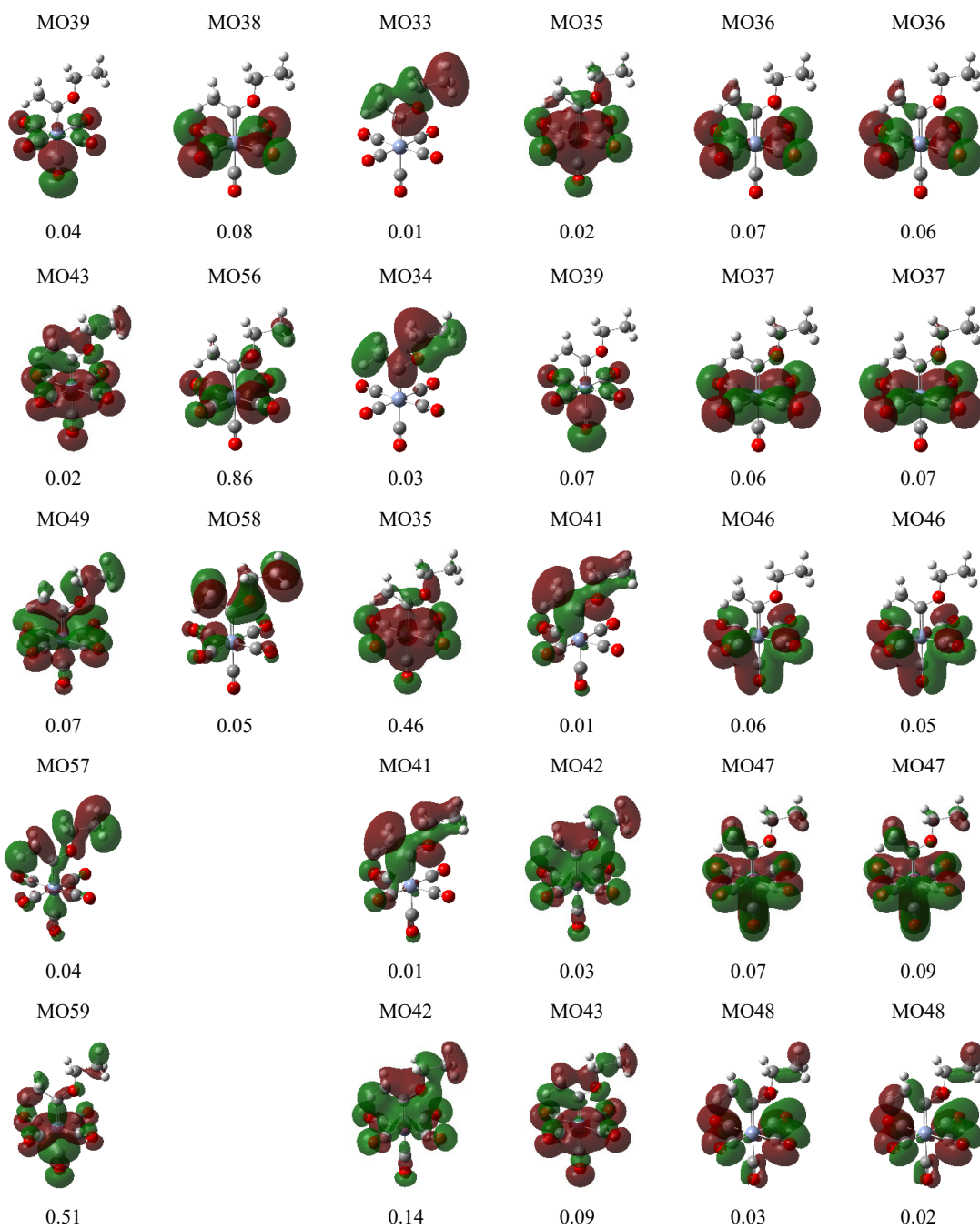
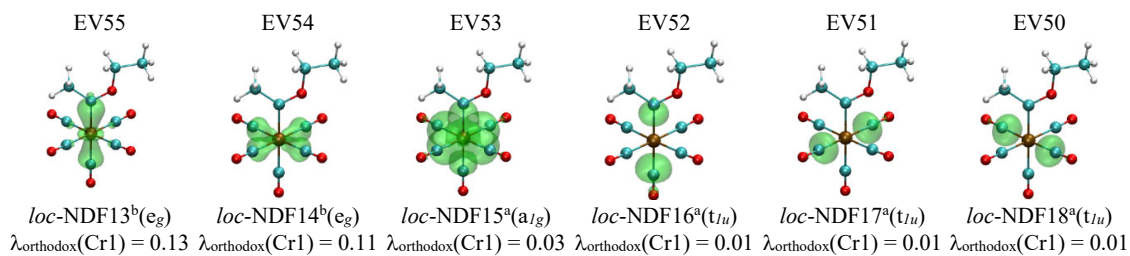
Section 6:  $\text{Cr}(\text{CO})_5[\text{C}(\text{OEt})(\text{Me})]$  Natural Density Functions corresponded to the Molecular Orbitals

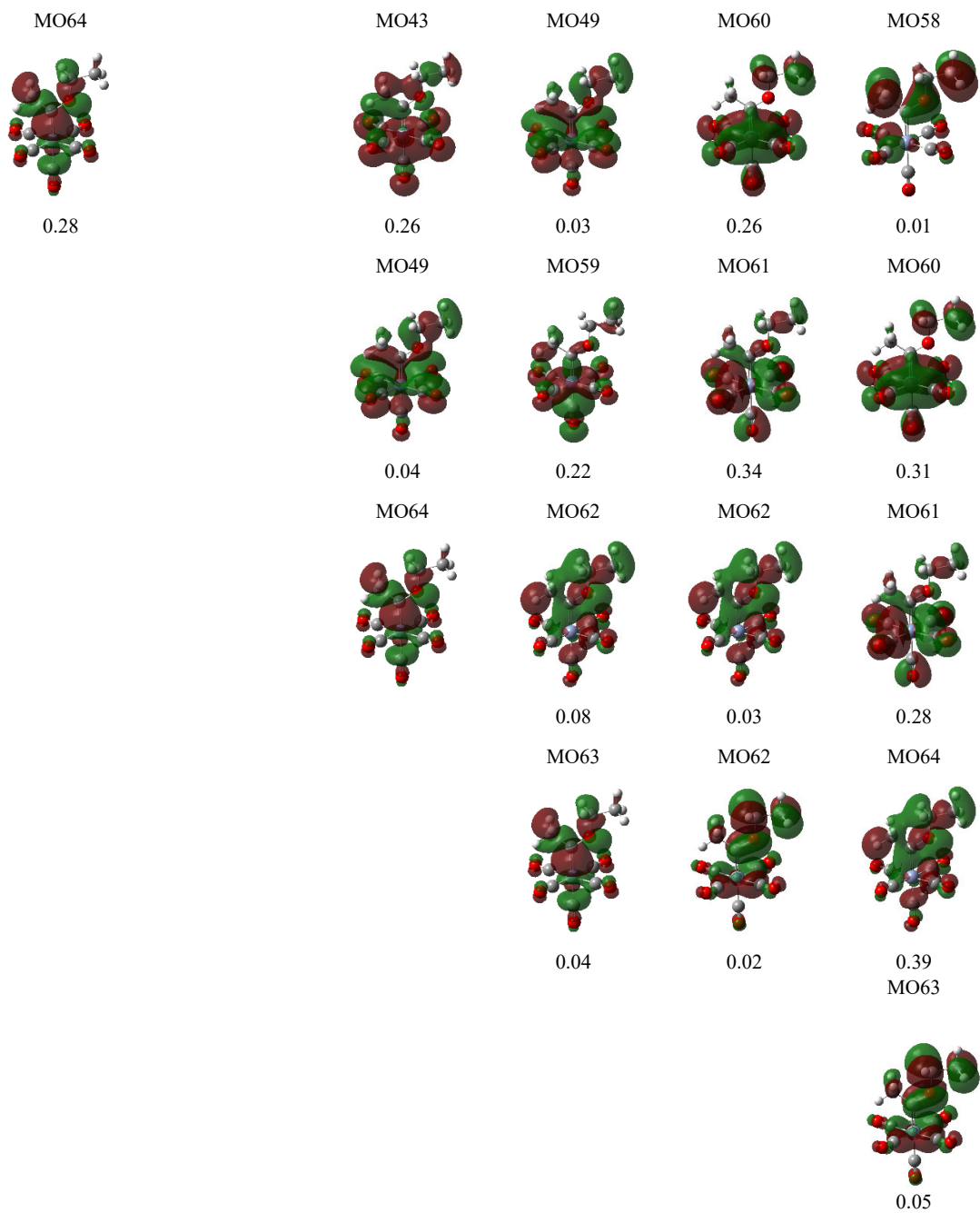


**Figure S3-1:** The full compilation of Molecular orbitals through the NDF analysis for  $\text{Cr}(\text{CO})_5[\text{C}(\text{OEt})(\text{Me})]$  with isovalues of  $a=0.0001\text{au}$  and  $b=0.001\text{au}$  and EV=Eigenvalue



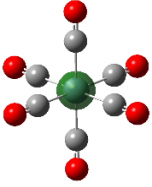
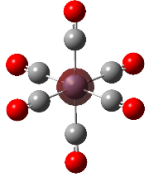
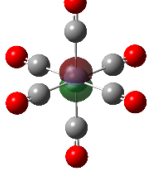
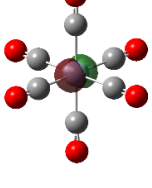
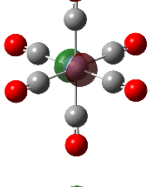
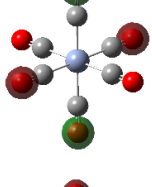
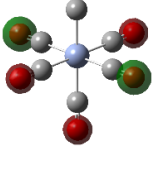
**Figure S3-2:** The full compilation of Molecular orbitals through the NDF analysis for  $\text{Cr}(\text{CO})_5[\text{C}(\text{OEt})(\text{Me})]$  with isovalues of  $a=0.0001\text{au}$  and  $b=0.001\text{au}$  and  $\text{EV}=\text{Eigenvalue}$

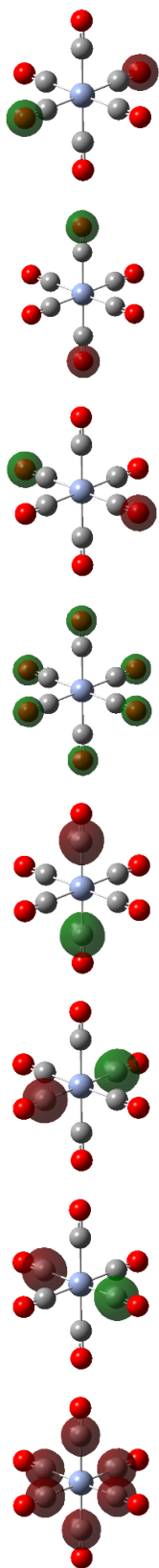




**Figure S3-3:** The full compilation of Molecular orbitals through the NDF analysis for  $\text{Cr}(\text{CO})_5[\text{C}(\text{OEt})(\text{Me})]$  with isovalues of  $a=0.0001\text{au}$  and  $b=0.001\text{au}$  and  $\text{EV}=\text{Eigenvalue}$

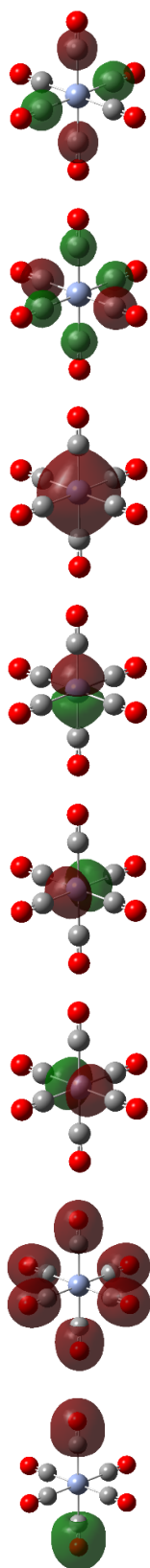
**Table S8:** The full list of Molecular Orbitals for Cr(CO)<sub>6</sub>

Molecular Orbital	Energy	Isosurface	Symmetry Label	
	$\chi_1$	-215.808	0.0002	s or a <sub>1g</sub>
	$\chi_2$	-24.789	0.002	s or a <sub>1g</sub>
	$\chi_3$	-21.0874	0.002	p or t <sub>1u</sub>
	$\chi_4$	-21.0874	0.002	p or t <sub>1u</sub>
	$\chi_5$	-21.0874	0.002	p or t <sub>1u</sub>
	$\chi_6$	-19.2342	0.002	b <sub>1g</sub>
	$\chi_7$	-19.2342	0.002	a <sub>1g</sub>

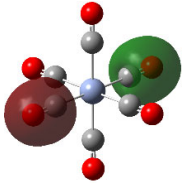
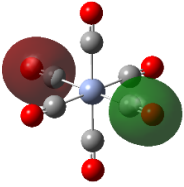
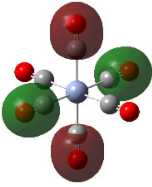
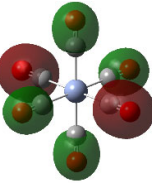
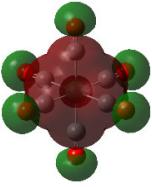
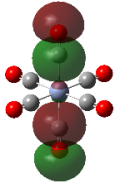
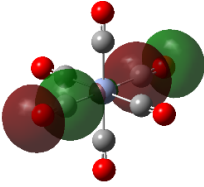
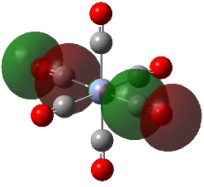


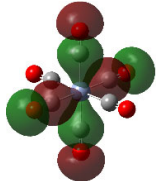
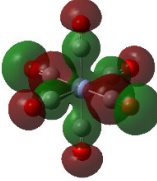
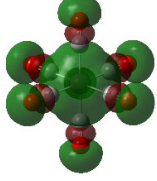
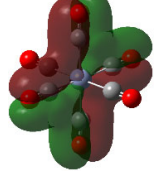
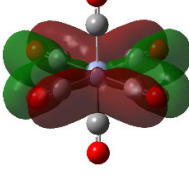
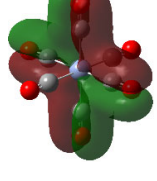
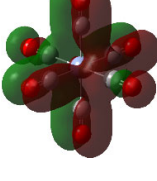
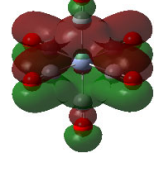
$\chi^8$	-19.2342	0.002	$e_u$
$\chi^9$	-19.2342	0.002	$e_u$
$\chi^{10}$	-19.2342	0.002	$e_u$
$\chi^{11}$	-19.234	0.002	$a_{1g}$
$\chi^{12}$	-10.3196	0.002	$e_u$
$\chi^{13}$	-10.3196	0.002	$e_u$
$\chi^{14}$	-10.3196	0.002	$e_u$
$\chi^{15}$	-10.3196	0.002	$a_{1g}$

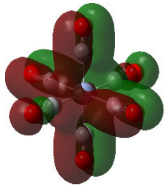
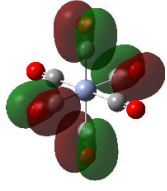
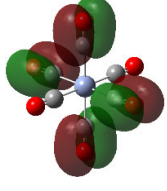
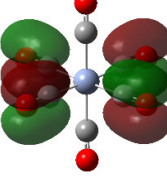
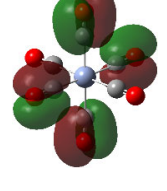
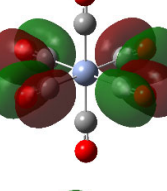
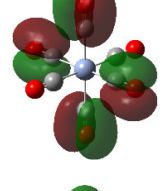
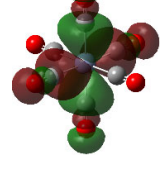


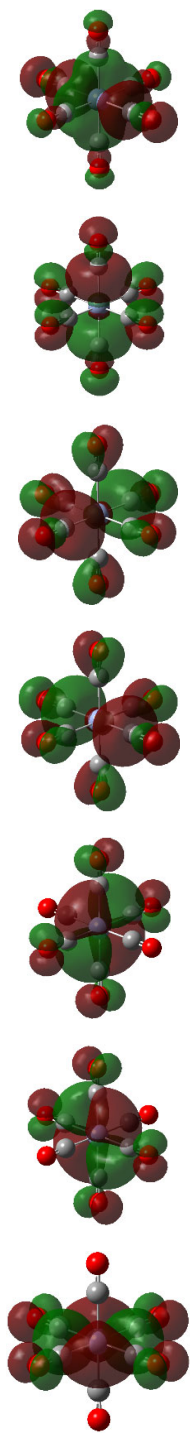


$\chi_{16}$	-10.3195	0.002	$t_{1u}$
$\chi_{17}$	-10.3195	0.002	$a_{1g}$
$\chi_{18}$	-2.9052	0.002	s or $a_{1g}$
$\chi_{19}$	-1.85187	0.02	p or $t_{1u}$
$\chi_{20}$	-1.85187	0.02	p or $t_{1u}$
$\chi_{21}$	-1.85187	0.02	p or $t_{1u}$
$\chi_{22}$	-1.14387	0.02	$a_{1g}$
$\chi_{23}$	-1.14283	0.02	$t_{1u}$

	$\chi_{24}$	-1.14283	0.02	$t_{1u}$
	$\chi_{25}$	-1.14283	0.02	$t_{1u}$
	$\chi_{26}$	-1.14247	0.02	$t_{1u}$
	$\chi_{27}$	-1.14247	0.02	$a_{1g}$
	$\chi_{28}$	-0.61256	0.02	$a_{1g}$
	$\chi_{29}$	-0.57053	0.02	$e_u$
	$\chi_{30}$	-0.57053	0.02	$e_u$
	$\chi_{31}$	-0.57053	0.02	$e_u$

	$\chi_{32}$	-0.56719	0.02	$b_{1g}$
	$\chi_{33}$	-0.56719	0.02	$a_{1g}$
	$\chi_{34}$	-0.51146	0.02	$a_{1g}$
	$\chi_{35}$	-0.49002	0.02	$t_{1g}$
	$\chi_{36}$	-0.49002	0.02	$t_{1g}$
	$\chi_{37}$	-0.49002	0.02	$t_{1g}$
	$\chi_{38}$	-0.48644	0.02	$t_{2u}$
	$\chi_{39}$	-0.48644	0.02	$t_{2u}$

	$\chi_{40}$	-0.48644	0.02	$t_{2u}$
	$\chi_{41}$	-0.47187	0.02	$t_{2u}$
	$\chi_{42}$	-0.47187	0.02	$t_{2u}$
	$\chi_{43}$	-0.47187	0.02	$t_{2u}$
	$\chi_{44}$	-0.46527	0.02	$t_{1g}$
	$\chi_{45}$	-0.46527	0.02	$t_{1g}$
	$\chi_{46}$	-0.46527	0.02	$t_{1g}$
	$\chi_{47}$	-0.45164	0.02	$e_g$



$\chi_{48}$	-0.45164	0.02	$e_g$
$\chi_{49}$	-0.41885	0.02	$t_{1u}$
$\chi_{50}$	-0.41885	0.02	$t_{1u}$
$\chi_{51}$	-0.41885	0.02	$t_{1u}$
$\chi_{52}$	-0.25553	0.02	$t_{2g}$
$\chi_{53}$	-0.25553	0.02	$t_{2g}$
$\chi_{54}$	-0.25553	0.02	$t_{2g}$

# **Appendix B**

## **Supplementary Information for Chapter 4**

## Section 1: Cartesian Coordinates and Energies of All Molecules Studied.

**Table B 1. 1.** Cartesian coordinates of  $\text{Cr}(\text{CO})_5\{\text{C}(\text{OEt})(\text{H})\}$  single point calculation at CAM-B3LYP/dev2svp(p) level in n-hexane.

Atom	X	Y	Z
Cr	0.0003	0.0000	-0.0367
C	0.0000	0.0000	-0.0014
O	0.0000	0.0000	0.0001
C	0.0001	0.0000	0.0025
O	0.0000	0.0000	0.0000
C	0.0000	0.0000	0.0001
O	0.0000	0.0000	0.0000
C	0.0000	0.0001	-0.0015
O	0.0000	0.0001	0.0001
C	0.0000	0.0000	-0.0050
O	0.0000	0.0000	0.0022
C	-0.0003	0.0021	0.3377
O	0.0017	0.0005	-0.0421
C	-0.0184	-0.0186	-0.0159
H	-0.0078	0.0063	0.0003
H	0.0067	-0.0084	0.0182
C	0.3791	0.3778	-0.0013
H	-0.0167	-0.0179	0.0000
H	0.5493	-0.0241	0.0002
H	-0.0241	0.5631	0.0003

H	0.0002	0.0003	0.6376
---	--------	--------	--------

---

Molecular Energy of Cr(CO)<sub>5</sub>{C(OEt)(H)}: -1803.30058518 a.u.

**Table B 1. 2.** Cartesian coordinates of Cr(CO)<sub>5</sub>{C(OEt)(CCH)} single point calculation at CAM-B3LYP/dev2svp(p) level in n-hexane.

Atom	X	Y	Z
Cr	-0.64426	0.0088	0.07138
C	-0.94801	-1.86568	0.32859
O	-1.11273	-2.98938	0.4902
C	-0.0348	-0.33919	-1.70901
O	0.29502	-0.54257	-2.78825
C	-2.42129	0.24964	-0.59251
O	-3.4865	0.39322	-0.99694
C	-0.26001	1.87046	-0.15998
O	-0.01191	2.98315	-0.29064
C	-1.28105	0.35715	1.83426
O	-1.70388	0.57209	2.87995
C	1.24177	-0.24962	0.72218
O	2.21642	-0.57231	-0.10971
C	3.60286	-0.73692	0.28298
H	3.98517	-1.50987	-0.40147
H	3.64449	-1.11853	1.31587



C	4.3653	0.56802	0.12723
H	5.43437	0.40279	0.35098
H	4.28207	0.94919	-0.905
H	3.98438	1.33844	0.81944
C	1.60088	-0.09601	2.09771
C	1.79755	0.06246	3.29026
H	1.95495	0.20614	4.34478

---

Molecular Energy of  $\text{Cr}(\text{CO})_5\{\text{C}(\text{OEt})(\text{CCH})\}$ : -1879.34725695 a.u.

**Table B 1. 3.** Cartesian coordinates of  $\text{Cr}(\text{CO})_5\{\text{C}(\text{OEt})(\text{CHCH}_2)\}$  single point calculation at CAM-B3LYP/dev2svp(p) level in n-hexane.

Atom	X	Y	Z
Cr	0.78239	-0.10041	-0.00318
C	1.28446	1.19428	-1.3145
O	1.61618	1.9557	-2.1078
C	0.32891	-1.30483	-1.40846
O	0.10761	-2.03601	-2.2686
C	2.56092	-0.76456	-0.03181
O	3.63942	-1.16451	-0.04814
C	0.35119	-1.42245	1.29882
O	0.15706	-2.2322	2.09265
C	1.27762	1.09805	1.39907
O	1.59544	1.80829	2.24377
C	-1.09636	0.75494	0.0397
O	-2.29365	0.21414	0.07715
C	-2.56694	-1.19843	0.11173
H	-2.24232	-1.5865	1.08975
H	-1.98475	-1.69657	-0.67658
C	-4.05803	-1.38859	-0.09094
H	-4.30032	-2.46483	-0.05468
H	-4.63417	-0.87717	0.69932
H	-4.37796	-0.99427	-1.07086
C	-1.25566	2.23131	0.02938
H	-0.33033	2.81246	0.04164

C	-2.43184	2.88676	-0.0038
H	-3.38718	2.35201	-0.02229
H	-2.46243	3.98237	-0.01715

---

Molecular Energy of  $\text{Cr}(\text{CO})_5\{\text{C}(\text{OEt})(\text{CHCH}_2)\}$ : -1880.59449520 a.u.

**Table B 1. 4.** Cartesian coordinates of  $\text{Cr}(\text{CO})_5\{\text{C}(\text{OEt})(\text{CHCHPh})\}$  single point calculation at CAM-B3LYP/dev2svp(p) level in n-hexane.

Atom	X	Y	Z
Cr	1.94168	-0.51579	0.00117
C	1.09657	-1.62512	1.30284
O	0.61641	-2.31163	2.08951
C	2.72963	0.4861	1.41654
O	3.23529	1.04817	2.2842
C	3.42923	-1.68794	0.01851
O	4.33154	-2.40302	0.0278
C	2.84739	0.5458	-1.29493
O	3.44134	1.13381	-2.08616
C	1.16404	-1.5428	-1.40689
O	0.71145	-2.17297	-2.25438
C	0.22103	0.65533	-0.02854
O	0.07602	1.96685	-0.05708
C	1.15037	2.91943	-0.10548
H	1.6341	2.84509	-1.09207
H	1.8902	2.67113	0.66901
C	0.55988	4.29971	0.11409

H	1.36313	5.05558	0.07095
H	-0.18461	4.54146	-0.66406
H	0.07177	4.36886	1.10159
C	-1.10721	0.02965	-0.01881
H	-1.1169	-1.06156	-0.0071
C	-2.28716	0.70847	-0.02276
H	-2.23664	1.80237	-0.03601
C	-3.63587	0.14849	-0.01017
C	-3.90235	-1.2394	0.01658
C	-4.73356	1.0367	-0.02513
C	-5.2125	-1.71235	0.02693
H	-3.07688	-1.95566	0.03065
C	-6.04603	0.56249	-0.01499
H	-4.54522	2.11488	-0.04523
C	-6.28973	-0.81462	0.01099
H	-5.3993	-2.79024	0.04803
H	-6.88152	1.26888	-0.02716
H	-7.31717	-1.19118	0.01931

---

Molecular Energy of Cr(CO)<sub>5</sub>{C(OEt)(CHCHPh)}: -2111.35055333 a.u.

**Table B 1. 5.** Cartesian coordinates of Cr(CO)<sub>5</sub>{C(NMe<sub>2</sub>)(H)} single point calculation at CAM-B3LYP/dev2svp(p) level in n-hexane.

Atom	X	Y	Z
Cr	0.58736	0.01555	0.00008
C	0.97327	1.30757	-1.34744
O	1.21332	2.08592	-2.15928
C	0.17423	-1.25466	-1.35229
O	-0.06304	-2.0234	-2.17578
C	2.39255	-0.53756	0.00008
O	3.49395	-0.87738	-0.0001
C	0.17382	-1.25464	1.35226
O	-0.06371	-2.02339	2.17568
C	0.97311	1.30743	1.3477
O	1.21314	2.08564	2.15968
C	-1.34138	0.77024	-0.00021
H	-1.40789	1.87281	-0.00047
N	-2.56893	0.29252	-0.0002
C	-2.89611	-1.13367	0.00002
H	-3.49467	-1.37735	0.89562
H	-3.49275	-1.37812	-0.89667
H	-1.98033	-1.73265	0.00124
C	-3.76201	1.1491	-0.00026
H	-4.37489	0.94217	-0.89561
H	-4.37428	0.94311	0.89572
H	-3.4634	2.20712	-0.00092

Molecular Energy of  $\text{Cr}(\text{CO})_5\{\text{C}(\text{NMe}_2)(\text{H})\}$ : -1783.46135026 a.u.

**Table B 1. 6.** Cartesian coordinates of Cr(CO)<sub>5</sub>{C(NMe<sub>2</sub>)(CCH)} single point calculation at CAM-B3LYP/dev2svp(p) level in n-hexane.

Atom	X	Y	Z
Cr	0.55005	0.07546	0.00044
C	1.03431	1.34508	-1.3465
O	1.35942	2.09715	-2.15038
C	0.11231	-1.16738	-1.37189
O	-0.12314	-1.91811	-2.21178
C	2.31996	-0.57701	0.00074
O	3.39758	-0.98273	0.00102
C	0.11216	-1.16662	1.37341
O	-0.12332	-1.91691	2.21369
C	1.03401	1.34584	1.34676
O	1.35898	2.09836	2.15028
C	-1.42285	0.88098	-0.00011
N	-2.6285	0.31	-0.00051
C	-2.83723	-1.13505	-0.00042
H	-3.41596	-1.42629	0.89478
H	-3.41251	-1.42701	-0.89762
H	-1.88162	-1.66396	0.00163
C	-3.90107	1.04245	-0.00128
H	-4.48686	0.76696	-0.89673
H	-4.48715	0.76844	0.89445
H	-3.72331	2.12497	-0.00214
C	-1.43586	2.30876	-0.00026

C	-1.34731	3.52415	-0.00034
H	-1.24423	4.59447	-0.00045

---

Molecular Energy of Cr(CO)<sub>5</sub>{C(NMe<sub>2</sub>)(CCH)}: -1859.50508810 a.u.

**Table B 1. 7.** Cartesian coordinates of Cr(CO)<sub>5</sub>{C(NMe<sub>2</sub>)(CHCH<sub>2</sub>)} single point calculation at CAM-B3LYP/dev2svp(p) level in n-hexane.

Atom	X	Y	Z
Cr	0.77475	-0.01979	0.00153
C	0.89722	1.71866	-0.78016
O	1.02505	2.75607	-1.25767
C	0.61938	-0.74839	-1.74864
O	0.54624	-1.17672	-2.81487
C	2.6468	-0.14849	-0.08857
O	3.79584	-0.23366	-0.1443
C	0.75026	-1.74274	0.80294
O	0.79428	-2.77873	1.30443
C	0.90295	0.74242	1.73902
O	0.99728	1.2042	2.78921
C	-1.36196	0.19334	0.15135
C	-1.79091	1.58234	0.44178
H	-1.3783	2.02224	1.35894
C	-2.49029	2.36929	-0.39259
H	-2.87901	2.00133	-1.35066
H	-2.6528	3.4285	-0.16325



N	-2.33034	-0.70225	0.04504
C	-3.7516	-0.47144	0.37018
H	-4.35638	-0.42965	-0.55275
H	-4.10916	-1.31652	0.98279
H	-3.8787	0.4642	0.92595
C	-2.10658	-2.09408	-0.35835
H	-2.11314	-2.75424	0.52673
H	-2.92233	-2.40352	-1.03331
H	-1.15288	-2.19651	-0.88242

---

Molecular Energy of  $\text{Cr}(\text{CO})_5\{\text{C}(\text{NMe}_2)(\text{CHCH}_2)\}$ : -1860.74376978 a.u.

**Table B 1. 8.** Cartesian coordinates of  $\text{Cr}(\text{CO})_5\{\text{C}(\text{NMe}_2)(\text{CHCHPh})\}$  single point calculation at CAM-B3LYP/dev2svp(p) level in n-hexane.

Atom	X	Y	Z
Cr	-1.84291	-0.50768	-0.06475
C	-0.48661	-1.58558	-0.87209
O	0.28812	-2.27336	-1.36938
C	-2.25105	0.19096	-1.78644
O	-2.50097	0.59042	-2.83706
C	-3.05718	-1.91716	-0.32242
O	-3.80781	-2.77892	-0.48038
C	-3.24895	0.47676	0.75033
O	-4.13174	1.01795	1.25498
C	-1.38681	-1.19602	1.64684

O	-1.1155	-1.62571	2.68003
C	-0.4024	1.05935	0.28167
C	0.95341	0.54968	0.56098
H	1.01774	-0.22572	1.33187
C	2.0461	0.8299	-0.18828
H	1.94691	1.57244	-0.9908
N	-0.54946	2.37746	0.28476
C	0.44725	3.34951	0.77359
H	0.90487	3.89787	-0.06854
H	-0.06975	4.07839	1.42108
H	1.23422	2.84655	1.34727
C	-1.78109	3.05609	-0.1286
H	-2.36994	3.35736	0.75567
H	-1.51336	3.9633	-0.69641
H	-2.38653	2.40584	-0.7654
C	3.37588	0.21456	-0.08969
C	3.68757	-0.82239	0.81603
C	4.40341	0.68408	-0.93413
C	4.97412	-1.3558	0.87757
H	2.91436	-1.22497	1.47611
C	5.69256	0.15021	-0.87286
H	4.18213	1.48295	-1.64975
C	5.98434	-0.87247	0.0348
H	5.1915	-2.16127	1.58591
H	6.47172	0.53273	-1.5395

H	6.99197	-1.2964	0.08396
---	---------	---------	---------

---

Molecular Energy of  $\text{Cr}(\text{CO})_5\{\text{C}(\text{NMe}_2)(\text{CHCHPh})\}$ : -2091.49689229 a.u.

**Section 2: Inter-fragment delocalization of all the molecules in their respective fragments.**

**Table B 2. 1.** Inter-fragment Delocalization when X=OEt.

Fragment A	Fragment B	Delocalized electrons			
		R=H	R=CHCH <sub>2</sub>	R=CHCHPh	R=CCH
[M]	C <sub>carbene</sub>	1.3367	1.1463	1.1082	1.2059
[M]	[X]	0.2440	0.3190	0.3085	0.2403
[M]	[R]	0.0601	0.2182	0.2318	0.2441
[M]	[L]	1.6408	1.6835	1.6484	1.6903
[X]	[R]	0.1362	0.2548	0.2759	0.2977

Several key features stand out. The  $[\text{M}] \cdots \text{C}_{\text{carbene}}$  decreases with more conjugation when X=OEt except when R= -CHCHPh. For the  $[\text{M}] \cdots [\text{X}]$  adding the Phenyl (Ph) group decreases this interaction, suggesting the Ph absorbs electron density from the X=OEt. The  $[\text{M}] \cdots [\text{R}]$  increases perfectly with more conjugation as the R-group becomes richer in electron density the  $[\text{M}] \cdots [\text{R}]$  interaction strengthens. With the  $[\text{M}] \cdots [\text{L}]$  interaction the Ph takes away density suggesting the Ph is likely acting as a  $\pi$ -accepting group. Finally, the  $[\text{X}] \cdots [\text{R}]$  group follows the trend of the  $[\text{M}] \cdots [\text{R}]$  group increasing with more conjugation, so the more conjugation that is added the more the X- and R-group interact.

**Table B 2. 2.** Inter-fragment Delocalization when X=NMe<sub>2</sub>.

Fragment A	Fragment B	Delocalized electrons			
		R=H	R=CHCH <sub>2</sub>	R=CHCHPh	R=CCH
[M]	C <sub>carbene</sub>	1.1048	0.9326	0.9273	0.9427
[M]	[X]	0.2866	0.2949	0.2938	0.2959
[M]	[R]	0.0546	0.2200	0.2286	0.2328

[M]	[L]	1.4460	1.4475	1.4497	1.4713
[X]	[R]	0.1455	0.3133	0.3340	0.3453

Similar to X=OEt the  $[M]\cdots C_{\text{carbene}}$  decreases with more conjugation when X=NMe<sub>2</sub> except when R= -CCH. For the  $[M]\cdots[X]$  adding the phenyl (Ph) decreases this interaction suggesting the Ph absorbs electron density from the X=NMe<sub>2</sub>. Then  $[M]\cdots[R]$  increases perfectly with more conjugation as the R-group becomes richer in electron density the  $[M]\cdots[R]$  interaction strengthens. The  $[M]\cdots[L]$  increases with more conjugation and finally the  $[X]\cdots[R]$  group follows the trend of the  $[M]\cdots[R]$  group increasing with conjugation, so the more conjugation that is added the more the X- and R-group interact.

### Section 3: Method of assigning symmetry labels (LMAT) and correlating to the DI contribution (DMAT) on a Molecular orbital level.

This section shows how the results that follow were obtained in terms of achieving the symmetry classifications linked to the DI values of the complexes. All the molecules followed the same procedure:

1. FALDI was run to obtain the LMAT of the metal centre (Cr) from which the *loc*-NDFs can be obtained in the investigation of  $[U_{ij}^{AA}]^2$  and symmetry labels assigned through visual analysis of the *loc*-NDF.
2. FALDI was run to obtain the DMAT and designated into Fragments. The fragments decomposed into the DI contribution of each MO. This was run twice, once for all the fragments and a second time for the  $[M]\cdots[L]$  fragment (illustrated below).
3. The DMAT MOs were then correlated to the LMAT assigned symmetry of the MOs and their percentage contributions were weighted with respect to the DI value and the weighted molecular energy of the orbital was calculated with its DI contribution.
4. For illustration purposes we demonstrate the process using  $\text{Cr}(\text{CO})_5\{\text{C}(\text{OEt})(\text{H})\}$  providing the full data set.

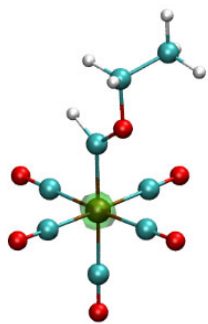
All **Tables below (B 3.)** have been simplified by inserting blank spaces where the cell value is less than 0.01, in the energetics (**Table B 3. 7.**) the blank inserts were for cell values above -0.001 (since all orbitals considered had negative energies).

**Table B 3. 1.** The LMAT for Cr and visual assignment symmetry labels to the *loc*-NDFs followed by the MOs for Cr(CO)<sub>5</sub>{C(OEt)(H)}.

Evec Matrix	a <sub>1g</sub>	a <sub>1g</sub>	t <sub>1u</sub>	t <sub>1u</sub>	t <sub>1u</sub>	a <sub>1g</sub>	t <sub>1u</sub>	t <sub>1u</sub>	t <sub>1u</sub>	t <sub>2g</sub>	t <sub>2g</sub>	t <sub>2g</sub>	e <sub>g</sub>	e <sub>g</sub>	a <sub>1g</sub>	t <sub>1u</sub>	t <sub>1u</sub>	t <sub>1u</sub>	NL	MO Classifications									
	1	2	3	4	5	6	7	8	9	10	11	12	13	14	15	16	17	18	19	a <sub>1g</sub>	t <sub>1u</sub>	t <sub>2g</sub>	e <sub>g</sub>	NL	Ratio	Character 1	Character 2		
MO1	0.91	0.09																			1.00					1.00	a <sub>1g</sub>		
MO2	0.09	0.88		0.03																	0.97	0.03				0.97	a <sub>1g</sub>		
MO3					1.00																	1.00				1.00	t <sub>1u</sub>		
MO4		0.02	0.33	0.65																	0.02	0.98				0.98	t <sub>1u</sub>		
MO5		0.01	0.67	0.32																	0.01	0.99				0.99	t <sub>1u</sub>		
MO6																								1.00		1.00	NL		
MO7																								1.00		1.00	NL		
MO8																								1.00		1.00	NL		
MO9																								1.00		1.00	NL		
MO10																								1.00		1.00	NL		
MO11																								1.00		1.00	NL		
MO12																								1.00		1.00	NL		
MO13																								1.00		1.00	NL		
MO14																								1.00		1.00	NL		
MO15																								1.00		1.00	NL		
MO16																								1.00		1.00	NL		
MO17																								1.00		1.00	NL		
MO18																								1.00		1.00	NL		
MO19																								1.00		1.00	NL		
MO20						1.00																1.00				1.00	a <sub>1g</sub>		
MO21									0.99																1.00		1.00	t <sub>1u</sub>	
MO22							0.05	0.94																	1.00		1.00	t <sub>1u</sub>	
MO23							0.94	0.05																	1.00		1.00	t <sub>1u</sub>	
MO24																									1.00		1.00	NL	
MO25																									1.00		1.00	NL	

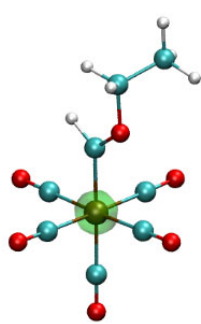
MO26										1.00	1.00	NL			
MO27										1.00	1.00	NL			
MO28										1.00	1.00	NL			
MO29										1.00	1.00	NL			
MO30										0.99	1.00	NL			
MO31					0.02				0.02		0.96	0.98	NL		
MO32					0.04			0.12	0.04	0.01		0.94	0.95	NL	
MO33					0.46	0.02			0.46	0.02		0.52	0.11	NL	a <sub>1g</sub>
MO34							0.01	0.12		0.13		0.87	0.85	NL	t <sub>1u</sub>
MO35							0.11	0.01	0.02	0.13		0.87	0.85	NL	t <sub>1u</sub>
MO36				0.07							0.08	0.92	0.91	NL	
MO37			0.03			0.07				0.07	0.04	0.89	0.92	NL	
MO38								0.25				1.00	1.00	NL	
MO39				0.01	0.08	0.02		0.10	0.08	0.02	0.01	0.88	0.91	NL	
MO40					0.26			0.03	0.26	0.01		0.73	0.65	NL	a <sub>1g</sub>
MO41				0.01	0.07	0.07			0.07	0.08	0.01	0.82	0.90	NL	t <sub>1u</sub>
MO42		0.04									0.04	0.95	0.95	NL	
MO43			0.02					0.08		0.08	0.03	0.89	0.91	NL	
MO44	0.02						0.11		0.20	0.11	0.02	0.87	0.87	NL	t <sub>1u</sub>
MO45						0.05		0.06		0.11		0.87	0.87	NL	t <sub>1u</sub>
MO46							0.03		0.13	0.03	0.01	0.96	0.97	NL	
MO47			0.02			0.01		0.04		0.05		0.92	0.95	NL	
MO48												1.00	1.00	NL	
MO49												0.99	0.99	NL	
MO50												1.00	1.00	NL	
MO51												0.99	0.99	NL	
MO52				0.10	0.68						0.78	0.22	0.72	e <sub>g</sub>	NL
MO53				0.25	0.23	0.02		0.02	0.02	0.02	0.48	0.49	0.03	NL	e <sub>g</sub>
MO54				0.05		0.02	0.01	0.01	0.01	0.04	0.05	0.91	0.95	NL	
MO55				0.20		0.26		0.03		0.29	0.20	0.51	0.42	NL	t <sub>1u</sub>

MO56																					0.01	0.01	0.51	0.54	0.46	0.15	t <sub>1u</sub>	NL														
MO57																						0.66	0.01	0.68	0.32	0.54	t <sub>1u</sub>	NL														
MO58																					0.01		0.07	0.09	0.90	0.90	NL															
MO59																					0.01		0.03	0.04	0.95	0.96	NL															
MO60													0.30	0.03	0.37									0.03	0.38	0.30	0.29	0.21	t <sub>1u</sub>	e <sub>g</sub>												
MO61													0.85	0.11											0.95	0.05	0.95	t <sub>2g</sub>														
MO62													0.11	0.85											0.95	0.05	0.95	t <sub>2g</sub>														
MO63													0.96												0.96	0.04	0.96	t <sub>2g</sub>														
Cr1_EVals	NDF1	NDF2	NDF3	NDF4	NDF5	NDF6	NDF7	NDF8	NDF9	NDF10	NDF11	NDF12	NDF13	NDF14	NDF15	NDF16	NDF17	NDF18	NDF19																							
	2.00	2.00	2.00	2.00	2.00	1.99	1.97	1.96	1.96	0.71	0.60	0.51	0.12	0.09	0.03	0.01	0.01	0.01	0.00																							
	a <sub>1g</sub>	a <sub>1g</sub>	t <sub>1u</sub>	t <sub>1u</sub>	t <sub>1u</sub>	a <sub>1g</sub>	t <sub>1u</sub>	t <sub>1u</sub>	t <sub>1u</sub>	t <sub>2g</sub>	t <sub>2g</sub>	t <sub>2g</sub>	e <sub>g</sub>	e <sub>g</sub>	a <sub>1g</sub>	t <sub>1u</sub>	t <sub>1u</sub>	t <sub>1u</sub>	NL																							



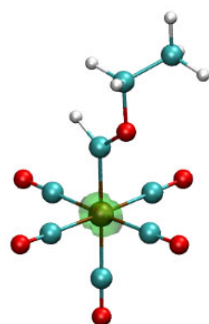
*loc-NDF1<sup>a</sup>(1s)*

$\lambda_{\text{orthodox}}(\text{Cr1}) = 2.00$



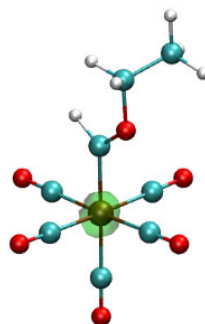
*loc-NDF2<sup>a</sup>(2s)*

$\lambda_{\text{orthodox}}(\text{Cr1}) = 2.00$



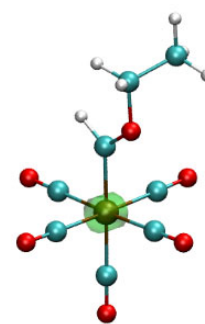
*loc-NDF3<sup>a</sup>(2p)*

$\lambda_{\text{orthodox}}(\text{Cr1}) = 2.00$



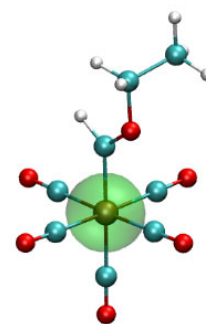
*loc-NDF4<sup>a</sup>(2p)*

$\lambda_{\text{orthodox}}(\text{Cr1}) = 2.00$



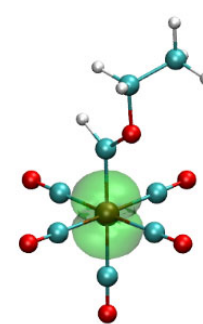
*loc-NDF5<sup>a</sup>(2p)*

$\lambda_{\text{orthodox}}(\text{Cr1}) = 2.00$



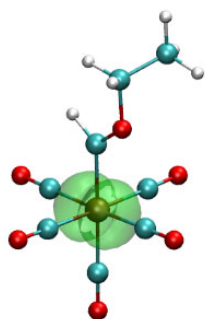
*loc-NDF6<sup>b</sup>(3s)*

$\lambda_{\text{orthodox}}(\text{Cr1}) = 1.99$



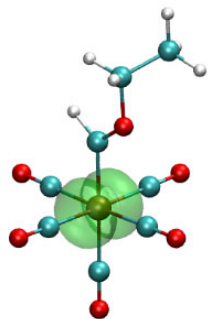
*loc-NDF7<sup>b</sup>(3p)*

$\lambda_{\text{orthodox}}(\text{Cr1}) = 1.97$



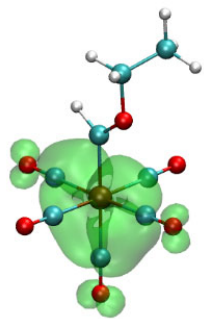
*loc*-NDF8<sup>b</sup>(3p)

$\lambda_{\text{orthodox}}(\text{Cr1}) = 1.96$



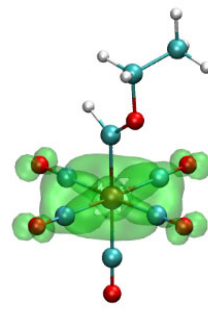
*loc*-NDF9<sup>b</sup>(3p)

$\lambda_{\text{orthodox}}(\text{Cr1}) = 1.96$



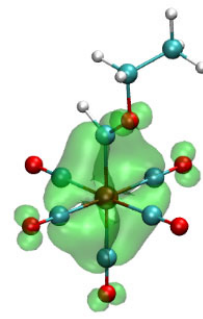
*loc*-NDF10<sup>b</sup>(t<sub>2g</sub>)

$\lambda_{\text{orthodox}}(\text{Cr1}) = 0.71$



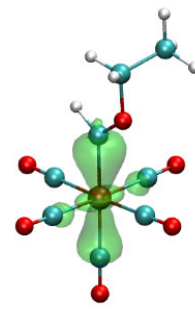
*loc*-NDF11<sup>b</sup>(t<sub>2g</sub>)

$\lambda_{\text{orthodox}}(\text{Cr1}) = 0.60$



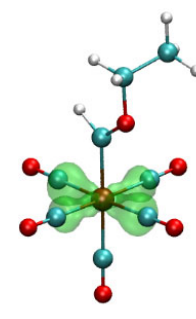
*loc*-NDF12<sup>b</sup>(t<sub>2g</sub>)

$\lambda_{\text{orthodox}}(\text{Cr1}) = 0.51$



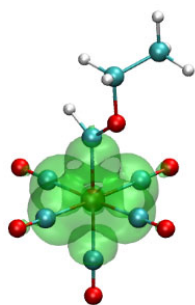
*loc*-NDF13<sup>b</sup>(e<sub>g</sub>)

$\lambda_{\text{orthodox}}(\text{Cr1}) = 0.12$



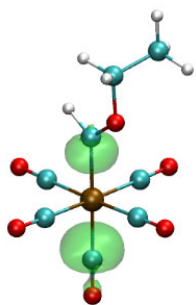
*loc*-NDF14<sup>b</sup>(e<sub>g</sub>)

$\lambda_{\text{orthodox}}(\text{Cr1}) = 0.09$



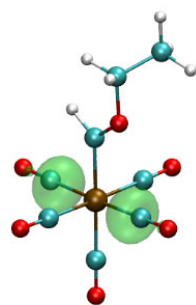
*loc*-NDF15<sup>a</sup>(a<sub>1g</sub>)

$\lambda_{\text{orthodox}}(\text{Cr1}) = 0.03$



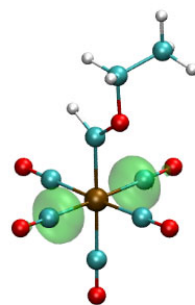
*loc*-NDF16<sup>a</sup>(t<sub>1u</sub>)

$\lambda_{\text{orthodox}}(\text{Cr1}) = 0.01$



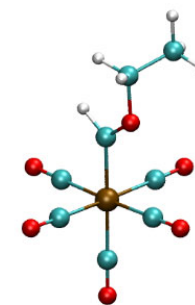
*loc*-NDF17<sup>a</sup>(t<sub>1u</sub>)

$\lambda_{\text{orthodox}}(\text{Cr1}) = 0.01$



*loc*-NDF18<sup>a</sup>(t<sub>1u</sub>)

$\lambda_{\text{orthodox}}(\text{Cr1}) = 0.01$



*loc*-NDF19<sup>a</sup>(NL)

$\lambda_{\text{orthodox}}(\text{Cr1}) = 0.00$



**Figure B 3. 1.** The Localized (*loc*) Natural Density Functions (NDF's) of  $\text{Cr}(\text{CO})_5\{\text{C}(\text{OEt})(\text{H})\}$  centered on the Chromium atom. The Isovalues are indicated as  $a = 0.0001$  a.u. and  $b = 0.001$  a.u. while  $\lambda^{\text{number}}$  refers to the eigenvalue retrieved from the Orthodox Localised Matrix.

**Table B 3. 2.** The DMATs MO contributions to inter-fragment population ([M]··[L] DI-value) for Cr(CO)<sub>5</sub>{C(OEt)(H)}.

Fragment A	Fragment B	MO1	MO2	MO3	MO4	MO5	MO6	MO7	MO8	MO9	MO10	MO11	MO12	MO13	MO14	MO15	MO16	MO17	MO18
[M]	[L]	0.00	0.00	0.00	0.00	0.00	0.00	0.00	0.00	0.00	0.00	0.00	0.00	0.00	0.00	0.00	0.00	0.00	0.00
MO19	MO20	MO21	MO22	MO23	MO24	MO25	MO26	MO27	MO28	MO29	MO30	MO31	MO32	MO33	MO34	MO35	MO36	MO37	
0.00	0.00	0.00	0.00	0.01	0.00	0.00	0.00	0.00	0.00	0.00	0.01	0.02	0.03	0.02	0.01	0.01	0.00	0.00	
MO38	MO39	MO40	MO41	MO42	MO43	MO44	MO45	MO46	MO47	MO48	MO49	MO50	MO51	MO52	MO53	MO54	MO55	MO56	
0.01	0.06	0.02	0.02	0.00	0.00	0.00	0.02	0.01	0.01	0.01	0.00	0.00	0.01	0.02	0.06	0.01	0.01	0.05	
MO57	MO58	MO59	MO60	MO61	MO62	MO63													
0.03	0.02	0.02	0.49	0.04	0.46	0.13													

**Table B 3. 3.** The DMATs DI values correlated to the MO symmetry labels of the Cr LMAT for the [M] ...[L] of Cr(CO)<sub>5</sub>{C(OEt)(H)}.

	DI						Character			
	Contribution	a <sub>1g</sub>	t <sub>1u</sub>	t <sub>2g</sub>	e <sub>g</sub>	NL	Ratio	1	2	
<i>MO60</i>	0.49		0.03	0.38		0.30	0.29	0.21	t <sub>1u</sub>	e <sub>g</sub>
<i>MO62</i>	0.46				0.95		0.05	0.95	t <sub>2g</sub>	
<i>MO63</i>	0.13				0.96		0.04	0.96	t <sub>2g</sub>	
<i>MO53</i>	0.06			0.02		0.48	0.49	0.03	NL	e <sub>g</sub>
<i>MO39</i>	0.06		0.08	0.02		0.01	0.88	0.91	NL	
<i>MO56</i>	0.05			0.54			0.46	0.15	t <sub>1u</sub>	NL
<i>MO61</i>	0.04				0.95		0.05	0.95	t <sub>2g</sub>	
<i>MO57</i>	0.03			0.68			0.32	0.54	t <sub>1u</sub>	NL
<i>MO32</i>	0.03		0.04	0.01			0.94	0.95	NL	
<i>MO45</i>	0.02			0.11			0.87	0.87	NL	t <sub>1u</sub>
<i>MO40</i>	0.02		0.26	0.01			0.73	0.65	NL	a <sub>1g</sub>
<i>MO58</i>	0.02			0.09			0.90	0.90	NL	
<i>MO41</i>	0.02		0.07	0.08		0.01	0.82	0.90	NL	t <sub>1u</sub>
<i>MO52</i>	0.02					0.78	0.22	0.72	e <sub>g</sub>	NL
<i>MO31</i>	0.02		0.02				0.96	0.98	NL	
<i>MO59</i>	0.02			0.04			0.95	0.96	NL	
<i>MO33</i>	0.02		0.46	0.02			0.52	0.11	NL	a <sub>1g</sub>
<i>MO47</i>	0.01			0.05		0.02	0.92	0.95	NL	
<i>MO23</i>	0.01			1.00				1.00	t <sub>1u</sub>	
<i>MO46</i>	0.01			0.03	0.01		0.96	0.97	NL	
<i>MO38</i>	0.01						1.00	1.00	NL	
<i>MO55</i>	0.01			0.29		0.20	0.51	0.42	NL	t <sub>1u</sub>

MO34		0.13		0.87	0.85	NL	t <sub>1u</sub>
MO35		0.13		0.87	0.85	NL	t <sub>1u</sub>
MO48				1.00	1.00	NL	
MO54		0.04	0.05	0.91	0.95	NL	
MO51				0.99	0.99	NL	
MO30				0.99	1.00	NL	
MO42			0.04	0.95	0.95	NL	
MO43		0.08	0.03	0.89	0.91	NL	
MO49				0.99	0.99	NL	
MO29				1.00	1.00	NL	
MO36			0.08	0.92	0.91	NL	
MO20	1.00				1.00	a <sub>1g</sub>	
MO22		1.00			1.00	t <sub>1u</sub>	
MO21		1.00			1.00	t <sub>1u</sub>	
MO37		0.07	0.04	0.89	0.92	NL	
MO44		0.11	0.02	0.87	0.87	NL	t <sub>1u</sub>
MO27				1.00	1.00	NL	
MO50				1.00	1.00	NL	
MO24				1.00	1.00	NL	
MO26				1.00	1.00	NL	
MO25				1.00	1.00	NL	
MO17				1.00	1.00	NL	
MO28				1.00	1.00	NL	
MO15				1.00	1.00	NL	
MO13				1.00	1.00	NL	
MO14				1.00	1.00	NL	

<i>MO12</i>				1.00	1.00	NL
<i>MO4</i>	0.02	0.98			0.98	<i>t<sub>1u</sub></i>
<i>MO6</i>				1.00	1.00	NL
<i>MO16</i>				1.00	1.00	NL
<i>MO3</i>		1.00			1.00	<i>t<sub>1u</sub></i>
<i>MO2</i>	0.97	0.03			0.97	<i>a<sub>1g</sub></i>
<i>MO5</i>	0.01	0.99			0.99	<i>t<sub>1u</sub></i>
<i>MO10</i>				1.00	1.00	NL
<i>MO9</i>				1.00	1.00	NL
<i>MO18</i>				1.00	1.00	NL
<i>MO8</i>				1.00	1.00	NL
<i>MO7</i>				1.00	1.00	NL
<i>MO19</i>				1.00	1.00	NL
<i>MO11</i>				1.00	1.00	NL
<i>MO1</i>	1.00				1.00	<i>a<sub>1g</sub></i>
Sum	1.64					
Absolute						
Sum	1.64					

**Table B 3. 4.** The MO DI Contributions of  $\text{Cr}(\text{CO})_5\{\text{C}(\text{OEt})(\text{H})\}$  for  $[\text{M}]\cdots[\text{L}]$ .

	<i>a<sub>1g</sub></i>	<i>t<sub>1u</sub></i>	<i>t<sub>2g</sub></i>	<i>e<sub>g</sub></i>	NL	Sum	
<i>MO60</i>	0.02	0.19			0.15	0.14	0.49
<i>MO62</i>				0.44		0.02	0.46

<i>MO63</i>		0.13		0.13
<i>MO53</i>			0.03	0.06
<i>MO39</i>			0.05	0.06
<i>MO56</i>	0.02		0.02	0.05
<i>MO61</i>		0.04		0.04
<i>MO57</i>	0.02		0.01	0.03
<i>MO32</i>			0.02	0.03
<i>MO45</i>			0.02	0.02
<i>MO40</i>			0.02	0.02
<i>MO58</i>			0.02	0.02
<i>MO41</i>			0.02	0.02
<i>MO52</i>			0.02	0.02
<i>MO31</i>			0.02	0.02
<i>MO59</i>			0.02	0.02
<i>MO33</i>				0.02
<i>MO47</i>			0.01	0.01
<i>MO23</i>	0.01			0.01
<i>MO46</i>			0.01	0.01
<i>MO38</i>			0.01	0.01
<i>MO55</i>				0.01

**Table B 3. 5.** A summary of the DI values in the assigned symmetry labels for  $\text{Cr}(\text{CO})_5\{\text{C}(\text{OEt})(\text{H})\}$  for the  $[\text{M}]\cdots[\text{L}]$  interaction and the MOs which contribute most to the interaction.

Summary						Sigma/Pi	
	DI	Absolute		Metal			
	Contribution	Contribution	%	%		Contribution	%
<i>a<sub>1g</sub></i>	0.0395	0.0395	2.40	3.55	$\sigma$	0.5064	30.86
<i>t<sub>1u</sub></i>	0.2691	0.2691	16.40	24.23	$\pi$	0.6045	36.84
<i>t<sub>2g</sub></i>	0.6045	0.6045	36.84	54.42	NL	0.5299	32.30
<i>e<sub>g</sub></i>	0.1978	0.1978	12.05	17.80			
<i>NL</i>	0.5299	0.5299	32.30				
<i>Total</i>	1.6408	1.6408					

#### Significant MOs

	DI		Character	Character		
	Contribution	Ratio	1	2	%	Running
<i>MO60</i>	0.49	0.212567912	<i>t<sub>1u</sub></i>	<i>e<sub>g</sub></i>	30.04	30.04
<i>MO62</i>	0.46	0.948687499	<i>t<sub>2g</sub></i>		28.27	58.31
<i>MO63</i>	0.13	0.95899982	<i>t<sub>2g</sub></i>		7.98	66.30
<i>MO53</i>	0.06	0.031975242	NL	<i>e<sub>g</sub></i>	3.91	70.21
<i>MO39</i>	0.06	0.910341955	NL		3.46	73.66
<i>MO56</i>	0.05	0.147637959	<i>t<sub>1u</sub></i>	NL	2.82	76.48
<i>MO61</i>	0.04	0.952197392	<i>t<sub>2g</sub></i>		2.25	78.73

*MO57*            0.03    0.536998562     $t_{1u}$             NL                            1.94            80.67

---

**Table B 3. 6.** The DMATs DI values correlated energies of the MOs with symmetry labels of the LMAT for  $\text{Cr}(\text{CO})_5\{\text{C}(\text{OEt})(\text{H})\}$  for the  $[\text{M}]\cdots[\text{L}]$  interaction.

MO	MO Classifications									
	DI contribution	MO Energy (a.u.)	$a_{1g}$	$t_{1u}$	$t_{2g}$	$e_g$	NL	Ratio	Character 1	Character 2
<i>MO1</i>	0.000	-215.840	0.997	0.003				0.997	$a_{1g}$	
<i>MO2</i>	0.000	-24.820	0.971	0.029				0.970	$a_{1g}$	
<i>MO3</i>	0.000	-21.123		1.000				1.000	$t_{1u}$	
<i>MO4</i>	0.000	-21.120	0.019	0.981				0.981	$t_{1u}$	
<i>MO5</i>	0.000	-21.119	0.014	0.986				0.986	$t_{1u}$	
<i>MO6</i>	0.000	-19.293					1.000	1.000	NL	
<i>MO7</i>	0.000	-19.285					1.000	1.000	NL	
<i>MO8</i>	0.000	-19.285					1.000	1.000	NL	
<i>MO9</i>	0.000	-19.284					1.000	1.000	NL	
<i>MO10</i>	0.000	-19.282					1.000	1.000	NL	
<i>MO11</i>	0.000	-19.278					1.000	1.000	NL	
<i>MO12</i>	0.000	-10.376					1.000	1.000	NL	
<i>MO13</i>	0.000	-10.376					1.000	1.000	NL	
<i>MO14</i>	0.000	-10.370					1.000	1.000	NL	
<i>MO15</i>	0.000	-10.370					1.000	1.000	NL	



<i>MO16</i>	0.000	-10.369			1.000	1.000	NL		
<i>MO17</i>	0.000	-10.355			1.000	1.000	NL		
<i>MO18</i>	0.000	-10.340			1.000	1.000	NL		
<i>MO19</i>	0.000	-10.272			1.000	1.000	NL		
<i>MO20</i>	0.002	-2.945	0.998	0.002		0.998	$a_{1g}$		
<i>MO21</i>	0.002	-1.896		1.000		1.000	$t_{1u}$		
<i>MO22</i>	0.002	-1.890		1.000		1.000	$t_{1u}$		
<i>MO23</i>	0.014	-1.887	0.002	0.998		0.998	$t_{1u}$		
<i>MO24</i>	0.000	-1.200	0.002		0.998	0.998	NL		
<i>MO25</i>	0.000	-1.199		0.002	0.998	0.998	NL		
<i>MO26</i>	0.000	-1.197			0.999	0.999	NL		
<i>MO27</i>	0.001	-1.197		0.001	0.998	0.999	NL		
<i>MO28</i>	0.000	-1.192		0.001	0.999	0.999	NL		
<i>MO29</i>	0.003	-1.188		0.001	0.998	0.999	NL		
<i>MO30</i>	0.005	-0.878	0.003	0.003	0.001	0.992	0.997	NL	
<i>MO31</i>	0.020	-0.763	0.022	0.009	0.006	0.963	0.977	NL	
<i>MO32</i>	0.025	-0.696	0.045	0.011	0.004	0.940	0.952	NL	
<i>MO33</i>	0.018	-0.656	0.458	0.022	0.003	0.516	0.112	NL	$a_{1g}$
<i>MO34</i>	0.008	-0.623		0.132		0.868	0.848	NL	$t_{1u}$
<i>MO35</i>	0.008	-0.622		0.130	0.001	0.868	0.850	NL	$t_{1u}$
<i>MO36</i>	0.003	-0.618		0.004	0.078	0.917	0.914	NL	
<i>MO37</i>	0.002	-0.615		0.068	0.039	0.893	0.924	NL	
<i>MO38</i>	0.011	-0.606			0.004	0.995	0.996	NL	

<i>MO39</i>	0.057	-0.576	0.079	0.024	0.002	0.012	0.883	0.910	NL	
<i>MO40</i>	0.021	-0.557	0.258	0.011	0.003	0.001	0.727	0.645	NL	$a_{1g}$
<i>MO41</i>	0.021	-0.544	0.073	0.085	0.007	0.014	0.822	0.897	NL	$t_{1u}$
<i>MO42</i>	0.005	-0.538		0.002	0.045		0.953	0.953	NL	
<i>MO43</i>	0.004	-0.533		0.082	0.025		0.893	0.908	NL	
<i>MO44</i>	0.001	-0.533		0.110	0.018		0.872	0.873	NL	$t_{1u}$
<i>MO45</i>	0.022	-0.528	0.008	0.114	0.003	0.008	0.867	0.869	NL	$t_{1u}$
<i>MO46</i>	0.013	-0.524		0.032	0.010		0.958	0.967	NL	
<i>MO47</i>	0.014	-0.524	0.010	0.048	0.004	0.016	0.922	0.947	NL	
<i>MO48</i>	0.007	-0.517		0.001			0.998	0.999	NL	
<i>MO49</i>	0.003	-0.511		0.008			0.991	0.992	NL	
<i>MO50</i>	0.001	-0.510					1.000	1.000	NL	
<i>MO51</i>	0.006	-0.510		0.009		0.002	0.989	0.991	NL	
<i>MO52</i>	0.020	-0.493	0.003	0.004		0.777	0.216	0.722	$e_g$	NL
<i>MO53</i>	0.064	-0.485	0.005	0.021		0.479	0.495	0.032	NL	$e_g$
<i>MO54</i>	0.006	-0.478		0.044		0.046	0.909	0.950	NL	
<i>MO55</i>	0.010	-0.473		0.294		0.197	0.508	0.420	NL	$t_{1u}$
<i>MO56</i>	0.046	-0.466		0.538	0.002		0.459	0.148	$t_{1u}$	NL
<i>MO57</i>	0.032	-0.456		0.682		0.002	0.316	0.537	$t_{1u}$	NL
<i>MO58</i>	0.021	-0.440		0.087	0.003	0.006	0.904	0.904	NL	
<i>MO59</i>	0.018	-0.432		0.041	0.003	0.006	0.950	0.957	NL	
<i>MO60</i>	0.493	-0.359	0.031	0.378	0.002	0.298	0.291	0.213	$t_{1u}$	$e_g$
<i>MO61</i>	0.037	-0.277				0.954	0.046	0.952	$t_{2g}$	

<i>MO62</i>	0.464	-0.273		0.951	0.049	0.949	<i>t</i> <sub>2g</sub>
<i>MO63</i>	0.131	-0.267		0.960	0.039	0.959	<i>t</i> <sub>2g</sub>
Sum	1.641	-536.229					
Abs							
Sum	1.641	536.229					

**Table B 3. 7.** The MO DI valued weighted energetic contributions for Cr(CO)<sub>5</sub>{C(OEt)(H)} for the [M]··[L] interaction.

MO	<i>a</i> <sub>1g</sub>	<i>t</i> <sub>1u</sub>	<i>t</i> <sub>2g</sub>	<i>e</i> <sub>g</sub>	NL	Sum	Summary	Energy (a.u.)
<i>MO1</i>						0.000		
<i>MO2</i>						0.000	<i>a</i> <sub>1g</sub>	-0.023
<i>MO3</i>						0.000	<i>t</i> <sub>1u</sub>	-0.125
<i>MO4</i>						0.000	<i>t</i> <sub>2g</sub>	-0.164
<i>MO5</i>						0.000	<i>e</i> <sub>g</sub>	-0.075
<i>MO6</i>						0.000	NL	-0.257
<i>MO7</i>						0.000		
<i>MO8</i>						0.000	Total	-0.645
<i>MO9</i>						0.000		
<i>MO10</i>						0.000		
<i>MO11</i>						0.000		
<i>MO12</i>						0.000		

MO13			0.000
MO14			0.000
MO15			0.000
MO16			0.000
MO17			0.000
MO18			0.000
MO19			0.000
MO20	-0.007		-0.007
MO21		-0.004	-0.004
MO22		-0.004	-0.004
MO23		-0.027	-0.027
MO24			0.000
MO25			0.000
MO26			0.000
MO27			0.000
MO28			0.000
MO29		-0.003	-0.003
MO30		-0.005	-0.005
MO31		-0.014	-0.014
MO32		-0.016	-0.016
MO33	-0.005	-0.006	-0.011
MO34		-0.005	-0.005
MO35		-0.004	-0.004

<i>MO36</i>			-0.001	-0.001
<i>MO37</i>			-0.001	-0.001
<i>MO38</i>			-0.007	-0.007
<i>MO39</i>	-0.003		-0.029	-0.031
<i>MO40</i>	-0.003		-0.009	-0.012
<i>MO41</i>			-0.009	-0.009
<i>MO42</i>			-0.002	-0.002
<i>MO43</i>			-0.002	-0.002
<i>MO44</i>				0.000
<i>MO45</i>		-0.001	-0.010	-0.011
<i>MO46</i>			-0.006	-0.006
<i>MO47</i>			-0.007	-0.007
<i>MO48</i>			-0.004	-0.004
<i>MO49</i>			-0.002	-0.002
<i>MO50</i>				0.000
<i>MO51</i>			-0.003	-0.003
<i>MO52</i>			-0.008	-0.002
<i>MO53</i>			-0.015	-0.015
<i>MO54</i>			-0.003	-0.003
<i>MO55</i>		-0.001	-0.003	-0.004
<i>MO56</i>		-0.012	-0.010	-0.021
<i>MO57</i>		-0.010	-0.005	-0.014
<i>MO58</i>			-0.008	-0.008

<i>MO59</i>					-0.007	-0.007
<i>MO60</i>	-0.005	-0.067		-0.053	-0.052	-0.177
<i>MO61</i>			-0.010			-0.010
<i>MO62</i>			-0.120		-0.006	-0.126
<i>MO63</i>			-0.034		-0.001	-0.035
Sum	-0.023	-0.125	-0.164	-0.075	-0.257	-0.645

**Section 4: Symmetry decomposition with Inter-fragment delocalization of each R-group for all molecules.**

**Table B 4. 1.** Symmetry decomposition for R= -H from DI.

	MO DI Contributions							
	X=OEt				X=NMe <sub>2</sub>			
	[M]...C <sub>carbene</sub>	[M]...[X]	[M]...[R]	[M]...[L]	[M]...C <sub>carbene</sub>	[M]...[X]	[M]...[R]	[M]...[L]
a <sub>1g</sub>	0.0379	0.0001	0.0014	0.0395	0.0440	0.0030	0.0004	0.0474
t <sub>1u</sub>	0.2265	0.0257	0.0169	0.2691	0.2886	0.0359	0.0160	0.3405
t <sub>2g</sub>	0.4244	0.1561	0.0240	0.6045	0.2497	0.1404	0.0204	0.4105
e <sub>g</sub>	0.1673	0.0201	0.0104	0.1978	0.1475	0.0217	0.0077	0.1768
NL	0.4805	0.0420	0.0074	0.5299	0.3750	0.0856	0.0102	0.4708
<b>Total</b>	<b>1.3367</b>	<b>0.2440</b>	<b>0.0601</b>	<b>1.6408</b>	<b>1.1048</b>	<b>0.2866</b>	<b>0.0546</b>	<b>1.4460</b>
σ	0.4317	0.0459	0.0288	0.5064	0.4801	0.0606	0.0240	0.5647
π	0.4244	0.1561	0.0240	0.6045	0.2497	0.1404	0.0204	0.4105
NL	0.4805	0.0420	0.0074	0.5299	0.3750	0.0856	0.0102	0.4708

**Table B 4. 2.** Symmetry decomposition for R= -CHCH<sub>2</sub> from DI.

	MO DI Contributions							
	X=OEt				X=NMe <sub>2</sub>			
	[M]...C <sub>carbene</sub>	[M]...[X]	[M]...[R]	[M]...[L]	[M]...C <sub>carbene</sub>	[M]...[X]	[M]...[R]	[M]...[L]
a <sub>1g</sub>	0.0413	0.00498	0.00236	0.0486	0.0224	0.00368	0.00263	0.0287
t <sub>1u</sub>	0.1929	0.05314	0.02660	0.2726	0.1524	0.02900	0.02756	0.2090
t <sub>2g</sub>	0.3257	0.10738	0.09914	0.5322	0.2021	0.10608	0.05971	0.3679
e <sub>g</sub>	0.1365	0.02256	0.01469	0.1738	0.0686	0.01681	0.01209	0.0975
NL	0.4499	0.13099	0.07542	0.6563	0.4870	0.13934	0.11800	0.7444
<b>Total</b>	<b>1.1463</b>	<b>0.31904</b>	<b>0.21821</b>	<b>1.6835</b>	<b>0.9326</b>	<b>0.29490</b>	<b>0.21998</b>	<b>1.4475</b>
σ	0.3707	0.0807	0.0437	0.4950	0.2434	0.0495	0.0423	0.3352
π	0.3257	0.1074	0.0991	0.5322	0.2021	0.1061	0.0597	0.3679
NL	0.4499	0.1310	0.0754	0.6563	0.4870	0.1393	0.1180	0.7444

**Table B 4. 3.** Symmetry decomposition for R= -CHCHPh from DI.

MO DI Contributions								
	X=OEt				X=NMe <sub>2</sub>			
	[M]...C <sub>carbene</sub>	[M]...[X]	[M]...[R]	[M]...[L]	[M]...C <sub>carbene</sub>	[M]...[X]	[M]...[R]	[M]...[L]
a <sub>1g</sub>	0.0332	0.0037	0.0025	0.0394	0.0174	0.0026	0.0014	0.0214
t <sub>1u</sub>	0.1938	0.0527	0.0253	0.2718	0.1298	0.0263	0.0202	0.1764
t <sub>2g</sub>	0.2502	0.0722	0.1321	0.4546	0.1891	0.0928	0.0770	0.3589
e <sub>g</sub>	0.1369	0.0231	0.0131	0.1731	0.0614	0.0142	0.0074	0.0830
NL	0.4941	0.1567	0.0588	0.7096	0.5296	0.1578	0.1225	0.8100
<b>Total</b>	<b>1.1082</b>	<b>0.3085</b>	<b>0.2318</b>	<b>1.6484</b>	<b>0.9273</b>	<b>0.2938</b>	<b>0.2286</b>	<b>1.4497</b>
σ	0.3638	0.0796	0.0409	0.4843	0.2086	0.0432	0.0291	0.2808
π	0.2502	0.0722	0.1321	0.4546	0.1891	0.0928	0.0770	0.3589
NL	0.4941	0.1567	0.0588	0.7096	0.5296	0.1578	0.1225	0.8100

**Table B 4. 4.** Symmetry decomposition for R= -CCH from DI.

MO DI Contributions								
	X=OEt				X=NMe <sub>2</sub>			
	[M]...C <sub>carbene</sub>	[M]...[X]	[M]...[R]	[M]...[L]	[M]...C <sub>carbene</sub>	[M]...[X]	[M]...[R]	[M]...[L]
a <sub>1g</sub>	0.0306	0.0004	0.0028	0.0338	0.0202	0.0033	0.0028	0.0263
t <sub>1u</sub>	0.1514	0.0187	0.0219	0.1921	0.1802	0.0255	0.0252	0.2310
t <sub>2g</sub>	0.3657	0.1328	0.1327	0.6313	0.2190	0.1244	0.0765	0.4199
e <sub>g</sub>	0.1046	0.0125	0.0144	0.1315	0.0679	0.0154	0.0118	0.0950
NL	0.5536	0.0758	0.0722	0.7016	0.4554	0.1272	0.1164	0.6991
<b>Total</b>	<b>1.2059</b>	<b>0.2403</b>	<b>0.2441</b>	<b>1.6903</b>	<b>0.9427</b>	<b>0.2959</b>	<b>0.2328</b>	<b>1.4713</b>
σ	0.2866	0.0316	0.0392	0.3574	0.2683	0.0442	0.0398	0.3523
π	0.3657	0.1328	0.1327	0.6313	0.2190	0.1244	0.0765	0.4199
NL	0.5536	0.0758	0.0722	0.7016	0.4554	0.1272	0.1164	0.6991



**Section 5: Symmetry decomposition in terms of energy for each fragment.**

**Table B 5. 1.** Symmetry decomposition in terms of energy (a.u.).

	MO-DI weighted energetic contributions							
	X=OEt				X=NMe <sub>2</sub>			
	[M]...C <sub>carbene</sub>				[M]...C <sub>carbene</sub>			
	R=H	R=CHCH <sub>2</sub>	R=CHCHPh	R=CCH	R=H	R=CHCH <sub>2</sub>	R=CHCHPh	R=CCH
a <sub>1g</sub>	-0.0251	-0.0252	-0.0202	-0.0214	-0.0271	-0.0148	-0.0123	-0.0139
t <sub>1u</sub>	-0.1167	-0.0932	-0.0906	-0.0861	-0.1305	-0.0743	-0.0653	-0.0888
t <sub>2g</sub>	-0.1157	-0.0885	-0.0666	-0.0987	-0.0654	-0.0530	-0.0494	-0.0575
e <sub>g</sub>	-0.0666	-0.0503	-0.0497	-0.0426	-0.0547	-0.0254	-0.0230	-0.0260
NL	-0.2465	-0.2263	-0.2370	-0.2689	-0.1903	-0.2204	-0.2347	-0.2129
<b>Total</b>	<b>-0.5707</b>	<b>-0.4835</b>	<b>-0.4640</b>	<b>-0.5177</b>	<b>-0.4679</b>	<b>-0.3880</b>	<b>-0.3847</b>	<b>-0.3990</b>

**Table B 5. 2.** Symmetry decomposition in terms of energy (a.u.).

	MO-DI weighted energetic contributions							
	X=OEt				X=NMe <sub>2</sub>			
	[M]...[X]				[M]...[X]			
	R=H	R=CHCH <sub>2</sub>	R=CHCHPh	R=CCH	R=H	R=CHCH <sub>2</sub>	R=CHCHPh	R=CCH
a <sub>1g</sub>	0.0002	-0.0024	-0.0016	-0.0001	-0.0014	-0.0019	-0.0013	-0.0017
t <sub>1u</sub>	-0.0094	-0.0213	-0.0207	-0.0072	-0.0134	-0.0116	-0.0107	-0.0102
t <sub>2g</sub>	-0.0425	-0.0292	-0.0194	-0.0357	-0.0367	-0.0278	-0.0243	-0.0327
e <sub>g</sub>	-0.0075	-0.0077	-0.0078	-0.0049	-0.0082	-0.0069	-0.0058	-0.0064
NL	-0.0140	-0.0627	-0.0707	-0.0292	-0.0407	-0.0668	-0.0731	-0.0614
<b>Total</b>	<b>-0.0732</b>	<b>-0.1233</b>	<b>-0.1202</b>	<b>-0.0771</b>	<b>-0.1004</b>	<b>-0.1152</b>	<b>-0.1153</b>	<b>-0.1125</b>

**Table B 5. 3.** Symmetry decomposition in terms of energy (a.u.).

MO-DI weighted energetic contributions

	X=OEt				X=NMe <sub>2</sub>			
	[M]···[R]				[M]···[R]			
	R=H	R=CHCH <sub>2</sub>	R=CHCHPh	R=CCH	R=H	R=CHCH <sub>2</sub>	R=CHCHPh	R=CCH
a <sub>1g</sub>	-0.0006	-0.0011	-0.0011	-0.0013	0.0000	-0.0013	-0.0007	-0.0013
t <sub>1u</sub>	-0.0063	-0.0107	-0.0100	-0.0082	-0.0061	-0.0105	-0.0082	-0.0095
t <sub>2g</sub>	-0.0065	-0.0269	-0.0349	-0.0357	-0.0053	-0.0156	-0.0199	-0.0201
e <sub>g</sub>	-0.0036	-0.0056	-0.0047	-0.0053	-0.0028	-0.0044	-0.0029	-0.0044
NL	-0.0003	-0.0366	-0.0322	-0.0291	-0.0037	-0.0545	-0.0572	-0.0508
<b>Total</b>	<b>-0.0173</b>	<b>-0.0809</b>	<b>-0.0830</b>	<b>-0.0796</b>	<b>-0.0180</b>	<b>-0.0863</b>	<b>-0.0888</b>	<b>-0.0861</b>

**Table B 5. 4.** Symmetry decomposition in terms of energy (a.u.).

MO-DI weighted energetic contributions								
	X=OEt				X=NMe <sub>2</sub>			
	[M]···[L]				[M]···[L]			
	R=H	R=CHCH <sub>2</sub>	R=CHCHPh	R=CCH	R=H	R=CHCH <sub>2</sub>	R=CHCHPh	R=CCH
a <sub>1g</sub>	-0.0255	-0.0287	-0.0229	-0.0228	-0.0285	-0.0180	-0.0144	-0.0169
t <sub>1u</sub>	-0.1324	-0.1252	-0.1212	-0.1015	-0.1500	-0.0965	-0.0842	-0.1085
t <sub>2g</sub>	-0.1646	-0.1446	-0.1209	-0.1701	-0.1074	-0.0965	-0.0936	-0.1103
e <sub>g</sub>	-0.0777	-0.0636	-0.0623	-0.0527	-0.0657	-0.0367	-0.0316	-0.0368
NL	-0.2608	-0.3256	-0.3400	-0.3272	-0.2347	-0.3418	-0.3650	-0.3250
<b>Total</b>	<b>-0.6611</b>	<b>-0.6877</b>	<b>-0.6672</b>	<b>-0.6744</b>	<b>-0.5863</b>	<b>-0.5895</b>	<b>-0.5888</b>	<b>-0.5976</b>

The [M]···[L] does an excellent job at summarizing the interaction of the ligands with the metal, likewise, the energetics data is very complimentary and insightful, illustrated in **Table B 5. 4**. The energetics correlate rather well with the DI values (some discrepancies) where X=OEt relative to X=NMe<sub>2</sub> and a constant R-group is always lower in energy (stabilized). The energetic order for X=OEt is CHCH<sub>2</sub><CCH<CHCHPh<H (with CHCH<sub>2</sub> most stabilized) and a DI order of CCH <CHCH<sub>2</sub><CHCHPh<H the discrepancy coming from the NL term contribution. For X=NMe<sub>2</sub> this energetic order is CCH<CHCH<sub>2</sub><CHCHPh<H and the DI order is H<CHCH<sub>2</sub><CHCHPh<CCH,

there is a discrepancy in the R-groups, with the styryl and vinyl, they virtually comparable with energy values of -0.5888a.u. for the styryl and -0.5895a.u. for the vinyl. This difference comes in from the  $\sigma$ -orbitals being lower in energy for the vinyl group but the NL of the styryl closing the gap. Since X=NMe<sub>2</sub> is rich in  $\sigma$ -type interactions, adding a phenyl group to the vinyl will cause delocalization towards the metal. The phenyl mostly contributes conjugation in terms of  $\pi$ -character, therefore the distribution of electrons is more delocalized throughout and not as localized in the styryl compared to the vinyl which then affects the energetics. This effect causes the average energy in the styryl to be higher than vinyl, even if this effect is only marginal. However, it is to be noted that the DI relating to weighted energetics trend discrepancies is mainly as a result of the NL term affecting the weighed energetics.

### Section 6: Symmetry decomposition in terms of energy for each R-group.

**Table B 6. 1.** Symmetry decomposition for R= -H in terms of energy (a.u.).

MO-DI weighted energetic contributions								
	X=OEt				X=NMe <sub>2</sub>			
	[M]...C <sub>carbene</sub>	[M]...[X]	[M]...[R]	[M]...[L]	[M]...C <sub>carbene</sub>	[M]...[X]	[M]...[R]	[M]...[L]
a <sub>1g</sub>	-0.0251	0.0002	-0.0006	-0.0255	-0.0271	-0.0014	0.0000	-0.0285
t <sub>1u</sub>	-0.1167	-0.0094	-0.0063	-0.1324	-0.1305	-0.0134	-0.0061	-0.1500
t <sub>2g</sub>	-0.1157	-0.0425	-0.0065	-0.1646	-0.0654	-0.0367	-0.0053	-0.1074
e <sub>g</sub>	-0.0666	-0.0075	-0.0036	-0.0777	-0.0547	-0.0082	-0.0028	-0.0657
NL	-0.2465	-0.0140	-0.0003	-0.2608	-0.1903	-0.0407	-0.0037	-0.2347
<b>Total</b>	<b>-0.5707</b>	<b>-0.0732</b>	<b>-0.0173</b>	<b>-0.6611</b>	<b>-0.4679</b>	<b>-0.1004</b>	<b>-0.0180</b>	<b>-0.5863</b>

**Table B 6. 2.** Symmetry decomposition for R= -CHCH<sub>2</sub> in terms of energy (a.u.).

MO-DI weighted energetic contributions								
	X=OEt				X=NMe <sub>2</sub>			
	[M]...C <sub>carbene</sub>	[M]...[X]	[M]...[R]	[M]...[L]	[M]...C <sub>carbene</sub>	[M]...[X]	[M]...[R]	[M]...[L]

$a_{1g}$	-0.0252	-0.0024	-0.0011	-0.0287	-0.0148	-0.0019	-0.0013	-0.0180
$t_{1u}$	-0.0932	-0.0213	-0.0107	-0.1252	-0.0743	-0.0116	-0.0105	-0.0965
$t_{2g}$	-0.0885	-0.0292	-0.0269	-0.1446	-0.0530	-0.0278	-0.0156	-0.0965
$e_g$	-0.0503	-0.0077	-0.0056	-0.0636	-0.0254	-0.0069	-0.0044	-0.0367
NL	-0.2263	-0.0627	-0.0366	-0.3256	-0.2204	-0.0668	-0.0545	-0.3418
<b>Total</b>	<b>-0.4835</b>	<b>-0.1233</b>	<b>-0.0809</b>	<b>-0.6877</b>	<b>-0.3880</b>	<b>-0.1152</b>	<b>-0.0863</b>	<b>-0.5895</b>

**Table B 6. 3.** Symmetry decomposition for R= -CHCHPh in terms of energy (a.u.).

	MO-DI weighted energetic contributions							
	X=OEt				X=NMe <sub>2</sub>			
	[M]...C <sub>carbene</sub>	[M]...[X]	[M]...[R]	[M]...[L]	[M]...C <sub>carbene</sub>	[M]...[X]	[M]...[R]	[M]...[L]
$a_{1g}$	-0.0202	-0.0016	-0.0011	-0.0229	-0.0123	-0.0013	-0.0007	-0.0144
$t_{1u}$	-0.0906	-0.0207	-0.0100	-0.1212	-0.0653	-0.0107	-0.0082	-0.0842
$t_{2g}$	-0.0666	-0.0194	-0.0349	-0.1209	-0.0494	-0.0243	-0.0199	-0.0936
$e_g$	-0.0497	-0.0078	-0.0047	-0.0623	-0.0230	-0.0058	-0.0029	-0.0316
NL	-0.2370	-0.0707	-0.0322	-0.3400	-0.2347	-0.0731	-0.0572	-0.3650
<b>Total</b>	<b>-0.4640</b>	<b>-0.1202</b>	<b>-0.0830</b>	<b>-0.6672</b>	<b>-0.3847</b>	<b>-0.1153</b>	<b>-0.0888</b>	<b>-0.5888</b>

**Table B 6. 4.** Symmetry decomposition for R= -CCH in terms of energy (a.u.).

	MO-DI weighted energetic contributions							
	X=OEt				X=NMe <sub>2</sub>			
	[M]...C <sub>carbene</sub>	[M]...[X]	[M]...[R]	[M]...[L]	[M]...C <sub>carbene</sub>	[M]...[X]	[M]...[R]	[M]...[L]
$a_{1g}$	-0.0214	-0.0001	-0.0013	-0.0228	-0.0139	-0.0017	-0.0013	-0.0169
$t_{1u}$	-0.0861	-0.0072	-0.0082	-0.1015	-0.0888	-0.0102	-0.0095	-0.1085
$t_{2g}$	-0.0987	-0.0357	-0.0357	-0.1701	-0.0575	-0.0327	-0.0201	-0.1103
$e_g$	-0.0426	-0.0049	-0.0053	-0.0527	-0.0260	-0.0064	-0.0044	-0.0368
NL	-0.2689	-0.0292	-0.0291	-0.3272	-0.2129	-0.0614	-0.0508	-0.3250
<b>Total</b>	<b>-0.5177</b>	<b>-0.0771</b>	<b>-0.0796</b>	<b>-0.6744</b>	<b>-0.3990</b>	<b>-0.1125</b>	<b>-0.0861</b>	<b>-0.5976</b>

**Section 7: MOs contributing majority of the DI in specific interactions for the [M]···[L] interaction.**

**Table B 7. 1.** Significant MOs in the [M]···[L] interaction for Cr(CO)<sub>5</sub>{C(OEt)(H)}.

	DI Contribution	Ratio	Character 1	Character 2	%	Running
<i>MO60</i>	0.49	0.212568	t <sub>1u</sub>	e <sub>g</sub>	30.04	30.04
<i>MO62</i>	0.46	0.948687	t <sub>2g</sub>		28.27	58.31
<i>MO63</i>	0.13	0.959000	t <sub>2g</sub>		7.98	66.30
<i>MO53</i>	0.06	0.031975	NL	e <sub>g</sub>	3.91	70.21
<i>MO39</i>	0.06	0.910342	NL		3.46	73.66
<i>MO56</i>	0.05	0.147638	t <sub>1u</sub>	NL	2.82	76.48
<i>MO61</i>	0.04	0.952197	t <sub>2g</sub>		2.25	78.73
<i>MO57</i>	0.03	0.536999	t <sub>1u</sub>	NL	1.94	80.67
<i>MO32</i>	0.03	0.952312	NL		1.53	82.21
<i>MO45</i>	0.02	0.868565	NL	t <sub>1u</sub>	1.32	83.53

**Table B 7. 2.** Significant MOs in the [M]···[L] interaction of Cr(CO)<sub>5</sub>{C(OEt)(CHCH<sub>2</sub>)}.

	DI Contribution	Ratio	Character 1	Character 2	%	Running
<i>MO67</i>	0.51	0.230677	t <sub>1u</sub>	e <sub>g</sub>	30.28	30.28
<i>MO69</i>	0.41	0.945383	t <sub>2g</sub>		24.43	54.71
<i>MO70</i>	0.12	0.960760	t <sub>2g</sub>		7.33	62.04
<i>MO44</i>	0.05	0.625302	NL	a <sub>1g</sub>	3.00	65.04
<i>MO35</i>	0.04	0.901014	NL		2.55	67.59
<i>MO63</i>	0.04	0.878838	NL	t <sub>1u</sub>	2.30	69.90
<i>MO61</i>	0.04	0.337538	t <sub>1u</sub>	NL	2.25	72.15
<i>MO49</i>	0.03	0.912481	NL		1.84	73.99
<i>MO51</i>	0.03	0.883683	NL	e <sub>g</sub>	1.80	75.79
<i>MO62</i>	0.03	0.380420	t <sub>1u</sub>	NL	1.72	77.51

**Table B 7. 3.** Significant MOs in the [M]···[L] interaction of Cr(CO)<sub>5</sub>{C(OEt)(CHCHPh)}.

	DI Contribution	Ratio	Character 1	Character 2	%	Running
<i>MO85</i>	0.51	0.257377	t <sub>1u</sub>	e <sub>g</sub>	31.20	31.20
<i>MO90</i>	0.36	0.864974	t <sub>2g</sub>	NL	21.55	52.75
<i>MO89</i>	0.12	0.959893	t <sub>2g</sub>		7.31	60.06
<i>MO87</i>	0.04	0.920062	NL		2.50	62.56
<i>MO56</i>	0.04	0.708396	NL	a <sub>1g</sub>	2.41	64.98
<i>MO77</i>	0.04	0.299520	t <sub>1u</sub>	NL	2.22	67.19
<i>MO66</i>	0.03	0.895519	NL	e <sub>g</sub>	1.97	69.17
<i>MO80</i>	0.03	0.864690	NL	t <sub>1u</sub>	1.80	70.96
<i>MO46</i>	0.03	0.836390	NL	a <sub>1g</sub>	1.75	72.71
<i>MO78</i>	0.03	0.290305	t <sub>1u</sub>	NL	1.60	74.32

**Table B 7. 4.** Significant MOs in the [M]···[L] interaction of Cr(CO)<sub>5</sub>{C(OEt)(CCH)}.

	DI Contribution	Ratio	Character 1	Character 2	%	Running
<i>MO68</i>	0.50	0.946044	t <sub>2g</sub>		29.38	29.38
<i>MO66</i>	0.36	0.427218	NL	t <sub>1u</sub>	21.12	50.50
<i>MO69</i>	0.14	0.956923	t <sub>2g</sub>		8.53	59.03
<i>MO64</i>	0.14	0.828001	NL	t <sub>1u</sub>	8.49	67.52
<i>MO43</i>	0.06	0.952202	NL		3.26	70.78
<i>MO63</i>	0.04	0.952202	NL		2.57	73.34
<i>MO57</i>	0.04	0.025617	NL	e <sub>g</sub>	2.53	75.87
<i>MO60</i>	0.04	0.235186	NL	t <sub>1u</sub>	2.17	78.04
<i>MO61</i>	0.03	0.484534	t <sub>1u</sub>	NL	1.80	79.84
<i>MO56</i>	0.02	0.390055	e <sub>g</sub>	NL	1.47	81.31

**Table B 7. 5.** Significant MOs in the [M]···[L] interaction of Cr(CO)<sub>5</sub>{C(NMe<sub>2</sub>)(H)}.

	DI Contribution	Ratio	Character 1	Character 2	%	Running
<i>MO60</i>	0.5390	0.409167	t <sub>1u</sub>	e <sub>g</sub>	37.28	37.28
<i>MO62</i>	0.2994	0.936890	t <sub>2g</sub>		20.70	57.98
<i>MO63</i>	0.1120	0.958012	t <sub>2g</sub>		7.75	65.73

<i>MO40</i>	0.0642	0.697952	NL	$a_{1g}$	4.44	70.17
<i>MO32</i>	0.0440	0.741716	NL	$a_{1g}$	3.04	73.21
<i>MO57</i>	0.0430	0.460378	$t_{1u}$	NL	2.98	76.19
<i>MO58</i>	0.0325	0.505165	$t_{1u}$	NL	2.25	78.44
<i>MO55</i>	0.0256	0.993317	NL		1.77	80.21
<i>MO45</i>	0.0217	0.926113	NL		1.50	81.71
<i>MO46</i>	0.0204	0.914588	NL		1.41	83.12

**Table B 7. 6.** Significant MOs in the [M]...[L] interaction of  $Cr(CO)_5\{C(NMe_2)(CHCH_2)\}$ .

	DI Contribution	Ratio	Character 1	Character 2	%	Running
<i>MO67</i>	0.30	0.502136	NL	$t_{1u}$	20.75	20.75
<i>MO66</i>	0.25	0.633664	NL	$t_{1u}$	17.15	37.90
<i>MO69</i>	0.23	0.945738	$t_{2g}$		15.56	53.46
<i>MO70</i>	0.13	0.946106	$t_{2g}$		9.16	62.62
<i>MO44</i>	0.04	0.832609	NL	$a_{1g}$	2.85	65.47
<i>MO63</i>	0.03	0.434546	$t_{1u}$	NL	2.38	67.85
<i>MO62</i>	0.03	0.166282	$t_{1u}$	NL	2.27	70.11
<i>MO64</i>	0.03	0.800626	NL	$t_{1u}$	2.10	72.22
<i>MO35</i>	0.03	0.947741	NL		1.82	74.04
<i>MO60</i>	0.02	0.963434	NL		1.67	75.71

**Table B 7. 7.** Significant MOs in the [M]...[L] interaction of  $Cr(CO)_5\{C(NMe_2)(CHCHPh)\}$ .

	DI Contribution	Ratio	Character 1	Character 2	%	Running
<i>MO85</i>	0.31	0.423742	NL	$t_{1u}$	21.22	21.22
<i>MO89</i>	0.21	0.947507	$t_{2g}$		14.39	35.62
<i>MO90</i>	0.14	0.863675	$t_{2g}$	NL	9.86	45.48
<i>MO84</i>	0.12	0.863473	NL	$t_{1u}$	8.20	53.68
<i>MO87</i>	0.11	0.866602	NL	$t_{2g}$	7.80	61.48
<i>MO56</i>	0.04	0.902338	NL		2.51	63.99
<i>MO83</i>	0.03	0.976444	NL		2.25	66.24
<i>MO80</i>	0.03	0.344134	$t_{1u}$	NL	2.24	68.48

<i>MO77</i>	0.02	0.383850	NL	$t_{1u}$	1.71	70.20
<i>MO88</i>	0.02	0.940472	$t_{2g}$		1.69	71.88

**Table B 7. 8.** Significant MOs in the  $[M]\cdots[L]$  interaction of  $Cr(CO)_5\{C(NMe_2)(CCH)\}$ .

	DI Contribution	Ratio	Character 1	Character 2	%	Running
<i>MO66</i>	0.31	0.405610	NL	$t_{1u}$	21.15	21.15
<i>MO68</i>	0.29	0.945193	$t_{2g}$		19.77	40.92
<i>MO64</i>	0.24	0.567818	NL	$t_{1u}$	16.63	57.55
<i>MO69</i>	0.12	0.951625	$t_{2g}$		8.20	65.75
<i>MO44</i>	0.05	0.926552	NL		3.32	69.08
<i>MO61</i>	0.04	0.248862	$t_{1u}$	NL	2.51	71.59
<i>MO62</i>	0.03	0.445926	$t_{1u}$	NL	2.29	73.88
<i>MO59</i>	0.02	0.954989	NL		1.69	75.57
<i>MO67</i>	0.02	0.951520	$t_{2g}$		1.67	77.23
<i>MO35</i>	0.02	0.950815	NL		1.67	78.90

**Section 8: MOs contributing majority of the DI in specific interactions for the  $[M]\cdots C_{\text{carbene}}$  bond.**

**Table B 8. 1.** Significant MOs in the  $[M]\cdots C_{\text{carbene}}$  bond of  $Cr(CO)_5\{C(OEt)(H)\}$ .

	DI Contribution	Ratio	Character 1	Character 2	%	Running
<i>MO60</i>	0.40	0.212568	$t_{1u}$	$e_g$	29.61	29.61
<i>MO62</i>	0.32	0.948687	$t_{2g}$		24.00	53.61
<i>MO63</i>	0.09	0.959000	$t_{2g}$		6.81	60.42
<i>MO39</i>	0.06	0.910342	NL		4.62	65.04
<i>MO53</i>	0.06	0.031975	NL	$e_g$	4.50	69.54
<i>MO56</i>	0.05	0.147638	$t_{1u}$	NL	4.02	73.56
<i>MO41</i>	0.03	0.896856	NL	$t_{1u}$	2.45	76.01
<i>MO61</i>	0.03	0.952197	$t_{2g}$		2.36	78.37



<i>MO32</i>	0.03	0.952312	NL		2.07	80.44
<i>MO31</i>	0.03	0.977458	NL		2.04	82.47

**Table B 8. 2.** Significant MOs in the  $[M]\cdots C_{\text{carbene}}$  bond of  $\text{Cr}(\text{CO})_5\{\text{C}(\text{OEt})(\text{CHCH}_2)\}$ .

	DI Contribution	Ratio	Character 1	Character 2	%	Running
<i>MO67</i>	0.39	0.230677	$t_{1u}$	$e_g$	34.14	34.14
<i>MO69</i>	0.25	0.945383	$t_{2g}$		21.49	55.62
<i>MO70</i>	0.08	0.960760	$t_{2g}$		7.08	62.71
<i>MO44</i>	0.05	0.625302	NL	$a_{1g}$	4.52	67.23
<i>MO35</i>	0.03	0.901014	NL		3.03	70.26
<i>MO58</i>	0.03	0.940850	NL		2.35	72.61
<i>MO45</i>	0.03	0.831485	NL	$t_{1u}$	2.23	74.84
<i>MO51</i>	0.02	0.883683	NL	$e_g$	2.06	76.89
<i>MO63</i>	0.02	0.878838	NL	$t_{1u}$	1.93	78.82
<i>MO50</i>	0.02	0.925050	NL		1.61	80.43

**Table B 8. 3.** Significant MOs in the  $[M]\cdots C_{\text{carbene}}$  bond of  $\text{Cr}(\text{CO})_5\{\text{C}(\text{OEt})(\text{CHCHPh})\}$ .

	DI Contribution	Ratio	Character 1	Character 2	%	Running
<i>MO85</i>	0.40	0.257377	$t_{1u}$	$e_g$	35.70	35.70
<i>MO90</i>	0.18	0.864974	$t_{2g}$	NL	16.12	51.83
<i>MO89</i>	0.08	0.959893	$t_{2g}$		7.14	58.96
<i>MO87</i>	0.05	0.920062	NL		4.34	63.30
<i>MO56</i>	0.04	0.708396	NL	$a_{1g}$	3.63	66.93
<i>MO66</i>	0.04	0.895519	NL	$e_g$	3.40	70.33
<i>MO46</i>	0.03	0.836390	NL	$a_{1g}$	2.51	72.84
<i>MO73</i>	0.02	0.935671	NL		2.18	75.02
<i>MO80</i>	0.02	0.864690	NL	$t_{1u}$	1.71	76.74
<i>MO88</i>	0.01	0.951938	$t_{2g}$		1.20	77.94

**Table B 8. 4.** Significant MOs in the  $[M]\cdots C_{\text{carbene}}$  bond of  $\text{Cr}(\text{CO})_5\{\text{C}(\text{OEt})(\text{CCH})\}$ .

	DI Contribution	Ratio	Character 1	Character 2	%	Running
<i>MO68</i>	0.28	0.946044	t <sub>2g</sub>		23.26	23.26
<i>MO66</i>	0.26	0.427218	NL	t <sub>1u</sub>	21.79	45.05
<i>MO64</i>	0.10	0.828001	NL	t <sub>1u</sub>	8.51	53.56
<i>MO69</i>	0.09	0.956923	t <sub>2g</sub>		7.13	60.69
<i>MO43</i>	0.05	0.952202	NL		4.46	65.16
<i>MO60</i>	0.05	0.235186	NL	t <sub>1u</sub>	3.88	69.04
<i>MO45</i>	0.04	0.937024	NL		2.98	72.02
<i>MO57</i>	0.04	0.025617	NL	e <sub>g</sub>	2.90	74.92
<i>MO63</i>	0.03	0.952202	NL		2.82	77.74
<i>MO58</i>	0.02	0.364386	NL	e <sub>g</sub>	1.96	79.70

**Table B 8. 5.** Significant MOs in the [M]...C<sub>carbene</sub> bond of Cr(CO)<sub>5</sub>{C(NMe<sub>2</sub>)(H)}.

	DI Contribution	Ratio	Character 1	Character 2	%	Running
<i>MO60</i>	0.45	0.409167	t <sub>1u</sub>	e <sub>g</sub>	40.79	40.79
<i>MO62</i>	0.17	0.936890	t <sub>2g</sub>		15.57	56.37
<i>MO63</i>	0.08	0.958012	t <sub>2g</sub>		6.82	63.19
<i>MO40</i>	0.07	0.697952	NL	a <sub>1g</sub>	6.08	69.27
<i>MO57</i>	0.05	0.460378	t <sub>1u</sub>	NL	4.52	73.78
<i>MO32</i>	0.04	0.741716	NL	a <sub>1g</sub>	3.78	77.57
<i>MO59</i>	0.03	0.976703	NL		2.77	80.34
<i>MO46</i>	0.02	0.914588	NL		1.76	82.10
<i>MO41</i>	0.02	0.732798	NL	a <sub>1g</sub>	1.46	83.56
<i>MO58</i>	0.02	0.505165	t <sub>1u</sub>	NL	1.42	84.98

**Table B 8. 6.** Significant MOs in the [M]...C<sub>carbene</sub> bond of Cr(CO)<sub>5</sub>{C(NMe<sub>2</sub>)(CHCH<sub>2</sub>)}.

	DI Contribution	Ratio	Character 1	Character 2	%	Running
<i>MO67</i>	0.22	0.502136	NL	t <sub>1u</sub>	23.41	23.41
<i>MO66</i>	0.20	0.633664	NL	t <sub>1u</sub>	20.96	44.37
<i>MO69</i>	0.13	0.945738	t <sub>2g</sub>		13.77	58.13
<i>MO70</i>	0.07	0.946106	t <sub>2g</sub>		7.41	65.55

<i>MO44</i>	0.04	0.832609	NL	$a_{1g}$	4.48	70.02
<i>MO62</i>	0.03	0.166282	$t_{1u}$	NL	3.57	73.60
<i>MO65</i>	0.03	0.984653	NL		2.70	76.29
<i>MO35</i>	0.02	0.947741	NL		2.31	78.61
<i>MO64</i>	0.02	0.800626	NL	$t_{1u}$	1.74	80.35
<i>MO43</i>	0.01	0.990413	NL		1.52	81.87

**Table B 8. 7.** Significant MOs in the  $[M] \cdots C_{\text{carbene}}$  bond of  $\text{Cr}(\text{CO})_5\{\text{C}(\text{NMe}_2)(\text{CHCHPh})\}$ .

	DI Contribution	Ratio	Character 1	Character 2	%	Running
<i>MO85</i>	0.25	0.423742	NL	$t_{1u}$	26.84	26.84
<i>MO89</i>	0.12	0.947507	$t_{2g}$		12.87	39.70
<i>MO84</i>	0.10	0.863473	NL	$t_{1u}$	10.71	50.42
<i>MO87</i>	0.08	0.866602	NL	$t_{2g}$	8.46	58.88
<i>MO90</i>	0.06	0.863675	$t_{2g}$	NL	6.90	65.78
<i>MO56</i>	0.04	0.902338	NL		4.09	69.87
<i>MO77</i>	0.03	0.383850	NL	$t_{1u}$	2.79	72.66
<i>MO83</i>	0.03	0.976444	NL		2.73	75.39
<i>MO46</i>	0.02	0.765965	NL	$a_{1g}$	1.99	77.39
<i>MO55</i>	0.01	0.991210	NL		1.45	78.83

**Table B 8. 8.** Significant MOs in the  $[M] \cdots C_{\text{carbene}}$  bond of  $\text{Cr}(\text{CO})_5\{\text{C}(\text{NMe}_2)(\text{CCH})\}$ .

	DI Contribution	Ratio	Character 1	Character 2	%	Running
<i>MO66</i>	0.23	0.405610	NL	$t_{1u}$	24.49	24.49
<i>MO64</i>	0.19	0.567818	NL	$t_{1u}$	20.61	45.10
<i>MO68</i>	0.15	0.945193	$t_{2g}$		15.65	60.76
<i>MO69</i>	0.07	0.951625	$t_{2g}$		7.18	67.93
<i>MO44</i>	0.05	0.926552	NL		5.43	73.36
<i>MO61</i>	0.05	0.248862	$t_{1u}$	NL	5.26	78.62
<i>MO35</i>	0.02	0.950815	NL		2.25	80.87
<i>MO50</i>	0.02	0.918964	NL		1.67	82.55
<i>MO62</i>	0.01	0.445926	$t_{1u}$	NL	1.43	83.98

<i>MO60</i>	0.01	0.573473	$e_g$	NL	1.29	85.27
-------------	------	----------	-------	----	------	-------

---

**Section 9: MOs contributing majority of the DI in specific interactions for the [M]...[X] interaction.**

**Table B 9. 1.** Significant MOs in the [M]... [X] interaction of  $\text{Cr}(\text{CO})_5\{\text{C}(\text{OEt})(\text{H})\}$ .

	DI Contribution	Ratio	Character 1	Character 2	%	Running
<i>MO62</i>	0.14	0.948687	$t_{2g}$		41.37	41.37
<i>MO60</i>	0.06	0.212568	$t_{1u}$	$e_g$	17.70	59.08
<i>MO63</i>	0.02	0.959000	$t_{2g}$		6.74	65.82
<i>MO58</i>	0.01	0.904065	NL		3.94	69.76
<i>MO57</i>	0.01	0.536999	$t_{1u}$	NL	3.37	73.13
<i>MO47</i>	0.01	0.947394	NL		2.45	75.58
<i>MO53</i>	0.01	0.031975	NL	$e_g$	2.00	77.57
<i>MO59</i>	0.01	0.957016	NL		1.93	79.50
<i>MO46</i>	0.01	0.967047	NL		1.59	81.09
<i>MO61</i>	0.00	0.952197	$t_{2g}$		1.34	82.43

---

**Table B 9. 2.** Significant MOs in the [M]...[X] interaction of  $\text{Cr}(\text{CO})_5\{\text{C}(\text{OEt})(\text{CHCH}_2)\}$ .

	DI Contribution	Ratio	Character 1	Character 2	%	Running
<i>MO69</i>	0.08	0.945383	$t_{2g}$		22.93	22.93
<i>MO67</i>	0.08	0.230677	$t_{1u}$	$e_g$	21.91	44.84
<i>MO70</i>	0.02	0.960760	$t_{2g}$		6.83	51.68
<i>MO61</i>	0.02	0.337538	$t_{1u}$	NL	6.15	57.83
<i>MO49</i>	0.02	0.912481	NL		5.95	63.78
<i>MO66</i>	0.01	0.995171	NL		3.57	67.35
<i>MO65</i>	0.01	0.990401	NL		3.51	70.86
<i>MO63</i>	0.01	0.878838	NL	$t_{1u}$	2.70	73.57
<i>MO52</i>	0.01	0.999765	NL		2.46	76.03
<i>MO62</i>	0.01	0.380420	$t_{1u}$	NL	2.33	78.35

---

**Table B 9. 3.** Significant MOs in the [M]...[X] interaction of Cr(CO)<sub>5</sub>{C(OEt)(CHCHPh)}.

	DI Contribution	Ratio	Character 1	Character 2	%	Running
<i>MO85</i>	0.08	0.257377	t <sub>1u</sub>	e <sub>g</sub>	22.59	22.59
<i>MO90</i>	0.05	0.864974	t <sub>2g</sub>	NL	13.42	36.01
<i>MO87</i>	0.03	0.920062	NL		9.55	45.56
<i>MO89</i>	0.02	0.959893	t <sub>2g</sub>		6.84	52.40
<i>MO77</i>	0.02	0.299520	t <sub>1u</sub>	NL	5.87	58.27
<i>MO82</i>	0.01	0.991119	NL		3.51	61.78
<i>MO62</i>	0.01	0.936520	NL		3.19	64.96
<i>MO78</i>	0.01	0.290305	t <sub>1u</sub>	NL	2.65	67.61
<i>MO65</i>	0.01	0.999181	NL		2.51	70.13
<i>MO63</i>	0.01	0.931517	NL		2.38	72.50

**Table B 9. 4.** Significant MOs in the [M]...[X] interaction of Cr(CO)<sub>5</sub>{C(OEt)(CCH)}.

	DI Contribution	Ratio	Character 1	Character 2	%	Running
<i>MO68</i>	0.12	0.946044	t <sub>2g</sub>		36.38	36.38
<i>MO66</i>	0.04	0.427218	NL	t <sub>1u</sub>	11.41	47.80
<i>MO64</i>	0.02	0.828001	NL	t <sub>1u</sub>	7.20	55.00
<i>MO69</i>	0.02	0.956923	t <sub>2g</sub>		6.14	61.14
<i>MO62</i>	0.01	0.802545	NL	t <sub>1u</sub>	3.58	64.72
<i>MO61</i>	0.01	0.484534	t <sub>1u</sub>	NL	2.73	67.45
<i>MO51</i>	0.01	0.921984	NL		2.71	70.16
<i>MO63</i>	0.01	0.952202	NL		2.55	72.72
<i>MO57</i>	0.01	0.025617	NL	e <sub>g</sub>	2.40	75.11
<i>MO65</i>	0.01	0.997843	NL		2.37	77.48

**Table B 9. 5.** Significant MOs in the [M]...[X] interaction of Cr(CO)<sub>5</sub>{C(NMe<sub>2</sub>)(H)}.

	DI Contribution	Ratio	Character 1	Character 2	%	Running
<i>MO62</i>	0.12	0.93689	t <sub>2g</sub>		35.40	35.40
<i>MO60</i>	0.06	0.40917	t <sub>1u</sub>	e <sub>g</sub>	18.16	53.56
<i>MO55</i>	0.03	0.99332	NL		7.49	61.05

<i>MO63</i>	0.02	0.95801	$t_{2g}$		5.85	66.90
<i>MO45</i>	0.01	0.92611	NL		3.99	70.89
<i>MO58</i>	0.01	0.50516	$t_{1u}$	NL	3.52	74.41
<i>MO52</i>	0.01	0.96673	NL		2.47	76.88
<i>MO42</i>	0.01	0.95463	NL		1.89	78.77
<i>MO47</i>	0.00	0.97549	NL		1.43	80.20
<i>MO61</i>	0.00	0.95171	$t_{2g}$		1.38	81.58

**Table B 9. 6.** Significant MOs in the [M]...[X] interaction of  $\text{Cr}(\text{CO})_5\{\text{C}(\text{NMe}_2)(\text{CHCH}_2)\}$ .

	DI Contribution	Ratio	Character 1	Character 2	%	Running
<i>MO69</i>	0.08	0.945738	$t_{2g}$		25.31	25.31
<i>MO67</i>	0.03	0.502136	NL	$t_{1u}$	10.72	36.03
<i>MO66</i>	0.03	0.633664	NL	$t_{1u}$	8.81	44.84
<i>MO60</i>	0.02	0.963434	NL		6.79	51.63
<i>MO70</i>	0.02	0.946106	$t_{2g}$		6.67	58.30
<i>MO50</i>	0.02	0.922588	NL		4.70	63.00
<i>MO63</i>	0.01	0.434546	$t_{1u}$	NL	4.11	67.11
<i>MO68</i>	0.01	0.950709	$t_{2g}$		2.17	69.28
<i>MO58</i>	0.01	0.900126	NL		2.06	71.35
<i>MO57</i>	0.01	0.985433	NL		2.03	73.38

**Table B 9. 7.** Significant MOs in the [M]...[X] interaction of  $\text{Cr}(\text{CO})_5\{\text{C}(\text{NMe}_2)(\text{CHCHPh})\}$ .

	DI Contribution	Ratio	Character 1	Character 2	%	Running
<i>MO89</i>	0.07	0.947507	$t_{2g}$		22.85	22.85
<i>MO85</i>	0.03	0.423742	NL	$t_{1u}$	10.95	33.80
<i>MO87</i>	0.03	0.866602	NL	$t_{2g}$	8.61	42.40
<i>MO75</i>	0.02	0.959903	NL		6.91	49.31
<i>MO90</i>	0.02	0.863675	$t_{2g}$	NL	5.30	54.61
<i>MO80</i>	0.01	0.344134	$t_{1u}$	NL	4.23	58.84
<i>MO63</i>	0.01	0.899364	NL	$t_{1u}$	4.06	62.90
<i>MO88</i>	0.01	0.940472	$t_{2g}$		2.60	65.50

<i>MO59</i>	0.01	0.978955	NL		2.58	68.08
<i>MO84</i>	0.01	0.863473	NL	$t_{1u}$	2.43	70.51

**Table B 9. 8.** Significant MOs in the [M]···[X] interaction of  $\text{Cr}(\text{CO})_5\{\text{C}(\text{NMe}_2)(\text{CCH})\}$ .

	DI Contribution	Ratio	Character 1	Character 2	%	Running
<i>MO68</i>	0.11	0.945193	$t_{2g}$		30.33	30.33
<i>MO66</i>	0.03	0.405610	NL	$t_{1u}$	9.42	39.75
<i>MO64</i>	0.03	0.567818	NL	$t_{1u}$	7.94	47.70
<i>MO59</i>	0.02	0.954989	NL		6.50	54.20
<i>MO69</i>	0.02	0.951625	$t_{2g}$		4.70	58.91
<i>MO62</i>	0.01	0.445926	$t_{1u}$	NL	4.30	63.20
<i>MO49</i>	0.01	0.928032	NL		4.14	67.34
<i>MO46</i>	0.01	0.957265	NL		3.79	71.13
<i>MO56</i>	0.01	0.994540	NL		2.43	73.57
<i>MO67</i>	0.01	0.951520	$t_{2g}$		2.42	75.99

**Section 10: MOs contributing majority of the DI in specific interactions for the [M]···[R] interaction.**

**Table B 10. 1.** Significant MOs in the [M]···[R] interaction of  $\text{Cr}(\text{CO})_5\{\text{C}(\text{OEt})(\text{H})\}$ .

	DI Contribution	Ratio	Character 1	Character 2	%	Running
<i>MO60</i>	0.04	0.212568	t <sub>1u</sub>	e <sub>g</sub>	40.26	40.26
<i>MO63</i>	0.02	0.959000	t <sub>2g</sub>		18.52	58.78
<i>MO62</i>	0.01	0.948687	t <sub>2g</sub>		6.55	65.32
<i>MO57</i>	0.00	0.536999	t <sub>1u</sub>	NL	4.21	69.53
<i>MO46</i>	0.00	0.967047	NL		2.24	71.77
<i>MO48</i>	0.00	0.998774	NL		1.50	73.27
<i>MO40</i>	0.00	0.645490	NL	a <sub>1g</sub>	1.31	74.58
<i>MO61</i>	0.00	0.952197	t <sub>2g</sub>		1.10	75.68
<i>MO33</i>	0.00	0.111642	NL	a <sub>1g</sub>	0.97	76.65
<i>MO51</i>	0.00	0.991311	NL		0.91	77.56

**Table B 10. 2.** Significant MOs in the [M]···[R] interaction of Cr(CO)<sub>5</sub>{C(OEt)(CHCH<sub>2</sub>)}.

	DI Contribution	Ratio	Character 1	Character 2	%	Running
<i>MO69</i>	0.08	0.945383	t <sub>2g</sub>		35.35	35.35
<i>MO67</i>	0.04	0.230677	t <sub>1u</sub>	e <sub>g</sub>	16.85	52.20
<i>MO70</i>	0.02	0.960760	t <sub>2g</sub>		7.52	59.72
<i>MO62</i>	0.01	0.380420	t <sub>1u</sub>	NL	4.91	64.64
<i>MO64</i>	0.01	0.967867	NL		3.71	68.35
<i>MO51</i>	0.01	0.883683	NL	e <sub>g</sub>	3.54	71.88
<i>MO63</i>	0.01	0.878838	NL	t <sub>1u</sub>	2.97	74.85
<i>MO56</i>	0.01	0.990957	NL		2.31	77.16
<i>MO68</i>	0.00	0.952122	t <sub>2g</sub>		2.01	79.17
<i>MO52</i>	0.00	0.999765	NL		1.90	81.08

**Table B 10. 3.** Significant MOs in the [M]···[R] interaction of Cr(CO)<sub>5</sub>{C(OEt)(CHCHPh)}.

	DI Contribution	Ratio	Character 1	Character 2	%	Running
<i>MO90</i>	0.13	0.864974	t <sub>2g</sub>	NL	38.66	38.66
<i>MO85</i>	0.04	0.257377	t <sub>1u</sub>	e <sub>g</sub>	11.62	50.28
<i>MO89</i>	0.02	0.959893	t <sub>2g</sub>		5.16	55.44
<i>MO64</i>	0.01	0.949998	NL		3.57	59.01



<i>MO79</i>	0.01	0.950240	NL		3.24	62.26
<i>MO78</i>	0.01	0.290305	$t_{1u}$	NL	2.62	64.88
<i>MO88</i>	0.00	0.951938	$t_{2g}$		1.42	66.30
<i>MO65</i>	0.00	0.999181	NL		1.36	67.65
<i>MO84</i>	0.00	0.998201	NL		1.34	69.00
<i>MO48</i>	0.00	0.967318	NL		1.22	70.22

**Table B 10. 4.** Significant MOs in the [M]...[R] interaction of  $\text{Cr}(\text{CO})_5\{\text{C}(\text{OEt})(\text{CCH})\}$ .

	DI Contribution	Ratio	Character 1	Character 2	%	Running
<i>MO68</i>	0.10	0.946044	$t_{2g}$		35.94	35.94
<i>MO66</i>	0.06	0.427218	NL	$t_{1u}$	20.81	56.76
<i>MO69</i>	0.04	0.956923	$t_{2g}$		13.98	70.74
<i>MO64</i>	0.02	0.828001	NL	$t_{1u}$	6.36	77.11
<i>MO62</i>	0.01	0.802545	NL	$t_{1u}$	2.46	79.56
<i>MO61</i>	0.01	0.484534	$t_{1u}$	NL	2.18	81.75
<i>MO49</i>	0.00	0.880699	NL	$t_{1u}$	1.73	83.47
<i>MO50</i>	0.00	0.945860	NL		1.57	85.05
<i>MO52</i>	0.00	0.998047	NL		1.47	86.51
<i>MO54</i>	0.00	0.989777	NL		1.26	87.77

**Table B 10. 5.** Significant MOs in the [M]...[R] interaction of  $\text{Cr}(\text{CO})_5\{\text{C}(\text{NMe}_2)(\text{H})\}$ .

	DI Contribution	Ratio	Character 1	Character 2	%	Running
<i>MO60</i>	0.02	0.409167	$t_{1u}$	$e_g$	35.38	35.38
<i>MO63</i>	0.02	0.958012	$t_{2g}$		23.22	58.60
<i>MO58</i>	0.00	0.505165	$t_{1u}$	NL	6.54	65.14
<i>MO62</i>	0.00	0.936890	$t_{2g}$		5.65	70.79
<i>MO47</i>	0.00	0.975486	NL		3.04	73.83
<i>MO42</i>	0.00	0.954627	NL		2.45	76.28
<i>MO57</i>	0.00	0.460378	$t_{1u}$	NL	1.66	77.94
<i>MO61</i>	0.00	0.951714	$t_{2g}$		1.43	79.37
<i>MO48</i>	0.00	0.999851	NL		1.35	80.72

*MO59*                      0.00    0.976703    NL                                      1.21            81.92

---

**Table B 10. 6.** Significant MOs in the [M]···[R] interaction of Cr(CO)<sub>5</sub>{C(NMe<sub>2</sub>)(CHCH<sub>2</sub>)}.

	DI Contribution	Ratio	Character 1	Character 2	%	Running
<i>MO67</i>	0.05	0.502136	NL	t <sub>1u</sub>	21.25	21.25
<i>MO70</i>	0.04	0.946106	t <sub>2g</sub>		18.76	40.01
<i>MO66</i>	0.02	0.633664	NL	t <sub>1u</sub>	10.84	50.86
<i>MO69</i>	0.01	0.945738	t <sub>2g</sub>		6.55	57.40
<i>MO52</i>	0.01	0.981734	NL		4.82	62.22
<i>MO63</i>	0.01	0.434546	t <sub>1u</sub>	NL	3.69	65.91
<i>MO64</i>	0.01	0.800626	NL	t <sub>1u</sub>	3.56	69.47
<i>MO65</i>	0.01	0.984653	NL		3.39	72.87
<i>MO53</i>	0.01	0.997226	NL		3.10	75.97
<i>MO46</i>	0.01	0.961504	NL		2.58	78.55

---

**Table B 10. 7.** Significant MOs in the [M]···[R] interaction of Cr(CO)<sub>5</sub>{C(NMe<sub>2</sub>)(CHCHPh)}.

	DI Contribution	Ratio	Character 1	Character 2	%	Running
<i>MO90</i>	0.06	0.863675	t <sub>2g</sub>	NL	26.98	26.98
<i>MO85</i>	0.02	0.423742	NL	t <sub>1u</sub>	10.67	37.65
<i>MO89</i>	0.02	0.947507	t <sub>2g</sub>		7.82	45.47
<i>MO65</i>	0.01	0.948265	NL		6.22	51.70
<i>MO84</i>	0.01	0.863473	NL	t <sub>1u</sub>	5.18	56.88
<i>MO79</i>	0.01	0.651550	NL	t <sub>1u</sub>	4.85	61.73
<i>MO83</i>	0.01	0.976444	NL		4.80	66.52
<i>MO80</i>	0.01	0.344134	t <sub>1u</sub>	NL	3.42	69.94
<i>MO87</i>	0.01	0.866602	NL	t <sub>2g</sub>	3.35	73.29
<i>MO66</i>	0.01	0.998278	NL		2.45	75.75

---

**Table B 10. 8.** Significant MOs in the [M]···[R] interaction of Cr(CO)<sub>5</sub>{C(NMe<sub>2</sub>)(CCH)}.

	DI Contribution	Ratio	Character 1	Character 2	%	Running
--	-----------------	-------	-------------	-------------	---	---------

---

<i>MO66</i>	0.05	0.405610	NL	$t_{1u}$	19.70	19.70
<i>MO68</i>	0.04	0.945193	$t_{2g}$		15.77	35.47
<i>MO69</i>	0.04	0.951625	$t_{2g}$		15.18	50.65
<i>MO65</i>	0.02	0.997357	NL		9.69	60.34
<i>MO64</i>	0.02	0.567818	NL	$t_{1u}$	9.48	69.82
<i>MO51</i>	0.01	0.948165	NL		5.51	75.33
<i>MO63</i>	0.01	0.897301	NL	$t_{1u}$	4.74	80.07
<i>MO62</i>	0.01	0.445926	$t_{1u}$	NL	2.18	82.25
<i>MO67</i>	0.00	0.951520	$t_{2g}$		1.89	84.14
<i>MO52</i>	0.00	0.999691	NL		1.72	85.87

# **Appendix C**

## **Supplementary Information for Chapter 5**

## Section 1: Cartesian Coordinates of and Energies of All Molecules Studied.

**Table C 1. 1.** Cartesian coordinates of  $\text{Cr}(\text{CO})_5\{\text{C}(\text{OEt})(2\text{-}(\text{N}\text{-Methyl})\text{pyrrolyl})\}$  in the crystal structure.

Atom	X	Y	Z
Cr	1.6734	1.9624	1.8963
C	0.4147	1.9624	0.5080
O	-0.3463	1.9624	-0.3469
C	0.6714	0.5793	2.7449
O	0.0668	-0.2637	3.2088
C	2.6162	0.6240	0.9479
O	3.1224	-0.1845	0.3201
C	3.0087	1.9624	3.5270
O	4.3383	1.9624	3.4877
C	2.6147	1.9624	4.9043
C	1.3235	1.9624	5.4477
H	0.5331	1.9624	4.9579
C	1.4087	1.9624	6.8278
H	0.6990	1.9624	7.4287
C	2.7390	1.9624	7.1364
H	3.0846	1.9624	8.0000
N	3.4743	1.9624	6.0170
C	4.9529	1.9624	6.0448
H	5.2564	1.9624	6.9553
C	5.1306	1.9624	2.2926
C	6.5559	1.9624	2.6788
H	7.1024	1.9624	1.8891
H	5.2819	1.1782	5.5982
H	4.9306	1.1759	1.7616
H	6.7468	2.7466	3.2002
C	0.6714	3.3455	2.7449
O	0.0668	4.1885	3.2088
C	2.6162	3.3008	0.9479
O	3.1224	4.1093	0.3201
H	5.2819	2.7466	5.5982

H	4.9306	2.7489	1.7616
H	6.7468	1.1782	3.2002

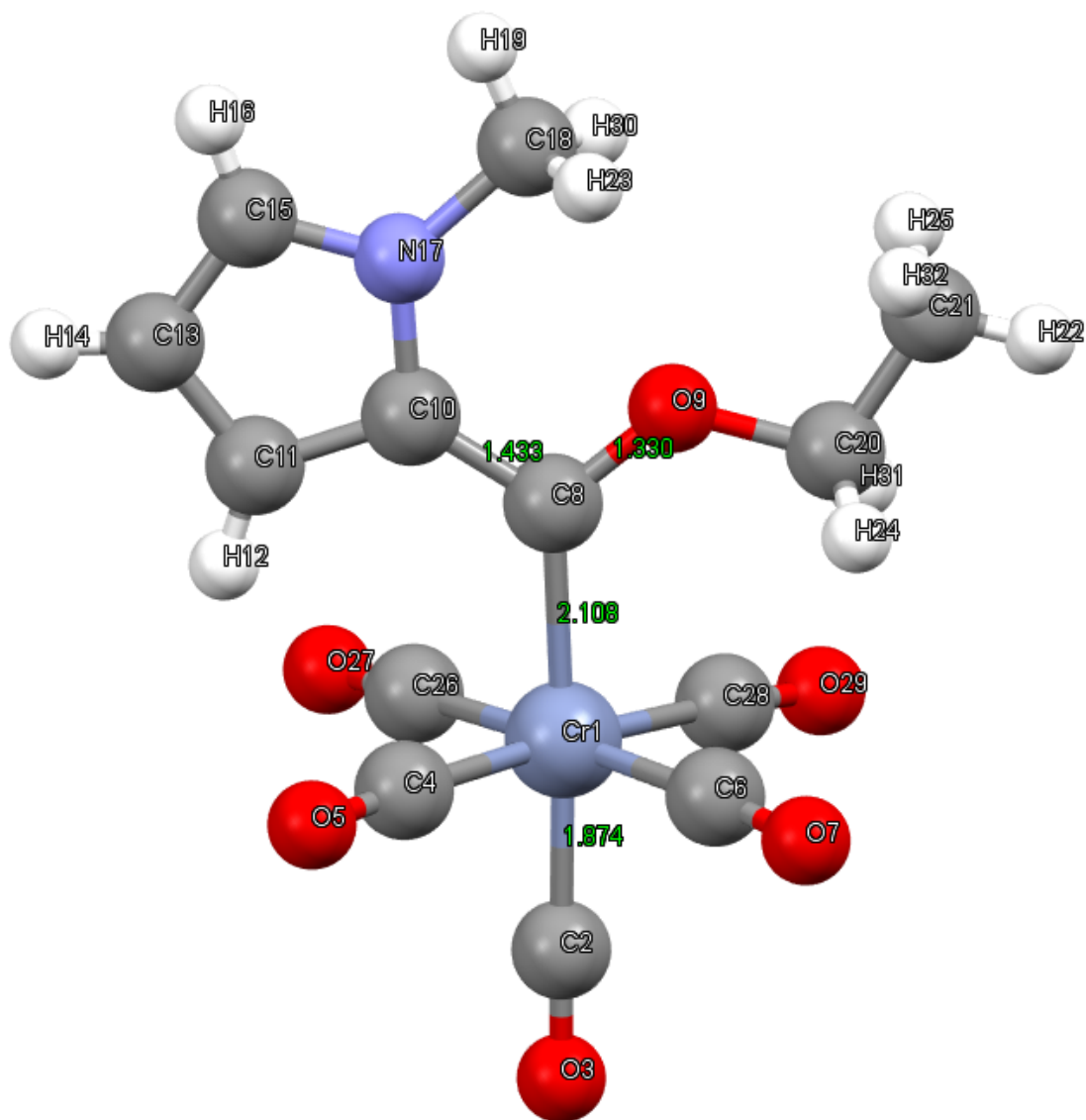


**Figure C 1. 1.** Crystal structure of  $\text{Cr(CO)}_5\{\text{C(OEt)(2-(N-Methyl)pyrrolyl)}\}$  in Mercury with bond lengths.

**Table C 1. 2.** Cartesian coordinates of Cr(CO)<sub>5</sub>{C(OEt)(2-(N-Methyl)pyrrolyl)} with the R-group frozen to a dihedral DA(Cr,C,C,N) of 180° at CAM-B3LYP/dev2svp(p) level in n-hexane.

Atom	X	Y	Z
Cr	1.6530	1.9624	1.8662
C	0.3933	1.9624	0.4697
O	-0.3827	1.9624	-0.3833
C	0.6540	0.5823	2.7188
O	0.0361	-0.2667	3.1867
C	2.6015	0.5994	0.9415
O	3.1064	-0.2393	0.3336
C	3.0098	1.9624	3.5214
O	4.3360	1.9624	3.4646
C	2.6158	1.9624	4.9137
C	1.3079	1.9622	5.4485
H	0.3911	1.9622	4.8688
C	1.3851	1.9622	6.8444
H	0.5582	1.9621	7.5532
C	2.7415	1.9623	7.1621
H	3.2255	1.9623	8.1392
N	3.4852	1.9624	6.0301
C	4.9431	1.9624	6.0744
H	5.2472	1.9624	7.1326
C	5.1313	1.9625	2.2680
C	6.5946	1.9625	2.6725
H	7.2227	1.9626	1.7648
H	5.3554	1.0695	5.5822
H	4.8872	1.0685	1.6763
H	6.8477	2.8594	3.2641
C	0.6543	3.3428	2.7186
O	0.0365	4.1921	3.1862
C	2.6017	3.3251	0.9413
O	3.1068	4.1636	0.3333
H	5.3553	2.8554	5.5823
H	4.8871	2.8565	1.6764

H	6.8477	1.0656	3.2640
---	--------	--------	--------

---

Molecular Energy of  $\text{Cr}(\text{CO})_5\{\text{C}(\text{OEt})(2\text{-(N-Methyl)pyrrolyl})\}$ : -2051.71850815 a.u.

**Table C 1. 3.** Cartesian coordinates of  $\text{Cr}(\text{CO})_5\{\text{C}(\text{OEt})(2\text{-(N-Methyl)pyrrolyl})\}$  with the R-group frozen to a dihedral  $\text{DA}(\text{Cr},\text{C},\text{C},\text{N})$  of  $170^\circ$  at CAM-B3LYP/dev2svp(p) level in n-hexane.

Atom	X	Y	Z
Cr	1.6589	1.9597	1.8703
C	0.4154	1.8851	0.4606
O	-0.3498	1.8401	-0.4008
C	0.5967	0.6729	2.7897
O	-0.0684	-0.1221	3.2867
C	2.6097	0.5099	1.0902
O	3.1407	-0.3819	0.5904
C	3.0051	2.0100	3.5288
O	4.3309	2.0546	3.4770
C	2.6083	1.9383	4.9182
C	1.3095	2.0639	5.4591
H	0.4013	2.2214	4.8866
C	1.3869	1.9804	6.8532
H	0.5667	2.0455	7.5667
C	2.7322	1.7900	7.1610
H	3.2106	1.6566	8.1318
N	3.4711	1.7704	6.0255
C	4.9126	1.5501	6.0517
H	5.2023	1.3364	7.0922
C	5.1237	2.1927	2.2873
C	6.5699	1.8961	2.6402
H	7.1962	2.0156	1.7392
H	5.1920	0.6939	5.4206
H	4.7534	1.5037	1.5167
H	6.9460	2.5888	3.4130
C	0.7055	3.4207	2.6341



O	0.1226	4.3139	3.0636
C	2.6369	3.2241	0.8406
O	3.1532	3.9946	0.1571
H	5.4589	2.4378	5.6999
H	5.0107	3.2247	1.9199
H	6.6879	0.8611	3.0054

Molecular Energy of  $\text{Cr}(\text{CO})_5\{\text{C}(\text{OEt})(2\text{-(N-Methyl)pyrrolyl)}\}$ : -2051.71856549 a.u.

**Table C 1. 4.** Cartesian coordinates of  $\text{Cr}(\text{CO})_5\{\text{C}(\text{OEt})(2\text{-(N-Methyl)pyrrolyl)}\}$  with the R-group frozen to a dihedral  $\text{DA}(\text{Cr,C,C,N})$  of  $90^\circ$  at CAM-B3LYP/dev2svp(p) level in n-hexane.

Atom	X	Y	Z
Cr	1.6398	2.0070	1.9493
C	0.2861	1.9122	0.6155
O	-0.5272	1.8569	-0.1953
C	0.4654	0.9993	3.0786
O	-0.2826	0.3932	3.7029
C	2.4180	0.4046	1.2858
O	2.8773	-0.5728	0.8873
C	3.0040	2.0673	3.4728
O	4.3167	2.0601	3.4833
C	2.5672	1.9907	4.9030
C	2.1036	3.0041	5.7309
H	2.0419	4.0596	5.4688
C	1.7102	2.4000	6.9596
H	1.2982	2.9059	7.8328
C	1.9279	1.0427	6.8325
H	1.7592	0.2236	7.5309
N	2.4403	0.7921	5.5788
C	2.9252	-0.5000	5.1283
H	2.4512	-1.2899	5.7310
C	5.1504	2.1185	2.3025
C	6.5807	1.8622	2.7349

H	7.2470	1.9213	1.8569
H	2.6610	-0.6682	4.0720
H	4.7975	1.3678	1.5800
H	6.9102	2.6127	3.4734
C	0.8874	3.6271	2.6412
O	0.4367	4.6042	3.0386
C	2.6661	3.0397	0.7235
O	3.2118	3.6675	-0.0716
H	4.0223	-0.5805	5.2339
H	5.0339	3.1199	1.8609
H	6.6860	0.8593	3.1834

Molecular Energy of  $\text{Cr}(\text{CO})_5\{\text{C}(\text{OEt})(2\text{-(N-Methyl)pyrrolyl})\}$ : -2051.70269228 a.u.

**Table C 1. 5.** Cartesian coordinates of  $\text{Cr}(\text{CO})_5\{\text{C}(\text{NH}_2)(2\text{-(N-Methyl)pyrrolyl})\}$  in the crystal structure.

Atom	X	Y	Z
Cr	3.3968	6.4864	2.5787
C	4.5019	7.9167	2.0948
O	5.166	8.7917	1.783
C	4.6737	5.7192	3.7283
O	5.4371	5.2332	4.4134
C	2.8048	7.5189	4.0383
O	2.516	8.1744	4.9307
C	1.9713	7.1177	1.4629
O	1.1123	7.4832	0.8319
C	4.2085	5.5329	1.1419
O	4.797	5.0097	0.3238
C	2.0759	4.9136	3.0313
N	1.2275	2.6324	2.3177
C	2.2492	3.5377	2.613
C	3.4386	2.8417	2.4727
H	4.2909	3.1917	2.6011
C	3.1443	1.5301	2.1077
H	3.7573	0.8455	1.9664

C	1.7949	1.4402	1.9967
H	1.3289	0.6787	1.739
C	-0.1847	2.9113	2.0847
H	-0.2781	3.782	1.6904
H	-0.6578	2.8863	2.9194
H	-0.5478	2.2502	1.4913
N	0.9674	5.1471	3.6944
H	0.7942	5.898	3.953
H	0.5064	4.554	3.9347

---

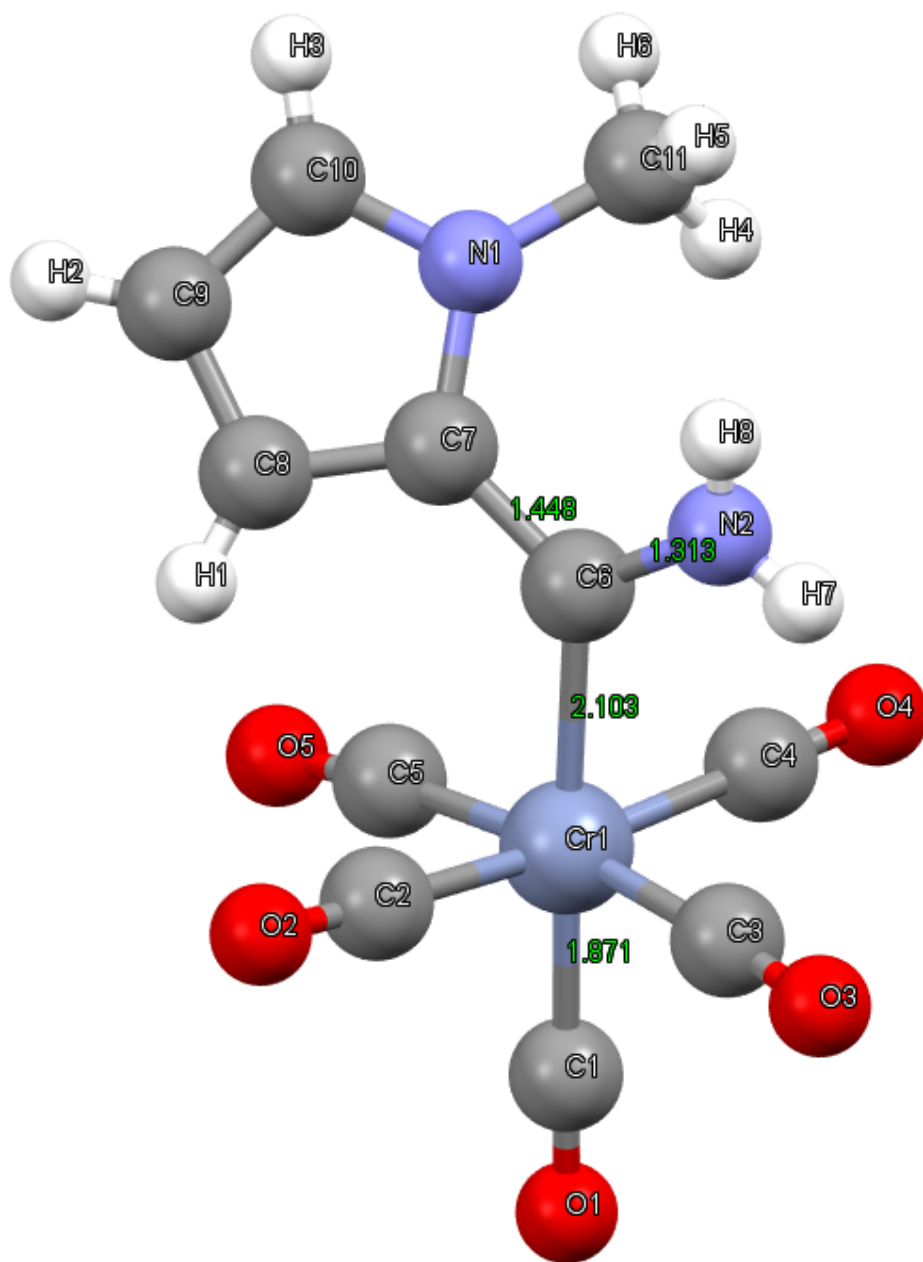


**Figure C 1. 2.** Crystal structure of  $\text{Cr}(\text{CO})_5\{\text{C}(\text{NH}_2)(2\text{-}(\text{N-Methyl})\text{pyrrolyl})\}$  in Mercury with bond lengths.

**Table C 1. 6.** Cartesian coordinates of Cr(CO)<sub>5</sub>{C(NH<sub>2</sub>)(2-(N-Methyl)pyrrolyl)} with the R-group frozen to a dihedral DA(Cr,C,C,N) of 180° at CAM-B3LYP/dev2svp(p) level in n-hexane.

Atom	X	Y	Z
Cr	3.6347	6.4203	2.9648
C	4.9641	7.7386	3.0568
O	5.7822	8.5514	3.1142
C	4.6541	5.3104	4.1285
O	5.2872	4.6725	4.8469
C	2.7880	7.1629	4.4924
O	2.2842	7.6300	5.4176
C	2.6041	7.5277	1.8186
O	1.9883	8.2133	1.1267
C	4.4717	5.6863	1.4204
O	4.9934	5.2797	0.4790
C	2.0625	4.9280	2.8665
N	1.2377	2.4964	2.5835
C	2.2310	3.5055	2.6548
C	3.4572	2.8372	2.4776
H	4.4298	3.3179	2.4776
C	3.2198	1.4661	2.3039
H	3.9574	0.6810	2.1445
C	1.8437	1.2965	2.3752
H	1.2474	0.3875	2.2896
C	-0.2085	2.6049	2.6941
H	-0.6312	3.2391	1.8946
H	-0.5131	2.9893	3.6837
H	-0.6442	1.6009	2.5826
N	0.8172	5.3845	3.0197
H	0.6625	6.3759	3.1694
H	-0.0247	4.8170	3.0006

Molecular Energy of Cr(CO)<sub>5</sub>{C(NH<sub>2</sub>)(2-(N-Methyl)pyrrolyl)}: -1953.31949327 a.u.

**Table C 1. 7.** Cartesian coordinates of  $\text{Cr}(\text{CO})_5\{\text{C}(\text{NH}_2)(2\text{-(N-Methyl)pyrrolyl})\}$  with the R-group frozen to a dihedral  $\text{DA}(\text{Cr,C,C,N})$  of  $150^\circ$  at CAM-B3LYP/dev2svp(p) level in n-hexane.

Atom	X	Y	Z
Cr	3.6142	6.3910	2.9359
C	4.9341	7.7062	3.1883
O	5.7416	8.5152	3.3447
C	4.7620	5.1396	3.8071
O	5.4867	4.4309	4.3488
C	2.8081	6.7933	4.6088
O	2.3055	7.0310	5.6171
C	2.5266	7.6870	2.0861
O	1.8811	8.4979	1.5796
C	4.3270	5.9206	1.2356
O	4.7590	5.6476	0.2045
C	2.1059	4.9029	2.7053
N	1.4257	2.4780	3.1060
C	2.3291	3.4688	2.6753
C	3.4193	2.7922	2.1095
H	4.2824	3.2721	1.6550
C	3.1717	1.4074	2.1759
H	3.8133	0.6050	1.8140
C	1.9513	1.2521	2.8180
H	1.4332	0.3441	3.1277
C	0.2373	2.6410	3.9350
H	-0.6809	2.7611	3.3298
H	0.3477	3.5104	4.6001
H	0.1137	1.7438	4.5612
N	0.8251	5.2693	2.6346
H	0.5684	6.2517	2.6614
H	0.0608	4.6214	2.4457

Molecular Energy of  $\text{Cr}(\text{CO})_5\{\text{C}(\text{NH}_2)(2\text{-(N-Methyl)pyrrolyl})\}$ : -1953.32123683 a.u.

**Table C 1. 8.** Cartesian coordinates of  $\text{Cr}(\text{CO})_5\{\text{C}(\text{NH}_2)(2\text{-(N-Methyl)pyrrolyl})\}$  with the R-group frozen to a dihedral  $\text{DA}(\text{Cr},\text{C},\text{C},\text{N})$  of  $90^\circ$  at CAM-B3LYP/dev2svp(p) level in n-hexane.

Atom	X	Y	Z
Cr	3.5722	6.3420	3.1730
C	4.9432	7.6336	3.0032
O	5.7754	8.4238	2.9054
C	4.0424	5.9534	4.9750
O	4.3037	5.7013	6.0671
C	2.4077	7.7036	3.7837
O	1.7177	8.5474	4.1605
C	2.9860	6.6368	1.3823
O	2.6187	6.8064	0.3066
C	4.8089	5.0216	2.5543
O	5.5905	4.2629	2.1892
C	2.0621	4.9153	3.2769
N	2.6650	2.4614	3.1950
C	2.1353	3.5900	2.6002
C	1.6809	3.2397	1.3342
H	1.2112	3.9169	0.6213
C	1.9701	1.8568	1.1504
H	1.7531	1.2567	0.2668
C	2.5734	1.4101	2.3091
H	2.9424	0.4233	2.5865
C	3.3053	2.3957	4.4974
H	2.7460	2.9935	5.2349
H	4.3447	2.7666	4.4586
H	3.3177	1.3487	4.8379
N	0.8724	5.1133	3.8151
H	0.6373	5.9914	4.2766
H	0.1294	4.4113	3.7599

Molecular Energy of  $\text{Cr}(\text{CO})_5\{\text{C}(\text{NH}_2)(2\text{-(N-Methyl)pyrrolyl})\}$ : -1953.31517477 a.u.

**Table C 1. 9.** Cartesian coordinates of  $\text{Cr}(\text{CO})_5\{\text{C}(\text{NMe}_2)(2\text{-(N-Methyl)pyrrolyl})\}$  in the crystal structure.

Atom	X	Y	Z
Cr	0.5781	13.0125	6.7608
C	-0.8223	12.5235	5.5820
O	-1.7250	12.2646	4.9263
C	1.2472	14.4134	5.3407
N	2.4614	14.7952	5.0128
C	3.6821	14.2733	5.6511
C	2.7930	15.7939	3.9918
C	0.2027	15.1020	4.5210
N	-0.0944	14.6802	3.2553
C	-1.0430	15.5221	2.7161
C	-1.3482	16.4715	3.6423
C	-0.5717	16.1977	4.7940
C	0.5177	13.5547	2.5622
C	-0.6722	14.2448	7.4352
O	-1.4785	14.9559	7.8463
C	-0.0245	11.7377	7.9819
O	-0.3727	10.9310	8.7325
C	1.7356	11.6785	6.0064
O	2.3750	10.8503	5.5562
C	1.8124	13.6237	8.0685
O	2.4770	14.0023	8.9272
H	4.4352	14.2846	5.0436
H	3.9091	14.8178	6.4083
H	3.5293	13.3740	5.9581
H	3.3977	16.4537	4.3455
H	1.9979	16.2300	3.6989
H	3.2114	15.3352	3.2495
H	-1.4047	15.4572	1.8515
H	-1.9488	17.1722	3.5483
H	-0.5822	16.6683	5.5945
H	-0.0977	13.2113	1.9148
H	1.3167	13.8688	2.1203



H            0.7380    12.8588    3.1929

---

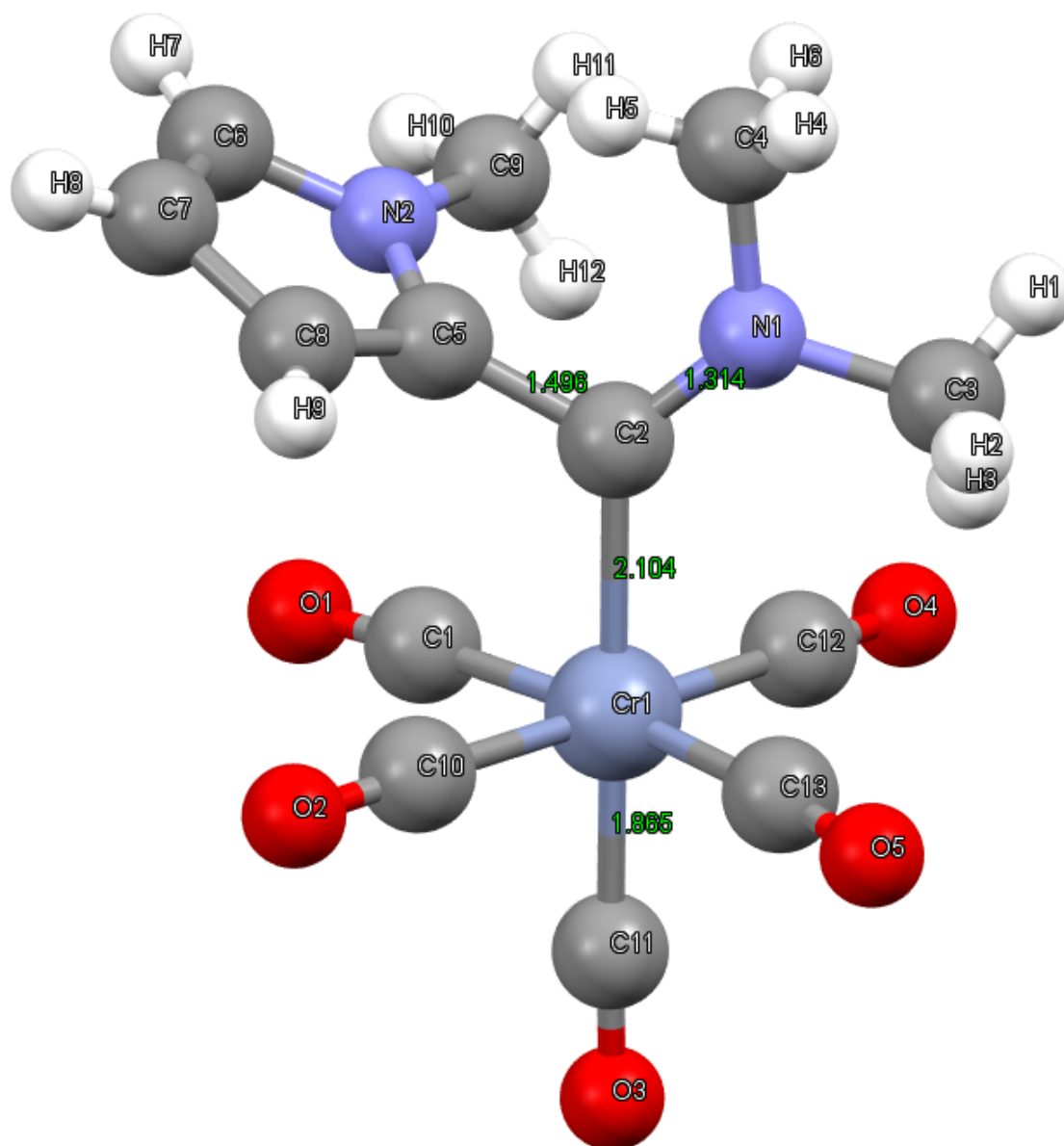


**Figure C 1. 3.** Crystal structure of  $\text{Cr}(\text{CO})_5\{\text{C}(\text{NMe}_2)(2\text{-(N-Methyl)pyrrolyl})\}$  in Mercury with bond lengths.

**Table C 1. 10.** Cartesian coordinates of  $\text{Cr}(\text{CO})_5\{\text{C}(\text{NMe}_2)(2\text{-(N-Methyl)pyrrolyl})\}$  with the R-group frozen to a dihedral  $\text{DA}(\text{Cr},\text{C},\text{C},\text{N})$  of  $180^\circ$  at CAM-B3LYP/dev2svp(p) level in n-hexane.

Atom	X	Y	Z
Cr	0.6011	12.8849	6.6607
C	-0.8612	12.3300	5.5681
O	-1.7442	11.9258	4.9520
C	1.2198	14.3747	5.1234
N	2.4716	14.8910	5.1440
C	3.6546	14.1037	5.4868
C	2.8077	16.3240	5.1216
C	0.2410	15.1150	4.3407
N	0.5259	16.0822	3.3409
C	-0.6232	16.7322	3.0064
C	-1.6695	16.2643	3.7869
C	-1.1374	15.2499	4.6019
C	1.6377	16.0299	2.3903
C	-0.3663	14.3051	7.4716
O	-0.9370	15.1422	8.0191
C	-0.0382	11.7208	7.9752
O	-0.4410	10.9927	8.7764
C	1.6273	11.4926	5.8646
O	2.2381	10.6335	5.4005
C	2.0135	13.2984	7.8565
O	2.8133	13.4910	8.6653
H	4.4519	14.3474	4.7605
H	4.0302	14.3460	6.4960
H	3.4397	13.0336	5.4203
H	3.3065	16.5631	6.0792
H	1.9076	16.9421	5.0344
H	3.5110	16.5730	4.3086
H	-0.6282	17.4490	2.1841
H	-2.6996	16.6181	3.7666

H	-1.6902	14.7112	5.3631
H	1.2651	15.7643	1.3863
H	2.1493	17.0051	2.3331
H	2.3575	15.2632	2.7015

Molecular Energy of  $\text{Cr}(\text{CO})_5\{\text{C}(\text{NMe}_2)(2\text{-(N-Methyl)pyrrolyl})\}$ : -2031.84597457 a.u.

**Table C 1. 11.** Cartesian coordinates of  $\text{Cr}(\text{CO})_5\{\text{C}(\text{NMe}_2)(2\text{-(N-Methyl)pyrrolyl})\}$  with the R-group frozen to a dihedral  $\text{DA}(\text{Cr},\text{C},\text{C},\text{N})$  of  $110^\circ$  at CAM-B3LYP/dev2svp(p) level in n-hexane.

Atom	X	Y	Z
Cr	0.5519	12.9689	6.7206
C	-0.4435	12.0897	5.3533
O	-1.0429	11.5175	4.5556
C	1.2174	14.3956	5.2724
N	2.4496	14.7214	4.8920
C	3.6635	14.1677	5.4986
C	2.7742	15.6135	3.7624
C	0.1651	15.1981	4.5951
N	0.0012	16.5569	4.8373
C	-1.0317	17.0270	4.0576
C	-1.5125	15.9892	3.2841
C	-0.7692	14.8272	3.6338
C	0.5952	17.3135	5.9268
C	-0.9361	14.1108	7.0882
O	-1.8409	14.7692	7.3507
C	-0.1218	11.7564	7.9907
O	-0.5286	11.0129	8.7733
C	1.9689	11.7513	6.3774
O	2.7886	10.9617	6.1983
C	1.5428	13.8499	8.0799
O	2.1306	14.3859	8.9137
H	4.0532	13.3358	4.8860
H	4.4312	14.9583	5.5448
H	3.4611	13.8099	6.5116

H	3.1338	16.5920	4.1287
H	1.8965	15.7595	3.1208
H	3.5813	15.1478	3.1721
H	-1.3584	18.0630	4.1423
H	-2.3141	16.0538	2.5485
H	-0.8765	13.8325	3.2057
H	0.5864	18.3844	5.6690
H	0.0353	17.1704	6.8689
H	1.6381	17.0043	6.0925

Molecular Energy of  $\text{Cr}(\text{CO})_5\{\text{C}(\text{NMe}_2)(2\text{-}(\text{N-Methyl})\text{pyrrolyl})\}$ : -2031.86213489 a.u.

**Table C 1. 12.** Cartesian coordinates of  $\text{Cr}(\text{CO})_5\{\text{C}(\text{NMe}_2)(2\text{-}(\text{N-Methyl})\text{pyrrolyl})\}$  with the R-group frozen to a dihedral  $\text{DA}(\text{Cr},\text{C},\text{C},\text{N})$  of  $90^\circ$  at CAM-B3LYP/dev2svp(p) level in n-hexane.

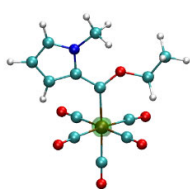
Atom	X	Y	Z
Cr	0.5570	12.9354	6.7023
C	-0.4022	12.1095	5.2721
O	-0.9788	11.5788	4.4318
C	1.2187	14.4108	5.2963
N	2.4440	14.7681	4.9384
C	3.6597	14.1930	5.5234
C	2.7692	15.7617	3.8969
C	0.1451	15.1821	4.5993
N	-0.3591	16.3642	5.1110
C	-1.3875	16.8004	4.3027
C	-1.5536	15.8952	3.2746
C	-0.5881	14.8632	3.4629
C	0.1782	17.1157	6.2306
C	-0.9828	13.9920	7.1048
O	-1.9327	14.5712	7.3940
C	-0.1017	11.6538	7.9108
O	-0.4966	10.8664	8.6555
C	1.9950	11.7456	6.3460
O	2.8231	10.9665	6.1604

C	1.5126	13.7938	8.0992
O	2.0789	14.3211	8.9536
H	4.0452	13.3818	4.8816
H	4.4285	14.9798	5.5950
H	3.4568	13.8004	6.5237
H	3.2024	16.6641	4.3640
H	1.8722	16.0305	3.3263
H	3.5197	15.3288	3.2135
H	-1.9198	17.7213	4.5378
H	-2.2996	15.9527	2.4820
H	-0.4535	13.9721	2.8513
H	0.9798	17.8089	5.9121
H	-0.6294	17.7034	6.6949
H	0.5860	16.4310	6.9897

Molecular Energy of  $\text{Cr}(\text{CO})_5\{\text{C}(\text{NMe}_2)(2\text{-}(\text{N-Methyl})\text{pyrrolyl})\}$ : -2031.86124045 a.u.

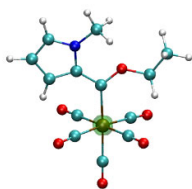
## Section 2: Assigning symmetry labels (LMAT) to each of the lowest energy structures.

Assigning the symmetry labels at any dihedral ( $\text{DA}(\text{Cr},\text{C},\text{C},\text{N})$ ) will give the same result (pattern remains the same) the only difference being the contribution each symmetry makes. The lowest energy structures have been used to show the symmetry labels as an example.



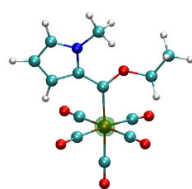
*loc*-NDF1<sup>a</sup>(1s)

$$\lambda_{\text{orthodox}}(\text{Cr1}) = 2.00$$



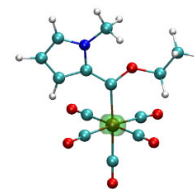
*loc*-NDF2<sup>a</sup>(2s)

$$\lambda_{\text{orthodox}}(\text{Cr1}) = 2.00$$



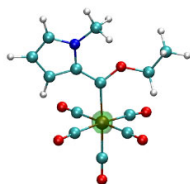
*loc*-NDF3<sup>a</sup>(2p)

$$\lambda_{\text{orthodox}}(\text{Cr1}) = 2.00$$



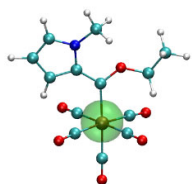
*loc*-NDF4<sup>a</sup>(2p)

$$\lambda_{\text{orthodox}}(\text{Cr1}) = 2.00$$



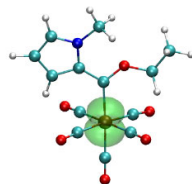
*loc*-NDF5<sup>a</sup>(2p)

$$\lambda_{\text{orthodox}}(\text{Cr1}) = 2.00$$



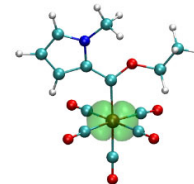
*loc*-NDF6<sup>b</sup>(3s)

$$\lambda_{\text{orthodox}}(\text{Cr1}) = 1.99$$



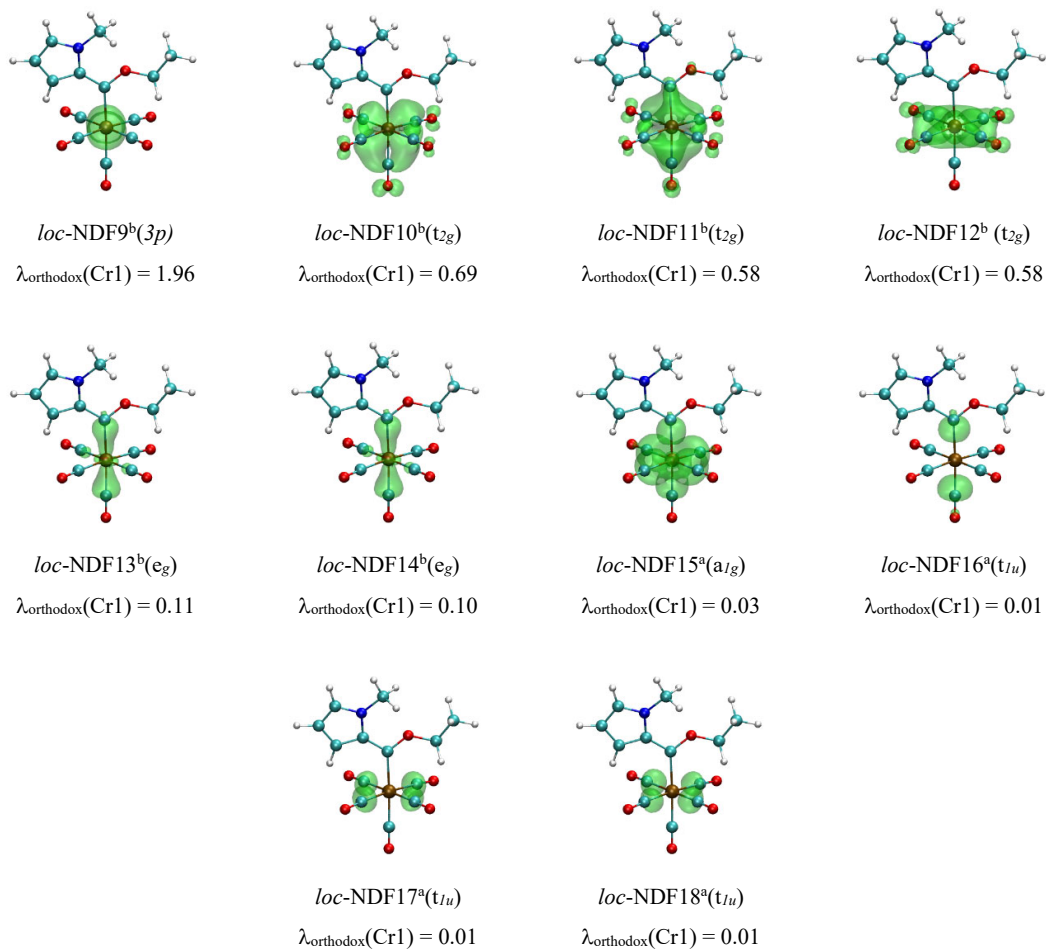
*loc*-NDF7<sup>b</sup>(3p)

$$\lambda_{\text{orthodox}}(\text{Cr1}) = 1.97$$

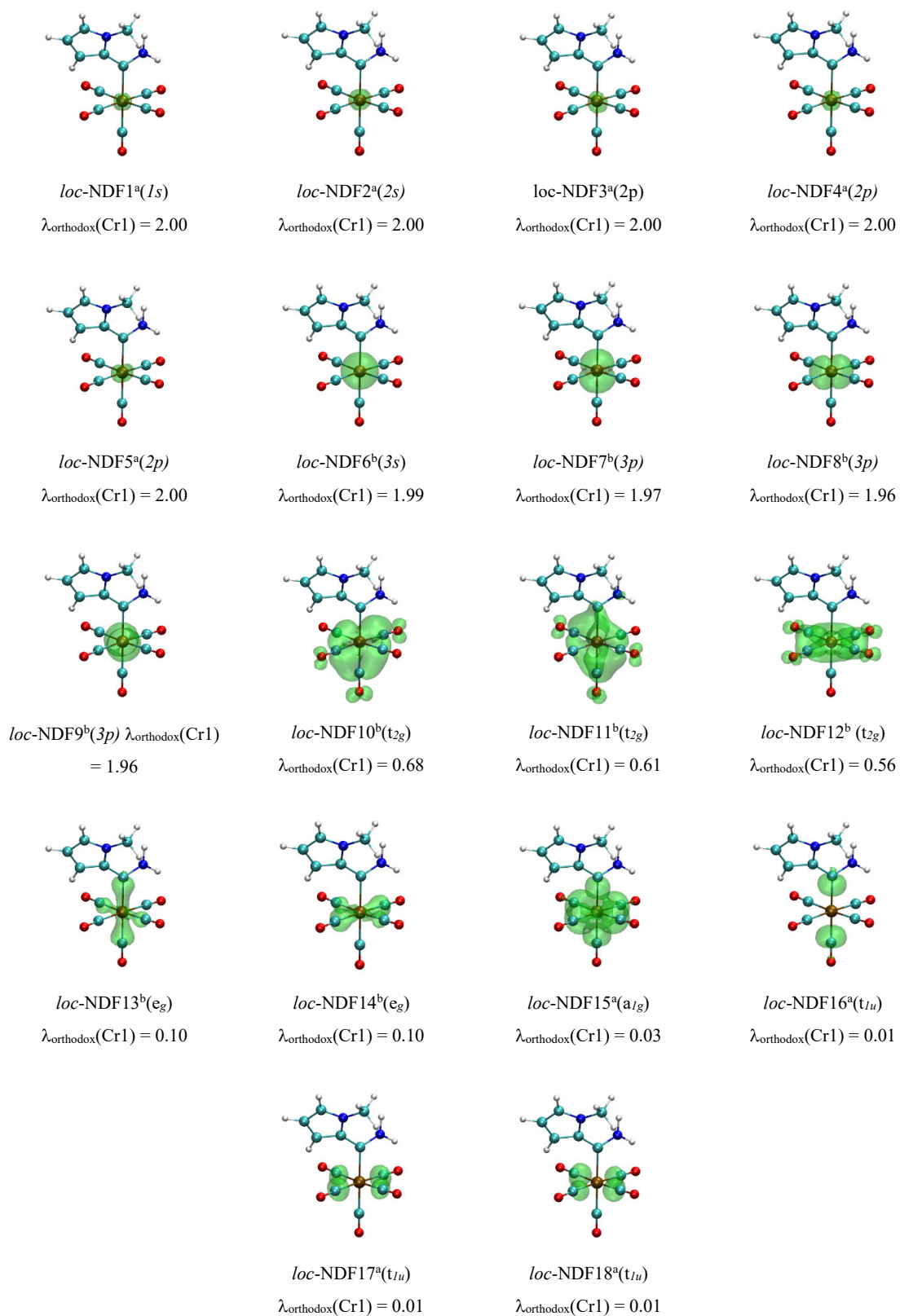


*loc*-NDF8<sup>b</sup>(3p)

$$\lambda_{\text{orthodox}}(\text{Cr1}) = 1.96$$

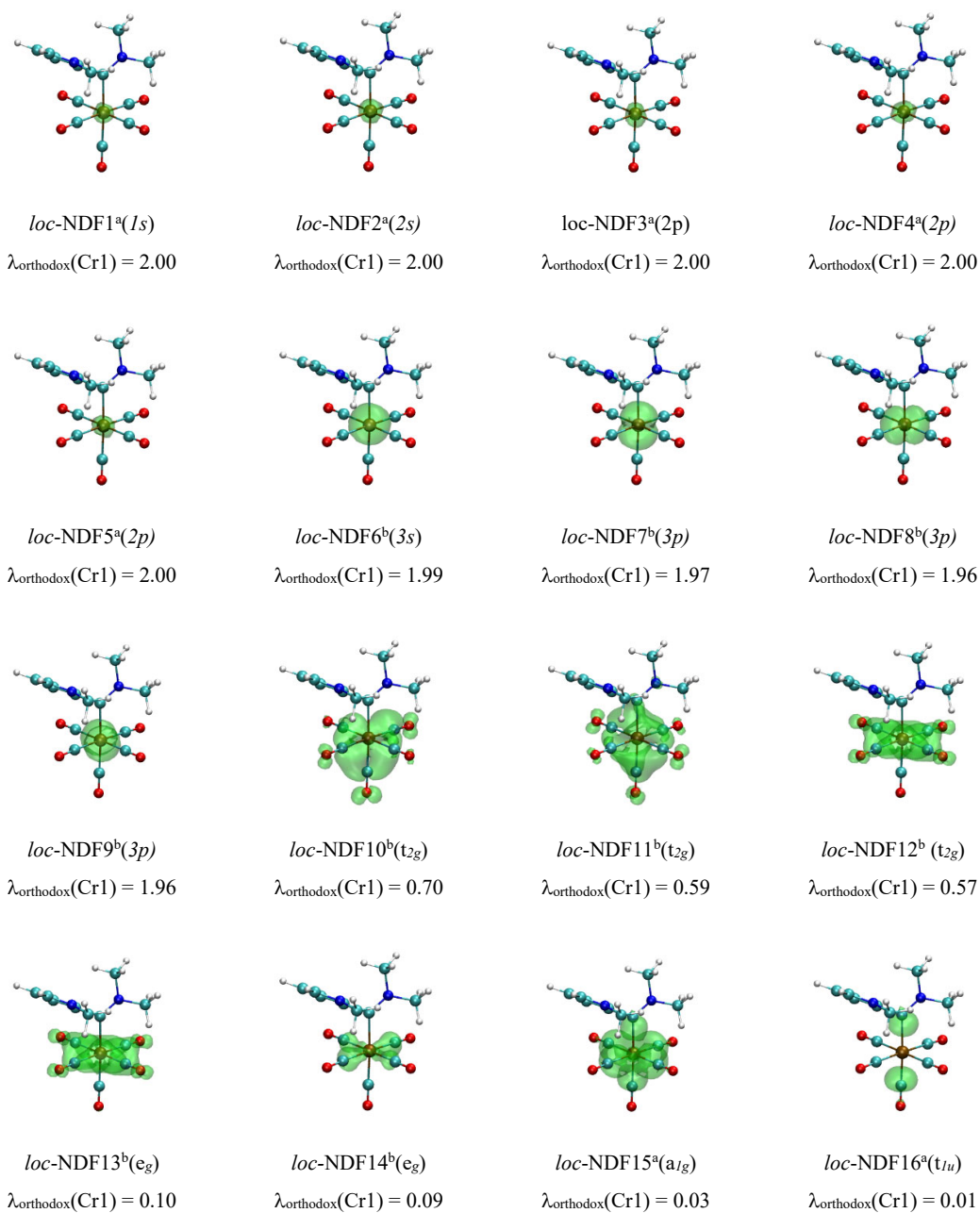


**Figure C 2. 1.** The Localized (*loc*) Natural Density Functions (NDF's) of  $\text{Cr}(\text{CO})_5\{\text{C}(\text{OEt})(2\text{-(N-Methyl)pyrrolyl})\}$  centred on the Chromium atom for the lowest energy structure (dihedral DA(Cr,C,C,N) frozen to  $170^\circ$ ). The Isovalues are indicated as  $a = 0.0001$  a.u. and  $b = 0.001$  a.u. while  $\lambda^{\text{number}}$  refers to the eigenvalue retrieved from the Orthodox Localised Matrix.



**Figure C 2. 2.** The Localized (*loc*) Natural Density Functions (NDF's) of Cr(CO)<sub>5</sub>{C(NH<sub>2</sub>)(2-(N-Methyl)pyrrolyl)} centred on the Chromium atom for the lowest energy structure (dihedral

DA(Cr,C,C,N) frozen to 150°). The Isovalues are indicated as  $a = 0.0001$  a.u. and  $b = 0.001$  a.u. while  $\lambda^{\text{number}}$  refers to the eigenvalue retrieved from the Orthodox Localised Matrix.





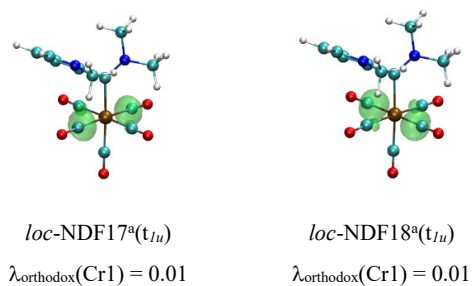


**Figure C 2. 3.** The Localized (*loc*) Natural Density Functions (NDF's) of  $\text{Cr}(\text{CO})_5\{\text{C}(\text{NMe}_2)(2\text{-}(\text{N}\text{-Methyl})\text{pyrrolyl})\}$  centred on the Chromium atom for the lowest energy structure (dihedral  $\text{DA}(\text{Cr},\text{C},\text{C},\text{N})$  frozen to  $110^\circ$ ). The Isovalues are indicated as  $a = 0.0001$  a.u. and  $b = 0.001$  a.u. while  $\lambda^{\text{number}}$  refers to the eigenvalue retrieved from the Orthodox Localised Matrix.

**Section 3: The metal cluster interacting with the all ligands [M]...[L] for all frozen dihedrals.**

**Table C 3. 1.** The [M]...[L] interaction of structure **5a** (OEt) at the various frozen dihedrals DA(Cr,C,C,N).

Frozen Dihedral Angle (°)					180				
Summary					$\sigma/\pi$				
DI					Summary				
	Contribution	Absolute Contribution	%	Metal %		Contribution	%		Energy (a.u.)
a <sub>1g</sub>	0.0410	0.0410	2.60	4.80	$\sigma$	0.4810	30.57	a <sub>1g</sub>	-0.0237
t <sub>1u</sub>	0.2897	0.2897	18.41	33.96	$\pi$	0.3720	23.64	t <sub>1u</sub>	-0.1244
t <sub>2g</sub>	0.3720	0.3720	23.64	43.61	NL	0.7203	45.78	t <sub>2g</sub>	-0.0977
e <sub>g</sub>	0.1503	0.1503	9.56	17.63				e <sub>g</sub>	-0.0541
NL	0.7203	0.7203	45.78		$\sigma + \pi$	0.8530	54.22	NL	-0.3449
Total	1.5733	1.5733						Total	-0.6449

Frozen Dihedral Angle (°)					170				
Summary					$\sigma/\pi$				
DI					Summary				
	Contribution	Absolute Contribution	%	Metal %		Contribution	%		Energy (a.u.)
a <sub>1g</sub>	0.0401	0.0401	2.55	4.67	$\sigma$	0.4788	30.41	a <sub>1g</sub>	-0.0235
t <sub>1u</sub>	0.2874	0.2874	18.25	33.48	$\pi$	0.3798	24.12	t <sub>1u</sub>	-0.1239
t <sub>2g</sub>	0.3798	0.3798	24.12	44.23	NL	0.7162	45.48	t <sub>2g</sub>	-0.0997

e <sub>g</sub>	0.1513	0.1513	9.61	17.62				e <sub>g</sub>	-0.0546
NL	0.7162	0.7162	45.48		σ + π	0.8586	54.52	NL	-0.3437
Total	1.5747	1.5747						Total	-0.6454

Frozen Dihedral Angle (°)					90				
Summary					σ/π				
DI					Summary				
	Contribution	Absolute Contribution	%	Metal %		Contribution	%		Energy (a.u.)
a <sub>1g</sub>	0.0451	0.0451	2.51	4.71	σ	0.4032	22.46	a <sub>1g</sub>	-0.0288
t <sub>1u</sub>	0.2206	0.2206	12.29	23.07	π	0.5530	30.80	t <sub>1u</sub>	-0.1093
t <sub>2g</sub>	0.5530	0.5530	30.80	57.83	NL	0.8391	46.74	t <sub>2g</sub>	-0.1530
e <sub>g</sub>	0.1375	0.1375	7.66	14.38				e <sub>g</sub>	-0.0523
NL	0.8391	0.8391	46.74		σ + π	0.9562	53.26	NL	-0.3982
Total	1.7953	1.7953						Total	-0.7416

**Table C 3. 2.** The [M]···[L] interaction of structure **5b** (NH<sub>2</sub>) at the various frozen dihedrals DA(Cr,C,C,N).

Frozen Dihedral Angle (°)					180				
Summary					σ/π				
DI					Summary				
	Contribution	Absolute Contribution	%	Metal %		Contribution	%		Energy (a.u.)

a <sub>1g</sub>	0.0325	0.0325	2.39	3.72	σ	0.5700	41.92	a <sub>1g</sub>	-0.0184
t <sub>1u</sub>	0.3699	0.3699	27.20	42.26	π	0.3053	22.45	t <sub>1u</sub>	-0.1512
t <sub>2g</sub>	0.3053	0.3053	22.45	34.88	NL	0.4846	35.64	t <sub>2g</sub>	-0.0785
e <sub>g</sub>	0.1676	0.1676	12.32	19.14				e <sub>g</sub>	-0.0609
NL	0.4846	0.4846	35.64		σ + π	0.8753	64.36	NL	-0.2433
Total	1.3599	1.3599						Total	-0.5522

---

Frozen Dihedral Angle (°)

150

Summary					σ/ π	Summary				
DI										
	Contribution	Absolute Contribution	%	Metal %		Contribution	%		Energy (a.u.)	
a <sub>1g</sub>	0.0300	0.0300	2.14	3.59	σ	0.4936	35.2	a <sub>1g</sub>	-0.0185	
t <sub>1u</sub>	0.3143	0.3143	22.43	37.61	π	0.3420	24.4	t <sub>1u</sub>	-0.1367	
t <sub>2g</sub>	0.3420	0.3420	24.41	40.93	NL	0.5659	40.4	t <sub>2g</sub>	-0.0887	
e <sub>g</sub>	0.1493	0.1493	10.65	17.86				e <sub>g</sub>	-0.0559	
NL	0.5659	0.5659	40.38		σ + π	0.8356	59.6244	NL	-0.2690	
Total	1.4015	1.4015						Total	-0.5688	

---

Frozen Dihedral Angle (°)

90

Summary					σ/ π	Summary				
---------	--	--	--	--	------	---------	--	--	--	--

DI										
Contribution					Metal %		Contribution		Energy (a.u.)	
	Contribution	Absolute Contribution	%		Metal %		Contribution	%		Energy (a.u.)
a <sub>1g</sub>	0.0351	0.0351	2.32	4.05	$\sigma$	0.4333	28.55	a <sub>1g</sub>	-0.0232	
t <sub>1u</sub>	0.2600	0.2600	17.13	29.93	$\pi$	0.4354	28.69	t <sub>1u</sub>	-0.1227	
t <sub>2g</sub>	0.4354	0.4354	28.69	50.12	NL	0.6490	42.76	t <sub>2g</sub>	-0.1163	
e <sub>g</sub>	0.1382	0.1382	9.11	15.91				e <sub>g</sub>	-0.0540	
NL	0.6490	0.6490	42.76		$\sigma + \pi$	0.8687	57.24	NL	-0.3088	
Total	1.5177	1.5177						Total	-0.6250	

**Table C 3. 3.** The [M]···[L] interaction of structure **5c** (NMe<sub>2</sub>) at the various frozen dihedrals DA(Cr,C,C,N).

Frozen Dihedral Angle (°)					180					
Summary					$\sigma/\pi$		Summary			
DI										
	Contribution	Absolute Contribution	%		Metal %		Contribution	%		Energy (a.u.)
a <sub>1g</sub>	0.0211	0.0211	1.48	3.56	$\sigma$	0.2875	20.17	a <sub>1g</sub>	-0.0135	
t <sub>1u</sub>	0.1881	0.1881	13.19	31.69	$\pi$	0.3060	21.46	t <sub>1u</sub>	-0.0839	
t <sub>2g</sub>	0.3060	0.3060	21.46	51.56	NL	0.8321	58.37	t <sub>2g</sub>	-0.0792	
e <sub>g</sub>	0.0783	0.0783	5.49	13.20				e <sub>g</sub>	-0.0293	
NL	0.8321	0.8321	58.37		$\sigma + \pi$	0.5935	41.63	NL	-0.3722	
Total	1.4255	1.4255						Total	-0.5781	

Frozen Dihedral Angle (°)					110				
Summary					Summary				
DI					Summary				
	Contribution	Absolute Contribution	%	Metal %		Contribution	%		Energy (a.u.)
a <sub>1g</sub>	0.0245	0.0245	1.60	3.15	σ	0.3755	24.52	a <sub>1g</sub>	-0.0157
t <sub>1u</sub>	0.2344	0.2344	15.30	30.19	π	0.4008	26.17	t <sub>1u</sub>	-0.1068
t <sub>2g</sub>	0.4008	0.4008	26.17	51.63	NL	0.7550	49.31	t <sub>2g</sub>	-0.1049
e <sub>g</sub>	0.1167	0.1167	7.62	15.03				e <sub>g</sub>	-0.0445
NL	0.7550	0.7550	49.31		σ + π	0.7763	50.69	NL	-0.3527
Total	1.5313	1.5313						Total	-0.6245

Frozen Dihedral Angle (°)					90				
Summary					Summary				
DI					Summary				
	Contribution	Absolute Contribution	%	Metal %		Contribution	%		Energy (a.u.)
a <sub>1g</sub>	0.0253	0.0253	1.65	3.23	σ	0.3776	24.56	a <sub>1g</sub>	-0.0162
t <sub>1u</sub>	0.2376	0.2376	15.46	30.34	π	0.4057	26.39	t <sub>1u</sub>	-0.1083
t <sub>2g</sub>	0.4057	0.4057	26.39	51.79	NL	0.7541	49.05	t <sub>2g</sub>	-0.1065
e <sub>g</sub>	0.1147	0.1147	7.46	14.64				e <sub>g</sub>	-0.0439
NL	0.7541	0.7541	49.05		σ + π	0.7833	50.95	NL	-0.3551

Total	1.5374	1.5374	Total	-0.6299
-------	--------	--------	-------	---------

**Section 4: The fragment analysis of the metal cluster interacting with the carbene carbon [M]...C<sub>carbene</sub> at the frozen dihedrals.**

**Table C 4. 1.** The [M]...C<sub>carbene</sub> interaction of structure **5a** (OEt) at the various frozen dihedrals DA(Cr,C,C,N).

Frozen Dihedral Angle (°)					180				
Summary					$\sigma/\pi$		Summary		
	DI Contribution	Absolute Contribution	%	Metal %	Contribution	%		Energy (a.u.)	
a <sub>1g</sub>	0.0338	0.0338	3.41	6.1	$\sigma$	0.3576	36.16	a <sub>1g</sub>	-0.0203
t <sub>1u</sub>	0.2080	0.2081	21.04	37.8	$\pi$	0.1931	19.52	t <sub>1u</sub>	-0.0927
t <sub>2g</sub>	0.1931	0.1931	19.52	35.1	NL	0.4368	44.32	t <sub>2g</sub>	-0.0508
e <sub>g</sub>	0.1158	0.1158	11.71	21.0				e <sub>g</sub>	-0.0418
NL	0.4368	0.4383	44.32		$\sigma + \pi$	0.55	55.68	NL	-0.2041
Total	0.9874	0.9891						Total	-0.4097

Frozen Dihedral Angle (°)					170				
Summary					$\sigma/\pi$		Summary		

	DI Contribution	Absolute Contribution	%	Metal %		Contribution	%		Energy (a.u.)
a <sub>1g</sub>	0.0331	0.0331	3.33	6.00	σ	0.3549	35.74	a <sub>1g</sub>	-0.0201
t <sub>1u</sub>	0.2061	0.2061	20.75	37.40	π	0.1960	19.74	t <sub>1u</sub>	-0.0922
t <sub>2g</sub>	0.1960	0.1960	19.74	35.58	NL	0.4418	44.51	t <sub>2g</sub>	-0.0515
e <sub>g</sub>	0.1158	0.1158	11.66	21.01				e <sub>g</sub>	-0.0418
NL	0.4418	0.4419	44.51		σ + π	0.55	55.49	NL	-0.2069
Total	0.9927	0.9929						Total	-0.4126

Frozen Dihedral Angle (°)					90				
Summary	DI Contribution	Absolute Contribution	%	Metal %	σ/π	Contribution	%	Summary	Energy (a.u.)
a <sub>1g</sub>	0.0364	0.0364	3.07	5.61	σ	0.2919	24.62	a <sub>1g</sub>	-0.0242
t <sub>1u</sub>	0.1532	0.1532	12.92	23.60	π	0.3573	30.14	t <sub>1u</sub>	-0.0817
t <sub>2g</sub>	0.3573	0.3573	30.14	55.04	NL	0.5363	45.24	t <sub>2g</sub>	-0.0991
e <sub>g</sub>	0.1023	0.1023	8.63	15.75				e <sub>g</sub>	-0.0388
NL	0.5363	0.5363	45.24		σ + π	0.65	54.76	NL	-0.2595
Total	1.1855	1.1855						Total	-0.5033

**Table C 4. 2.** The [M]...C<sub>carbene</sub> interaction of structure **5b** (NH<sub>2</sub>) at the various frozen dihedrals DA(Cr,C,C,N).

Frozen Dihedral Angle (°)	180
---------------------------	-----



Summary					$\sigma/\pi$		Summary			
DI										
	Contribution	Absolute Contribution	%	Metal %			Contribution	%	Energy (a.u.)	
a <sub>1g</sub>	0.0254	0.0254	2.79	4.07	$\sigma$		0.4538	49.99	a <sub>1g</sub>	-0.0148
t <sub>1u</sub>	0.2957	0.2971	32.63	47.57	$\pi$		0.1693	18.59	t <sub>1u</sub>	-0.1229
t <sub>2g</sub>	0.1693	0.1693	18.59	27.11	NL		0.2798	31.42	t <sub>2g</sub>	-0.0435
e <sub>g</sub>	0.1327	0.1327	14.57	21.25					e <sub>g</sub>	-0.0476
NL	0.2798	0.2861	31.42		$\sigma + \pi$		0.62	68.58	NL	-0.1431
Total	0.9029	0.9107							Total	-0.3718

---

Frozen Dihedral Angle (°)

150

Summary					$\sigma/\pi$		Summary			
DI										
	Contribution	Absolute Contribution	%	Metal %			Contribution	%	Energy (a.u.)	
a <sub>1g</sub>	0.0245	0.0245	2.52	4.13	$\sigma$		0.4020	41.41	a <sub>1g</sub>	-0.0156
t <sub>1u</sub>	0.2543	0.2551	26.23	42.92	$\pi$		0.1915	19.69	t <sub>1u</sub>	-0.1132
t <sub>2g</sub>	0.1915	0.1915	19.69	32.23	NL		0.3741	38.90	t <sub>2g</sub>	-0.0497
e <sub>g</sub>	0.1231	0.1231	12.66	20.72					e <sub>g</sub>	-0.0460
NL	0.3741	0.3783	38.90		$\sigma + \pi$		0.59	61.10	NL	-0.1799
Total	0.9675	0.9726							Total	-0.4044

Frozen Dihedral Angle (°)					90									
Summary					$\sigma/\pi$					Summary				
DI														
	Contribution	Absolute Contribution	%	Metal %			Contribution	%		Energy (a.u.)				
a <sub>1g</sub>	0.0277	0.0277	2.60	4.52	$\sigma$		0.3528	33.09	a <sub>1g</sub>	-0.0191				
t <sub>1u</sub>	0.2108	0.2110	19.78	34.36	$\pi$		0.2611	24.48	t <sub>1u</sub>	-0.1029				
t <sub>2g</sub>	0.2611	0.2611	24.48	42.52	NL		0.4508	42.43	t <sub>2g</sub>	-0.0699				
e <sub>g</sub>	0.1143	0.1143	10.71	18.61					e <sub>g</sub>	-0.0447				
NL	0.4508	0.4526	42.43		$\sigma + \pi$		0.61	57.57	NL	-0.2183				
Total	1.0647	1.0667							Total	-0.4550				

**Table C 4. 3.** The [M]...C<sub>carbene</sub> interaction of structure **5c** (NMe<sub>2</sub>) at the various frozen dihedrals DA(Cr,C,C,N).

Frozen Dihedral Angle (°)					180									
Summary					$\sigma/\pi$					Summary				
DI														
	Contribution	Absolute Contribution	%	Metal %			Contribution	%		Energy (a.u.)				
a <sub>1g</sub>	0.0156	0.0156	1.84	4.3	$\sigma$		0.2075	24.50	a <sub>1g</sub>	-0.0104				
t <sub>1u</sub>	0.1366	0.1366	16.12	37.5	$\pi$		0.1565	18.47	t <sub>1u</sub>	-0.0626				
t <sub>2g</sub>	0.1565	0.1565	18.47	43.0	NL		0.4832	57.03	t <sub>2g</sub>	-0.0405				
e <sub>g</sub>	0.0554	0.0554	6.54	15.2					e <sub>g</sub>	-0.0199				
NL	0.4832	0.4832	57.03		$\sigma + \pi$		0.36	42.97	NL	-0.2067				

Total	0.8472	0.8472						Total	-0.3402
-------	--------	--------	--	--	--	--	--	-------	---------

Frozen Dihedral Angle (°)	110
---------------------------	-----

Summary					$\sigma/\pi$	Summary				
DI										
	Contribution	Absolute Contribution	%	Metal %		Contribution	%		Energy (a.u.)	
a <sub>1g</sub>	0.0186	0.0186	1.92	3.64	$\sigma$	0.2925	30.27	a <sub>1g</sub>	-0.0127	
t <sub>1u</sub>	0.1830	0.1830	18.94	35.92	$\pi$	0.2171	22.47	t <sub>1u</sub>	-0.0862	
t <sub>2g</sub>	0.2171	0.2171	22.47	42.60	NL	0.4566	47.26	t <sub>2g</sub>	-0.0569	
e <sub>g</sub>	0.0909	0.0909	9.41	17.84				e <sub>g</sub>	-0.0342	
NL	0.4566	0.4566	47.26		$\sigma + \pi$	0.51	52.74	NL	-0.2103	
<b>Total</b>	<b>0.9662</b>	<b>0.9662</b>						<b>Total</b>	<b>-0.4003</b>	

Frozen Dihedral Angle (°)	90
---------------------------	----

Summary					$\sigma/\pi$	Summary				
DI										
	Contribution	Absolute Contribution	%	Metal %		Contribution	%		Energy (a.u.)	
a <sub>1g</sub>	0.0185	0.0185	1.95	3.60	$\sigma$	0.2920	30.680	a <sub>1g</sub>	-0.0127	
t <sub>1u</sub>	0.1861	0.1861	19.55	36.20	$\pi$	0.2221	23.335	t <sub>1u</sub>	-0.0876	
t <sub>2g</sub>	0.2221	0.2221	23.34	43.20	NL	0.4377	45.985	t <sub>2g</sub>	-0.0584	
e <sub>g</sub>	0.0874	0.0874	9.18	17.00				e <sub>g</sub>	-0.0329	

NL	0.4377	0.4377	45.99	$\sigma + \pi$	0.51	54.01	NL	-0.2037
Total	0.9518	0.9518					Total	-0.3954

From the above results it is clear that the  $\pi$ -contribution is favoured when  $DA(\text{Cr,C,C,N}) = 90^\circ$  for each X-group. The result being that the  $\pi$ -character increases from  $180^\circ$  to  $90^\circ$ .

**Section 5: The fragment analysis of the metal cluster interacting with the X-group [M]...[X] at the frozen dihedrals.**

**Table C 5. 1.** The [M]...[X] interaction of structure **5a** (OEt) at the various frozen dihedrals  $DA(\text{Cr,C,C,N})$ .

Frozen Dihedral Angle ( $^\circ$ )					180				
Summary					$\sigma / \pi$				
DI					Summary				
	Contribution	Absolute Contribution	%	Metal %		Contribution	%		Energy (a.u.)
$a_{1g}$	0.0045	0.0055	1.68	4.24	$\sigma$	0.0762	23.85	$a_{1g}$	-0.0021
$t_{1u}$	0.0497	0.0501	15.21	38.39	$\pi$	0.0519	15.78	$t_{1u}$	-0.0189
$t_{2g}$	0.0519	0.0520	15.78	39.81	NL	0.1787	60.37	$t_{2g}$	-0.0138

e <sub>g</sub>	0.0221	0.0229	6.96	17.56				e <sub>g</sub>	-0.0078
NL	0.1787	0.1989	60.37		σ + π	0.1281	39.63	NL	-0.0834
Total	0.3068	0.3294						Total	-0.1262

Frozen Dihedral Angle (°)

170

Summary					σ/π	Summary				
DI										
	Contribution	Absolute Contribution	%	Metal %		Contribution	%		Energy (a.u.)	
a <sub>1g</sub>	0.0046	0.0056	1.71	4.24	σ	0.0773	24.21	a <sub>1g</sub>	-0.0023	
t <sub>1u</sub>	0.0498	0.0502	15.32	37.89	π	0.0531	16.23	t <sub>1u</sub>	-0.0190	
t <sub>2g</sub>	0.0531	0.0532	16.23	40.14	NL	0.1758	59.56	t <sub>2g</sub>	-0.0141	
e <sub>g</sub>	0.0229	0.0235	7.17	17.73				e <sub>g</sub>	-0.0082	
NL	0.1758	0.1951	59.56		σ + π	0.1305	40.44	NL	-0.0820	
Total	0.3062	0.3276						Total	-0.1256	

Frozen Dihedral Angle (°)

90

Summary					σ/π	Summary				
DI										
	Contribution	Absolute Contribution	%	Metal %		Contribution	%		Energy (a.u.)	
a <sub>1g</sub>	0.0044	0.0066	1.71	3.11	σ	0.0712	19.84	a <sub>1g</sub>	-0.0024	
t <sub>1u</sub>	0.0448	0.0471	12.23	22.23	π	0.1351	35.15	t <sub>1u</sub>	-0.0182	

t <sub>2g</sub>	0.1351	0.1353	35.15	63.92	NL	0.1216	45.01	t <sub>2g</sub>	-0.0376
e <sub>g</sub>	0.0220	0.0227	5.90	10.74				e <sub>g</sub>	-0.0082
NL	0.1216	0.1732	45.01		$\sigma + \pi$	0.2064	54.99	NL	-0.0565
Total	0.3280	0.3849						Total	-0.1229

**Table C 5. 2.** The [M]...[X] interaction of structure **5b** (NH<sub>2</sub>) at the various frozen dihedrals DA(Cr,C,C,N).

Frozen Dihedral Angle (°)						180			
Summary					$\sigma/\pi$		Summary		
DI									
	Contribution	Absolute Contribution	%	Metal %		Contribution	%		Energy (a.u.)
a <sub>1g</sub>	0.0037	0.0038	1.53	3.06	$\sigma$	0.0546	26.21	a <sub>1g</sub>	-0.0019
t <sub>1u</sub>	0.0347	0.0452	18.12	36.33	$\pi$	0.0589	23.67	t <sub>1u</sub>	-0.0127
t <sub>2g</sub>	0.0589	0.0590	23.67	47.45	NL	0.0982	50.12	t <sub>2g</sub>	-0.0152
e <sub>g</sub>	0.0161	0.0164	6.56	13.16				e <sub>g</sub>	-0.0059
NL	0.0982	0.1250	50.12		$\sigma + \pi$	0.1135	49.88	NL	-0.0460
Total	0.2117	0.2494						Total	-0.0817

Frozen Dihedral Angle (°)						150			
---------------------------	--	--	--	--	--	-----	--	--	--

Summary					$\sigma/\pi$		Summary			
DI										
	Contribution	Absolute Contribution	%	Metal %			Contribution	%		Energy (a.u.)
a <sub>1g</sub>	0.0032	0.0033	1.32	2.71	$\sigma$		0.0487	23.11	a <sub>1g</sub>	-0.0016
t <sub>1u</sub>	0.0306	0.0390	15.62	32.22	$\pi$		0.0632	25.38	t <sub>1u</sub>	-0.0115
t <sub>2g</sub>	0.0632	0.0633	25.38	52.34	NL		0.0974	51.51	t <sub>2g</sub>	-0.0164
e <sub>g</sub>	0.0149	0.0154	6.17	12.73					e <sub>g</sub>	-0.0055
NL	0.0974	0.1285	51.51		$\sigma + \pi$		0.1119	48.49	NL	-0.0427
Total	0.2093	0.2494							Total	-0.0777

---

Frozen Dihedral Angle (°)

90

Summary					$\sigma/\pi$		Summary			
DI										
	Contribution	Absolute Contribution	%	Metal %			Contribution	%		Energy (a.u.)
a <sub>1g</sub>	0.0032	0.0034	1.15	2.06	$\sigma$		0.0412	17.94	a <sub>1g</sub>	-0.0018
t <sub>1u</sub>	0.0255	0.0341	11.70	20.96	$\pi$		0.1101	37.89	t <sub>1u</sub>	-0.0098
t <sub>2g</sub>	0.1101	0.1105	37.89	67.87	NL		0.0713	44.17	t <sub>2g</sub>	-0.0294
e <sub>g</sub>	0.0124	0.0148	5.09	9.11					e <sub>g</sub>	-0.0047
NL	0.0713	0.1289	44.17		$\sigma + \pi$		0.1513	55.83	NL	-0.0305
Total	0.2226	0.2918							Total	-0.0761

**Table C 5. 3.** The [M]···[X] interaction of structure **5c** (NMe<sub>2</sub>) at the various frozen dihedrals DA(Cr,C,C,N).

Frozen Dihedral Angle (°)						180					
Summary						$\sigma/\pi$		Summary			
DI											
	Contribution	Absolute Contribution	%	Metal %		Contribution	%		Energy (a.u.)		
a <sub>1g</sub>	0.0032	0.0033	1.05	2.66	$\sigma$	0.0462	14.94	a <sub>1g</sub>	-0.0017		
t <sub>1u</sub>	0.0292	0.0293	9.44	23.92	$\pi$	0.0760	24.53	t <sub>1u</sub>	-0.0118		
t <sub>2g</sub>	0.0760	0.0760	24.53	62.14	NL	0.1839	60.53	t <sub>2g</sub>	-0.0197		
e <sub>g</sub>	0.0138	0.0138	4.45	11.28				e <sub>g</sub>	-0.0056		
NL	0.1839	0.1876	60.53		$\sigma + \pi$	0.1222	39.47	NL	-0.0883		
Total	0.3061	0.3099						Total	-0.1271		

Frozen Dihedral Angle (°)						110					
Summary						$\sigma/\pi$		Summary			
DI											
	Contribution	Absolute Contribution	%	Metal %		Contribution	%		Energy (a.u.)		
a <sub>1g</sub>	0.0031	0.0036	1.02	2.10	$\sigma$	0.0485	15.07	a <sub>1g</sub>	-0.0016		
t <sub>1u</sub>	0.0282	0.0315	9.01	18.48	$\pi$	0.1174	33.66	t <sub>1u</sub>	-0.0110		
t <sub>2g</sub>	0.1174	0.1178	33.66	69.07	NL	0.1398	51.26	t <sub>2g</sub>	-0.0309		
e <sub>g</sub>	0.0171	0.0177	5.05	10.36				e <sub>g</sub>	-0.0069		
NL	0.1398	0.1793	51.26		$\sigma + \pi$	0.1658	48.74	NL	-0.0670		



Frozen Dihedral Angle (°)					90				
Summary					Summary				
DI									
	Contribution	Absolute Contribution	%	Metal %		Contribution	%		Energy (a.u.)
a <sub>1g</sub>	0.0030	0.0035	0.98	1.95	σ	0.0470	15.11	a <sub>1g</sub>	-0.0016
t <sub>1u</sub>	0.0270	0.0327	9.25	18.42	π	0.1236	35.07	t <sub>1u</sub>	-0.0105
t <sub>2g</sub>	0.1236	0.1239	35.07	69.89	NL	0.1347	49.82	t <sub>2g</sub>	-0.0326
e <sub>g</sub>	0.0170	0.0173	4.89	9.74				e <sub>g</sub>	-0.0069
NL	0.1347	0.1760	49.82		σ + π	0.1705	50.18	NL	-0.0654
Total	0.3052	0.3534						Total	-0.1169

From the above results it is clear that the  $\pi$ -contribution is favoured when  $DA(\text{Cr,C,C,N}) = 90^\circ$  for each X-group. The result being that the  $\pi$ -character decreases from  $180^\circ$  to  $90^\circ$ .

### Section 6: The fragment analysis of the metal cluster interacting with the R-group [M]...[R] at the frozen dihedrals.

**Table C 6. 1.** The [M]...[R] interaction of structure **5a** (OEt) at the various frozen dihedrals  $DA(\text{Cr,C,C,N})$ .

Frozen Dihedral Angle (°)						180					
Summary						$\sigma/\pi$		Summary			
	DI Contribution	Absolute Contribution	%	Metal %		Contribution	%			Energy (a.u.)	
a <sub>1g</sub>	0.0027	0.0032	0.82	1.75	$\sigma$	0.0472	12.40	a <sub>1g</sub>		-0.0013	
t <sub>1u</sub>	0.0321	0.0323	8.32	17.65	$\pi$	0.1270	34.71	t <sub>1u</sub>		-0.0128	
t <sub>2g</sub>	0.1270	0.1346	34.71	73.67	NL	0.1049	52.89	t <sub>2g</sub>		-0.0331	
e <sub>g</sub>	0.0124	0.0127	3.26	6.92				e <sub>g</sub>		-0.0045	
NL	0.1049	0.2051	52.89		$\sigma + \pi$	0.1742	47.11	NL		-0.0574	
Total	0.2791	0.3878						Total		-0.1091	

Frozen Dihedral Angle (°)						170					
Summary						$\sigma/\pi$		Summary			
	DI Contribution	Absolute Contribution	%	Metal %		Contribution	%			Energy (a.u.)	
a <sub>1g</sub>	0.0024	0.0030	0.78	1.60	$\sigma$	0.0466	12.52	a <sub>1g</sub>		-0.0011	
t <sub>1u</sub>	0.0316	0.0320	8.37	17.18	$\pi$	0.1306	36.18	t <sub>1u</sub>		-0.0126	
t <sub>2g</sub>	0.1306	0.1382	36.18	74.30	NL	0.0986	51.31	t <sub>2g</sub>		-0.0340	
e <sub>g</sub>	0.0126	0.0129	3.37	6.92				e <sub>g</sub>		-0.0046	
NL	0.0986	0.1960	51.31		$\sigma + \pi$	0.1772	48.69	NL		-0.0548	
Total	0.2758	0.3820						Total		-0.1072	

Frozen Dihedral Angle (°)						90					
---------------------------	--	--	--	--	--	----	--	--	--	--	--

Summary						$\sigma/\pi$		Summary	
	DI Contribution	Absolute Contribution	%	Metal %		Contribution	%		Energy (a.u.)
a <sub>1g</sub>	0.0042	0.0048	1.67	4.72	$\sigma$	0.0401	14.19	a <sub>1g</sub>	-0.0022
t <sub>1u</sub>	0.0226	0.0226	7.89	22.36	$\pi$	0.0605	21.11	t <sub>1u</sub>	-0.0094
t <sub>2g</sub>	0.0605	0.0606	21.11	59.81	NL	0.1812	64.70	t <sub>2g</sub>	-0.0163
e <sub>g</sub>	0.0133	0.0133	4.63	13.11				e <sub>g</sub>	-0.0053
NL	0.1812	0.1857	64.70		$\sigma + \pi$	0.1006	35.30	NL	-0.0823
Total	0.2818	0.2870						Total	-0.1154

**Table C 6. 2.** The [M]...[R] interaction of structure **5b** (NH<sub>2</sub>) at the various frozen dihedrals DA(Cr,C,C,N).

Frozen Dihedral Angle (°)					180				
Summary	DI				$\sigma/\pi$		Summary		
	Contribution	Absolute Contribution	%	Metal %		Contribution	%		Energy (a.u.)
a <sub>1g</sub>	0.0033	0.0035	1.27	2.48	$\sigma$	0.0616	22.84	a <sub>1g</sub>	-0.0017
t <sub>1u</sub>	0.0395	0.0398	14.64	28.51	$\pi$	0.0770	28.49	t <sub>1u</sub>	-0.0155
t <sub>2g</sub>	0.0770	0.0774	28.49	55.50	NL	0.1065	48.66	t <sub>2g</sub>	-0.0198
e <sub>g</sub>	0.0188	0.0188	6.94	13.51				e <sub>g</sub>	-0.0074
NL	0.1065	0.1322	48.66		$\sigma + \pi$	0.1387	51.34	NL	-0.0542
Total	0.2452	0.2717						Total	-0.0987

Frozen Dihedral Angle (°)					150									
Summary					$\sigma/\pi$					Summary				
DI														
	Contribution	Absolute Contribution	%	Metal %		Contribution	%		Energy (a.u.)					
a <sub>1g</sub>	0.0023	0.0025	0.97	1.86	$\sigma$	0.0429	17.60	a <sub>1g</sub>	-0.0012					
t <sub>1u</sub>	0.0294	0.0306	11.99	22.99	$\pi$	0.0873	34.57	t <sub>1u</sub>	-0.0120					
t <sub>2g</sub>	0.0873	0.0881	34.57	66.26	NL	0.0944	47.83	t <sub>2g</sub>	-0.0226					
e <sub>g</sub>	0.0113	0.0118	4.63	8.88				e <sub>g</sub>	-0.0044					
NL	0.0944	0.1220	47.83		$\sigma + \pi$	0.1303	52.17	NL	-0.0464					
Total	0.2247	0.2549						Total	-0.0867					

Frozen Dihedral Angle (°)					90									
Summary					$\sigma/\pi$					Summary				
DI														
	Contribution	Absolute Contribution	%	Metal %		Contribution	%		Energy (a.u.)					
a <sub>1g</sub>	0.0042	0.0043	1.78	4.13	$\sigma$	0.0393	16.55	a <sub>1g</sub>	-0.0023					
t <sub>1u</sub>	0.0237	0.0242	10.00	23.21	$\pi$	0.0642	26.52	t <sub>1u</sub>	-0.0099					
t <sub>2g</sub>	0.0642	0.0642	26.52	61.57	NL	0.1270	56.92	t <sub>2g</sub>	-0.0170					
e <sub>g</sub>	0.0114	0.0116	4.78	11.09				e <sub>g</sub>	-0.0047					
NL	0.1270	0.1378	56.92		$\sigma + \pi$	0.1035	43.08	NL	-0.0600					

Total	0.2305	0.2421	Total	-0.0939
-------	--------	--------	-------	---------

**Table C 6. 3.** The [M]...[R] interaction of structure **5c** (NMe<sub>2</sub>) at the various frozen dihedrals DA(Cr,C,C,N).

Frozen Dihedral Angle (°)						180					
Summary						$\sigma/\pi$		Summary			
DI											
	Contribution	Absolute Contribution	%	Metal %		Contribution	%			Energy (a.u.)	
a <sub>1g</sub>	0.0023	0.0027	0.95	2.47	$\sigma$	0.0337	12.27	a <sub>1g</sub>		-0.0013	
t <sub>1u</sub>	0.0223	0.0226	8.01	20.90	$\pi$	0.0735	26.07	t <sub>1u</sub>		-0.0094	
t <sub>2g</sub>	0.0735	0.0735	26.07	68.00	NL	0.1650	61.66	t <sub>2g</sub>		-0.0191	
e <sub>g</sub>	0.0091	0.0093	3.31	8.63				e <sub>g</sub>		-0.0038	
NL	0.1650	0.1739	61.66		$\sigma + \pi$	0.1072	38.34	NL		-0.0772	
Total	0.2722	0.2820						Total		-0.1107	

Frozen Dihedral Angle (°)						110					
Summary						$\sigma/\pi$		Summary			
DI											
	Contribution	Absolute Contribution	%	Metal %		Contribution	%			Energy (a.u.)	
a <sub>1g</sub>	0.0028	0.0030	1.13	2.95	$\sigma$	0.0345	13.48	a <sub>1g</sub>		-0.0014	
t <sub>1u</sub>	0.0231	0.0242	9.06	23.64	$\pi$	0.0663	24.87	t <sub>1u</sub>		-0.0095	
t <sub>2g</sub>	0.0663	0.0663	24.87	64.85	NL	0.1586	61.65	t <sub>2g</sub>		-0.0170	

e <sub>g</sub>	0.0086	0.0087	3.28	8.56				e <sub>g</sub>	-0.0034
NL	0.1586	0.1643	61.65		σ + π	0.1008	38.35	NL	-0.0754
Total	0.2594	0.2665						Total	-0.1068

Frozen Dihedral Angle (°)					90				
Summary					Summary				
DI									
	Contribution	Absolute Contribution	%	Metal %		Contribution	%		Energy (a.u.)
a <sub>1g</sub>	0.0038	0.0040	1.40	4.01	σ	0.0386	13.71	a <sub>1g</sub>	-0.0020
t <sub>1u</sub>	0.0245	0.0245	8.66	24.82	π	0.0600	21.16	t <sub>1u</sub>	-0.0101
t <sub>2g</sub>	0.0600	0.0600	21.16	60.69	NL	0.1817	65.13	t <sub>2g</sub>	-0.0155
e <sub>g</sub>	0.0104	0.0104	3.65	10.48				e <sub>g</sub>	-0.0041
NL	0.1817	0.1847	65.13		σ + π	0.0987	34.87	NL	-0.0860
Total	0.2804	0.2836						Total	-0.1176

**Section 7: Inter-fragment delocalization of all the molecules in their respective fragments for the geometric analysis.**

**Table C 7. 1.** The electrons population in the Fischer Carbenes for X=OEt.

Total Electron Population, N([A])	Total intra-fragment population N <sup>intra</sup> ([A])
-----------------------------------	---

Structure	Frozen Dihedral Angle (°)	[M]	C <sub>carbene</sub>	[X]	[R]	[M]	C <sub>carbene</sub>	[X]	[R]
		5a	90	94.03	5.52	25.50	42.95	92.27	3.79
	170	94.14	5.53	25.53	42.81	92.43	3.81	24.65	41.80
	180	94.14	5.53	25.53	42.81	92.43	3.81	24.64	41.80

**Table C 7. 2.** The electrons population in the Fischer Carbenes for X=OEt.

Structure	Frozen Dihedral Angle (°)	Electrons shared DI([A], [B])					
		[M]···C <sub>carbene</sub>	[M]···[X]	[M]···[R]	C <sub>carbene</sub> ···[X]	C <sub>carbene</sub> ···[R]	[X]···[R]
		5a	90	1.1855	0.3280	0.2818	1.1390
	170	0.9927	0.3062	0.2758	1.0785	1.3685	0.3720
	180	0.9874	0.3068	0.2791	1.0785	1.3711	0.3760

**Table C 7. 3.** The electrons population in the Fischer Carbenes for X=NH<sub>2</sub>.

Structure	Frozen Dihedral Angle (°)	Total Electron Population, N([A])				Total intra-fragment population N <sup>intra</sup> ([A])			
		[M]	C <sub>carbene</sub>	[X]	[R]	[M]	C <sub>carbene</sub>	[X]	[R]
5b	90	94.12	5.51	9.40	42.97	92.45	3.76	8.51	42.16
	150	94.17	5.53	9.42	42.88	92.53	3.77	8.52	41.95
	180	94.19	5.53	9.43	42.85	92.56	3.78	8.53	41.88

**Table C 7. 4.** The electrons population in the Fischer Carbenes for X=NH<sub>2</sub>.

Structure	Frozen Dihedral Angle (°)	Electrons shared DI([A], [B])					
		[M]...C <sub>carbene</sub>	[M]...[X]	[M]...[R]	C <sub>carbene</sub> ...[X]	C <sub>carbene</sub> ...[R]	[X]...[R]
5b	90	1.0647	0.2226	0.2305	1.3070	1.1426	0.2406
	150	0.9675	0.2093	0.2247	1.2516	1.3057	0.3311
	180	0.9029	0.2117	0.2452	1.2511	1.3498	0.3502



**Table C 7. 5.** The electrons population in the Fischer Carbenes for X=NMe<sub>2</sub>.

Structure	Frozen Dihedral Angle (°)	Total Electron Population, N([A])				Total intra-fragment population N <sup>intra</sup> ([A])			
		[M]	C <sub>carbene</sub>	[X]	[R]	[M]	C <sub>carbene</sub>	[X]	[R]
5c	90	94.14	5.55	25.32	42.99	92.56	3.79	24.28	42.10
	110	94.15	5.56	25.32	42.97	92.55	3.79	24.28	42.07
	180	94.19	5.59	25.34	42.88	92.65	3.83	24.28	41.84

**Table C 7. 6.** The electrons shared in the Fischer Carbenes for X=NMe<sub>2</sub>.

Structure	Frozen Dihedral Angle (°)	Electrons shared DI([A], [B])					
		[M]···C <sub>carbene</sub>	[M]···[X]	[M]···[R]	C <sub>carbene</sub> ···[X]	C <sub>carbene</sub> ···[R]	[X]···[R]
5c	90	0.9518	0.3052	0.2804	1.4197	1.1466	0.3446
	110	0.9662	0.3056	0.2594	1.3979	1.1660	0.3843
	180	0.8472	0.3061	0.2722	1.3265	1.3374	0.4824

**Section 8: Inter-fragment delocalization of all the molecules in their respective fragments for the electronic analysis.**

**Table C 8. 1.** The electrons population in the Fischer Carbenes for all X's frozen to  $DA(Cr,C,C,N) = 90^\circ$ .

Structure	Frozen Dihedral Angle ( $^\circ$ )	Total Electron Population, N([A])				Total intra-fragment population $N^{intra}$ ([A])			
		[M]	$C_{\text{carbene}}$	[X]	[R]	[M]	$C_{\text{carbene}}$	[X]	[R]
5a	90	94.03	5.52	25.50	42.95	92.27	3.79	24.66	42.14
5b	90	94.12	5.51	9.40	42.97	92.45	3.76	8.51	42.16
5c	90	94.14	5.55	25.32	42.99	92.56	3.79	24.28	42.10

**Table C 8. 2.** The electrons population in the Fischer Carbenes for all X's frozen  $DA(Cr,C,C,N)$  to the lowest energy structure.

Structure	Frozen Dihedral	Total Electron Population, N([A])				Total intra-fragment population $N^{intra}$ ([A])			
		[M]	$C_{\text{carbene}}$	[X]	[R]	[M]	$C_{\text{carbene}}$	[X]	[R]

	Angle (°)								
5a	170	94.14	5.53	25.53	42.81	92.43	3.81	24.65	41.80
5b	150	94.17	5.53	9.42	42.88	92.53	3.77	8.52	41.95
5c	110	94.15	5.56	25.32	42.97	92.55	3.79	24.28	42.07

**Table C 8. 3.** The electrons population in the Fischer Carbenes for all X's frozen to  $DA(Cr,C,C,N) = 180^\circ$ .

Structure	Frozen Dihedral Angle (°)	Total Electron Population, N([A])				Total intra-fragment population $N^{intra}$ ([A])			
		[M]	$C_{carbene}$	[X]	[R]	[M]	$C_{carbene}$	[X]	[R]
		5a	180	94.14	5.53	25.53	42.81	92.43	3.81
5b	180	94.19	5.53	9.43	42.85	92.56	3.78	8.53	41.88
5c	180	94.19	5.59	25.34	42.88	92.65	3.83	24.28	41.84

**Section 9: Hypothesis testing of the carbonyls interacting with [X] and [R] fragments.**

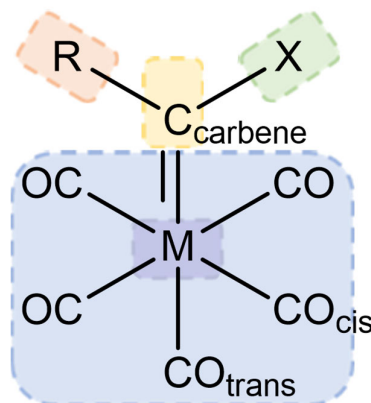


**Figure C 9. 1.** The fragmentation of the Fischer carbene used in the FALDI Fragments Molecular Orbital Analysis to investigate chromium interacting with the various fragments.

**Figure C 9. 1.** illustrates the general fragmentation of the molecule in a pictorial format, the X-group was the only parameter changed. The metal cluster [M] is defined as the metal and the five carbonyls, indicated in blue, the carbene carbon as yellow, the R-group as orange and the X-group as green. Finally, M or Cr which is in purple, represents only the metal (Chromium) and the carbonyls are then separately represented by the blue. From the above results we developed a hypothesis to describe some of the interactions with the carbonyls and substituents on the carbene, it is however important to note these interactions are weak relative to the  $[M] \cdots C_{\text{carbene}}$  interaction. The hypothesis was that the R-group interacts more with carbonyls, which is why we separated the metal cluster into Cr and the five carbonyls ([CO]) in **Figure C 9. 1**. This fragmenting pattern allowed for isolating whether the R-group was interacting with the carbonyls only, metal only or both collectively as the metal cluster.

**Table C 9. 1.** The electrons shared in the Fischer Carbene when X=OEt with Cr as an independent fragment.

Structure	Frozen Dihedral Angle (°)	Total Electron Population, N([A])					Total intra-fragment population N <sup>intra</sup> ([A])				
		Cr	C <sub>carbene</sub>	[X]	[R]	[CO]	Cr	C <sub>carbene</sub>	[X]	[R]	[CO]
		5a	90	22.89	5.52	25.50	42.95	71.14	19.99	3.79	24.66
5a	170	22.89	5.53	25.53	42.81	71.24	20.00	3.81	24.65	41.80	68.31
5a	180	22.90	5.53	25.53	42.81	71.25	20.00	3.81	24.64	41.80	68.31

By separating the metal cluster into the carbonyls ([CO]) and metal only (Cr), the metal population remained the same at dihedral  $DA(\text{Cr,C,C,N}) = 90^\circ$ ,  $170^\circ$  and approximately the same at  $180^\circ$  which is expected from the hypothesis, indicating the change in electron population stems from the carbonyls. This illustrates that the hypothesis is correct and that electrons are being shared between the carbonyls and R-group depending on the dihedral angle. The low energy structure at  $DA(\text{Cr,C,C,N}) = 170^\circ$  and  $180^\circ$  has more electrons on the carbonyls than at  $90^\circ$ , while  $90^\circ$  has more electrons on the R-group. Showing that the R-group is taking electron density from the carbonyls at  $DA(\text{Cr,C,C,N}) = 90^\circ$ . While the carbonyls are richer in electrons when the dihedral is set to  $DA(\text{Cr,C,C,N}) = 170^\circ$  and  $180^\circ$ . These electron populations provide a glimpse of what is expected when the electrons are shared between the fragments, which can be found in **Table C 9. 2.**

**Table C 9. 2.** The electrons shared in the Fischer Carbene when X=OEt with Cr as an independent fragment.

Structure	Frozen Dihedral Angle (°)	Electrons shared DI([A], [B])								
		Cr···C <sub>carbene</sub>	Cr···[X]	Cr···[R]	C <sub>carbene</sub> ···[X]	C <sub>carbene</sub> ···[R]	[X]···[R]	C <sub>carbene</sub> ···[CO]	[X]···[CO]	[R]···[CO]
5a	90	0.7256	0.1127	0.0684	1.1390	1.1312	0.2209	0.4599	0.2152	0.2134
5a	170	0.5934	0.0830	0.0736	1.0785	1.3685	0.3720	0.3994	0.2232	0.2022
5a	180	0.5911	0.0808	0.0740	1.0785	1.3711	0.3760	0.3963	0.2260	0.2051

The results of separating Cr from the metal cluster show that the carbonyls are interacting with the R-group. The most electrons are shared when the R-group is at  $DA(\text{Cr,C,C,N}) = 90^\circ$  to the carbonyls. This fragment analysis does not show how the electrons are shared but only how many electrons are shared, this is where the FALDI MO analysis comes into play. The FALDI MO analysis revealed that there is a strange trend that occurs when the dihedral of the R-group is rotated from  $DA(\text{Cr,C,C,N}) = 180^\circ$  to  $90^\circ$  in that the  $\pi$ -character increased. Therefore, the result of the FALDI fragment analysis and the FALDI MO analysis suggests that the increase in  $\pi$ -character from  $DA(\text{Cr,C,C,N}) = 180^\circ$  to  $90^\circ$  results from the R-group interacting with the carbonyls, so their orbital alignment is optimal to allow a  $\pi$ -transfer of electrons when at  $DA(\text{Cr,C,C,N}) = 90^\circ$ . The flip side of the trend showed that the  $\sigma$ -relationship increased from  $DA(\text{Cr,C,C,N}) = 90^\circ$  to  $180^\circ$  and this can mostly be found in the [X]···[R] interaction as the electrons shared increases from  $DA(\text{Cr,C,C,N}) = 90^\circ$  to  $180^\circ$ . Showing that the  $\sigma$ -character increase is likely from through bond electrons sharing in a  $\sigma$ -fashion.

The extent to which the fragments interact is best illustrated by visualizing the interaction, which can be found below in **Figure C 9. 2**. From **Table C 9. 2**. It is seen that there is a mostly inverse relationship between the [X]···[R] group interaction and the R-group interacting with the carbonyls. Speculating then that the  $DA(\text{Cr,C,C,N}) = 90^\circ$  dihedral most likely pays the energy penalty because of the R-groups geometry even

though the R-group interaction with the carbonyls is at its highest, sharing the most electrons, while the [X]...[R] interaction decreased and fewer electrons were shared.

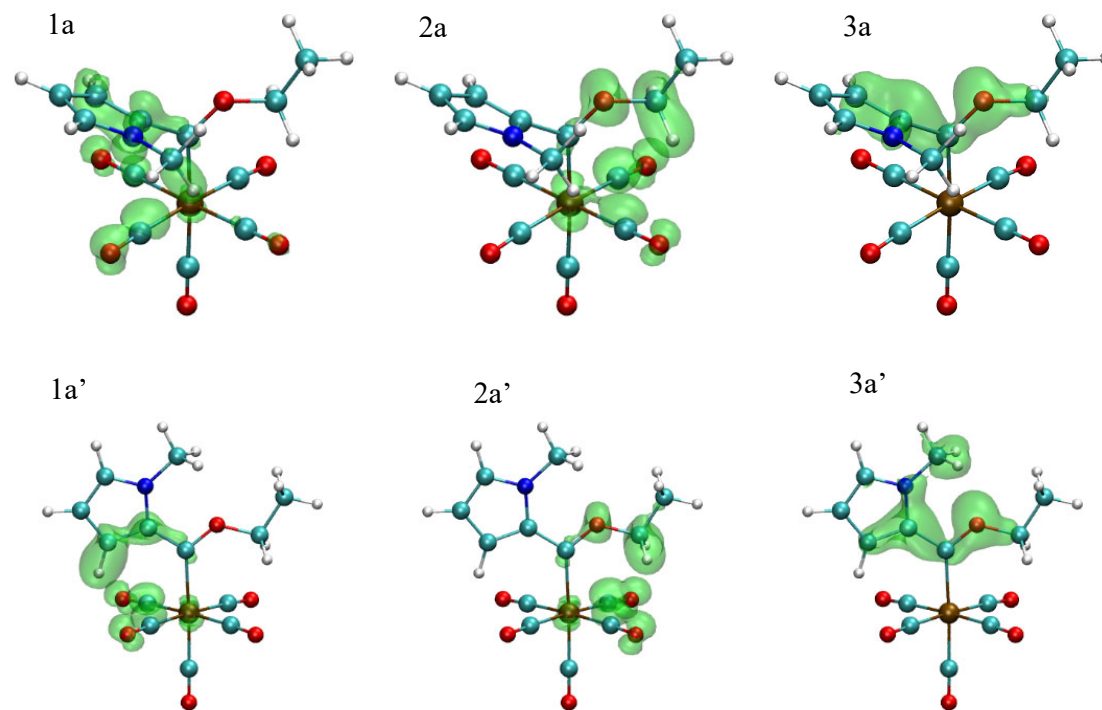


**Figure C 9. 2.** The Fragment interaction where the OEt (**5a**) is compared at dihedrals of  $DA(\text{Cr,C,C,N}) = 90^\circ$  (a) and  $DA(\text{Cr,C,C,N}) = 180^\circ$  (a'). The electrons are shared between fragments (1a) Carbonyls and R-group, (2a) the Carbonyls and X-group and (3a) the X- and R-group interaction.<sup>a</sup>

<sup>a</sup>All the isovalues were at 0.001 a.u.

The visualization of electrons shared between fragments provides a much better grasp of what is happening in the system when the R-group is rotated. From 1a and 1a' it can be seen that the R-group better overlaps with the carbonyls when at  $DA(\text{Cr,C,C,N}) = 90^\circ$ , such that the NMe on the R-group is involved in this interaction with the carbonyls. The carbonyls interacting with the X-group does not provide such a striking argument as the  $[\text{CO}] \cdots [\text{R}]$  interaction, and there is only slightly better overlap, which is visible when the molecule is freely rotated. How the carbonyls interact with the X-group is less obvious and more visible when the isovalues are changed, however, at an isovalue of 0.001 a.u. the overlap and interaction seem to be better at  $DA(\text{Cr,C,C,N}) = 180^\circ$  as illustrated in 2a', matching the results of **Table C 9. 2**. The opposite is seen for the  $[\text{X}] \cdots [\text{R}]$  interaction in 3a and 3a' which shows at  $DA(\text{Cr,C,C,N}) = 90^\circ$  the methylamine of the R-group is not involved in the interaction. Moving over to  $DA(\text{Cr,C,C,N}) = 180^\circ$  the inverse is seen, where the  $[\text{X}] \cdots [\text{R}]$  interaction has maximum overlap and the methylamine of R-group is involved in the interaction with the X-group. The same analysis has been performed for structure **5b** and **5c** and these figures and tables are available in under **Section 10** in **Figure C 10. 1.** and **C 10. 2.** and **Tables C 10. 1. to C 10. 4.** The same general trends and results are seen with the prominent visuals being the  $[\text{CO}] \cdots [\text{R}]$  and the  $[\text{X}] \cdots [\text{R}]$  interaction.

**Section 10. The fragment analysis of the metal and carbonyls separated interacting with the different fragments at the frozen dihedrals as a geometric analysis.**

**Table C 10. 1.** The electrons population in the Fischer Carbene when  $\text{X}=\text{NH}_2$  with Cr as an independent fragment.

Structure	Frozen Dihedral Angle ( $^\circ$ )	Total Electron Population, $N([\text{A}])$					Total intra-fragment population $N^{\text{intra}}([\text{A}])$				
		Cr	$\text{C}_{\text{carbene}}$	[X]	[R]	[CO]	Cr	$\text{C}_{\text{carbene}}$	[X]	[R]	[CO]
		5b	90	22.89	5.51	9.40	42.97	71.23	19.99	3.76	8.51
5b	150	22.89	5.53	9.42	42.88	71.27	20.00	3.77	8.52	41.95	68.39



5b	180	22.90	5.53	9.43	42.85	71.30	20.01	3.78	8.53	41.88	68.40
----	-----	-------	------	------	-------	-------	-------	------	------	-------	-------

**Table C 10. 2.** The electrons shared in the Fischer Carbene when X=NH<sub>2</sub> with Cr as an independent fragment.

		Electrons shared DI([A], [B])								
Frozen Dihedral Angle										
Structure	(°)	Cr···C <sub>carbene</sub>	Cr···[X]	Cr···[R]	C <sub>carbene</sub> ···[X]	C <sub>carbene</sub> ···[R]	[X]···[R]	C <sub>carbene</sub> ···[CO]	[X]···[CO]	[R]···[CO]
5b	90	0.6319	0.0962	0.0569	1.3070	1.1426	0.2406	0.4328	0.1263	0.1736
5b	150	0.5692	0.0806	0.0593	1.2516	1.3057	0.3311	0.3984	0.1287	0.1654
5b	180	0.5316	0.0773	0.0585	1.2511	1.3498	0.3502	0.3714	0.1345	0.1866

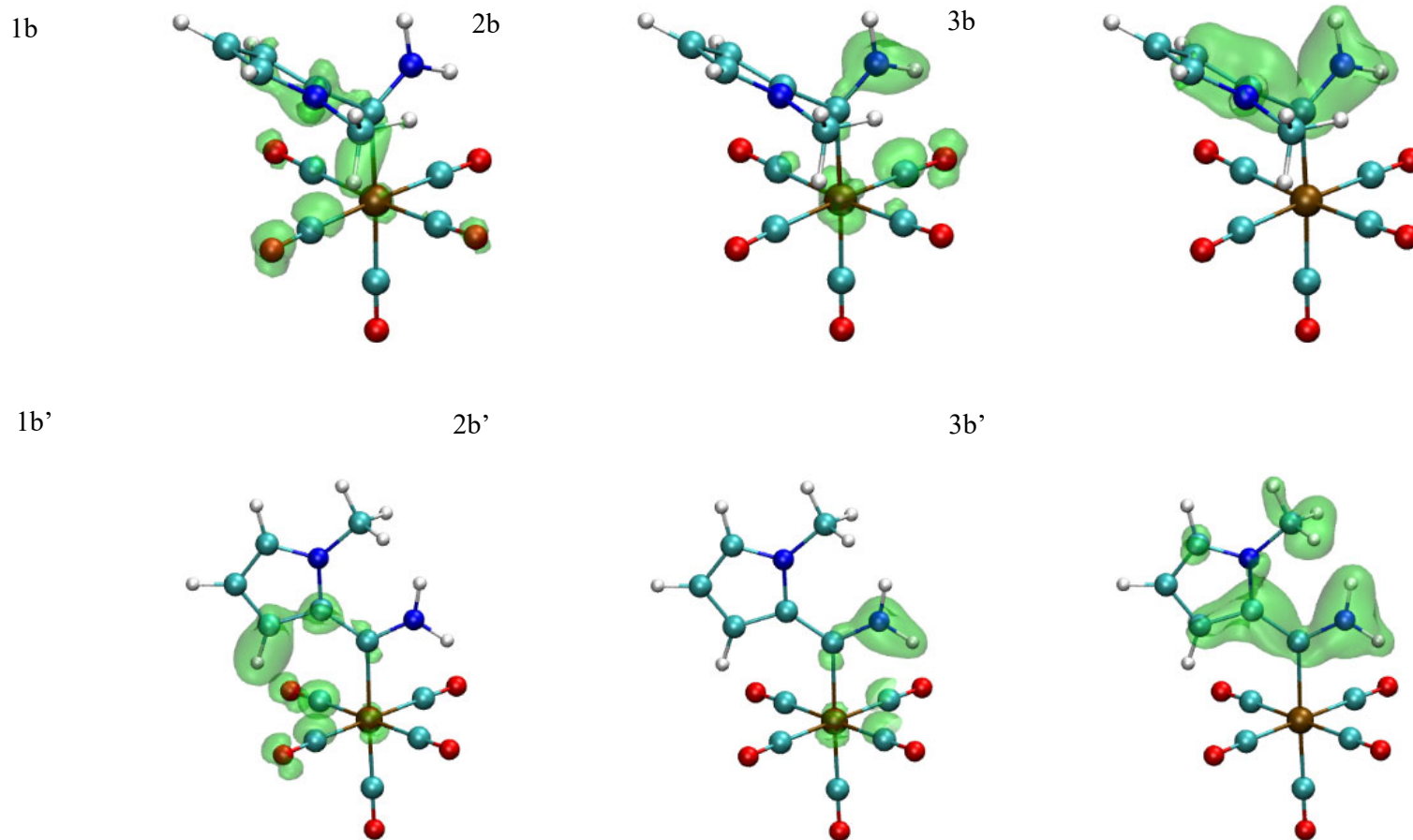


**Figure C 10. 1.** The Fragment interaction where the NH<sub>2</sub> (**5b**) is compared at dihedrals of DA(Cr,C,C,N) = 90°(b) and DA(Cr,C,C,N) = 180° (b'). The electrons are shared between fragments (1b) Carbonyls and R-group, (2b) the Carbonyls and X-group and (3b) the X- and R-group interaction.<sup>a</sup>

<sup>a</sup>All the isovalues were at 0.001 a.u.

**Table C 10. 3.** The electrons population in the Fischer Carbene when X=NMe<sub>2</sub> with Cr as an independent fragment.

Structure	Frozen Dihedral Angle (°)	Total Electron Population, N([A])					Total intra-fragment population N <sup>intra</sup> ([A])				
		Cr	C <sub>carbene</sub>	[X]	[R]	[CO]	Cr	C <sub>carbene</sub>	[X]	[R]	[CO]
		5c	90	22.89	5.55	25.32	42.99	71.25	20.01	3.79	24.28
5c	110	22.89	5.56	25.32	42.97	71.25	20.00	3.79	24.28	42.07	68.33
5c	180	22.90	5.59	25.34	42.88	71.29	20.02	3.83	24.28	41.84	68.34

**Table C 10. 4.** The electrons shared in the Fischer Carbene when X=NMe<sub>2</sub> with Cr as an independent fragment.

Structure	Frozen Dihedral Angle (°)	Electrons shared DI([A], [B])								
		Cr...C <sub>carbene</sub>	Cr...[X]	Cr...[R]	C <sub>carbene</sub> ...[X]	C <sub>carbene</sub> ...[R]	[X]...[R]	C <sub>carbene</sub> ...[CO]	[X]...[CO]	[R]...[CO]
		5b	90	0.5709	0.0996	0.0608	1.4197	1.1466	0.3446	0.3809
5b	110	0.5768	0.0986	0.0572	1.3979	1.1660	0.3843	0.3894	0.2071	0.2022
5b	180	0.4986	0.0809	0.0642	1.3265	1.3374	0.4824	0.3486	0.2252	0.2080

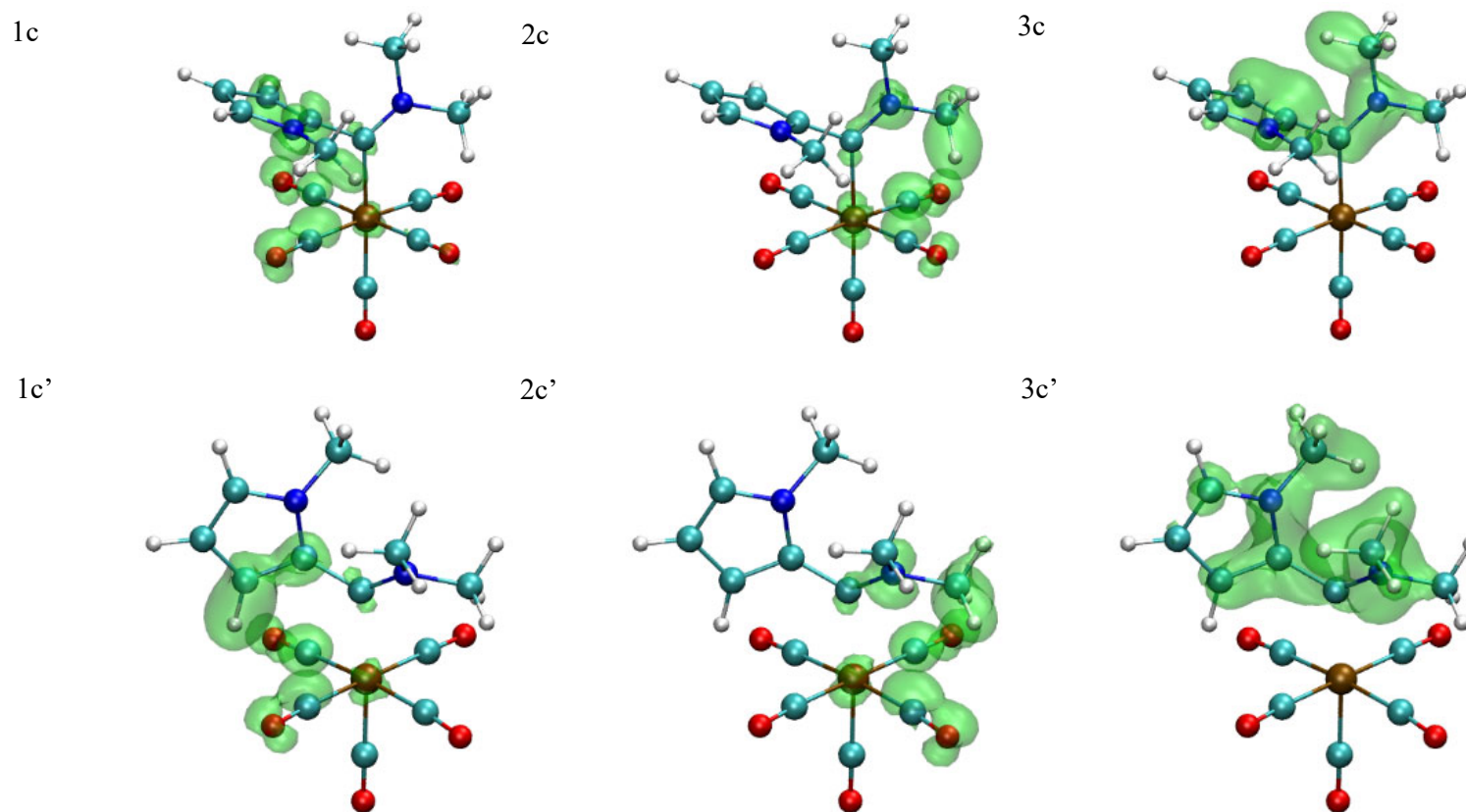


**Figure C 10. 2.** The Fragment interaction where the NMe<sub>2</sub> (**5c**) is compared at dihedrals of DA(Cr,C,C,N) = 90°(c) and DA(Cr,C,C,N) = 180° (c'). The electrons are shared between fragments (1c) Carbonyls and R-group, (2c) the Carbonyls and X-group and (3c) the X- and R-group interaction.<sup>a</sup>

<sup>a</sup>All the isovalues were at 0.001 a.u.

Looking deeper into the interactions as with the geometric effect analysis with a constant X-group, but where the carbonyls are separated from the metal produces **Table C 10. 5**.

**Table C 10. 5.** The electrons shared between fragments for different X-groups with Cr as an independent fragment.

Electrons shared DI([A], [B])										
Structure	Frozen Dihedral Angle	Cr...C <sub>carbene</sub>	Cr...[X]	Cr...[R]	C <sub>carbene</sub> ...[X]	C <sub>carbene</sub> ...[R]	[X]...[R]	C <sub>carbene</sub> ...[CO]	[X]...[CO]	[R]...[CO]
	(°)									
5a	90	0.7256	0.1127	0.0684	1.1390	1.1312	0.2209	0.4599	0.2152	0.2134
5b	90	0.6319	0.0962	0.0569	1.3070	1.1426	0.2406	0.4328	0.1263	0.1736
5c	90	0.5709	0.0996	0.0608	1.4197	1.1466	0.3446	0.3809	0.2056	0.2196

Electrons shared DI([A], [B])										
Structure	Frozen Dihedral Angle	Cr...C <sub>carbene</sub>	Cr...[X]	Cr...[R]	C <sub>carbene</sub> ...[X]	C <sub>carbene</sub> ...[R]	[X]...[R]	C <sub>carbene</sub> ...[CO]	[X]...[CO]	[R]...[CO]
	(°)									

5a	170	0.5934	0.0830	0.0736	1.0785	1.3685	0.3720	0.3994	0.2232	0.2022
5b	150	0.5692	0.0806	0.0593	1.2516	1.3057	0.3311	0.3984	0.1287	0.1654
5c	110	0.5768	0.0986	0.0572	1.3979	1.1660	0.3843	0.3894	0.2071	0.2022

---

Electrons shared DI([A], [B])

Frozen Dihedral Angle										
Structure	(°)	Cr···C <sub>carbene</sub>	Cr···[X]	Cr···[R]	C <sub>carbene</sub> ···[X]	C <sub>carbene</sub> ···[R]	[X]···[R]	C <sub>carbene</sub> ···[CO]	[X]···[CO]	[R]···[CO]
5a	180	0.5911	0.0808	0.0740	1.0785	1.3711	0.3760	0.3963	0.2260	0.2051
5b	180	0.5316	0.0773	0.0585	1.2511	1.3498	0.3502	0.3714	0.1345	0.1866
5c	180	0.4986	0.0809	0.0642	1.3265	1.3374	0.4824	0.3486	0.2252	0.2080

---

Throughout  $X=OEt$  has the most DI between the  $Cr \cdots C_{\text{carbene}}$  bond for all dihedrals  $DA(Cr,C,C,N)$  in **Table C 10. 5**. The trend at the dihedral of  $DA(Cr,C,C,N) = 90^\circ$  and  $180^\circ$  shows the electrons shared rank as  $OEt > NH_2 > NMe_2$ . While for the lowest energy structures, the electrons shared changes to  $OEt > NMe_2 > NH_2$ . Indicating Cr interacts best with the  $C_{\text{carbene}}$  when the X-group is ethoxy. The next interesting interaction is in the  $[CO] \cdots [X]$  interaction for which all dihedrals  $DA(Cr,C,C,N)$  follow the same trend, with the most electrons shared in ethoxy but the least with dihydrogen amine ( $OEt > NMe_2 > NH_2$ ) indicating the effect is electronic and not geometric. The  $[CO] \cdots [R]$  interaction also has a constant trend for all dihedrals with the most electrons shared in the dimethylamine and the least in dihydrogen amine ( $NMe_2 > OEt > NH_2$ ) indicating the effect is also electronic. Relating this information to classical interpretation is challenging in the sense that these long-range interactions where the carbonyls interact with the R- and X-group are not common thinking in Fischer carbene chemistry and bond lengths are rather looked at but this type of interaction is through space and bond lengths are redundant.

